

UNIVERSITY OF BIRMINGHAM

NON-FOSTER ANTENNA MATCHING NETWORKS USING REFLECTION-MODE NEGATIVE-GROUP-DELAY NETWORKS

BY

ALHASAN ALI MOFTAH ALMAHROUG

A thesis submitted to

University of Birmingham

for the degree of

DOCTOR OF PHILOSOPHY

Department of Electronic, Electrical and Systems Engineering

School of Engineering

University of Birmingham

June 2018

UNIVERSITY OF
BIRMINGHAM

University of Birmingham Research Archive

e-theses repository

This unpublished thesis/dissertation is copyright of the author and/or third parties. The intellectual property rights of the author or third parties in respect of this work are as defined by The Copyright Designs and Patents Act 1988 or as modified by any successor legislation.

Any use made of information contained in this thesis/dissertation must be in accordance with that legislation and must be properly acknowledged. Further distribution or reproduction in any format is prohibited without the permission of the copyright holder.

ABSTRACT

Wireless communication devices are required to cover an increasingly wide frequency band with low profile and low manufacturing antennas cost. Electrically small antennas can help designers to comply with these requirements. However, these antennas are characterised by large reactance and small radiation resistance which are very difficult to impedance match. Moreover, they are subject to gain-bandwidth limits derived by Bode and Fano that would inhibit continuous broadband matching with passive matching networks. Non-Foster reactive elements are proposed as a means to bypass those restrictions. These reactive non-Foster elements are susceptible to instability when realised using the transistorised negative impedance converters (NICs) and negative impedance inverters (NIIs), due to the difficulty in controlling the feedback in the circuitry at microwave frequencies and this limits the achievable top frequency.

This thesis explores the connection between loss-compensated negative group delay (NGD) networks and non-Foster reactive elements in a bandwidth from 1 to 2 GHz. A new perspective in designing NGD-based non-Foster reactive elements in the microwave frequencies is investigated. A novel reflection-mode NGD network is designed using NI AWRDE Microwave Office, fabricated and tested. Simulation and experimental results show that the proposed topology generates NGD of -1.62 ns over a bandwidth of 0.3 GHz between 1.2 GHz to 1.37 GHz. Subsequently, a novel approach which contains a negative resistance amplifier and a Lange coupler is modelled with the aid of Microwave Office to compensate the inevitable losses of

the NGD networks. The merit of this novel design is that the main NGD response is obtained by circuits which should make it easier to achieve stable behaviour.

The potential use of the NGD-based non-Foster network in antenna matching applications is theoretically investigated. A new analysis to explore an equivalent circuit model for the non-Foster NGD network based on the impedance trajectory of the network in the frequency range of interest has been investigated and introduced. The NGD-based non-Foster network was implemented as a shunt matching network with a designed planar monopole patch antenna (PMPA) and by the addition of an external impedance transformer to the antenna's terminal, the bandwidth of the antenna is increased over a wider frequency range. This is a significant achievement compared with the performance of the antenna alone and when it is matched with a passive matching network. Stability analysis using the Nyquist criteria to detect the instability of the NGD-based non-Foster circuit connected to a PMPA was carried out. Simulation results revealed that the overall circuit with the antenna is working stable. Finally, approximate calculations of the non-linearity and noise performance addressing the operational limitations of the proposed circuit in transmit and receive applications have been introduced.

DEDICATIONS

This thesis is dedicated to

My beloved parents

And

My beloved wife and children, Anas, Osama and MaisAlreem

And

My beloved brother and sister

ACKNOWLEDGMENTS

In the name of Allah, Most Gracious, and Most Merciful

Praise be to Allah the Cherisher and Sustainer of the Worlds. With his permission and blessing, I have completed this work.

I wish to express my sincere and deepest gratitude and appreciation to my supervisors, Professor Peter Gardner, Head of Department of Electronic, Electrical and Systems Engineering and Dr Alexandros Feresidis, Senior Lecturer in Communications Engineering, for their kindness, constant endeavour, and guidance and the numerous moments of attention they devoted throughout my long journey of study.

I extend my deepest gratitude to Mr Alan Yates, Senior Research Technician, Wireless Communications & Remote Sensing Group, for providing all the technical support in fabricating the PCBs and teaching me very useful practical skills and sharing his wealth of experience with me.

I would like also to thank all members in the Communication Engineering Research Group for their help, including Professor Costas Constantinou and Mr James Churm for their support during my studies. Special thanks go to my brilliant colleagues and very nice friends, including Abdullah Altamimi, Waleed Al Abri, Zafar Khan, Bader Alharbi, Hasan Gunduz, and Dr Mohammad Milani.

Family support plays a vital role in the success of any individual. I would like to convey a heartfelt thanks to my parents, my wife and children, my brother Husain Almahroug and my sister for their endless love, emotional support and belief in me without them I would never come up to this stage.

My biggest gratitude is to all my friends in Libya and appreciation is also extending to all my relatives back home.

Finally, this thesis was copy-edited for the conventions of language, grammar and spelling by Janet's Proofreading Service.

LIST OF PUBLICATIONS

[1] A. A. Almahroug, A. P. Feresidis, and P. Gardner, "Non-Foster antenna matching networks using reflection-mode negative-group-delay networks," in 2016 Loughborough Antennas & Propagation Conference (LAPC), 2016, pp. 1-4.

[2] A. A. Almahroug, A. P. Feresidis, and P. Gardner, "Antenna matching network using new class of non-Foster reactive elements," in 2017 International Workshop on Electromagnetics: Applications and Student Innovation Competition, 2017, pp. 180-182.

TABLE OF CONTENTS

CHAPTER 1 1

INTRODUCTION 1

1.1 Motivation and Background 1

1.1.1 Specific Systems Requirements – need for wide-band smal antennas……...4

1.2 Objectives 6

1.3 Thesis Contributions 7

1.4 Thesis Layout 8

References 11

CHAPTER 2 13

REACTIVE NON-FOSTER ELEMENTS AND THEIR APPLICATIONS 13

2.1 Non-Foster Impedances 13

2.2 Realisation of Non-Foster Impedances 15

2.2.1 Negative Impedance Converters (NICs) and Inverters (NIIs) 15

2.2.2 Stability within NICs 17

2.3 Non-Foster Reactive Elements Applications 20

2.3.1 Implementation of Non-Foster Reactive Elements in Matching Networks 21

2.3.1.1 Conventional versus Non-Foster Matching Techniques 21

2.3.1.2 Literature Review regarding Using Non-Foster Impedances as Matching Networks with Antennas 22

2.3.2 Using Non-Foster Reactive Elements in Other Applications 33

2.4 Summary 39

References..... 40

CHAPTER 3 47

NEGATIVE-GROUP-DELAY NETWORKS AND THEIR APPLICATIONS.... 47

3.1 Basic Theory of Negative Group Delay 47

3.2 Realisation of Negative- Group Delay Networks..... 48

3.3 Negative- Group -Delay Networks Applications 51

3.4 Relationship between NGD Networks and Networks with Non-Foster Behaviour..... 54

3.5 Loss-Compensation Methods for NGD Networks 59

3.5.1 Active Circuits for Loss-Compensation 59

3.5.2 Loss-Compensation scheme for Transmission-mode NGD Networks 62

3.5.3 Loss-Compensation scheme for Reflection-Mode NGD Networks……...63

3.6 Summary..... 66

References..... 68

CHAPTER 4 74

REALISATION OF NON-FOSTER REACTIVE CIRCUITS USING REFLECTION–MODE NGD NETWORKS..... 74

4.1 Reflection-mode NGD Network Design 74

4.2 Reflection-mode NGD Network Design Using Ideal Components..... 75

4.3 Design and Experimental Verification of Realistic Reflection-Type NGD Network..... 97

4.4 Reflection–Type NGD Network Design Using Open and Short Shunt Stubs……...105

4.5 Summary..... 114

References 115

CHAPTER 5 116

SYNTHESISED NON-FOSTER REACTIVE ELEMENTS USING LOSS-COMPENSATED REFLECTION-MODE NGD NETWORKS 116

5.1 A Novel Loss Compensation Technique for Reflection-mode NGD Networks 116

5.2 Negative Resistance Reflection Amplifier Design and Experiment 126

5.2.1 Design and Fabrication Procedure 128

5.2.2 Stability Analysis Methods 135

5.2.2.1 Nyquist Stability Measured with Modified Gamma Probe STABN_GP2 135

5.2.3 Stability Checks for the Prototype in the Laboratory 138

5.2.4 Simulation Results 144

5.3 Lange Coupler Design and Experiment 147

5.3.1 The Design Procedure 148

5.3.2 Coupler Assessment 153

5.3.3 The Fabrication Procedure 156

5.3.4 Lange Coupler Simulated and Measured Performance 158

5.4 The Implementation of the Lange Coupler with the NGD Networks. 164

5.4.1 Simulation and Measurement Results 167

5.5 Final Synthesised Non-Foster Reactive Element Using Loss-Compensated NGD Networks 174

5.5.1 Simulation Results 177

5.5.2 Stability Analysis of the NGD-Based Non-Foster Circuit 180

5.6 Summary 183

References 185

CHAPTER 6 186

ANTENNA MATCHING NETWORK USING NEW CLASS OF NON-FOSTER REACTIVE ELEMENTS 186

6.1 Realisation of an Equivalent Circuit Model for the Final Synthesised Non-Foster Element 187

6.2 Realisation of Pure Negative Capacitance from the LC Equivalent Circuit 193

6.3 Design of an Electrically Small Antenna 194

6.4 Antenna Matching Network Application 200

6.5 Circuit Model of Microstrip Patch Antenna 203

6.6 Realisation of a Pure Negative Inductance from the LC Equivalent Circuit of the Final Synthesised Non-Foster Element 206

6.7 Matching Network with the ESPA Circuit Model 208

6.8 Design of a Planar Monopole Patch Antenna (PMPA) 210

6.9 Impedance Transformer Network 213

6.10 Antenna Matching Network 216

6.11 Stability Analysis 218

6.12 Linearity and Noise Considerations 222

6.12.1 Non-Linearity 222

6.12.2 Noise Performance 223

6.13 Summary 226

References 228

CHAPTER 7 229

CONCLUSIONS AND FUTURE WORK 229

7.1 Summary 229

7.2 Conclusions 232

7.3 Future Work 233
References 236
APPENDIX A 237
COMPONENTS DATA SHEETS 237
Avago ATF-33143 237
Inductors- Coil craft 244
Capacitors_ ATC_600S 246
Resistors_ RK73B 251
Resistors _ Panasonic 253
Coupler _ipp_7047 255
Coupler_Anaren_11305-3S 256
Taconic _ RF _ 35 substrate 258
Tusonix_ Feedthrough capacitors 259
APPENDIX B 262
NI AWR Design Environnent 262
B. 1 Microwave Office (MWO) 262
B. 2 Starting NI AWR/ MWO 266
B. 3 Specifying the Simulation Frequency 267
B. 4 Creating a New Circuit Schematic for the Design 268
B. 5 Placing Elements in a Schematic 269
B. 6 Creating Output Graphs and Measurements 270

LIST OF FIGURES

Figure 2.1: (a) the reactance rotation of Foster and non-Foster elements around the Smith chart; (b) the reactance slope vs. frequency 14

Figure 2.2: Ideal Linvill NIC realising a negative capacitor..... 16

Figure 2.3: The operation of the NIC [4] 16

Figure 2.4: The operation of the NII [7] 17

Figure 2.5: An antenna matched with (a) a passive matching network (b) with a non-Foster matching network [4] 22

Figure 3.1: (a) S_{11} rotation of non-Foster elements on Smith chart; (b) complex S_{11} response of a reflection –mode NGD network shows an increasing reflection phase from f_1 to f_2 with zero loss amplitude..... 55

Figure 3.2: (a) circuit schematic of an ideal non-Foster T- network; (b) a circuit schematic of the loss-compensated NGD network realised by cascading an NGD filter with an amplifier; (c) transmission-type NGD network prototype [5]..... 56

Figure 3.3: S-parameters' results of the loss- compensated NGD network when compared with the same results obtained from an ideal T-network; (a) S_{21} magnitude response plot; (b) S_{21} phase response plot; (c) S_{22} response plot [5] 57

Figure 3.4: Symbolic examples of active circuits' blocks for loss compensation [5]..... 60

Figure 3.5: Loss-compensation technique for transmission-type NGD networks using regular amplifier [5] 63

Figure 3.6: Loss-compensation technique for transmission-type NGD networks using a bi-directional amplifier [5] 63

Figure 3.7: Loss-compensation technique for reflection–type NGD network using reflection amplifier [5] 64

Figure 3. 8: Loss-compensation technique for reflection–type NGD network using a bi-directional amplifier [5] 64

Figure 3.9: Loss-compensation technique for reflection–type NGD network using NGD network in transmission mode of Figure 3.5 and a circulator [5] 65

Figure 4. 1: Schematic layout of the proposed ideal reflection- type NGD network using 5 sections LC resonators 77

Figure 4. 2: The proposed NGD network is analysed using L-type impedance matching network to determine the values of a series combination of L_4 C_4 and a shunt combination of L_5 C_5 resonators 78

Figure 4. 3: L-type matching network 78

Figure 4. 4: The proposed NGD network is analysed using the Pi-type impedance matching network to determine the values of the shunt- series-shunt LC resonators 84

Figure 4. 5: Pi-type matching network 84

Figure 4. 6: Schematic layout of the proposed ideal reflection- type NGD network using the calculated values of the 5 sections LC resonators 92

Figure 4. 7: Simulated reflection coefficient (S_{11}) phase and magnitude of the proposed ideal NGD network using the calculated values of the 5 sections LC resonators 92

Figure 4. 8: Simulated group delay (GD) of the ideal NGD network using the calculated values of the 5 sections LC resonators 93

Figure 4. 9: Circuit schematic of the optimised reflection- type NGD network..... 94

Figure 4. 10: Simulated reflection coefficient (S_{11}) phase and magnitude of the optimised NGD network..... 95

Figure 4. 11: Simulated group delay (GD) of the optimised NGD network..... 95

Figure 4. 12: An ideal non-Foster network is modelled using an equivalent circuit of a negative capacitor in shunt with a negative inductor..... 98

Figure 4. 13: Circuit schematic of the ideal reflection-mode NGD network..... 98

Figure 4. 14: Circuit schematic of the realistic reflection-mode NGD network with distributed transmission lines 100

Figure 4. 15: Circuit layout of the NGD network 101

Figure 4. 16: Image of the NGD network prototype..... 101

Figure 4. 17: The S_{11} magnitude and phase plots of the NGD network from simulation and experiment..... 103

Figure 4. 18: Simulation and measurement results of the complex reflection coefficient plotted on the Smith chart..... 103

Figure 4. 19: Simulated and measured group delay (GD) responses obtained from the realistic reflection-type NGD network..... 104

Figure 4. 20: Circuit schematic of the NGD network realised using ideal components, where, MLSC denotes to a short microstrip line stub and MLEF denotes to an open microstrip line stub. 108

Figure 4. 21: Circuit schematic of the NGD network realised using open-short stubs 109

Figure 4. 22: NGD network circuit layout 110

Figure 4. 23: Image of the NGD network prototype..... 110

Figure 4. 24: Simulated and measured results of S_{11} magnitude and phase of the reflection-type NGD network realised using stubs 112

Figure 4. 25: Simulation and measurement results of the complex reflection coefficient (S_{11}) plotted on the Smith chart 112

Figure 4. 26: Simulated and measured group delay (GD) responses obtained from realistic reflection-type NGD network using stubs 113

Figure 5.1: Loss-compensated NGD network using reflection amplifier procedure 126

Figure 5.2: Schematic layout of an active two-port device configured as a negative resistance amplifier [1, 2] 127

Figure 5.3: AWR circuit schematic of the ideal negative resistance amplifier..... 128

Figure 5.4: The simulated input impedance of the ideal reflection amplifier..... 130

Figure 5.5: AWR circuit schematic of the realistic reflection amplifier with biasing networks at the gate and the drain terminals..... 132

Figure 5.6: The reflection amplifier layout with the biasing circuitry..... 133

Figure 5.7: Images of the fabricated reflection amplifier and the biasing circuitry: (a) front view; (b) back view 134

Figure 5.8: Nyquist Stability Measured with Modified Gamma-Probe applied to the FET-based reflection amplifier..... 137

Figure 5.9: Stability analysis through the Nyquist diagram to detect the instability of the FET-based reflection amplifier. The open loop function G, does not encircle the -1 point in the clockwise direction, meaning that the amplifier considered stable..... 138

Figure 5.10: Testing the reflection amplifier stability using a spectrum analyser (a) The amplifier was oscillating about 30 MHz spacing from 500 MHz to 3 GHz;

(b) the amplifier was oscillating only at 1.26 GHz; (c) the amplifier worked with no sign of oscillation..... 142

Figure 5.11: Photograph of the measured S_{11} magnitude of the reflection amplifier at the biasing stable conditions in the lab 143

Figure 5.12: Reflection gain obtained from negative resistance amplifier 145

Figure 5.13: Negative resistance plot of the reflection amplifier..... 146

Figure 5.14: Group delay obtained from negative resistance amplifier..... 146

Figure 5.15: Ideal Lange coupler schematic layout 148

Figure 5.16: Even- and odd-mode characteristic impedance design data for coupled microstrip lines [5]. This implementation uses a substrate with a dielectric constant of 3.5..... 153

Figure 5.17: Group delay and S_{11} magnitude obtained from the assessed couplers..... 154

Figure 5.18: Realistic Lange coupler schematic layout 155

Figure 5.19: Structure layout of the realistic Lange coupler..... 156

Figure 5.20: Image of the fabricated circuit board..... 157

Figure 5.21: Photograph of the measured S_{11} phase response of the fabricated circuit board in the test station..... 158

Figure 5.22: Coupling simulation and measurement results obtained from the Lange coupler 160

Figure 5.23: Output balance at ports 2 and 4 obtained from simulation and measurement..... 161

Figure 5.24: Return loss simulation and measurement results obtained from the Lange coupler 161

Figure 5.25: Isolation simulation and measurement results obtained from the Lange coupler 162

Figure 5.26: Group delay simulation and measurement results obtained from the Lange coupler 162

Figure 5.27: Electrical circuit schematic based on the combination of a Lange coupler with NGD networks 165

Figure 5. 28: Layout structure of the combination of a Lange coupler with NGD networks 166

Figure 5.29: Schematic of the combination of a Lange coupler with NGD networks, where the Lange coupler isolated port is connected to 50 Ω port. The "NGD network" sub-circuit is from Fig. 4.8. The "Lange coupler" sub-circuit is from Fig. 5.18. 168

Figure 5.30: Photograph of the S_{11} magnitude of the prototype. The prototype consists of a Lange coupler connected at its outputs to two NGD networks; whereas its input and isolated ports are connected to the VNA through 50 Ω measurement ports. 169

Figure 5.31: Reflection coefficient response plots obtained from measurement and simulation for the combination of the Lange coupler and NGD networks of Fig. 5.29 169

Figure 5.32: Simulated and measured group delay (GD) responses obtained from overall structure displayed in Fig. 5.29 170

Figure 5.33: Schematic of the combination between a Lange coupler with NGD networks. The "NGD network" sub-circuit is from Fig. 4.14. The "Lange coupler" sub-circuit is from Fig. 5.18. 171

Figure 5.34: Photograph of the S_{11} magnitude of the combined NGD networks with a Lange coupler. Two NGD networks are connected to the outputs of the

coupler, the coupler's input port is connected to the VNA through 50 Ω measurement port and the isolation port is connected to a short circuit..... 172

Figure 5.35: Reflection coefficient response plots obtained from measurement and simulation for the combination of the Lange coupler and NGD networks of Fig. 5.33 172

Figure 5.36: Measured and simulated group delay response obtained from overall structure displayed in Fig. 5.33..... 173

Figure 5. 37: Schematic presents the overall NGD-based non-Foster reactive element using loss compensation NGD networks technique. The "NGD Network" sub-circuit is from Fig. 4.14. The "Reflection Amplifier" sub-circuit is from Fig. 5.5. The "Lange Coupler" sub-circuit is from Fig. 5.18. 175

Figure 5. 38: Schematic of the final NGD-based non-Foster network 176

Figure 5.39: AWR circuit layout for the NGD-based non-Foster network..... 177

Figure 5.40: Reflection coefficient response plots for the overall NGD-based non-Foster network shown in Fig. 5.38 178

Figure 5.41: Rotation of the reflection coefficient of the NGD-based non-Foster network of Fig. 5.38..... 179

Figure 5.42: Group delay response for the final NGD-based non-Foster network Fig. 5.38 179

Figure 5.43: Stability analysis through the Nyquist diagram to detect the instability of the FET-based reflection amplifier. The open loop function G, does not encircle the -1 point in the clockwise direction, thus, the NGD-based non-Foster circuit is considered stable 181

Figure 5.44: S_{11} phase and magnitude plots obtained from the stand-alone NGD network of Fig. 4.14 and the loss-compensated NGD network of Fig. 5.38 . 182

Figure 6.1: Schematic of the LC equivalent circuit model for the NGD-based non-Foster network in the bandwidth of interest, where ($L < 0, C < 0$) 187

Figure 6.2: S_{11} phase response of the final synthesised non-Foster element of Fig 5.38 versus the phase response obtained from an ideal non-Foster network modelled using an equivalent circuit of Fig 6.1 with values of (C = -25.6 pF) and (L = -0.7 nH) 192

Figure 6.3: S_{11} phase response of the final synthesised non-Foster element of Fig 5.38 versus the phase response obtained from an ideal non-Foster network modelled using an equivalent circuit of Fig 6.1 with values of (C = -27 pF) and (L = -0.62 nH) 192

Figure 6.4: The input admittance imaginary parts response of the final non-Foster NGD network and the synthesised LC equivalent circuit of Fig 6.1 with values of (C = -27 pF) and (L = -0.62 nH) 193

Figure 6.5: AWR circuit schematic shows how a purely negative capacitor is realized from the equivalent circuit model presented in Fig 6.1 194

Figure 6.6: AWR circuit schematic of the ESPA with dimensions of (W = 23 mm) and (L = 14.1 mm), designed on a Taconic RF_35 substrate 197

Figure 6.7: The simulated return loss of the ESPA 198

Figure 6.8: The obtained susceptance and conductance values of the ESPA of Fig 6.7 199

Figure 6.9: The complex input impedance of the ESPA 199

Figure 6.10: AWR schematic of the ESPA matched with non-Foster matching technique 200

Figure 6.11: Simulated RL for the ESPA matched with different matching networks 201

Figure 6.12: RLC equivalent circuit of ESPA. The optimised RLC values are ... 203

Figure 6.13: Simulated return loss (RL) of the ESPA circuit model shown in Fig 6.12 204

Figure 6.14: The complex input impedance of the ESPA's equivalent circuit 205

Figure 6.15: The complex input admittance of the ESPA's equivalent circuit 205

Figure 6.16: AWR circuit schematic shows how a purely negative inductor is realized from the equivalent circuit model presented in Fig 6.1 206

Figure 6.17: The input impedance and the input admittance of the realised negative inductor from the non-Foster NGD network's equivalent circuit model 207

Figure 6.18: Comparison between the input impedance imaginary part response of the ESPA equivalent circuit and the realised pure negative inductor 208

Figure 6.19: Simulated return loss (RL) for the RLC resonant network matched with different matching networks 210

Figure 6.20: Geometry of the planar monopole patch antenna 211

Figure 6.21: Return loss response of the proposed simulated PMPA 211

Figure 6.22: Input impedance response of the PMPA 212

Figure 6.23: Input admittance response the PMPA 213

Figure 6.24: Schematic of the planar monopole antenna with the impedance transformer network, where (C = 8.36 pF) and (L = 9.46 nH) 214

Figure 6.25: Impedance response of the PMPA alone and when it is connected to the admittance transformer network on the Smith chart 214

Figure 6.26: Simulated return loss of the PMPA alone and when it is connected to the impedance transformer network 215

Figure 6.27: Schematic of the PMPA matched with non-Foster matching technique 216

Figure 6.28: Simulated return loss (RL) for the PMPA matched with different matching networks 217

Figure 6.29: Stability analysis through the Nyquist diagram to detect the instability of the NGD-based non-Foster circuit connected with a planar monopole patch antenna (PMPA). The open loop function G, does not encircle the -1 point in the clockwise direction, thus, the overall combination is considered to be having a stable operation. 219

LIST OF TABLES

Table 4. 1: Summary of the performance of the realised reflection-mode NGD networks 96

Table 4. 2: Component values and manufacturer for this implementation 99

Table 4. 3: Summary of the performance of the realised reflection-mode NGD network using LC resonators 104

Table 4. 4: Summary of the performance of the realised reflection-mode NGD networks 113

Table 5. 1: Biasing stable conditions……143

Table 5. 2: comparison between the proposed FET-based reflection amplifier and another tunnel diode-based reflection amplifier 147

Table 5. 3: Electrical specifications of the designed Lange coupler based on measurement and simulation results 163

Table 5. 4: Summary of the performance of both Lange couplers NGD network prototypes 173

Table 5. 5: Comparison between the proposed NGD-based non-Foster circuit and an NGD-based non-Foster circuit presented in [6] 181

Table 6. 1: Summary of the performance of the employed antennas ……220

Table 6. 2: Summary of the performance of the electrically small antennas matched with different matching networks 221

LIST OF ABBREVIATIONS

UHF	-	Ultra-High frequency
RF	-	Radio Frequency
NGD	-	Negative Group Delay
NIC	-	Negative Impedance Converter
NII	-	Negative Impedance Inverter
RHP	-	Right Half Plane
NI AWRDE	-	National Instruments Applied Wave Research Design Environment
AWR MWO	-	AWR Microwave Office
EM	-	Electromagnetic
ESPA	-	Electrically Small Patch Antenna
PMPA	-	Planar Monopole Patch antenna
FET	-	Field-Effect Transistor
VNA	-	Vector Network Analyser
SA	-	Spectrum Analyser

DC	-	Direct Current
PCB	-	Printed Circuit Board
NF	-	Noise Figure
SNR	-	Signal to Noise Ratio
GSM	-	Global System for Mobile Communication

CHAPTER 1

INTRODUCTION

1.1 Motivation and Background

Wireless communication devices such as mobile phones play a vital and increasingly significant part of our lives. These devices are required to cover an increasingly wide frequency band with low profile and low manufacturing cost antennas. Electrically small antennas are preferably chosen to comply with these requirements. An antenna is considered to be electrically small if the wavelength is bigger than its physical length as defined by Wheeler and Chu in [1, 2]. The Q-factor of a small antenna is inversely proportional to its electrical size and it increases inversely with the third power of electrical length; meaning these antennas are characterised by highly reactive (high-Q) input impedance and a large reactance [3, 4]. The following equation presents the relation between a small antenna radiation quality factor (Q) and its electrical length (kr) [3]:

$$\mathrm{Q} \propto 1/(\mathrm{kr})^3 \qquad (1.1)$$

This relation holds with $kr < 0.5$, but it is larger enough so the radiation resistance is ultimately larger than the loss resistance of the antenna [3].

Chu [2] and Harrington [5] have specified a relationship between a small antenna's Q-factor and its electrical size, where the minimum Q for linearly polarised antenna is computed by:

$$Q_{min} = \frac{1}{kr} + \frac{1}{(kr)^3} \qquad (1.2)$$

Where (k) is the wave number and is inversely proportional to the wavelength ($k = 2\pi/\lambda$) and (r) is the radius of the smallest sphere that can enclose the antenna. Thereby, the electrical size of a small antenna determines its achievable bandwidth and gain [5].

Electrically small antennas, regardless of their shape and type, present high-Q impedances characterised by large reactances and low radiation resistance. The problem is in transferring power to and from them, which consequently make them very difficult to match. These physical limits on antennas make it tough to have wideband small antennas with low- Q impedances. However, there are existing and future applications and systems that require the use of wideband small antennas.

Therefore, a matching network will usually be necessary to match the antenna radiation resistance to the transmission line.

Electrically small antennas are subject to gain-bandwidth limits derived by Bode [6] and Fano [7] with conventional matching technologies using passive elements. They suffer from poor gain due to a lossy impedance matching when attempting a broadband match and a narrow bandwidth due to the high Q of the antenna when attempting to maximise the gain. Circuits containing negative elements called non-Foster networks are not constrained by gain-bandwidth theory and can achieve wide matching bandwidths when they are integrated with electrically small antennas or other metamaterial structures.

Non-Foster reactive elements are susceptible to instability when realised using the transistorised negative impedance converters (NICs) and negative impedance inverters (NIIs), due to the generation of negative impedance and the difficulty in controlling the feedback in the circuitry at microwave frequencies and this limits the achievable top frequency.

The work considered in this thesis develops a novel method to realise non-Foster reactive elements using NGD networks which achieve a certain effective negative capacitance in a limited frequency range. These active circuits can deploy to cover GSM bands for example or to be integrated with electrically small antennas to pull

down their frequency of resonance and to broadband their matching bandwidth. Therefore, they can be potentially used and begin to approach the requirement for the systems described below.

1.1.1 Specific Systems Requirements – need for wide-band small antennas

With the tremendous growth of wireless communication technology, mobile phones are required to work over increasingly large frequency bands from 400 MHz to 4 GHz covering a host of communications standards such as DVB-H, GSM, Bluetooth, Wi-Fi, LTE, cognitive radios etc. Prior work on designing an antenna that is able to access a very large number of multiple wireless communications standards was presented in [8], where a single reconfigurable antenna with external matching circuits was designed. Simulations showed that the antenna was able to give a wide tuning range from 778 to 2896 MHz, thus, covering GSM 900, GPS 1575, GSM 1800, PCS 1900 and UMTS 2100 bands [8]. In another example presented in [9], 17 different matching networks were employed to match an antenna in the frequency range from 100 MHz to 2500 MHz. However, the implementations of multiple matching networks will result in narrow instantaneous bandwidths. Moreover, the use of multiple antennas is undesirable because it increases the size and the cost of the system. In addition, the electromagnetic interference between adjacent antennas may degrade the performance of the system. Wide-band small antennas are steadily increasing for wireless communication systems because of the need for compact multi-function devices. In particular, in many of these applications, electrically small

antennas are required due to the limited space available in the structures such as mobile phones, medical equipment etc.

For example, GSM 900 and GSM 1800 mobile communications systems consist of two bands, one for transmitting and the other for receiving. To integrate an antenna into a compact GSM 900 or GSM 1800 mobile devices, electrically small antennas are required to cover total frequencies range from (876- 960 MHz) and (1710 - 1880 MHz) respectively.

The proposed NGD-based non-Foster circuit achieves a certain effective negative capacitance with a bandwidth of 170 MHz at a centre frequency of 1.29 GHz over a frequency range from 1.2 - 1.37 GHz. At this specific frequency range, the non-Foster NGD network can be represented with an equivalent LC circuit of a negative capacitor in shunt with a negative inductor. Therefore, the performance of the circuit can be scaled with frequency to demonstrate its potential benefit in specific examples systems such as GSM 900 and 1800 systems.

Using frequency scaling argument to change the centre frequency of the NGD-based non-Foster circuit to 918 MHz instead of 1.29 GHz, thus, the scaled frequency range from 854 to 975 MHz would be achieved. Therefore, deploying the scaled version of the circuit would cover the GSM 900 band.

With the same manner, scaling the centre frequency of the circuit up to 1.8 GHz will result in a new scaled frequency range from 1670 to 1910 MHz. Deploying the new scaled version of the non-Foster NGD circuit using MIMIC technology will seamlessly cover the GSM 1800 band.

The realisable bandwidth of the proposed NGD prototype is 170 MHz from 1.2 – 1.37 GHz. This is not very broad in the context of ultra-wideband UWB (3 - 10 GHz) or a radio direction finding RDF system (0.8 - 6 GHz).

Other examples where the proposed NGD-based non-Foster network can be implemented are as a matching network with a monopole antenna to pull down its operating frequency or as with a small patch antenna to broadband its bandwidth as will be presented in Chapter 6. Moreover, these negative impedance elements can provide an approach to reducing the antenna size in many applications in handheld or mobile receivers where this is desirable.

1.2 Objectives

The main objective of this research is to investigate the means of achieving active reactive networks which exhibit a non-Foster response in the frequency range between 1 to 2 GHz realised by implementing novel synthesised structures using negative group delay (NGD) networks that can begin to approach the requirements for the systems described above.

The stability issues of the conventional implementation methods and applications of reactive non-Foster elements using negative impedance converters (NICs) and negative impedance inverters (NIIs) arise from the difficulty in controlling the feedback of the circuitry and the production of negative impedance. It limits their achieved top frequencies at HF and VHF bands and only a few successful demonstrations have been reported beyond that. This motivates the search for an alternative way to implement reactive elements with non-Foster behaviour in this thesis; hence, the work on NGD networks as a means to design stable non-Foster reactive elements proves important. Subsequently, the new synthesised non-Foster NGD circuit operating at 1.3 GHz can be employed as a non-Foster loading network to match suitable electrically small antennas before their resonance at the microwave frequency region and to broaden their bandwidths.

1.3 Thesis Contributions

The main contributions and novelties of this thesis are highlighted in this section in the order that they appear in the thesis:

- Based on the relation between NGD networks and non-Foster reactive elements, a new technique for designing reflection–type NGD networks is introduced.
- A novel technique to compensate the inherent losses of the NGD networks in the reflection mode is demonstrated. It provides a new route for synthesising networks with non-Foster behaviour over a limited frequency range.

- A new class of reactive non-Foster elements is realised using loss-compensated NGD networks. The advantage of this novel design is that the main NGD response is provided by separate passive circuits; which should make it easier to achieve stable behaviour.
- A new analysis of the equivalent circuit model for the non-Foster NGD network, based on the impedance trajectory of the network in the frequency range of interest has been developed.
- The employment of the final NGD-based non-Foster matching network is demonstrated theoretically.
- The operational limitations of this approach arise from the stability, noise and non-linearity, all stemming from the reflection amplifier. Approximate calculations of these limitations have been introduced.
- Different electrically small antennas are designed; and through simulation, the application to antenna matching is demonstrated.

1.4 Thesis Layout

The thesis is organised into seven chapters in the following manner:

Chapter 1 contains the introduction and motivations for the research of this thesis. It also highlights the systems that potentially require wide-band small antennas given specific system requirements examples. In addition, the objective of the thesis is addressed and the layout of the thesis is outlined.

Chapter 2 presents the background of the non-Foster reactive elements and reviews their properties and implementations using negative impedance converters (NICs) and negative impedance inverters (NIIs). Stability problems associated with NICs are noted. The fundamental limitations of electrically small antennas are stated and the limitations of the passive matching networks are addressed in this chapter. Moreover, prior work in the literature on the implementation of non-Foster impedances in antenna matching applications is discussed. Furthermore, other applications of non-Foster networks in electromagnetics and integrated circuit design are also highlighted.

Chapter 3 demonstrates the theoretical aspects of negative group delay NGD circuits; that exhibit NGD behaviour in different frequency regions. Moreover, the realisation of NGD networks in transmission and reflection modes is presented and the important implementations of these NGD networks in communication systems and microwaves are summarised. After that, the connection between NGD circuits and non-Foster reactive networks is explored. As a result, NGD networks are utilised as a means to realise stable non-Foster reactive elements such as negative capacitors and negative inductors in a certain frequency range. Active circuits and existing approaches to compensate the losses of the NGD networks are also discussed. Moreover, an example of the employment of a transmission-mode NGD network to obtain a non-Foster element, using regular amplifiers, and also its potential use to overcome beam-squinting issues in series-fed array antennas is presented.

In Chapters 4 and 5, the elements of this research are presented, including design, simulation and measurement work in the realisation of NGD networks in the reflection mode and the realisation of the synthesised non-Foster reactive circuits using loss-compensated NGD networks. In Chapter 4, a novel structure is designed by cascading LC resonators in parallel and series fashion along with transmission lines. Likewise, another new NGD network model is obtained using open and short stubs. Both prototypes are experimentally validated. The results from the simulation and experiment are in good agreement and demonstrate that both NGD networks act as non-Foster reactive elements within the 1 GHz to 2 GHz frequency range. The realised NGD networks have inherent losses and a method to compensate these losses is presented in the following chapter.

In Chapter 5, a novel technique to compensate the losses of the NGD networks in the reflection mode is demonstrated. It provides a new route for synthesising networks with non-Foster properties over a limited bandwidth. The new method is comprised of two NGD networks and a reflection amplifier in a balanced structure with a Lange coupler. Key steps in the methodology including the design of a negative resistance reflection amplifier and a Lange coupler are individually investigated and experimentally validated. Consequently, all the circuits are combined together to form the overall synthesised non-Foster NGD reactive network. The stability of the NGD-based non-Foster network was assessed by Nyquist techniques and simulation results showed that the proposed circuit is working stable. The proposed circuit operates as a shunt element, making it appealing in antenna matching applications;

as it enables both transmit and receive operations without having to switch the configuration, as presented in Chapter 6.

Chapter 6 investigates the potential use of the synthesised reactive non-Foster elements using reflection-type NGD networks in impedance matching networks for antennas. It explores a new analysis for modelling the non-Foster NGD network with an equivalent circuit in the frequency range of interest. The performance of electrically small antennas matched with the proposed NGD-based non-Foster network and other matching networks is demonstrated. Furthermore, the operational limitations associated with the implementation of the NGD-based non-Foster circuit in antenna matching systems are addressed in Chapter 6.

Chapter 7 contains the conclusions and a summary of the contributions of the thesis. It also outlines suggestions and recommendations for future work.

References

[1] H. A. Wheeler, “Fundamental Limitations of Small Antennas,” Proc. IRE, vol.35, pp. 1479-1484, Dec. 1947.

[2] L. J. Chu, “Physical Limitations of Omni-Directional Antennas,” J. App. Phys., vol. 19, pp. 1163-1175, Dec. 1948.

[3] S. E. Sussman-Fort and R. M. Rudish, "Non-Foster Impedance Matching of Electrically-Small Antennas," IEEE Transactions on Antennas and Propagation, vol. 57, pp. 2230-2241, Aug 2009.

[4] K. S. Song, "Non-Foster impedance matching and loading networks for electrically small antennas," PhD Thesis, Ohio State University, 2011.

[5] DR. F. Harrington, "Effect of Antenna Size on Gain, Bandwidth and Efficiency," Journal of Research of the National Bureau of Standards - D. Radio Propagation, vol. 64D, p. 12, June 29, 1959 1959.

[6] H. W. Bode, "Network analysis and feedback amplifier design," 1945.

[7] R. M. Fano, "Theoretical limitations on the broadband matching of arbitrary impedances," Journal of the Franklin Institute, vol. 249, pp. 57-83, 1950.

[8] Z. H. Hu, C. T. P. Song, J. Kelly, P. S. Hall, and P. Gardner, "Wide tunable dual-band reconfigurable antenna," Electronics Letters, vol. 45, pp. 1109-1110, 2009.

[9] D. Manteuffel and M. Arnold, "Considerations for Reconfigurable Multi-Standard Antennas for Mobile Terminals," in Antenna Technology: Small Antennas and Novel Metamaterials, 2008. iWAT 2008. International Workshop on, 2008, pp. 231-234.

CHAPTER 2

REACTIVE NON-FOSTER ELEMENTS AND THEIR APPLICATIONS

This chapter presents the background behind non-Foster reactive elements. It reviews their properties and implementations using negative impedance converters (NICs) and negative impedance inverters (NIIs). Stability issues with the NIC circuits are addressed. Furthermore, a comprehensive literature review on demonstrating the employment of non-Foster impedances in providing broadband small antenna matching networks is discussed and other applications in electromagnetics and integrated circuit design are noted.

2.1 Non-Foster Impedances

To understand the behaviour of the non-Foster reactive impedances, firstly Foster's reactance theorem as it applies to reactive elements is reviewed. In references [1,2], Foster established a reactance theorem, looking at a passive lossless element regarding its impedance $Z = jX$ or admittance $Y = jB$. The theory states that the input reactance (X) and the susceptance (B) must always have positive slopes with frequency and their locus on the Smith chart rotates clockwise (CW) with increasing

frequency. Simple representative examples of Foster reactive elements are positive inductors and positive capacitors.

$$\frac{\partial X}{\partial \omega} > 0 \text{ and } \frac{\partial B}{\partial \omega} > 0 \tag{2.1}$$

Non-Foster circuits are artificial structures whose reactance and susceptance characteristics disobey equation (2.1); thus, violating the condition of Foster's reactance theorem. These elements are characterised by a negative reactance slope as frequency increases. The associated reflection coefficient rotates counter-clockwise (CCW) around the Smith chart perimeter with increasing frequency, as shown in Figure 2.1. Examples of non-Foster elements include negative inductors and negative capacitors.

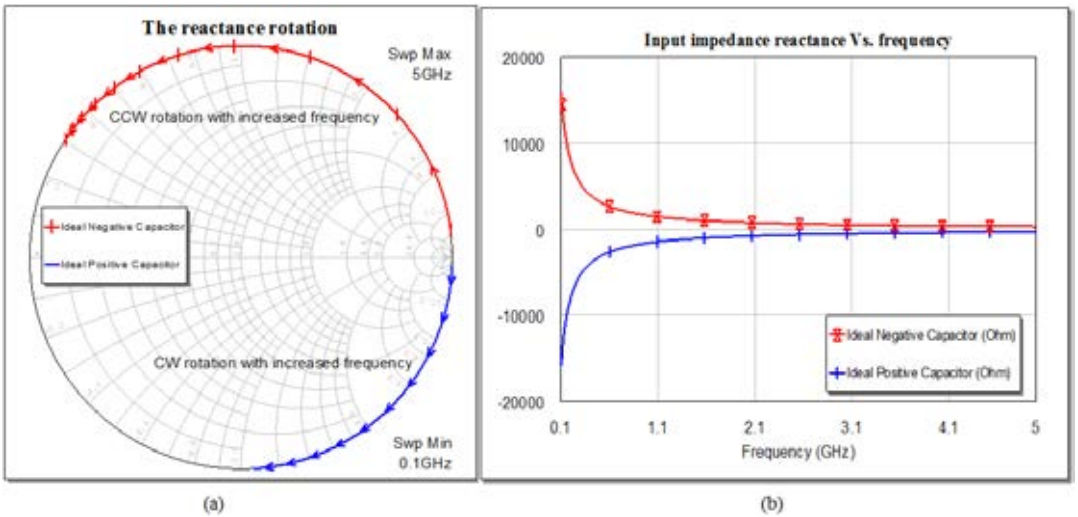


Figure 2.1: (a) the reactance rotation of Foster and non-Foster elements around the Smith chart; (b) the reactance slope vs. frequency

2.2 Realisation of Non-Foster Impedances

Non-Foster reactive impedances are traditionally realised by active circuits, called negative impedance converters (NICs) and negative impedance inverters (NIIs). These active networks and their stability are reviewed in this section.

2.2.1 Negative Impedance Converters (NICs) and Inverters (NIIs)

NICs have been widely employed in the realisation of negative capacitors and negative inductors as non-Foster elements. Linvill proposed the first floating and grounded NICs implemented using transistors in 1954. The NIC model is comprised of two transistors as shown in Figure 2.2.

The principle idea of generating a negative behaviour from a passive load (i.e. capacitor or inductor) is by swapping the sensing points of the reactive impedance and measuring the voltage across it. Therefore, if some current passes through an impedance element (i.e. a capacitor or an inductor) and the voltage is measured across it, then a positive impedance is measured. However, if the ac voltage measurement probes are swapped, then a negative impedance is measured because the current is still the same and the voltage is reversed.

This concept applies to Linvill's circuit the feedback paths are swapped over and sense the voltage through the gates of the transistors; the current does not change, but the sensing points where the voltage is measured changes because the voltage is reversed. The impedance inversion of Linvill's NIC analytically was proven in [3].

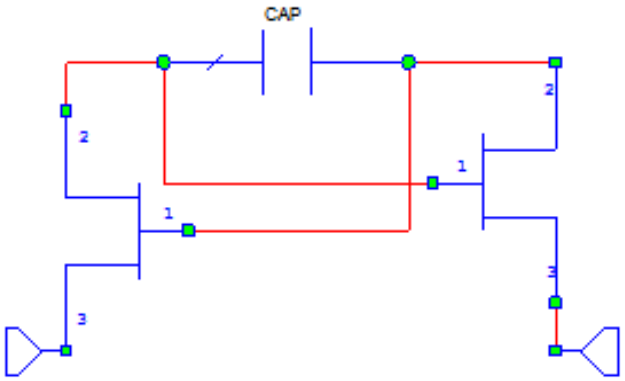


Figure 2.2: Ideal Linvill NIC realising a negative capacitor

The NIC was described in [4] as a two-port active circuit. Its input impedance (Z_{in}) seen at the input port (port 1) is equal to the negative termination of the load impedance (Z_L) looking into port 2, with a positive scaling factor (K > 0), as depicted in Figure 2.3.

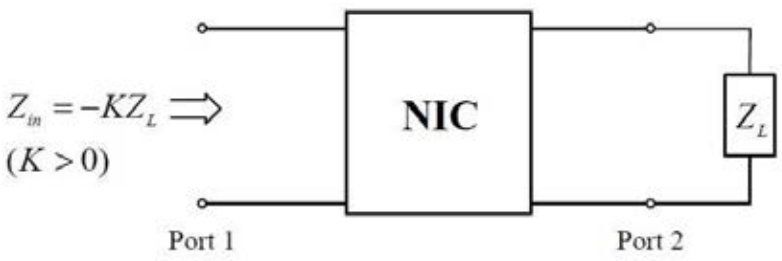


Figure 2.3: The operation of the NIC [4]

The NII is a two-port network where its input impedance (Z_{in}) at the input port is equivalent to the negative scaled load admittance termination at the other port as shown in Figure 2.4. Hence, the NII converts inductive termination impedance to a negative capacitor seen at the input port [5]. Likewise, an NII terminated with a capacitive impedance results in a negative inductor, observed at the input port [5]. References [6, 7] give examples of the realisation of NII using two FET transistors connected to a terminated load impedance.

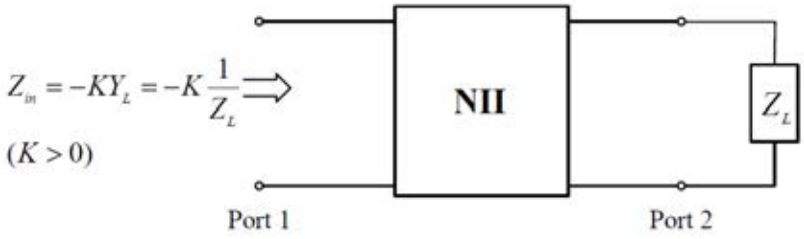


Figure 2.4: The operation of the NII [7]

2.2.2 Stability within NICs

The biggest challenge when designing non-Foster elements using NICs is stability concerns, because of the difficulty in controlling the feedback of the circuitry and the production of negative impedance [3]. To this end, it is necessary to assess the stability of the whole system including the NICs [3]. The NIC stability depends on many factors, such as the decoupling biasing circuitry, the printed circuit board (PCB) layout, the reactive impedance load and the external loads connected to the NIC [8].

The standard method for checking the stability of the NIC or any other two-port circuit is to use the stability K factor and B1 auxiliary factor. The unconditional stability conditions for such circuits are $K > 1$ and $B1 > 0$ [8]. However, there are many situations where they may fail in predicting the oscillation within the non-Foster circuits, caused by hidden modes which could not be assessed by a simple measure of K and B1 of the entire circuit [9- 11].

The Nyquist stability technique [12] is proposed as a reliable approach for calculating the loop gain in a feedback system such as a NIC circuit and assesses the stability. Based on [13- 14], the standard Nyquist test is carried out by plotting the loop gain of a feedback system in a polar plot with the frequency used as a parameter and checking the existence of the right-half plane (RHP) poles. A NIC circuit is stable if its configuration does not have RHP characteristic poles. In reference [15], the authors presented a successful implementation of the Nyquist test along with the Middlebrook technique [16] to calculate the loop gain in the NIC circuit and verify the stability. The NIC circuit was used as an embedded matching network with a reconfigurable antenna to broaden its performance.

In reference [17], stability analysis of a non-Foster circuit has been performed using normalised determinant function (NDF) technique. A stable floating-version negative capacitor based on Linvill's NIC was achieved by carefully considering several factors in the design, including the device parasitics, choice of dc biasing,

length of transmission lines in the layout, and the realistic load impedance. Furthermore, an electrically small monopole antenna was matched with the non-Foster circuit and the stability of the overall circuit was assessed. The NDF stability analysis was verified with experimental results. The measurement result showed a stable operation on a negative capacitor of - 4 pF from 30 to 500 MHz. Moreover, the NDF technique can be applied to multiple non- Foster elements.

In reference [18], a circuit analysis was implemented to determine the conditions on realising a stable non-Foster matching network realised by a negative capacitor with an adjacent single swamping element and a negative inductor. It was observed that the circuit cannot satisfy the stability conditions for any possible choice of values of the negative elements. Therefore, the network was potentially unstable. The reason was contributed to that there was no adjacent positive “swamping” element for the negative inductor [19]. Thus, it was stated that in order for non-Foster circuits consisting of multiple parallel or series negative elements to be stable, they must either have restricted topologies in which every negative element has an adjacent positive swamping element in series or in parallel, or using the method of bandpass negative elements described in [19], which was shown to satisfy the Nyquist criterion over a positive bandwidth. Two ideal non-Foster elements were introduced to provide non-Foster behaviour and acting as ideal negative inductors and negative capacitors only over a prescribed passband. These elements yield circuits that exhibit a desired non-Foster behaviour over positive, non-zero bandwidths and, more

important, were shown to be provably stable within the framework of linear circuit theory [19].

Other work presented in [20] showed that even the topologies restriction in [19], is not sufficient for stability on physical grounds. It has been demonstrated that the widely accepted stability criterion of positive “mesh” capacitance fails for the parallel combination of positive and ideal negative capacitor with connecting transmission line. Such a network is always unstable, regardless of the line length and capacitance values of positive and negative capacitor [20].

2.3 Non-Foster Reactive Elements Applications

When having access to electronic devices which exhibit the phenomenon of a negative reactance slope with frequency, it is possible to exceed the fundamental limitation in antenna matching applications. Also, many other applications in integrated circuit design, electromagnetics and microwaves are applicable. In this section, the important applications where the non-Foster reactive elements can be implemented are presented.

2.3.1 Implementation of Non-Foster Reactive Elements in Matching Networks

As it is related to the application presented in this thesis in Chapter 6, reactive non-Foster circuits used as matching networks with electrically small antennas are reviewed in detail. To appreciate the potential benefits of using these circuits in antenna matching, firstly the fundamental limits when electrically small antennas are impedance matched with passive matching networks are highlighted.

2.3.1.1 Conventional versus Non-Foster Matching Techniques

The input impedance of an electrically small antenna is dominated by a capacitive reactance below its resonance and has a relatively narrow operational bandwidth. It can be impedance matched to the desired frequency to deliver the maximum amount of energy to an arbitrary load impedance using an external passive inductor, as depicted in Figure 2.5(a). An inductor has a reactance which can negate the effect of a capacitive reactance of an electrically small antenna. Therefore, adding them in series, their reactances will cancel each other, resulting in a perfectly matched system where the whole energy is delivered to the resistor without any unwanted stored energy in the inductor or the capacitor. The problem here is that perfect impedance matching occurs only at a single frequency and results in a very limited bandwidth and gain. This gain-bandwidth limitation was derived by Bode and Fano [21, 22].

On the other hand, Figure 2.5(b) illustrates the anomalous reactance characteristic of a non-Foster reactive element (such as a negative capacitor), which provides a complete cancellation of the reactance of an electrically small antenna over a large frequency bandwidth. Therefore, the non-Foster impedance matching technique is proposed as a key to overcoming the restrictions of the gain-bandwidth theory that would inhibit continuous broadband passive matching of antennas [4].

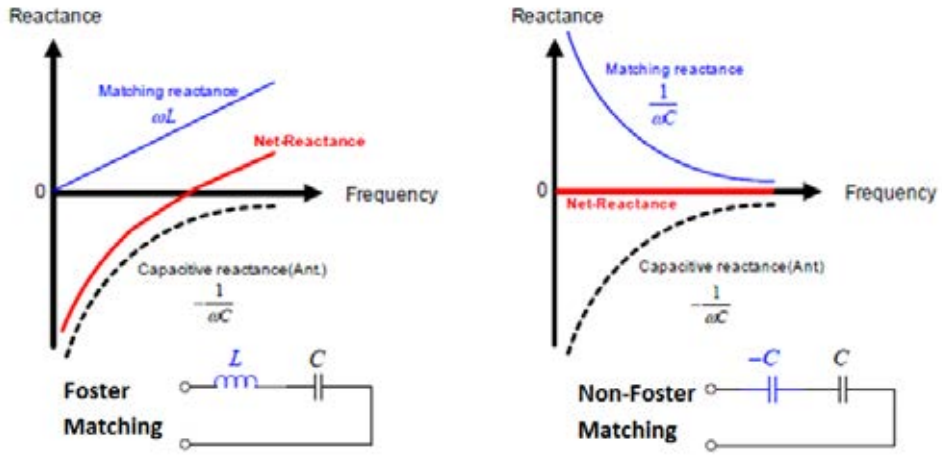


Figure 2.5: An antenna matched with (a) a passive matching network (b) with a non-Foster matching network [4]

2.3.1.2 Literature Review regarding Using Non-Foster Impedances as Matching Networks with Antennas

Most published works have focused on utilising negative capacitors realised by NICs, based on the Linvill transistorised model to be used as external matching networks with electrically small antennas. For instance, Susman-Fort [4] has

summarised his previous work in [23, 24] on non-Foster impedance matching networks with electrically small antennas for reception and transmission applications. He demonstrated that by using a non-Foster matching technique between a small antenna and a receiver, the signal-to-noise Ratio (SNR) and the gain of the antenna can be significantly improved [4].

During the initial work, monopole and dipole antennas connected to a conventional military receiver were designed. Linvill's balanced NIC was employed as a non-Foster impedance matching network connected in series with the antennas. With receivers, the noise added by the non-Foster matching network was determined. Without matching network, the receiver records environmental noise and its own noise, while with non-Foster matching the receiver records environmental noise, its own noise, plus non-Foster circuit noise. The measurements have been done using a low- noise receiver an 8 dB noise figure [4].

It was shown that the non-Foster receiving systems provide an SNR advantage over passive systems only in the cases where the system is device-noise limited, or when the receiver noise dominates over external noise, which is often the case for VHF receivers with electrically small antennas [4]. In the bandwidth from 20 MHz to 100 MHz, experimental results showed 9 dB of S/N improvement at 30 MHz of the non-Foster matched with a 6-inch monopole antenna when compared to a not matched passive antenna. It was mentioned that the NICs-based transistor circuits were low-noise themselves when they compared to NICs made using low- noise op-amps.

Experimental results showed that those NIC- based op-amp circuits generate at least 10 dB more noise at 30 MHz than the transistorised NICs [4]. Another experimental setup used to evaluate the S/N improvement of non-Foster matched with a 12-inch dipole antenna over a lossy-matched blade. It was observed 10 dB of S/N improvement in the bandwidth from 33 MHz to 63 MHz [4].

The paper presented a work on non-Foster matching networks for transmitting antennas as well. It has been experimentally shown that non-Foster matching to an electrically small monopole antenna achieved up to 20 dB more transducer gain (S_{21}) than any passive antenna design over bandwidth [4]. Moreover, experimental results showed that a non-Foster matching circuit achieved a factor-of-two improvement in power efficiency over the best passive match to an electrically-small antenna model (Q is approximately 250 at 20 MHz) with 5% bandwidth and an average signal power of over 1W to the radiation resistance, by carefully applying a class-C NIC biasing strategy which was developed in [24]. Experimental results for a class C non-Foster circuit with a power BJT showed a power efficiency advantage of 2.2 over a bandwidth of 1.2 MHz (21 - 22.2 MHz) when compared to the best possible passive match over the indicated bandwidth [4]. An important measurement factor in transmitting applications which are the circuit linearity, however, was not considered.

The origin and the development of the non-Foster impedance matching networks were explored for the first time in [4]. The potential benefit of using the non-Foster

approach with electrically small antennas was also demonstrated. Moreover, all measured data of non-Foster matching networks with the antennas have been shown in his previous works in [23- 25]. However, none of these articles has shown in detail how to stabilise the whole network. Besides, the maximum achieved frequencies from the matched antennas were all reported at the HF and the VHF bands and could not go beyond these ranges because of the challenging stability problems caused by the generation of negative impedance at higher frequencies.

In references [3, 8 and 29] the authors have presented and discussed the potential of employing non-Foster impedance matching networks realised by negative impedance converters (NICs) for achieving broadband antenna matching. A stand-alone negative capacitor based on the Linvill NIC model with two transistors was designed and built as a double layer structure to minimise the feedback length [8]. A mobile chassis antenna was chosen, and its equivalent circuit was investigated. The antenna was impedance matched with both passive and non-Foster matching networks. Simulation results showed that the associated reflection coefficient S_{11} of the antenna with non-Foster matching network reveals a wideband performance, with a magnitude lower than -10 dB between 0.80 GHz- 2.4 GHz. It was a significant improvement over the same antenna when it was passively matched. When the NIC circuit was fabricated, there was an oscillation at 2.4 GHz and a higher harmonics order, which was not revealed by the standard simulation stability K and B1 auxiliary factors.

Benefitting from the symmetry and based on the loop gain transfer function of the NIC circuit, an even-odd modes stability analysis was developed and applied to treat the stability. As a result, a stable NIC working up to 1.5 GHz was designed and built. The prototype exhibited non-Foster performance by its anticlockwise rotation around the Smith chart with increasing frequency between 0.595 GHz and 1.5 GHz [8].

Owing to the complexity involved in achieving the NIC, a new matching network was made up of a single element NIC and a positive inductor was designed. The NIC matching network obtained a better than -6 dB return loss was between 647 and 1500 MHz. It was a better performance than what was obtained through the use of passive matching networks which showed a -6 dB return loss bandwidth of 137 MHz. The NIC matched antenna has an efficiency advantage of 5 dB over a bandwidth of 300 MHz from 1000 MHz to 700 MHz when compared to resistive matching and lossy matching which offer wideband performance. However, the passive match does better over narrower bandwidth [8].

It was not possible to fabricate the complete NIC matched chassis antenna because it requires a sizable amount of the ground plane which might not be available in practical devices; the antenna was replaced with an equivalent lumped element circuit to allow an assessment of the noise and linearity properties [8].

The antenna equivalent consists of CPW transmission lines and lumped elements and was designed to represent the antenna in the frequency ranges 0.7- 1 GHz. This small frequency range was chosen because it is hard to find a practical passive lumped element equivalent to an antenna which completely represents the antenna at over a wider bandwidth [8].

The noise and linearity performance of the NIC matched antenna was characterised by the frequency range. An SNR advantage of 4 dB or more was achieved across the measured frequency band of 700- 1000 MHz when it compared to a lossy matched antenna. As a measure of the non-linearity of the NIC, the third order intercept point has been shown to be comparable with other typical front-end components using similar transistors. Further research is required for producing NIC elements in more suitable technology, such as MMIC, facilitating reduced size, direct integration with a realistic antenna [8].

The same authors proposed another alternative method to the transistorised Linvill's NIC. It used a single transistor along with coupled lines, referred to as a coupled line NIC. Due to the reduced stability concerns within the coupled line NIC, it was possible to demonstrate a stable NIC working at 6 GHz [8].

To analyse the coupled line NIC, its equivalent circuit was investigated. The NIC schematic was simulated using the NI AWRDE. When the input and output

impedances were simulated and plotted on the Smith chart, the NIC circuit exhibited non-Foster characteristics with anti-clockwise rotation. Stability analysis was also performed to choose the suitable transistor to be used in the fabricated structure [8]. Then, the coupled line NIC was integrated with a planar monopole antenna. It was possible to have a wideband matching over the range from 1.7 GHz to 2.9 GHz and below the antenna self-resonant frequency of 3.5 GHz [8].

The gain of the different antennas, the reference antenna, the NIC matched antenna and the passively matched antenna have also been compared. With the NIC matched antenna, the gain within the matched bandwidth is significantly higher than that of the reference antenna over a wide bandwidth with 20 dB improvement at 2 GHz. It was concluded that the coupled line NIC outperforms the Linvill NIC version at microwave frequencies [8].

In reference [15], a design methodology for loading an internally matched monopole antenna with a non-Foster matching network was proposed to obtain broadband antennas. The embedded Linvill's NIC inside the antenna generates non-Foster impedance, to produce a small well-matched broadband antenna. This paper followed on from previous works published in [30, 31] where a dual-band monopole antenna was established. The antenna was redesigned to operate at the lower UHF band. These modifications were essential to provide the DC bias for the NIC and for stabilising it, which was difficult at microwave frequencies.

The stability of the embedded NIC circuit was verified with the aid of a full-wave simulator using the transfer function method. The existence of RHP poles of the NIC enclosing the antenna was checked using the Nyquist criterion technique. Moreover, the Middlebrook current and voltage injection technique is utilised to measure the loop gain of the NIC circuit [15]. From the Nyquist plot, it was observed that in the range of 0.1 GHz to 2.85 GHz the NIC as an embedded non-Foster matching network has no poles in the right half of the frequency plane and hence, was considered to be stable. Finally, the monopole antenna with the integrated NIC circuit was fabricated and tested as a receiver to transmit and receive (Tx/Rx) applications. The measured return loss results of the whole network showed a broader bandwidth when compared to the antenna without a matching network [15].

A non-Foster matching network for a loop antenna was designed and presented in [32]. Gain and noise measurements of the non-Foster matched antenna were compared with those of the passive antenna itself. The active matching network provided an average gain improvement of 7 dB over a matching bandwidth of 105 MHz from 30 to 135 MHz. In contrary to the finding in [4]; wherein noise measured results showed a signal- to- noise ratio SNR advantage with a non-Foster matching when a receiver of a noise figure NF of 8 dB was used.

In [32], the noise measurement performed using a receiver of an NF of 4 dB did not provide any improvement in the SNR compared with the antenna alone. The added noise from the non-Foster network was about 8.9 dB and could not be isolated from the total measured noise of the system.

After that, noise models were developed for the balanced and unbalanced Linvill NIC circuits and verified with simulations. Simulations were then done to analyse the NF of a non-Foster receiving system for various small antennas, different biasing conditions, and receiver noise levels [32]. These were then compared with NF simulations of small antennas attached to an amplifier and a noisy receiver. It was conceded that for receivers with low-noise floor levels, a receiving system consisting of a passive small antenna and an amplifier can provide better SNRs compared with a receiving system with a non-Foster matched small antenna [32]. However, stability analysis was not performed for the non-Foster matched antenna in the paper.

Another design of non-Foster matching circuits for electrically small monopole and loop printed antennas operating below their resonance frequencies has been presented in [33]. The non-Foster elements (negative capacitor and negative inductor) were realised as transistor-based NICs. An ideal non-Foster negative capacitance of -1 pF and an ideal negative inductance of -110 nH were employed to compensate partly the reactance of the monopole antenna and the loop antenna respectively. In addition, Lumped-element transformers were utilised to convert antennas resistance to 50 Ω. Stability analysis was performed using NDF technique. Since the locus of the NDF did not encircle the origin, both circuits were considered stable [33]. Although, the simulated reflection coefficients of both antennas connected with non-Foster matching networks based on realistic bipolar junction transistors revealed that the achieved matching was narrow compared to that of matching networks based on

ideal negative elements. The potential of employing such non-Foster elements for achieving broadband antennas was theoretically demonstrated [33].

Moreover, stability analysis of the non-Foster network connected to both antennas was carried out using the normalised determined function NDF technique. Simulation results revealed that the locus of the NDF does not encircle the origin, thus both circuits were anticipated to be stable. Consequently, a NIC circuit realising the negative inductance of -110 nH was fabricated [33].

To avoid instability, a 115 nH inductor was connected in series with the NIC circuit. The value of the negative inductance realized by the NIC was then obtained by de-embedding the positive inductor. The obtained reactance of the NIC circuit from measurement and simulation was compared to the same ones obtained from an ideal negative inductance. In the bandwidth from 150 to 250 MHz both measured and simulated results seemed to agree with each other and closely follow that of the ideal negative inductance [33]. Practical application where the realised non-Foster element can be implemented was not presented in the paper.

In reference [34], a non-Foster matching network for a small cylindrical slot antenna was designed and its broadband matching capability has been examined. It was noticed that the impedance of the non-Foster circuit changes dramatically as the signal power increases, hence, reducing its matching capability and introducing stability issues. To analyse its potential in transmit applications; the non-Foster

matched antenna was compared with an unmatched antenna for the same transmitting system. Despite being poorly matched, simulations on the gain-bandwidth product and the third order intermodulation output intercept point (OIP3) demonstrated that the unmatched antenna has a higher OIP3 and gain-bandwidth product [34]. However, increasing the bias currents for the non-Foster circuit can improve OIP3. It was conceded that for high power applications, the design of the non-Foster circuit should be a balance between power added efficiency, IP3, and gain-bandwidth product. Moreover, further studies should be done to investigate the linearization methods for non-Foster circuits [34].

In reference [35], a non-Foster network was designed and employed with a resistively loaded vee dipole antenna (RVD) for a low-frequency application. Two NICs based on operational amplifiers were used to realise the non-Foster network.

Stability analysis of the matching network was performed using the Barkhausen criterion [35]. Because of the capacitive characteristics of the input impedance of the RVD, it suffered from a large mismatch at the feed point, especially at low frequencies [35].

The non-Foster network was employed to reduce the reflection of the antenna at the feed point, thus, enhancing the performance of the RVD as an antenna used in impulse radar applications, such as ground penetrating radar (GRP) [35].

2.3.2 Using Non-Foster Reactive Elements in Other Applications

In addition to impedance matching, non-Foster reactive elements have been implemented in many other applications. For example, in electromagnetic applications, the authors of the references [36, 37] have demonstrated how the bandwidth of artificial magnetic conductors (AMCs) could be increased when loaded with non-Foster circuits. The AMCs are inherently limited by narrow bandwidths because of their specific electromagnetic properties of negative permittivity (ε) and permeability (μ). To overcome the bandwidth limitations associated with the AMC surfaces, a negative inductance circuit called an NFC, realised by a negative impedance inverter (NII), was designed and loaded in parallel with the AMC. The negative inductance circuit interacted with the AMC substrate inductance resulting in a large net inductance over a wide frequency range. The NFC was fabricated as an integrated circuit (IC). Details on the circuit design and fabrication procedure can be found in [38]. The IC was soldered between the patches of the AMC surface and biased through holes passing through the AMC ground plane. Measurement results showed an 80% improvement in the achieved bandwidth in the range from 160 to 391MHz at a resonant frequency of 263 MHz [38].

Another effort to use embedded non-Foster elements in an AMC and AMC absorber structures was presented in [39]. The negative elements (negative capacitors and negative inductors) were realised by floating Linvill NIC circuits. The stability analysis of the loaded NIC circuit was carried out using pole-zero analysis. It was addressed that the employment of floating NICs to form non-Foster AMC bandwidth

enhancement is challenging because it was impossible to satisfy the stability conditions within the NIC circuit at higher frequencies when both a negative capacitor and a negative inductor are implemented together with such structures and also suggested to use practical circuits which behave like their idealised ones [39].

Reference [40] showed that negative capacitors and negative inductors could be loaded in parallel and series, respectively, with transmission lines and as a result, wideband active transmission lines can be obtained. The non-Foster elements were realised by Linvill NICs and simulated using ADS software in the range of 150 to 350 MHz. The active transmission lines can be proposed as a solution for beam-squinting issues in series-fed array antennas as demonstrated in [41].

Synthesised networks with a non-Foster property can be employed in electronics and integrated circuit design applications too. For instance, in reference [42], negative capacitors were connected to the input transmission line nodes to compensate for the capacitive behaviour of the transistors due to their parasitic capacitors. As a result, a high-gain structure for the distributed amplifier (DA) was obtained. The structure had the capability of producing a high gain and maintaining the wideband frequency response of the amplifier simultaneously. Based on the proposed design, the implemented DA showed an average gain of 13.2 dB with a bandwidth of 29.4 GHz in 0.13μm IBM's CMRF8SF CMOS process, producing the highest gain per stage of many reported CMOS Das [42].

Furthermore, it was shown in [43], that the bandwidth of a 5-stage limiting amplifier could be increased and have a flat broadband response beyond its cut-off frequency when it was loaded with a negative capacitance to compensate for the limited bandwidth of its gain cells. Moreover, reference [44] presented synthesised capacitive multipliers using an operational amplifier-based NIC to generate the negative capacitance. The simulated topologies obtained tunable negative and positive capacitances, for the frequency range from 400 mHz up to 159 Hz, making it suitable for low frequency integrated applications. Finally, the association of a negative capacitance in series with an active varactor diode to increase the tuning range of the varactor in MMIC technology was presented in [45].

Table 2.1 illustrates a summary of the reviewed articles in the literature section and other published papers which are only included in the references for the important applications where the non-Foster reactive circuits can be implemented. The table includes the reference number and highlights some important parameters such as the type of non-Foster circuit (NFC); type of antenna or surface, stability analysis and achieved matching bandwidth. It also includes efficiency, noise figure and gain advantages over passive matches.

Table 2.1: Summary of NICs implementations

Ref No	Type of NFC	Antenna or Surface Type	Stability analysis	Noise Figure NF	Efficiency	Matching bandwidth	Gain
[4]	Linvill NIC	6-inch monopole & 12-inch dipole	Not given	20dB over (120/20) MHz	2.2 over a BW of 1.2 MHz (22.2/21) MHz	1.2 MHz over (22.2/21) MHz	14dB Over (22.2/21) MHz
[3,8, 29]	Linvill NIC	Antenna equivalent circuit	Based on the transfer function of the circuit	4 dB over (1000/700) MHz	5 dB over (1000/700) MHz	300 MHz over (1000/700) MHz	Not given
	Coupled line NIC	planar monopole		Not given	-0.16 dB	1200 MHz Over (2900/1700) MHz	20 dB at 2GHz Over (2900/1700) MHz
[15]	Linvill NIC	MTM-inspired small monopole	Nyquist test	Not given	Not given	14 MHzOver (382/368) MHz	Not given

[32]	Linvill NIC	Loop	Not given	8.9 dB added noise	Not given	105 MHz over (135/30) MHz	7 dB
[33]	Transistor-based NICs	Monopole and printed loop	NDF	Not given	Not given	100 MHz over (250/150)MHz & 20MHz over (210/190) MHz	Not given
[34]	Op amp-based NICs	vee dipole	Barkhausen criterion		0.4 %	45 MHz over (70/25) MHz	Not given
[36,37]	NII	AMC surface	Not given	Not given	Not Given	231 MHz over (391/160) MHz	Not given
[39]	Floating Linvill NIC	AMC and AMC absorber structures	pole-zero analysis	Not given	Not Given	253 MHz over (469/216) MHz	Not given
[40]	Linvill NIC	Transmission line	Not given	Not given	Not given	200 MHz over (250/150) MHz	Not given

[42]	NIC with two transistors	Transmission lines	Simulated K- factor	Added noise figure of 5.14 dB	Not given	29.4 GHz	13.2 dB
[44]	Op amp-based NIC		Not given	Not given	Not given	400mHz – 157 Hz	Not given
[46]	Linvill NIC	Two-port antenna model	Computer simulator	Not given	95% over (90/36) MHz	54 MHz over (90/36) MHz	Not given
[47]	Transistor-based NIC	Box Cage Loop	Transient simulations in ADS	Not given	Not given	100 MHz over (350/250) MHz	Not given
[48]	Linvill's balanced NIC	15-cm monopole	Transient simulations in ADS	Not given	Not given	170MHz Over (200/30) MHz	10 dB
[49]	Linvill's floating NIC	Monopole	Closed loop gain analysis	12.5 dB over (108/88) MHz	Not given	20MHz over (108/88) MHz	3 dB

2.4 Summary

In this chapter, a review of non-Foster reactive elements, their properties and realisation using NICs and NIIs was presented. Stability issues associated with these circuits were addressed. Furthermore, an inventory of some NICs and a development of non-Foster impedance matching networks were presented. In addition, the state of the art in non-Foster matching networks with electrically small antennas and metamaterial structures was explored.

Reference [8] developed a transistorised Linvill NIC circuit operating at 1.5 GHz. To the extent of our knowledge, this was the highest top frequency reported in the literature. The NIC was utilised to design a non-Foster negative capacitor. Subsequently, the synthesised negative capacitor was used as a non-Foster matching network to match a mobile phone chassis antenna [8].

Simulated results showed a significant improvement in the achievable bandwidth when compared with the results obtained from matching the same antenna using the conventional Foster technique. However, the fabricated non-Foster circuit had stability issues. Apart from that, all the reviewed papers had a limited top frequency at HF and VHF bands. Beyond these ranges, challenging stability issues arise because of the difficulty in controlling the feedback of the circuitry at higher frequencies and constraining their practical implementations.

This motivates the search for an alternative way of generating non-Foster behaviour; hence, the work on NGD networks as a means to design stable non-Foster reactive elements proves important and is appealing in order to overcome the stability problems of the traditional methods. Details on the concept of NGD networks and their implementations to synthesise non-Foster circuits are presented in Chapter 3 and Chapter 4.

References

[1] R. M. Foster, "A reactance theorem," Bell Syst. Tech. J., vol. 3, pp. 259-267, 1924.

[2] O. J. Zobel, "Theory and Design of Uniform and Composite Electric Wave-filters," Bell system technical journal, vol. 2, pp. 1-46, 1923.

[3] O. O. Tade, "Negative impedance converter for antenna matching," Ph.D. Thesis, University of Birmingham, Jul. 2014.

[4] S. E. Sussman-Fort and R. M. Rudish, "Non-Foster Impedance Matching of Electrically-Small Antennas," IEEE Transactions on Antennas and Propagation, vol. 57, pp. 2230-2241, Aug 2009.

[5] B. P. Bogert, "Some Gyrator and Impedance Inverter Circuits," Proceedings of the IRE, vol. 43, pp. 793-796, 1955.

[6] S. Kolev, B. Delacressonniere, and J. L. Gautier, "Using a negative capacitance to increase the tuning range of a varactor diode in MMIC

technology," IEEE Transactions on Microwave Theory and Techniques, vol. 49, pp. 2425-2430, 2001.

[7] K. L. Su, "A Method for Realizing the Negative-Impedance Inverter," IEEE Journal of Solid-State Circuits, vol. 2, pp. 22-25, 1967.

[8] O. O. Tade, P. Gardner, and P. S. Hall, "Antenna bandwidth broadening with a negative impedance converter," International Journal of Microwave and Wireless Technologies, vol. 5, no. 3, pp. 249–260, Jun. 2013.

[9] G. Gonzalez, Microwave transistor amplifiers: analysis and design 2nd ed. Upper Saddle River, N.J.: Prentice Hall, c1997, 1997.

[10] S. D. Stearns, "Incorrect stability criteria for non-foster circuits," in Proceedings of the 2012 IEEE International Symposium on Antennas and Propagation, 2012, pp. 1-2.

[11] S. D. Stearns, "Non-foster circuits and stability theory," in 2011 IEEE International Symposium on Antennas and Propagation (APSURSI), 2011, pp. 1942-1945.

[12] H. Nyquist, "Regeneration Theory," Bell system technical journal, vol. 11, pp. 126-147, 1932.

[13] Sedra, A.S. and K.C. Smith., Microelectronic Circuits. 5th ed.: Oxford University Press, Inc., 2004.

[14] K. S. Song, "Non-Foster impedance matching and loading networks for electrically small antennas," Ph.D. Thesis, The Ohio State University, 2011.

[15] H. Mirzaei and G. V. Eleftheriades, "A Resonant Printed Monopole Antenna With an Embedded Non-Foster Matching Network," IEEE Transactions on Antennas and Propagation, vol. 61, pp. 5363-5371, Nov 2013.

[16] R. D. Middlebrook, "Measurement of loop gain in feedback systems," International Journal of Electronics, vol. 38, pp. 485-512, 1975/04/01 1975.

[17] Q. Tang and H. Xin, "Stability Analysis of Non-Foster Circuit Using Normalized Determinant Function," *IEEE Transactions on Microwave Theory and Techniques*, vol. 65, pp. 3269-3277, 2017.

[18] S. D. Stearns, "Circuit analysis of the stability of a two-element non-Foster impedance matching network," in 2017 IEEE International Symposium on Antennas and Propagation & USNC/URSI National Radio Science Meeting, 2017, pp. 1485-1486.

[19] S. D. Stearns, "Stable band-pass non-Foster circuits," in 2015 IEEE International Symposium on Antennas and Propagation & USNC/URSI National Radio Science Meeting, 2015, pp. 1386-1387.

[20] J. Loncar, S. Hrabar, and D. Muha, "Stability of Simple Lumped-Distributed Networks With Negative Capacitors," IEEE Transactions on Antennas and Propagation, vol. 65, pp. 390-395, 2017.

[21] H. W. Bode, "Network analysis and feedback amplifier design," 1945.

[22] R. M. Fano, "Theoretical limitations on the broadband matching of arbitrary impedances," Journal of the Franklin Institute, vol. 249, pp. 57-83, 1950.

[23] S. E. Sussman-Fort and R. M. Rudish, “Non-Foster impedance matching of a lossy, electrically-small antenna over an extended frequency range,” the Antenna Applicat. Symp., Allerton Park, IL, pp.220-240, Sept. 2007.

[24] S. E. Sussman-Fort and R. M. Rudish, "Non-Foster Impedance Matching for Transmit Applications," in IEEE International Workshop on Antenna Technology Small Antennas and Novel Metamaterials, 2006, pp. 53-56.

[25] R. M. Rudish and S. E. Sussman-Fort, “Non-Foster Impedance Matching Improves S/N of Wideband Electrically Small VHF Antennas and Arrays,” Proceedings of the 2nd IASTED international conference on Antennas, Radar, and Wave Propagation, Banff, Alberta, Canada, Jul. 19-21, 2005.

[29] O. O. Tade, P. Gardner, and P. S. Hall, "Broadband matching of small antennas using negative impedance converters," in Antennas and Propagation Society International Symposium (APSURSI), 2012 IEEE, 2012, pp. 1-2.

[30] J. Zhu and G. V. Eleftheriades, "Dual-band metamaterial-inspired small monopole antenna for WiFi applications," Electronics Letters, vol. 45, pp. 1104-1106, 2009.

[31] H. Mirzaei and G. V. Eleftheriades, "A wideband metamaterial-inspired compact antenna using embedded non-Foster matching," in 2011 IEEE International Symposium on Antennas and Propagation (APSURSI), 2011, pp. 1950-1953.

[32] M. M. Jacob and D. F. Sievenpiper, "Gain and Noise Analysis of Non-Foster Matched Antennas," IEEE Transactions on Antennas and Propagation, vol. 64, pp. 4993-5004, 2016.

[33] N. Ivanov, B. Buyantuev, V. Turgaliev, and D. Kholodnyak, "Non-foster broadband matching networks for electrically-small antennas," in 2016 Loughborough Antennas & Propagation Conference (LAPC), 2016, pp. 1-4.

[34] M. M. Jacob and D. F. Sievenpiper, "Non-Foster Matched Antennas for High-Power Applications," IEEE Transactions on Antennas and Propagation, vol. 65, pp. 4461-4469, 2017.

[35] H. Yang, I. Kim, and K. Kim, "Non-Foster Matching of a Resistively Loaded Vee Dipole Antenna Using Operational Amplifiers," IEEE Transactions on Antennas and Propagation, vol. 64, pp. 1477-1482, 2016.

[36] D. J. Gregoire, C. R. White, and J. S. Colburn, "Wideband Artificial Magnetic Conductors Loaded With Non-Foster Negative Inductors," IEEE Antennas and Wireless Propagation Letters, vol. 10, pp. 1586-1589, 2011.

[37] D. J. Kern, D. H. Werner, and M. J. Wilhelm, "Active negative impedance loaded EBG structures for the realization of ultra-wideband Artificial Magnetic Conductors," in IEEE Antennas and Propagation Society International Symposium. Digest. Held in conjunction with: USNC/CNC/URSI North American Radio Sci. Meeting (Cat. No.03CH37450), 2003, pp. 427-430 vol.2.

[38] C. R. White, J. W. May, and J. S. Colburn, "A Variable Negative-Inductance Integrated Circuit at UHF Frequencies," IEEE Microwave and Wireless Components Letters, vol. 22, pp. 35-37, 2012.

[39] Y. Ding and V. Fusco, "Loading artificial magnetic conductor and artificial magnetic conductor absorber with negative impedance converter elements," Microwave and Optical Technology Letters, vol. 54, pp. 2111-2114, 2012.

[40] H. Mirzaei and G. V. Eleftheriades, "An active artificial transmission line for squint-free series-fed antenna array applications," in Microwave Conference (EuMC), 2011 41st European, 2011, pp. 503-506.

[41] H. Mirzaei and G. V. Eleftheriades, "Arbitrary-Angle Squint-Free Beamforming in Series-Fed Antenna Arrays Using Non-Foster Elements Synthesized by Negative-Group-Delay Networks," Antennas and Propagation, IEEE Transactions on, vol. 63, pp. 1997-2010, 2015.

[42] A. Ghadiri and K. Moez, "Gain-Enhanced Distributed Amplifier Using Negative Capacitance," IEEE Transactions on Circuits and Systems I: Regular Papers, vol. 57, pp. 2834-2843, 2010.

[43] J.-S. Youn, M.-J. Lee, K.-Y. Park, and W.-Y. Choi, "10-Gb/s 850-nm CMOS OEIC receiver with a silicon avalanche photodetector," IEEE Journal of quantum electronics, vol. 48, pp. 229-236, 2012.

[44] M. De, Ferri, and Stornelli, "NIC-based capacitance multipliers for low-frequency integrated active filter applications," in 2007 Ph.D Research in Microelectronics and Electronics Conference, 2007, pp. 225-228.

[45] S. Kolev, B. Delacressonniere, and J. L. Gautier, "Using a negative capacitance to increase the tuning range of a varactor diode in MMIC technology," IEEE Transactions on Microwave Theory and Techniques, vol. 49, pp. 2425-2430, 2001.

[46] J. T. Aberle, "Two-port representation of an antenna with application to non-foster matching networks," IEEE Transactions on Antennas and Propagation, vol. 56, pp. 1218-1222, May 2008.

[47] J. Church, J. C. S. Chieh, L. Xu, J. D. Rockway, and D. Arceo, "UHF Electrically Small Box Cage Loop Antenna With an Embedded Non-Foster Load," IEEE Antennas and Wireless Propagation Letters, vol. 13, pp. 1329-1332, 2014.

[48] C. R. White, J. S. Colburn, and R. G. Nagele, "A Non-Foster VHF Monopole Antenna," IEEE Antennas and Wireless Propagation Letters, vol. 11, pp. 584-587, 2012.

[49] Y. Shen and T. H. Chio, "Matching electrically small antenna using non-Foster circuit in the FM-band," in The 8th European Conference on Antennas and Propagation (EuCAP 2014), 2014, pp. 333-336.

CHAPTER 3

NEGATIVE-GROUP-DELAY NETWORKS AND THEIR APPLICATIONS

This chapter is devoted to the study of negative-group-delay (NGD) networks. It begins by reviewing the theory behind the NGD concept. Next, the existing approaches for realising networks that support NGD behaviour are presented. Following on, previous work presented in the literature concerning the implementation of NGD networks in different applications is summarised. Then, the relation between NGD networks and reactive non-Foster networks is discussed. Finally, a background about loss compensation schemes for NGD networks and existing techniques in the literature is outlined.

3.1 Basic Theory of Negative Group Delay

The phenomenon of the NGD is observed to exist when an electromagnetic wave propagates in a dispersive medium within an absorption band. It occurs when an output peak of a transient pulse of a wave packet appears before its input peak enters the medium (time advance) [1-3]. The NGD phenomenon includes anomalous group velocity called superluminal group velocity which is greater than the speed of light in a vacuum [2]. Group velocity can become negative in a specific frequency band

[4, 5]. A counterintuitive phenomenon but is does not breach the relationship of the causality system as the initial and the final points of a wave packet exhibit positive delay and never exceed the speed of light [6, 7]. The NGD behaviour occurs when a pulse propagates through a suitably configured network in a forward direction or a backward direction, forming transmission and reflection type NGD networks respectively. The existence of the group delay (GD) in a network can be mathematically examined from the phase response (φ) of its S-parameters using the following differential-phase group delay (τ_g) relation [5] :

$$\tau_g = -\frac{d\varphi}{d\omega} \tag{3.1}$$

The presence of negative group delay (NGD), ($-\tau_g$) in such a network is equivalent to an increasing phase with frequency in a limited bandwidth [5].

3.2 Realisation of Negative- Group Delay Networks

There has been a growing interest over the recent years on structures which exhibit NGDs at different frequency regions especially at microwave bands. For example, in references [8- 12], NGD networks were designed by forming RLC resonators in series and shunt fashions and used in microwave circuits. Furthermore, NGD behaviour can be synthesised, using circuits with distributed elements as a means to overcome the lumped elements' limitations such as poor quality at high frequencies

[13- 17]. Moreover, it has been shown in [18, 19] that NGD networks can be obtained by loading transmission lines with RLC resonant circuits and a capacitor in series, and with an inductor in parallel. A lossless NGD circuit has been designed and reported in [20] using a T-junction power divider and an amplifier to be integrated into a feed line to reduce the beam squint issues in series-fed array antennas.

In reference [21, 22], a new method was presented on the realisation of a broadband NGD network formed by a microstrip structure of coupled positive-index to negative-index transmission line. Despite the general conditions for observing anomalous group velocities such as a negative group velocity (NGV) requiring reflective and absorptive systems, reference [22] has experimentally proved that negative group velocity (NGV) could be observed in specific lossless materials like a guided-wave structure at microwave frequencies.

In reference [23], a compact NGD circuit with a size 50 mm x 25 mm was realised by implementing two-port open-circuited coupled lines, a short-circuited transmission line and two resistors connected by two transmission lines. The proposed NGD circuit was self-matched without the need for an external matching circuit. The coupled lines were employed for obtaining port matching. Measurement results showed that an NGD value of -8.75 ns over a bandwidth of 3.82 % and an attenuation of 20.8 dB at 1.57 GHz was obtained [23]. However, the proposed NGD circuit suffers from losses and no compensation techniques were presented in the

paper to compensate the associated insertion loss of the circuit. This can be done by amplification obtained from amplifiers.

In reference [24], a broadband negative group delay was synthesised in a circular waveguide system with an asymmetric cross-shaped slotted structure in the millimetre-wave region. With the polarization azimuthal angle of the incident at 45 degrees relative to the cross-shaped slots, NGDs were observed from 31.76 to 32.91 GHz with a fractional bandwidth of 3.57 %. In addition, the measured maximal group advancement was as large as -0.46 ns. The structure achieved a high fractional advancement of 12.10 % centred at 32.33 GHz. The NGD can be controlled by adjusting the polarization azimuthal angle of the incident pulse. The observed tunable NGD effect is attributed to the destructive cross-interference between the two polarization eigenstates, which effectively reduces the released field energy at the observed polarization channel [24].

In reference [25], a compact transmission-type negative group delay circuit NGDC with low signal attenuation and compact size was presented. A two-stage NGDC was designed using a full-wave simulation with Ansys HFSS and experimentally validated. The fabricated prototype exhibited an NGD of -7.7 ns over a bandwidth of 35 MHz with a centre frequency of 1.79 GHz and a corresponding signal attenuation of as low as 8.6 dB have been obtained. The measured reflection coefficients were better than -20 dB. The proposed prototype had a compact size of 30 mm x 18 mm [25]. However, no specific application was mentioned in the paper where the realised circuit can be employed

In another example in [26], a negative group-delay (NGD) topology of parallel interconnect lines PILs was presented. The proposed circuit was realised using passive distributed elements without lossy lumped elements. It consists of parallel interconnect lines configures as transmission type structure. It was shown that the NGD behaviour can be generated when the PIL is lossy and presenting different electrical lengths. The NGD concept was validated by designing two microstrip circuits. An NGD of - 4 ns at 1.75 GHz with attenuation loss of about -5 dB over a bandwidth of 50 MHz was obtained when the PIL prototype was built with a same characteristic impedance of the lines (50 Ω) [26]. Moreover, with PIL prototype having different characteristic impedance from the lines and having same physical lengths, an NGD of about - 4 ns happened at 1.99 GHz with an attenuation loss of - 2.5 dB over the NGD bandwidth of 50 MHz. The developed NGD circuit was anticipated to be useful for the correction of the signal delays in the high-speed electronic systems [26].

3.3 Negative- Group -Delay Networks Applications

When having access to circuits which exhibit abnormal group velocities including superluminal and negative group velocities, many interesting applications in communication systems and microwaves are applicable. In this section, the important applications of the NGD networks that have been implemented and reported in the literature are summarised.

For example in communication systems, NGD networks have been employed in [27] to enhance and increase the operating bandwidth of a feedback power amplifier. The proposed feedback amplifier with the proposed negative group delay topology experimentally achieved an adjacent channel leakage ratio of - 53:2 dBc with a cancellation bandwidth of over 50 MHz In another example, NGD circuits were utilised in [13] to improve the efficiency of feedforward amplifiers. The amplifier with the proposed NGD circuit experimentally achieved 19.4% power-added efficiency and - 53.2 dBc adjacent channel leakage ratio with 44 dBm average output power.

Furthermore, a predefined NGD network was implemented in a microwave filter design based on the transformation in frequency from a low-pass filter to a band-stop filter [6], [28]. Also, synthesised non-Foster circuits utilised by active NGD networks in [29], were loaded with transmission lines to enhance the inherent beam-squinting issues associated with beamforming in series-fed phased array antennas. Moreover, NGD networks were used to reduce beam-squinting and obtain zero phase delay, zero group delay, planar phase shifters in linear series-fed array antenna systems [30].

Moreover, NGD networks have been reported in new interesting electromagnetic and microwave applications. For example, in references [5, 8], NGD networks were implemented to realise non-Foster reactive elements such as negative capacitors and negative inductors between 1.4 to 1.8 GHz. These new methods have been proposed as a way around the stability challenges associated with the existing methods using

transistorised NICs and NIIs. Hence, new routes for the implementations of NGD circuits can be opened. For instance, synthesised non-Foster reactive elements can be integrated with transmission lines and employed in squint-free beamforming in series-fed antenna arrays [29, 31].

In another work presented in [32] a rat-race coupler with NGD characteristics working at a centre frequency of 2.14 GHz was designed with an arbitrary power division ratio. The NGD characteristics were obtained through various transmission paths and have small variations with the power division ratio. The power division ratio was determined by the characteristic impedances of the transmission lines. The NGD coupler was designed, fabricated and tested. Both measured and simulated results seemed to agree with each other. The NGD coupler was anticipated to be implemented in feed networks of series fed antenna arrays for minimizing beam-squint problem and in predistortion amplifier for group delay matching between different transmission paths [32].

In this work the synthesised non-Foster reactive element using reflection-mode NGD networks can be implemented as external matching networks with relatively small antennas to broaden the bandwidth and tune their operating frequencies.

3.4 Relationship between NGD Networks and Networks with Non-Foster Behaviour

In reference [5] a logical relation connecting networks with a NGD response and networks with a non-Foster behaviour was explored and presented. It states that to establish such a relationship, firstly, networks with NGD responses must represent reactive non-Foster elements at certain bandwidths. Likewise, networks exhibiting non-Foster reactance must operate as networks with NGD responses [5].

To explain the first connection: if a non-Foster reactive element is represented by its reactance *X* or susceptance *B*; these properties are characterised by negative slopes and can be expressed by the following equation [5]:

$$\frac{\partial X}{\partial \omega} < 0 \quad and \quad \frac{\partial B}{\partial \omega} < 0 \tag{3.2}$$

The reflection coefficient (S_{11}) associated with these reactive circuits rotates anti-clockwise on the Smith chart with frequency as depicted in Figure 3.1(a). Moreover, the presence of the negative group delay (NGD) is observed from the synthesised phase response of S_{11} [3]. An increasing phase from f_1 to f_2 implies NGD behaviour. Meanwhile, the network's response below f_1 and above f_2 is a Foster response with a decreasing phase response versus increasing frequency, as shown in Figure 3.1(b). Note that the NGD networks exhibit losses which could be compensated using amplifiers. As a result, loss-compensated NGD networks in a certain bandwidth can be obtained and satisfy the condition of equation (3.2) [5].

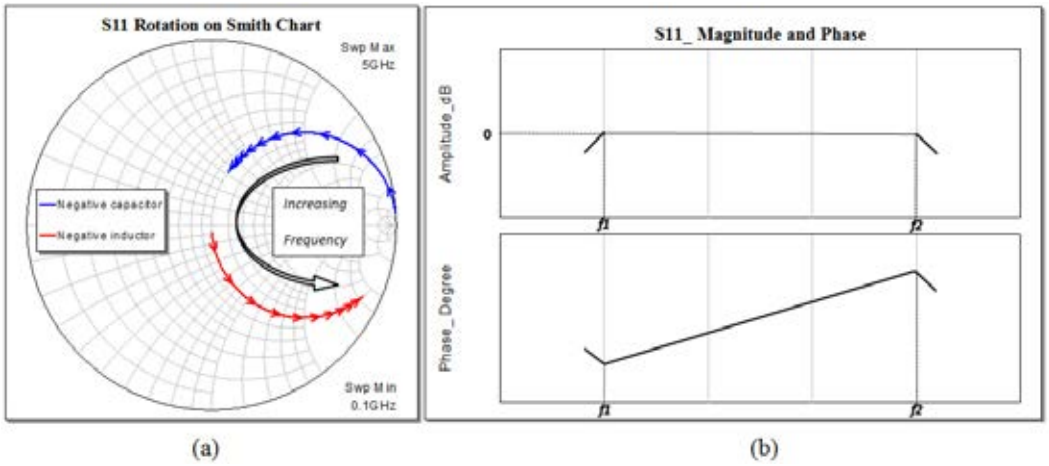


Figure 3.1: (a) S_{11} rotation of non-Foster elements on Smith chart; (b) complex S_{11} response of a reflection –mode NGD network shows an increasing reflection phase from f_1 to f_2 with zero loss amplitude

The second connection, where the NGD response can be synthesised using non-Foster impedances in different arrangements was established in [5]. It was demonstrated that grounded one-port, floating two -port, and shunting two-port non-Foster configurations can operate as networks with NGD responses and satisfy the condition in (3.1). For a complete background about the analogy of these two concepts, the readers are referred to [5] and the references therein. By establishing this two-way relationship, new techniques in the design and implementation of non-Foster circuits using NGD networks have been introduced. These approaches have the advantages of obtaining the non-Foster property mainly using passive circuits. Thus, they have minimal stability concerns compared to the traditional methods using NICs.

For instance, in [5], the authors have demonstrated the realisation of a stand-alone unilateral non-Foster T-network at microwave frequencies, as illustrated in Figure 3.2(a). The non-Foster circuit is realised by employing a transmission-type NGD network with a conventional amplifier, as shown in Figure 3.2(b). The NGD network was designed by cascading RLC resonators in series and parallel fashion. A regular amplifier was used to compensate the inherent losses of the NGD network. However, since regular amplifiers are unidirectional and provide gain in one direction and isolation in the reverse direction, the NGD network obtained in [5] cannot represent a full-fledged non-Foster reactive element. Rather, such a unidirectional NGD network. The prototype is shown in Figure 3.2(c). Stability assessment was not performed for the proposed circuit. In addition, another important parameter in the realisation of the NGD networks which is the amount of the group delay produced by the NGD network was not presented in [5].

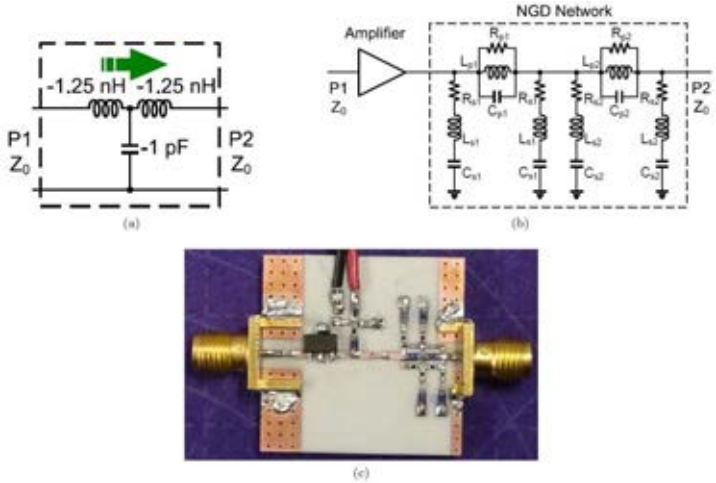


Figure 3.2: (a) circuit schematic of an ideal non-Foster T- network; (b) a circuit schematic of the loss-compensated NGD network realised by cascading an NGD filter with an amplifier; (c) transmission-type NGD network prototype [5]

Measurement and simulation results of the complex transmission coefficient (S_{21}) and the magnitude of the output reflection coefficient (S_{22}) were compared with the same S-parameter values obtained from an ideal non-Foster T-network as a reference and plotted in Figure 3.3.Good agreement can be observed, with an increasing transmission phase in the frequency band of interest. This implies NGD behaviour over a bandwidth of 0.4 GHz. The losses of the NGD networks were compensated by amplification from a regular amplifier and as a result, a transmission coefficient with a magnitude close to zero dB loss from 1.4 GHz to 1.8 GHz was obtained with good output matching [5].

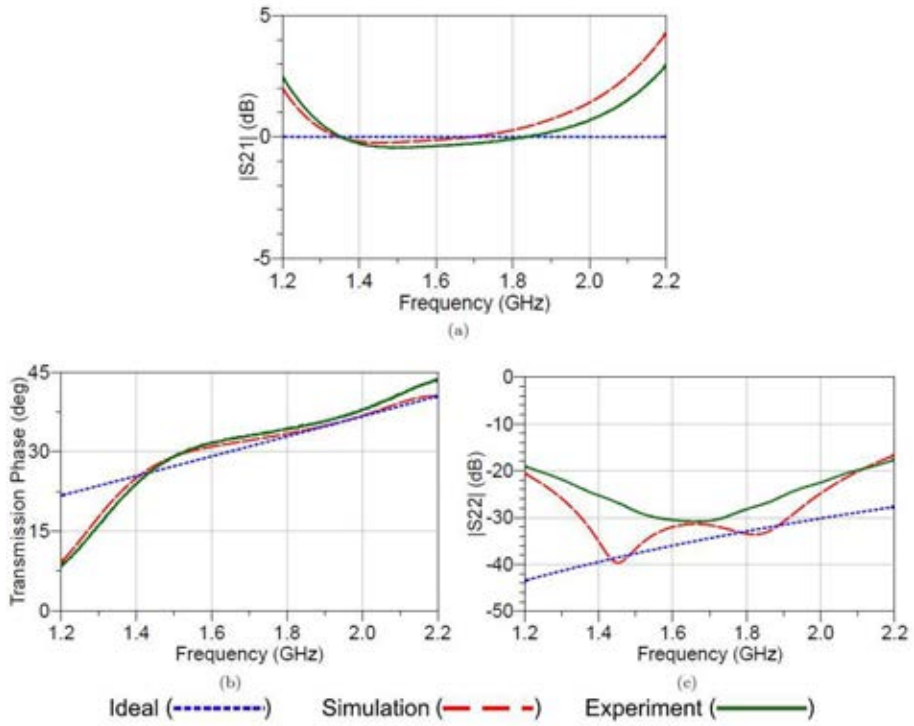


Figure 3.3: S-parameters' results of the loss- compensated NGD network when compared with the same results obtained from an ideal T-network; (a) S_{21} magnitude response plot; (b) S_{21} phase response plot; (c) S_{22} response plot [5]

Another example related to the realisation of a two-port unilateral non-Foster reactive element was presented in [8]. A (-2.4 pF) non-Foster capacitor was synthesised using a loss-compensated NGD network as depicted in Figure 3.4(a). The circuit schematic employed in this design was similar to that one shown in Figure 3.2 (b). The circuit was fabricated and experimentally tested. The S-parameter values were compared with the same values obtained from an ideal -2.4 pF capacitor as a reference [8]. An increasing transmission phase S_{21} was obtained with a positive slope from 1 GHz to 1.5 GHz, which was an indication of NGD. Also, a transmission coefficient amplitude close to 0 dB for the non-Foster circuit in the frequency region of interest was achieved with good output matching [8]. However, the amount of the group delay generated by the proposed circuit was not considered in the paper.

Another example based on the relation between NGD networks and non-Foster networks was recently presented in [33]. A non-Foster element using a microwave transversal-filter-based NGD circuit was introduced. The proposed circuit is realised by a distributed amplifier, in which the NGD response is synthesised by adjusting the ratio of transconductance of transistors in each stage. Simulated and measured results showed that the circuit could realise a unilateral non-Foster element composed of a -1 pF shunt capacitor and a -1.25 nH series inductor [33]. The circuit exhibited an increasing transmission phase response by 25 degrees over a bandwidth between 1.35 to 1.45 GHz and magnitude around 0 dB with ± 0.7 dB. However, before and after that bandwidth the circuit generates about 7 dB gain in the frequency

range from 1 to 2 GHz. Stability K and B1 factors were performed and it was anticipated to be unconditionally stable [33].

3.5 Loss-Compensation Methods for NGD Networks

It was discussed in the previous section that reactive non-Foster networks can be constructed using loss-compensated NGD networks. This was the implication of an established two-way relationship between them which was for the first time explored in [5]. However, the NGD networks are "lossy" structures, have inevitable losses associated with them, which must be compensated [5]. This can be accomplished by amplification. This section reviews suitable active circuits and methods which can be used to compensate the losses associated with the NGD networks.

3.5.1 Active Circuits for Loss-Compensation

The circuits that can be utilised to compensate the losses of the NGD networks are basically active components which provide an amplification and gain in a forward or backward direction or in both directions. Such representative examples are amplifiers, negative resistance reflection amplifiers and bi-directional amplifiers, as depicted in Figure 3.4. Although these active devices bring their own stability concerns, their stability can be successfully predicted using the standard methods for checking the stability of active two-port devices such as K and $B1$ factors or some other measure of stability. The reported implementations are narrowband and

produce an additional positive delay [5]. The associated positive group delay can be over using NGD networks. Broadband amplifiers generate a lower amount of positive group delay but have a large gain, which might lead to more stability problems [5].

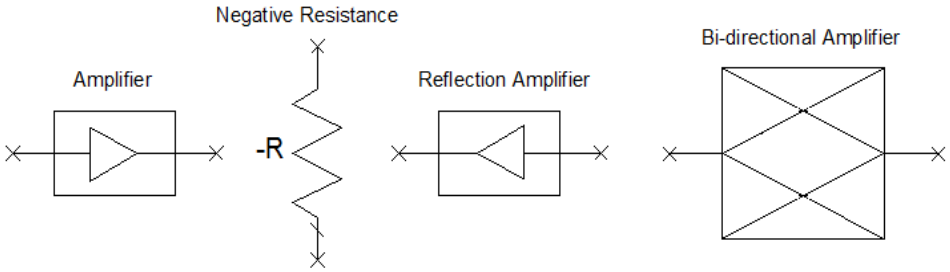


Figure 3.4: Symbolic examples of active circuits' blocks for loss compensation [5]

Conventional amplifiers, also known as transmission transistor amplifiers are well-behaved devices and usually do not have stability concerns with their configurations. They can be designed in many technologies and employed in a different frequency spectrum. Furthermore, they are widely available on the market in a different range of specifications.

Negative resistance reflection amplifiers are widely studied and reported in the literature. They can be realised using Gunn and tunnel diodes [34]. Their implementations using transistors were presented in [35]. Moreover, negative resistance circuits were employed in the design of microwave active filters in [36]. In this work presented in thesis, reflection amplifier is implemented in the realisation of loss-compensated NGD networks.

Two-port bi-directional amplifiers have the capability to amplify signals when passing through them in both directions. By employing these active devices at the terminals of the NGD networks, the losses of these networks can be equalised and compensated. As a result, transmission and reflection modes of NGD networks can be obtained [5]. Bi-directional amplifiers have been suggested as a means for designing fully established, bi-lateral non-Foster elements using loss-compensated NGD networks. An example of realising the two-way amplifiers by employing two reflection amplifiers and a 3-dB hybrid coupler was presented [37]. They were used as an alternative to negative resistance repeaters in telephone lines. However, the reported implementations of the bi-directional amplifiers have several limitations, such as narrow bandwidth, associated with an excessive group delay and stability issues. Therefore, designing stable broadband bi-directional amplifiers is still a challenge.

As a conclusion to the above discussion, using regular amplifiers is a preferable approach to compensate the losses of the NGD networks for the minimal stability concerns. However, all the above mentioned active devices are considered as narrow bandwidth and generate large positive group delay. Therefore, for future consideration, improving their performance will have a positive impact on designing NGD-based non-Foster networks.

3.5.2 Loss-Compensation scheme for Transmission-mode NGD Networks

The easiest way for compensating the losses associated with NGD networks in the transmission mode is by using regular amplifiers. These active devices amplify the signals passing through them in the forward direction and maintain isolation on the reverse side. These amplifiers can be connected to the terminals of the NGD networks as shown in Figure 3.5. With the right amount of gain and positive group delay produced by the amplifiers, the losses and the negative group delay of the NGD networks can be compensated. Consequently, two-port NGD networks with zero-dB transmission coefficient amplitude and a positive transmission phase slope in the frequency range of interest can be synthesised. An example of the realisation of stand-alone non-Foster elements using loss-compensated NGD networks in the transmission mode can be found in [8].

Another approach for compensating the losses of the transmission-mode NGD networks can be accomplished using bi-directional amplifiers. As a result, a synthesised two-port NGD network with zero losses at a frequency range of interest can be realised by connecting two NGD networks in both sides of the bi-directional amplifier, as depicted in Figure 3.6.

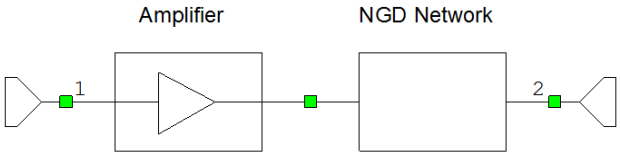


Figure 3.5: Loss-compensation technique for transmission-type NGD networks using regular amplifier [5]

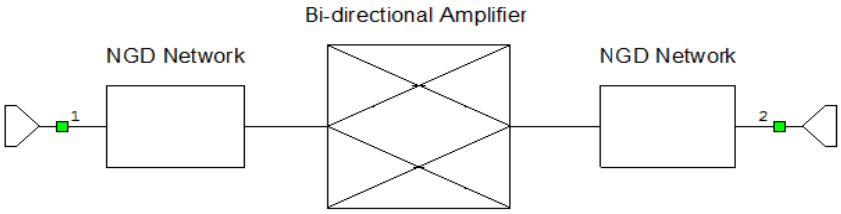


Figure 3.6: Loss-compensation technique for transmission-type NGD networks using a bi-directional amplifier [5]

3.5.3 Loss-Compensation scheme for Reflection-Mode NGD Networks

Reflection amplifiers are very attractive for compensating the losses of the NGD networks in the reflection mode, as shown in Figure 3.7. They provide a reflection gain greater than unity and amplify the signal from the NGD network travelling in a backward direction to the input port [5]. The positive delay of the amplifiers will be more than compensated by the NGD networks; as a result, one-port non-Foster networks can be synthesised in a limited frequency range [5].

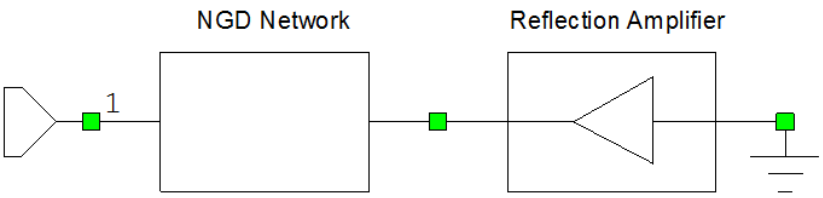


Figure 3.7: Loss-compensation technique for reflection–type NGD network using reflection amplifier [5]

The loss-compensation technique using a bi-directional amplifier of Figure 3.7 can be modified so that one NGD network is terminated to the ground and thus a one-port NGD network in the reflection mode with zero loss can be obtained, as depicted in Figure 3.8 [5]. These active devices will influence the travelling signals of the NGD network in both directions and because one of the NGD networks is terminated, the signals will be travelling in a backward direction to the input port [5].

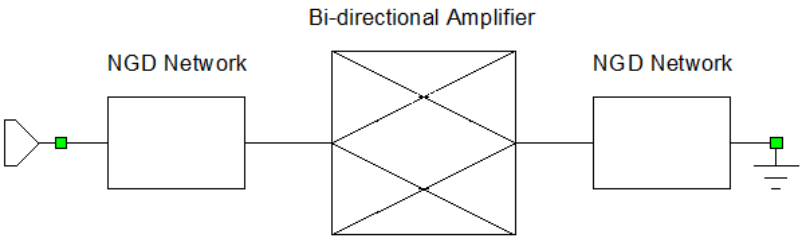


Figure 3. 8: Loss-compensation technique for reflection–type NGD network using a bi-directional amplifier [5]

Figure 3.9 demonstrates another interesting loss-compensation scheme for NGD networks in a reflection mode. It can be realised by combining the loss-compensated NGD network of Figure 3.6 with a circulator. The signal will be directed back to the

input port and the circulator will separate the received synthesised signal with the NGD from the transmitted signals. The positive group delay produced by the amplifier and the circulator will be over compensated by the NGD network and therefore, a one-port loss-compensated NGD network in the reflection mode can be achieved [5].

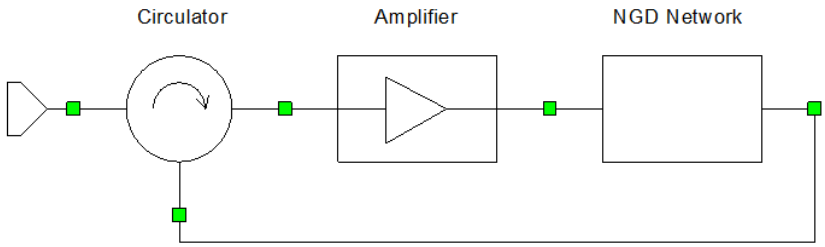


Figure 3.9: Loss-compensation technique for reflection–type NGD network using NGD network in transmission mode of Figure 3.5 and a circulator [5]

In this thesis, a novel technique for equalising the losses of the NGD networks in the reflection mode will be introduced in Chapter 5. It is a new perspective in the realisation of NGD networks with zero loss in the bandwidth between 1 G. The proposed technique is comprised of two reflection-type NGD networks. A negative resistance amplifier is employed to generate the required reflection gain to compensate for the losses of the NGD networks. A Lange coupler is used to double the effect of the NGDs' behaviour as a result of sending the signal through them twice in a balanced structure.

3.6 Summary

This chapter has summarised the concept of the NGD phenomenon. Circuits that support propagation with an NGD in different frequency regions were reviewed. Moreover, many practical applications where NGD networks have been implemented were outlined. To the best of our knowledge, the presented intimate relationship between NGD networks and non-Foster reactive networks was explored for the first time in references [5, 8]. Furthermore, rigorous proof has been presented aiming to unify the two concepts and to justify that a class of a non-Foster element can operate as an NGD network and vice versa; NGD response can be synthesised using non-Foster reactive elements in different configurations. Consequently, NGD networks were introduced as an alternative means for the design and the realisation of stable non-Foster circuits in limited bandwidths.

In [5, 8] the NGD network was realised in the transmission mode only; meaning that the NGD behaviour happened when the wave propagates through a network in the forward direction because the losses of the NGD networks were compensated using unidirectional amplifiers. These amplifiers produce a gain in one direction and isolation on the reverse side [5]. That led to the realisation of unilateral non-Foster elements. Subsequently, they have been employed in unilateral applications such as guided-wave applications. Finally, active circuits which could be used for the loss compensation of the NGD networks in the transmission and reflection modes, and further existing techniques in the literature were presented.

This thesis explores a novel technique in the realisation of NGD networks in the reflection-mode presented in Chapter 4. Consequently, a new method for compensating the losses of the NGD networks using a negative resistance reflection amplifier is demonstrated. Ultimately, a synthesised non-Foster reactive circuit using reflection-mode loss-compensated NGD networks is proposed in Chapter 5. This active circuit is suitable for transmit and receive applications. In Chapter 6, the NGD-based non-Foster circuit will be used to match suitable small antennas at microwave frequencies.

References

[1] E. L. Bolda, R. Y. Chiao, and J. C. Garrison, "Two theorems for the group velocity in dispersive media," Physical review A, vol. 48, p. 3890, 1993.

[2] G. Chaudhary and Y. Jeong, "Transmission-type negative group delay networks using coupled line doublet structure," IET Microwaves, Antennas & Propagation, vol. 9, pp. 748-754, 2015.

[3] L. Brillouin and H. Massey, "Wave propagation and group velocity," 1960.

[4] M. Kitano, T. Nakanishi, and K. Sugiyama, "Negative group delay and superluminal propagation: An electronic circuit approach," IEEE Journal of selected Topics in Quantum electronics, vol. 9, pp. 43-51, 2003.

[5] H. Mirzaei and G. V. Eleftheriades, "Realizing Non-Foster Reactive Elements Using Negative-Group-Delay Networks," Microwave Theory and Techniques, IEEE Transactions on, vol. 61, pp. 4322-4332, 2013.

[6] G. Chaudhary, Y. Jeong, and J. Lim, "Microstrip Line Negative Group Delay Filters for Microwave Circuits," IEEE Transactions on Microwave Theory and Techniques, vol. 62, pp. 234-243, 2014.

[7] D. Solli, R. Y. Chiao, and J. M. Hickmann, "Superluminal effects and negative group delays in electronics, and their applications," Physical Review E, vol. 66, p. 056601, 11/12/ 2002.

[8] H. Mirzaei and G. V. Eleftheriades, "Unilateral non-Foster elements using loss-compensated negative-group-delay networks for guided-wave

applications," in Microwave Symposium Digest (IMS), 2013 IEEE MTT-S International, 2013, pp. 1-4.

[9] S. Lucyszyn, I. Robertson, and A. Aghvami, "Negative group delay synthesiser," Electronics Letters, vol. 29, pp. 798-800, 1993.

[10] B. Ravelo, A. PÉrennec, M. L. Roy, and Y. G. Boucher, "Active Microwave Circuit With Negative Group Delay," IEEE Microwave and Wireless Components Letters, vol. 17, pp. 861-863, 2007.

[11] Y. Jeong, H. Choi, and C. D. Kim, "Experimental verification for time advancement of negative group delay in RF electronic circuits," Electronics Letters, vol. 46, pp. 306-307, 2010.

[12] C. D. Broomfield and J. K. A. Everard, "Broadband negative group delay networks for compensation of microwave oscillators and filters," Electronics Letters, vol. 36, pp. 1931-1933, 2000.

[13] H. Choi, Y. Jeong, C. D. Kim, and J. S. Kenney, "Efficiency Enhancement of Feedforward Amplifiers by Employing a Negative Group-Delay Circuit," IEEE Transactions on Microwave Theory and Techniques, vol. 58, pp. 1116-1125, 2010.

[14] B. Ravelo, M. Le Roy, and A. Pérennec, "Application of negative group delay active circuits to the design of broadband and constant phase shifters," Microwave and Optical Technology Letters, vol. 50, pp. 3078-3080, 2008.

[15] G. Chaudhary and Y. Jeong, "Negative Group Delay Phenomenon Analysis Using Finite Unloaded Quality Factor Resonators," Progress In Electromagnetics Research, vol. 156, pp. 55-62, 2016.

[16] M. Kandic and G. E. Bridges, "Asymptotic Limits of Negative Group Delay in Active Resonator-Based Distributed Circuits," IEEE Transactions on Circuits and Systems I: Regular Papers, vol. 58, pp. 1727-1735, 2011.

[17] H. Choi, G. Chaudhary, T. Moon, Y. Jeong, J. Lim, and K. Chul Dong, "A design of composite negative group delay circuit with lower signal attenuation for performance improvement of power amplifier linearization techniques," in 2011 IEEE MTT-S International Microwave Symposium, 2011, pp. 1-4.

[18] O. F. Siddiqui, M. Mojahedi, and G. V. Eleftheriades, "Periodically loaded transmission line with effective negative refractive index and negative group velocity," IEEE Transactions on Antennas and Propagation, vol. 51, pp. 2619-2625, 2003.

[19] O. F. Siddiqui, S. J. Erickson, G. V. Eleftheriades, and M. Mojahedi, "Time-domain measurement of negative group delay in negative-refractive-index transmission-line metamaterials," IEEE Transactions on Microwave Theory and Techniques, vol. 52, pp. 1449-1454, 2004.

[20] W. Alomar and A. Mortazawi, "Elimination of beam squint in uniformly excited serially fed antenna arrays using negative group delay circuits," in

Proceedings of the 2012 IEEE International Symposium on Antennas and Propagation, 2012, pp. 1-2.

[21] H. Mirzaei and G. V. Eleftheriades, "Negative and zero group velocity in microstrip/negative-refractive-index transmission-line couplers," in 2010 IEEE MTT-S International Microwave Symposium, 2010, pp. 37-40.

[22] H. Mirzaei, R. Islam, and G. V. Eleftheriades, "Anomalous Negative Group Velocity in Coupled Positive-Index/Negative-Index Guides Supporting Complex Modes," Antennas and Propagation, IEEE Transactions on, vol. 59, pp. 3412-3420, 2011.

[23] T. Shao, Z. Wang, S. Fang, H. Liu, and S. Fu, "A Compact Transmission-Line Self-Matched Negative Group Delay Microwave Circuit," IEEE Access, vol. 5, pp. 22836-22843, 2017.

[24] H. Y. Yao, N. C. Chen, T. H. Chang, and H. G. Winful, "Tunable Negative Group Delay in a Birefringent Fabry-Perot-Like Cavity With High Fractional Advancement Induced by Cross-Interference Effect," IEEE Transactions on Microwave Theory and Techniques, vol. 64, pp. 3121-3130, 2016.

[25] G. Liu and J. Xu, "Compact transmission-type negative group delay circuit with low attenuation," Electronics Letters, vol. 53, pp. 476-478, 2017.

[26] B. Ravelo, "Negative Group-Delay Phenomenon Analysis with Distributed Parallel Interconnect Line," IEEE Transactions on Electromagnetic Compatibility, vol. 58, pp. 573-580, 2016.

[27] H. Choi, Y. Jeong, C. D. Kim, and J. S. Kenney, "Bandwidth enhancement of an analog feedback amplifier by employing a negative group delay circuit," Progress In Electromagnetics Research, vol. 105, pp. 253-272, 2010.

[28] J. Park, G. Chaudhary, J. Jeong, and Y. Jeong, "Microwave Negative Group Delay Circuit Filter Synthesis Approach," Journal of electromagnetic engineering and science, vol. 16, pp. 7-12, 2016.

[29] H. Mirzaei and G. V. Eleftheriades, "Arbitrary-Angle Squint-Free Beamforming in Series-Fed Antenna Arrays Using Non-Foster Elements Synthesized by Negative-Group-Delay Networks," Antennas and Propagation, IEEE Transactions on, vol. 63, pp. 1997-2010, 2015.

[30] S. Keser and M. Mojahedi, "Removal of beam squint in series fed array antennas using abnormal group delay phase shifters," in Antennas and Propagation Society International Symposium (APSURSI), 2010 IEEE, 2010, pp. 1-4.

[31] H. Mirzaei and G. V. Eleftheriades, "Squint-free beamforming in series-fed antenna arrays using synthesized non-Foster elements," in 2013 IEEE Antennas and Propagation Society International Symposium (APSURSI), 2013, pp. 2209-2210.

[32] G. Chaudhary and Y. Jeong, "Arbitrary Power Division Ratio Rat-Race Coupler With Negative Group Delay Characteristics," IEEE Microwave and Wireless Components Letters, vol. 26, pp. 565-567, 2016.

[33] T. Zhang, R. Xu, and C. T. M. Wu, "Unconditionally Stable Non-Foster Element Using Active Transversal-Filter-Based Negative Group Delay Circuit," *IEEE Microwave and Wireless Components Letters*, vol. 27, pp. 921-923, 2017.

[34] P. Chan and V. Fusco, "An 8-to 12-GHz wideband negative resistance reflection amplifier," Microwave and Optical Technology Letters, vol. 54, pp. 553-555, 2012.

[35] P. Gardner and D. K. Paul, "Aspects of the design of low noise, negative resistance, reflection mode transistor amplifiers," Microwave Theory and Techniques, IEEE Transactions on, vol. 39, pp. 1869-1875, 1991.

[36] C. Chi-Yang and T. Itoh, "Microwave active filters based on coupled negative resistance method," Microwave Theory and Techniques, IEEE Transactions on, vol. 38, pp. 1879-1884, 1990.

[37] C. Shyh-Jong, C. Shing-Ming, and L. Yang-Chang, "A novel bi-directional amplifier with applications in active Van Atta retrodirective arrays," IEEE Transactions on Microwave Theory and Techniques, vol. 51, pp. 542-547, 2003.

CHAPTER 4

REALISATION OF NON-FOSTER REACTIVE CIRCUITS USING REFLECTION–MODE NGD NETWORKS

In the previous chapter, the background behind NGD networks and their properties were reviewed. In addition, the means of realising these structures and their implementation in various applications were also presented. Moreover, the potential of employing NGD networks in transmission mode to realise stand-alone reactive non-Foster elements was also introduced. In this chapter, original research including design, simulation and measurement work in the realisation of NGD networks is presented. In this approach, the NGD response occurs when the signal is reflected from a suitably configured network and travels in a backward direction. Thereby, it is called a reflection-type NGD network. The merit of the proposed technique lies in the potential uses in antenna matching applications where both transmit and receive capabilities are required.

4.1 Reflection-mode NGD Network Design

A new approach for the implementation of NGD networks in the reflection mode at microwave frequencies is presented. To demonstrate the physics of the NGD concept, the AWR Microwave Office circuit schematic simulator is used.

This simulation tool gives results with good accuracy and fast execution times. Initially, the NGD network is investigated using ideal components of a combination of parallel and series LC resonators in five stages. Subsequently, a realistic NGD network is constructed using realistic Modelithics models of Coilcraft inductors and ATC capacitors along with microstrip transmission line sections. The NGD structure is designed and modelled with the aid of AWR Microwave Office and experimentally verified as presented in section 4.3. The NGD network is studied and optimised to generate a reflection coefficient phase that has a positive gradient and increases with frequency within the bandwidth of interest, based on the reflection characteristics of the network.

4.2 Reflection-mode NGD Network Design Using Ideal Components

In this section, a circuit schematic simulator tool is used for the conceptual design stage of NGD networks. This fast simulator allows selection for appropriate NGD network configurations and for design optimisation, where the chosen LC component values can be optimised, aiming to achieve a reflection phase that increases with frequency within the range between 1 GHz - 2 GHz.

Simulations have been carried out for many different combinations and different physical dimensions and values of the LC resonators. Eventually, five sections LC resonators are chosen to demonstrate the NGD principle because more sections give

a bigger NGD slope, but too many become too complex, too expensive and too "lossy". Therefore, five LC sections are considered as a working practical compromise. Firstly, the design methodology of the proposed NGD structure is presented based on analytical equations to demonstrate how the LC component values are initially obtained in the design frequency of interest.

In this work, the concept of the reflection phase of an impedance-matching network is introduced. The approach is based on a parametric study of the design parameters and closed-form equations are obtained taking the desired increasing phase slope of the corresponding network into account. Subsequently, an optimised design of a realistic reflection-mode NGD network is introduced in the following section. The implementation of the NGD network in the reflection-mode using ideal components of five sections LC resonators aiming to achieve a positive phase gradient in the reflection phase response is depicted in Figures 4.1.

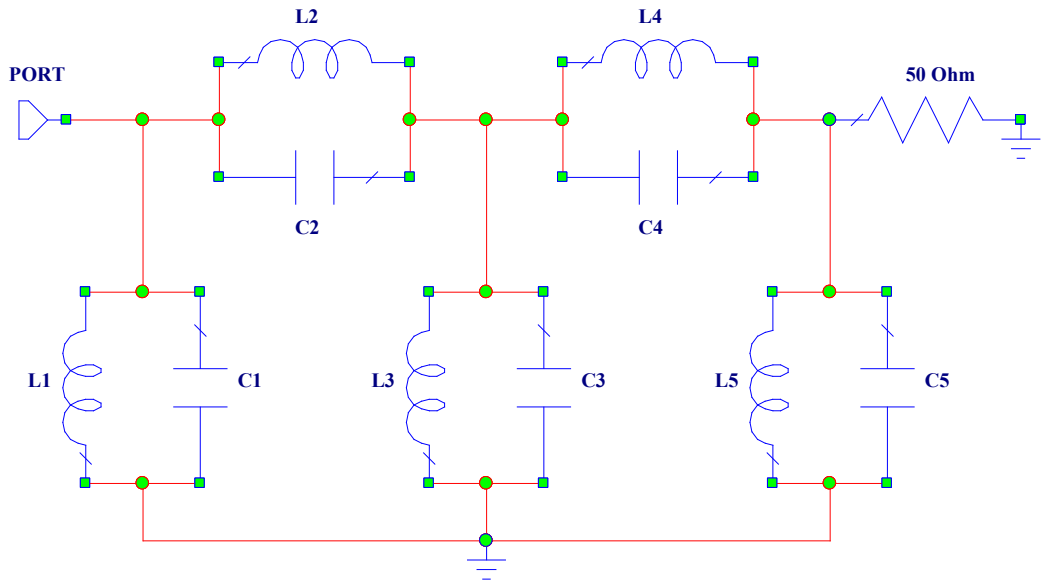


Figure 4. 1: Schematic layout of the proposed ideal reflection- type NGD network using 5 sections LC resonators

For a given source and load impedances of the proposed NGD network, it is possible to form a design procedure of L-type and Pi-type networks offering impedance matching for a required specification in terms of a reflection phase. Therefore, the design equations based on the loaded Q of the two matching networks are derived and analytically demonstrated. As a result, a reflection-mode NGD network will be designed, fabricated and measured to establish the proposed concept.

Firstly, a Q-based design procedure using L-type matching network is used to analyse the reflection-mode NGD network and calculate the values of the combinations of L_4 C_4, L_5 C_5 as depicted in Figure 4.2.

For a given source R_{in} and load R_l impedances, the equivalent L-type matching network is depicted in Figure 4.3.

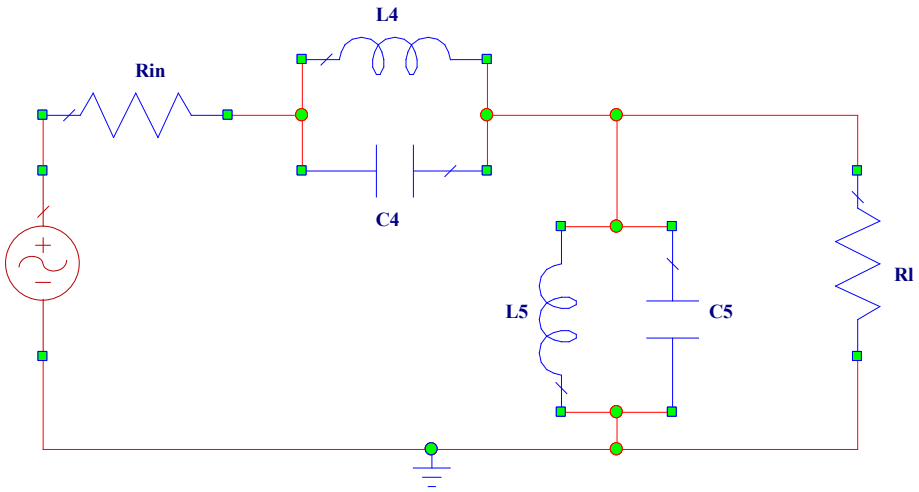


Figure 4. 2: The proposed NGD network is analysed using L-type impedance matching network to determine the values of a series combination of L_4 C_4 and a shut combination of L_5 C_5 resonators

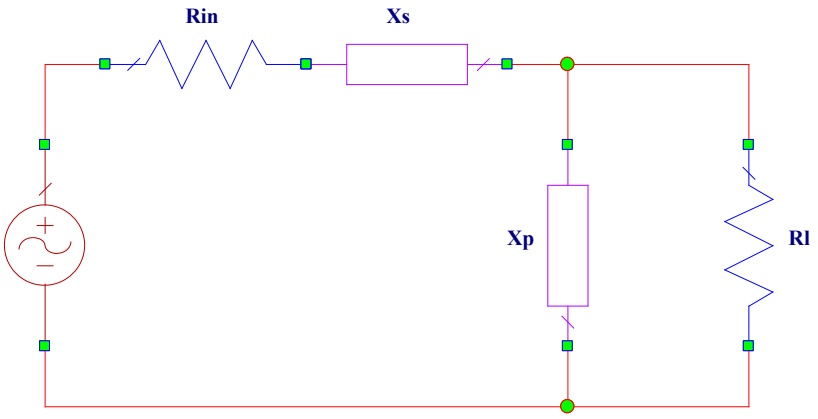


Figure 4. 3: L-type matching network

Assuming that the source impedance is purely resistive with a value of $R_{in} = 30\ \Omega$ and the load impedance is also resistive with a value of $R_l = 50\ \Omega$. The quality factor Q of the network can be calculated using the following formula [1]:

$$Q = \sqrt{\frac{R_l}{R_{in}} - 1} \tag{4.1}$$

$$Q_s = \sqrt{\frac{50}{30} - 1} = 0.816$$

The series matching reactance X_s is determined using the following equation [1]:

$$X_s = Q\ x\ R_{in} \tag{4.2}$$

$$X_s = 0.816\ x\ 30$$

Therefore, $\boldsymbol{X_s = 24.480\ \Omega}$

The parallel matching reactance X_p is calculated using the following equation [1]:

$$X_p = \frac{R_l}{Q} \tag{4.3}$$

$$X_p = \frac{50}{0.816}$$

Therefore, $\boldsymbol{X_p = 61.275\ \Omega}$

Knowing the operating frequency f_0 of the NGD network which is 1.3 GHz and assuming the resonance frequencies of the series and parallel sections f_4 and f_5 respectively, the values of L_4, C_4, L_5 and C_5 can be derived as follows:

Assuming that $f_4 > f_o$, for example $f_4 = 1.1f_0$, thus, $\omega_4 = 1.1\omega_0$

$f_5 < f_o$, for example $f_5 = 0.9f_0$, thus, $\omega_5 = 0.9\omega_0$

The susceptance of the series section of the combination of L_4 and C_4 at the operating frequency of f_0= 1.3 GHz can be derived as follows:

$$B = \frac{1}{X_s} = \frac{1}{\omega_0 L_4} - \omega_0 C_4 \tag{4.4}$$

Knowing that at the resonance $f_4 = \frac{1}{\sqrt{L_4 C_4}}$, therefore, $L_4 = \frac{1}{\omega_4^2 C_4}$

By substituting L_4 and ω_4 into equation 4, B becomes:

$$B = \frac{\omega_4^2 C_4}{\omega_0} - \omega_0 C_4$$

$$B = C_4 \left(\frac{1.21\omega_0^2}{\omega_0} - \omega_0 \right)$$

$$B = 0.21\ C_4 \omega_0 \qquad (4.5)$$

$\frac{1}{24.48}$=0.21x $2\pi\ x\ 1.3x\ 10^9 x\ C_4$

$$\boldsymbol{C_4 = 23.8\ pF}$$

$$L_4 = \frac{1}{\omega_4^2 C_4} = \frac{1}{4.84\ \pi^2 f_0^2 C_4}$$

$$L_4 = \frac{1}{4.84x\ \pi^2 x\ 1.3^2 x 10^{18} x\ 23.8\ x\ 10^{-12}}$$

$$\boldsymbol{L_4 = 0.5\ nH}$$

The susceptance of the parallel section of the combination of L_5 and C_5 at the operating frequency of f_0= 1.3 GHz can be derived as follows:

$$B = \frac{1}{X_p} = \omega_0 C_5 - \frac{1}{\omega_0 L_5} \qquad (4.6)$$

Knowing that at the resonance $f_5 = \frac{1}{\sqrt{L_5 C_5}}$, therefore, $L_5 = \frac{1}{\omega_5^2 C_5}$

By substituting L_5 and ω_5 into equation 6, B becomes:

$$B = \omega_0 C_5 - \frac{\omega_5^2 C_5}{\omega_0}$$

$$B = C_5 \left(\omega_{0-} \frac{\omega_5^2}{\omega_0} \right)$$

$$B = C_5 \left(\omega_{0-} \frac{0.9^2 \omega_0^2}{\omega_0} \right)$$

$$B = 0.19\ \omega_0 C_5 \tag{4.7}$$

$$\frac{1}{61.275} = 0.19\ x\ 2\pi\ x\ 1.3x\ 10^9 x\ C_5$$

$$\boldsymbol{C_5 = 10.5\ pF}$$

$$L_5 = \frac{1}{\omega_5^2 C_5} = \frac{1}{0.9^2 x\ 2^2 \pi^2 f_0^2 C_5}$$

$$L_5 = \frac{1}{3.24\ x\ \pi^2 x\ 1.3^2 x 10^{18} x\ 10.5x\ 10^{-12}}$$

$$\boldsymbol{L_5 = 1.8\ nH}$$

Secondly, a Q-based design procedure using Pi-type matching network is used to analyse the reflection-mode NGD network and calculate the values of the combinations of L_1 C_1, L_2 C_2 and L_3 C_3 as depicted in Figure 4.4. For a given source R_1 and load R_2 impedances, the equivalent Pi-type matching network is depicted in Figure 4.5.

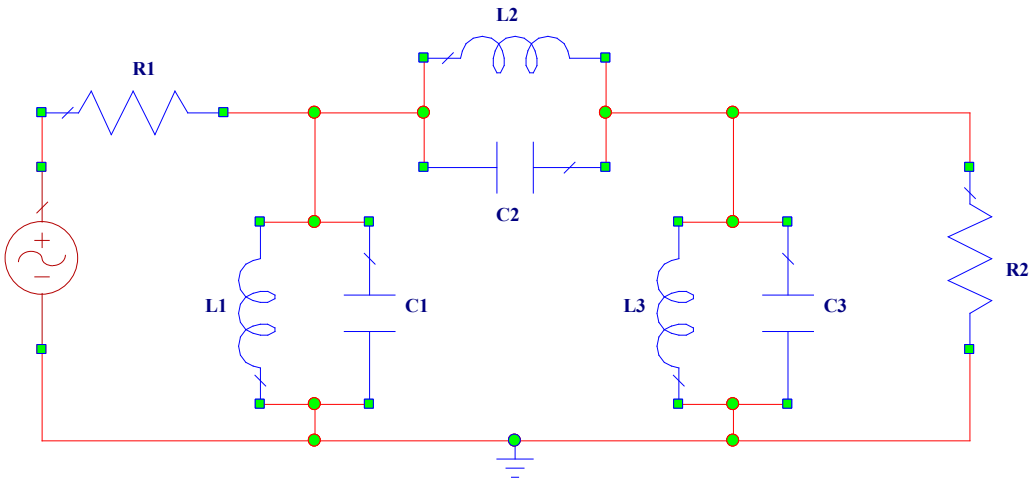


Figure 4. 4: The proposed NGD network is analysed using the Pi-type impedance matching network to determine the values of the shunt- series-shunt LC resonators

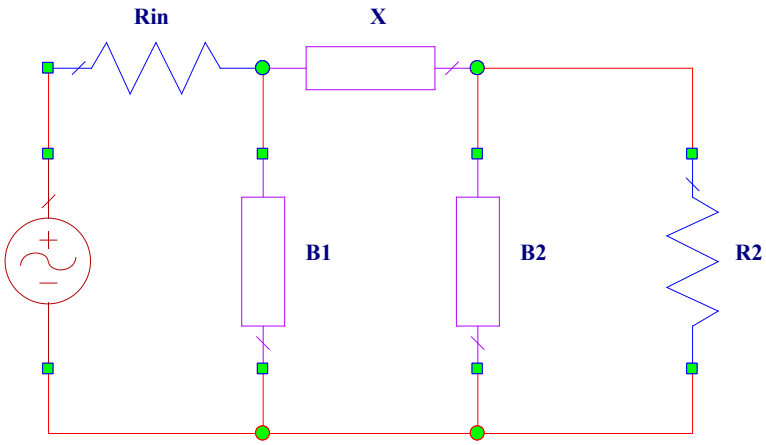


Figure 4. 5: Pi-type matching network

Assuming that the source impedance is purely resistive with a value of $R_1 = 20\ \Omega$ and the load impedance is also resistive with a value of $R_2 = 30\ \Omega$. Since $R_1 < R_2$, therefore, the quality factor Q of the network can be calculated using the following formula [2]:

$$Q = \frac{1}{2}\sqrt{\frac{R_2}{R_1} - 1} \qquad \text{for} \qquad R_1 < R_2 \tag{4.8}$$

$$Q = \frac{1}{2}\sqrt{\frac{30}{20} - 1} = 0.354$$

The first parallel matching susceptance B_1 of the network can be calculated using the following equation [2]:

$$B_1 = \frac{1}{R_1}\sqrt{\frac{R_1}{R_2}(1 + 4Q^2) - 1} \tag{4.9}$$

$$B_1 = \frac{1}{20}\sqrt{\frac{20}{30}(1 + 4 \text{ x } 0.354^2) - 1}$$

Therefore, $\mathbf{B_1 = 1.451 \text{ x } 10^{-3}\ S}$

The series matching reactance X of the network can be determined using the following equation [2]:

$$X = \frac{2QR_2}{1 + 4Q^2} \tag{4.10}$$

$$X = \frac{2 \text{ x } 0.354 \text{ x } 30}{1 + 4 \text{ x } (0.354)^2}$$

Therefore, $\mathbf{X = 14.148\ \Omega}$

The second parallel matching susceptance B_2 of the network can be calculated using the following equation [2]:

$$B_2 = \frac{2Q}{R_2} \tag{4.11}$$

$$B_2 = \frac{2 \text{ x } 0.354}{30}$$

Therefore, $\mathbf{B_2 = 0.024\ S}$

Knowing the centre frequency f_0 of the proposed NGD network which is 1.3 GHz and assuming the resonance frequencies of the parallel- series-parallel sections f_1, f_2 and f_3 respectively, the values of L_1, C_1, L_2, C_2 and L_3, C_3 can be derived as follows:

Assuming that $f_1 < f_o$, for example $f_1 = 0.9\, f_0$, therefore, $\omega_1 = 0.9\, \omega_0$,

$f_2 > f_o$, for example $f_2 = 1.1\, f_0$, therefore, $\omega_2 = 1.1\, \omega_0$,

$f_3 < f_o$, for example $f_3 = 0.88\, f_0$, therefore, $\omega_3 = 0.88\, \omega_0$

The susceptance of the shunt section of the combination of L_1 and C_1 at the operating frequency of f_0 = 1.3 GHz can be derived as follows:

$$B_1 = \omega_0 C_1 - \frac{1}{\omega_0 L_1} \tag{4.12}$$

Knowing that at the resonance $f_1 = \frac{1}{\sqrt{L_1 C_1}}$, therefore, $L_1 = \frac{1}{\omega_1^2 C_1}$

By substituting L_1 and ω_1 into equation 12, B_1 becomes:

$$B_1 = C_1\left(\omega_{0-}\frac{0.9^2\omega_0^2}{\omega_0}\right)$$

$$B_1 = 0.19\ \omega_0 C_1 \tag{4.13}$$

$$1.451 \text{ x } 10^{-3} = 0.19\ x\ 2\pi\ x\ 1.3x\ 10^9 x\ C_1$$

$$\mathbf{C_1 = 0.9\ pF}$$

$$L_1 = \frac{1}{\omega_1^2 C_1} = \frac{1}{0.9^2\omega_0^2 C_1}$$

$$L_1 = \frac{1}{0.9^2\ x\ 4\pi^2 x\ 1.3^2 x 10^{18} x\ 0.9x\ 10^{-12}}$$

$$\boldsymbol{L_1 = 20.5\ nH}$$

The susceptance of the series section of the combination of L_2 and C_2 at the operating frequency of f_0= 1.3 GHz can be derived as follows:

$$B = \frac{1}{X} = \frac{1}{\omega_0 L_2} - \omega_0 C_2 \qquad (4.14)$$

Knowing that at the resonance $f_2 = \frac{1}{\sqrt{L_2 C_2}}$, therefore, $L_2 = \frac{1}{\omega_2^2 C_2}$

By substituting L_2 into equation 14, B becomes:

$$B = \frac{\omega_2^2 C_2}{\omega_0} - \omega_0 C_2$$

$$B = \frac{1}{X} = C_2 \left(\frac{1.1^2 \omega_0^2}{\omega_0} - \omega_0 \right)$$

$$B = 0.21\ \omega_0 C_2 \qquad (4.15)$$

$\frac{1}{14.148}$ = 0.21 x 2π x 1.3 x 10^9x C_2

$$\mathbf{C_2 = 41.2pF}$$

$$L_2 = \frac{1}{\omega_2^2 C_2} = \frac{1}{1.1^2 \omega_0^2 C_2}$$

$$L_2 = \frac{1}{1.1^2 x\ 4\pi^2 x\ 1.3^2 x 10^{18} x\ 41.2\ x\ 10^{-12}}$$

$$\boldsymbol{L_2 = 0.3\ nH}$$

The susceptance of the shunt section of the combination of L_3 and C_3 at the operating frequency of f_0= 1.3 GHz can be derived as follows:

$$B_2 = \omega_0 C_3 - \frac{1}{\omega_0 L_3} \tag{4.16}$$

Knowing that at the resonance $f_3 = \frac{1}{\sqrt{L_3 C_3}}$, therefore, $L_3 = \frac{1}{\omega_3^2 C_3}$

By substituting L_3 and ω_3 into equation 4.16, B_2 becomes:

$$B_2 = 0.2256\omega_0 C_3 \tag{4.17}$$

$$0.024 = 0.2256 \text{ x } 2\pi \text{ x } 1.3 \text{ x } 10^9 \text{x } C_3$$

$$\mathbf{C_3 = 13\ pF}$$

$$L_3 = \frac{1}{\omega_3^2 C_3} = \frac{1}{0.88^2 \omega_0^2 C_3}$$

$$L_3 = \frac{1}{0.88^2\ x\ 4\pi^2 x\ 1.3^2 x 10^{18} x\ 13x\ 10^{-12}}$$

$$\boldsymbol{L_3 = 1.4\ nH}$$

The proposed NGD network using the initial calculated LC values is modelled in the Microwave Office as depicted in Figure 4.6 and its associated reflection coefficient and group delay are plotted in Figure 4.7 and Figure 4.8 respectively. As it can be seen, the calculated values of the LC resonators of the proposed NGD network give a good starting point in terms of an increasing reflection phase by 65 degrees in the frequency range from 1.2 to 1.28 GHz. However, the NGD network suffers from about 16 dB loss. Moreover, the proposed NGD network generates an NGD of - 4.34 ns over a bandwidth of 0.08 GHz from 1.2 to 1.28 GHz.

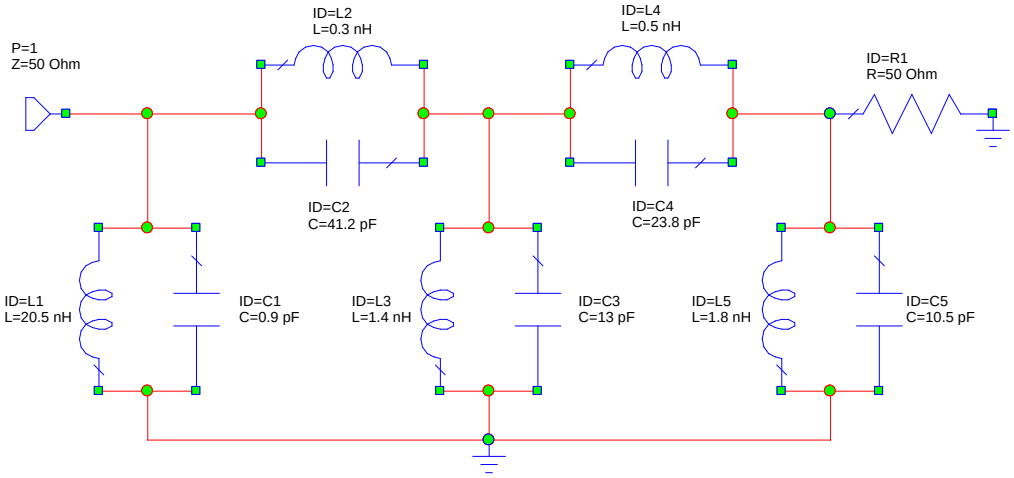


Figure 4. 6: Schematic layout of the proposed ideal reflection- type NGD network using the calculated values of the 5 sections LC resonators

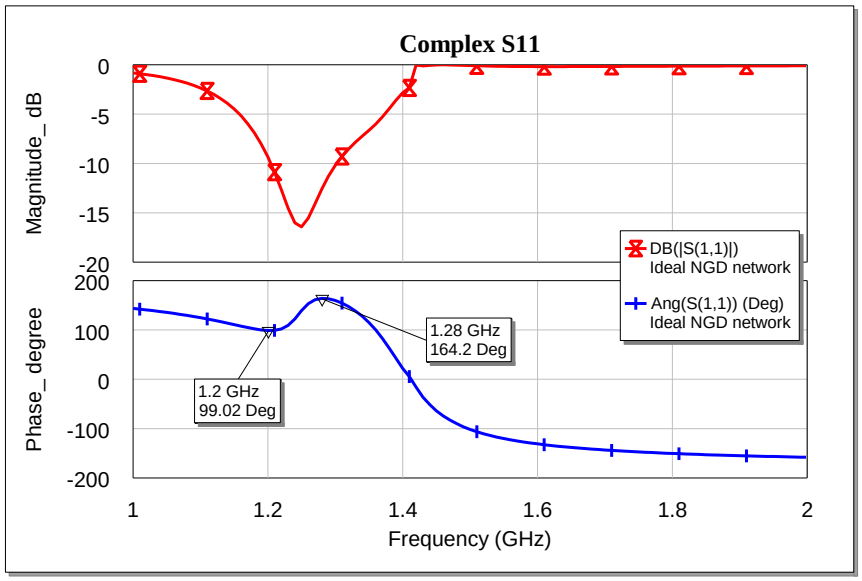


Figure 4. 7: Simulated reflection coefficient (S_{11}) phase and magnitude of the proposed ideal NGD network using the calculated values of the 5 sections LC resonators

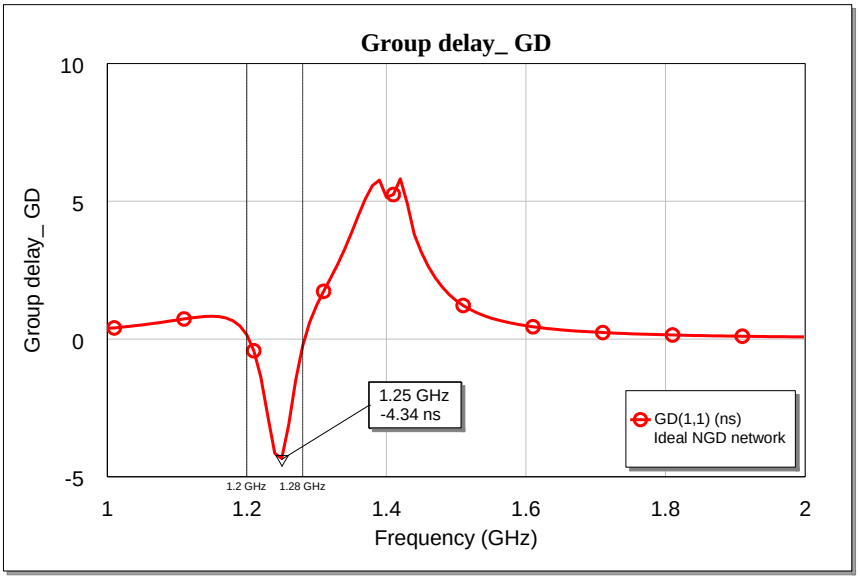


Figure 4. 8: Simulated group delay (GD) of the ideal NGD network using the calculated values of the 5 sections LC resonators

Consequently, Modelithics models of Coilcraft CLC 0603CS inductors and ATC 600S capacitors are employed in the simulation to obtain more accurate results. Moreover, tuning the values of the LC was carried out using Microwave Office for optimising the designs. This implementation uses a Taconic RF_35_0600 substrate with relative permittivity $\varepsilon_r = 3.5$ and a dielectric thickness H = 1.52 mm. The circuit schematic of the proposed NGD circuit using realistic LC components without transmission line sections is depicted in Figure 4.9. The associated reflection coefficient magnitude and phase responses for the NGD network are presented as a comparison in Figure 4.10. As it can be seen, the NGD circuit has NGD behaviour over a bandwidth of 0.45 GHz from 1.24 to 1.69 GHz with an increasing reflection phase by 42 degrees. This positive slope in the phase variation with frequency

indicates NGD behaviour and implies that the NGD network is acting as a non-Foster circuit in that certain bandwidth. However, the NGD network generates about 6 dB losses. These inherent losses can be compensated by amplifications. Furthermore, the group delay (GD) response obtained from the proposed NGD network is shown in Figure 4.11. The NGD circuit generates an NGD of - 0.6 ns over a bandwidth of 0.45 GHz from 1.24 to 1.69 GHz.

Table 4.1 presents a comparison between the reflection-type NGD networks realised from the initial calculated LC values and the optimised structure using realistic LC components in term of the realisable bandwidth, losses, reflection coefficient phase and group delay.

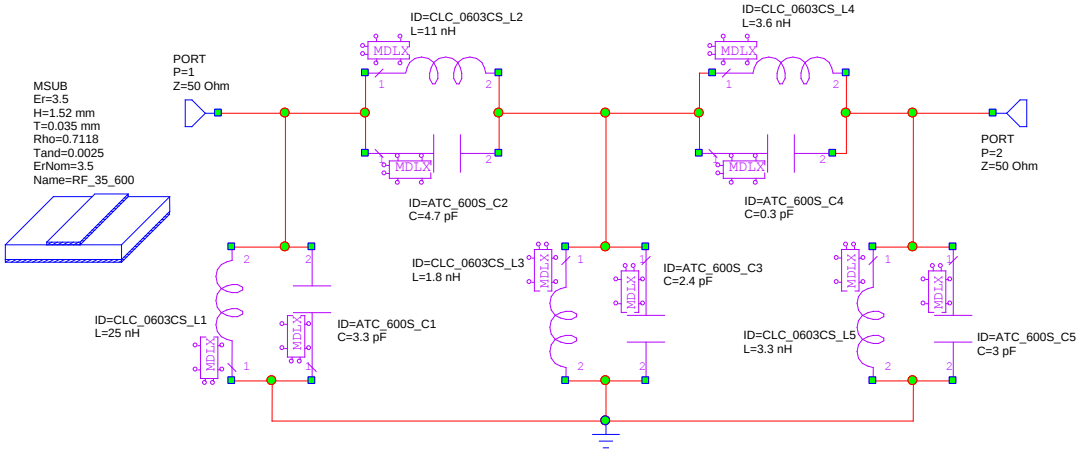


Figure 4. 9: Circuit schematic of the optimised reflection- type NGD network

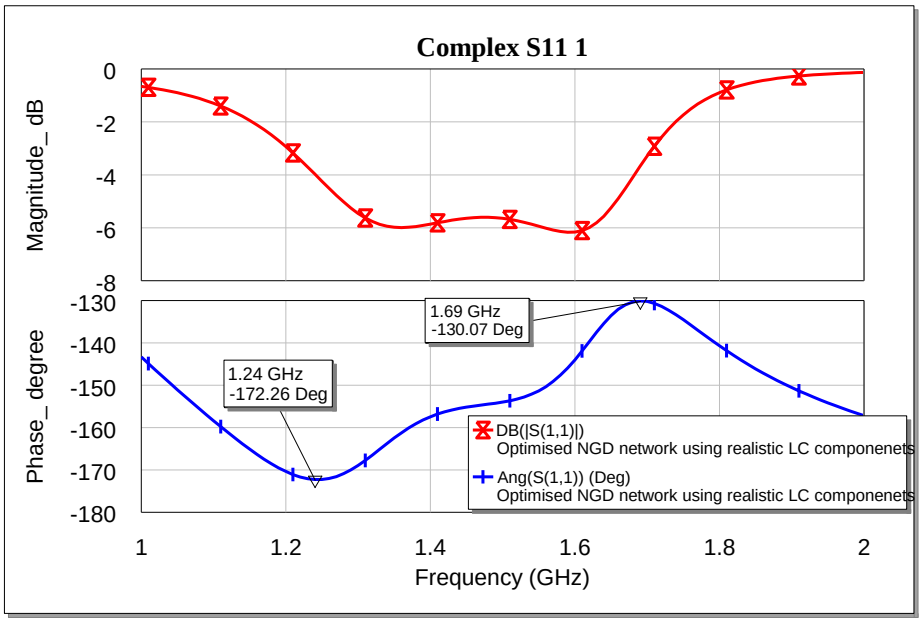


Figure 4. 10: Simulated reflection coefficient (S_{11}) phase and magnitude of the optimised NGD network

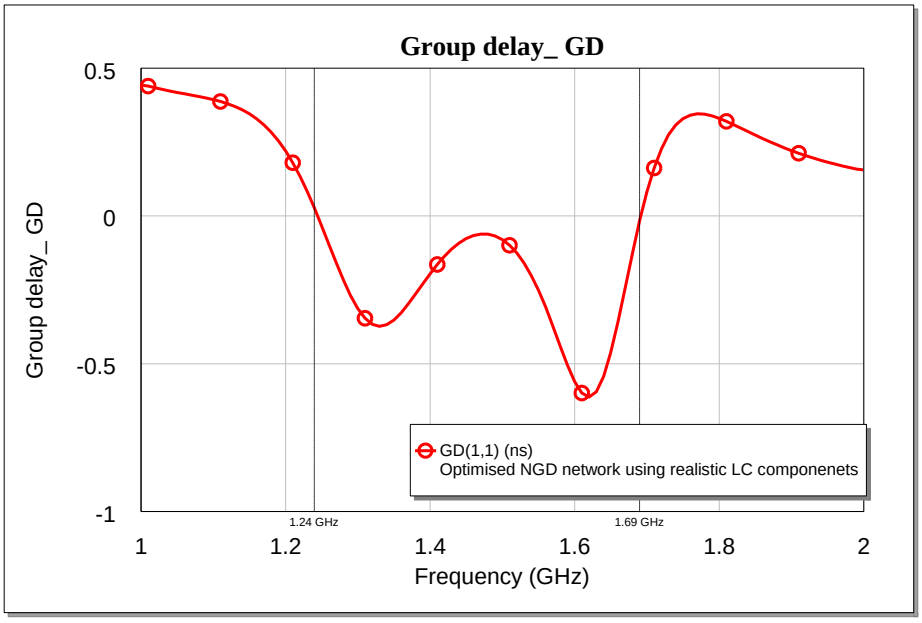


Figure 4. 11: Simulated group delay (GD) of the optimised NGD network

Table 4. 1: Summary of the performance of the realised reflection-mode NGD networks

NGD network	Realisable NGD Bandwidth	Losses dB	S_{11} Phase increased by	Group delay
Using the initial calculated LC values	70 MHz between 1.2- 1.28 GHz	16 dB	65 degrees	-4.34 ns
The optimised structure using realistic LC components	450 MHz between 1.24- 1.69 GHz	6 dB	42 degrees	- 0.65 ns

4.3 Design and Experimental Verification of Realistic Reflection-Type NGD Network

The implementation of a novel structure of a reflection-type NGD network in the range of 1 GHz to 2 GHz is presented. An ideal non-Foster network was modelled using an equivalent circuit of a negative capacitor in shunt with a negative inductor as depicted in Figure 4.12. This non-Foster element produces an image impedance of 50 Ω over a wide bandwidth and is suitable for antenna matching networks. A two-port realistic reflection-type NGD network has been designed with the aid of Microwave Office, fabricated and experimentally validated. This implementation uses a Taconic RF_35_0600 substrate with relative permittivity $\varepsilon_r = 3.5$ and a dielectric thickness $H = 1.52$ mm. A schematic of an ideal reflection- type NGD network structure is presented in Figure 4.13. To obtain more accurate results, realistic Modelithics models of ATC 600S capacitors and Coilcraft CLC 0603CS inductors are employed in the simulation amongst distributed microstrip transmission line sections. The values used for the Modelithics models are listed in Table 4.2 and their datasheets are presented in Appendix A. The circuit schematic, its associated layout and the fabricated prototype image of the proposed NGD circuit connected to two 50 Ω measurement ports are depicted in Figures 4.14, 4.15 and 4.16 respectively.

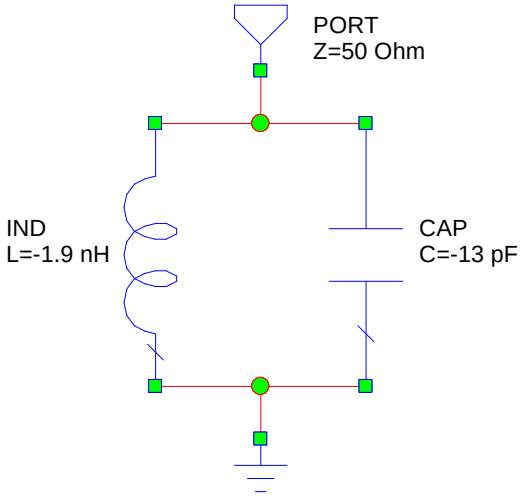


Figure 4. 12: An ideal non-Foster network is modelled using an equivalent circuit of a negative capacitor in shunt with a negative inductor

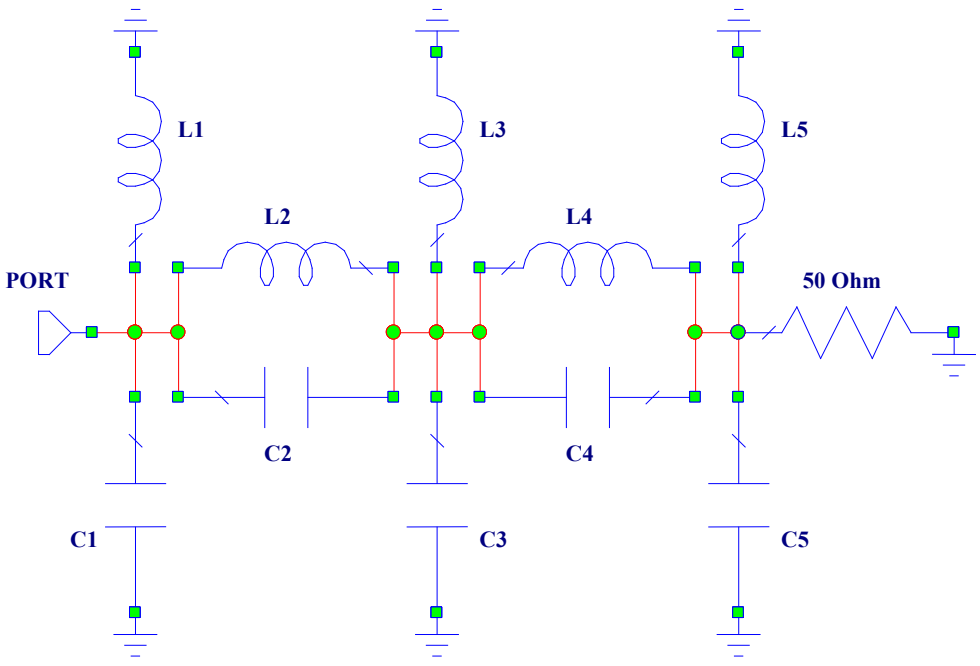


Figure 4. 13: Circuit schematic of the ideal reflection-mode NGD network

Table 4. 2: Component values and manufacturer for this implementation

Component	Value	Manufacturer
L1	10.2nH	Coilcraft_ CLC_0603CS
L2	6.8nH	Coilcraft_ CLC_0603CS
L3	3.2nH	Coilcraft_ CLC_0603CS
L4	1.8nH	Coilcraft_ CLC_0603CS
L5	6.8nH	Coilcraft_ CLC_0603CS
C1	2.7pF	ATC_600S
C2	2.4pf	ATC_600S
C3	0.7pF	ATC_600S
C4	0.6pF	ATC_600S
C5	1.3pF	ATC_600S

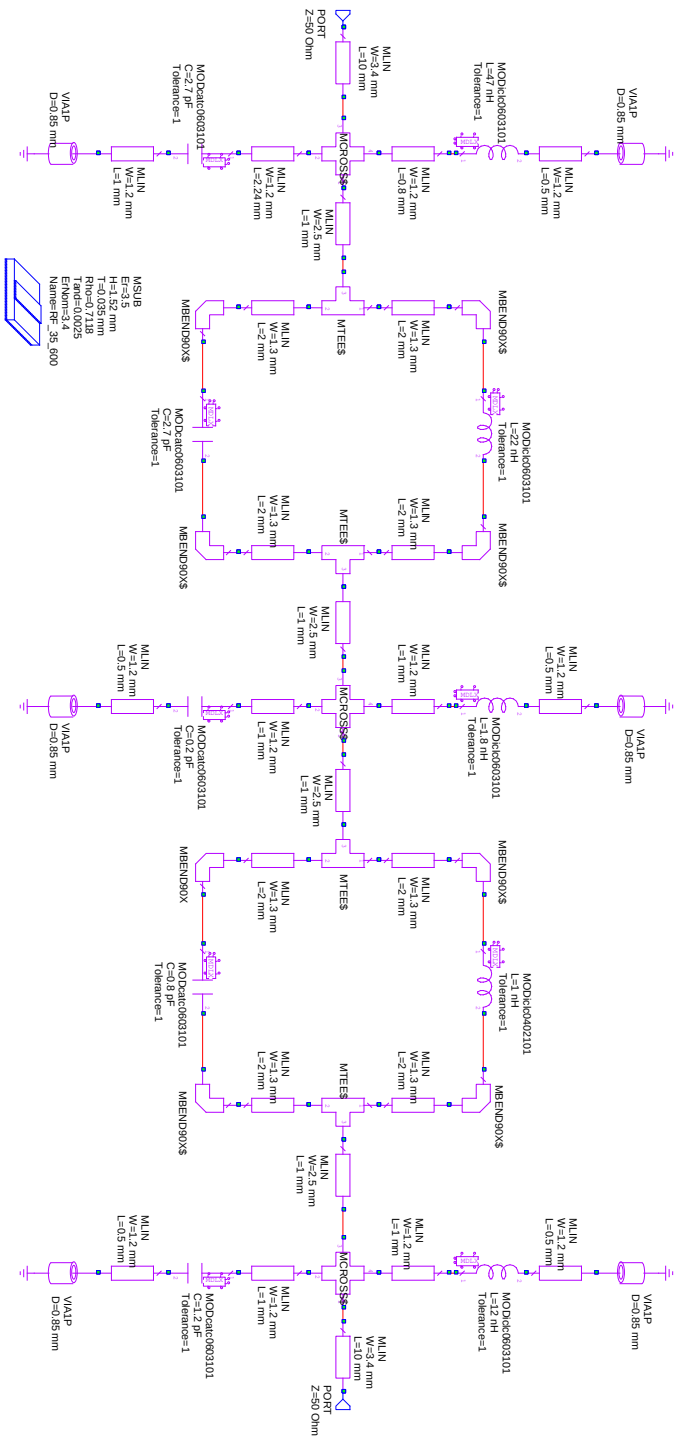


Figure 4. 14: Circuit schematic of the realistic reflection-mode NGD network with distributed transmission lines

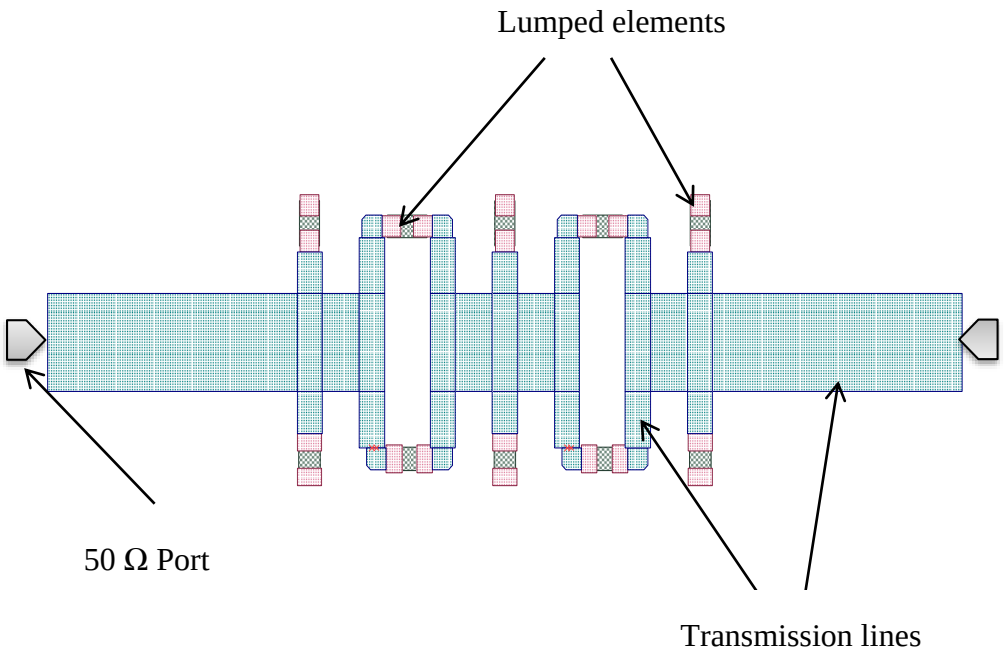


Figure 4. 15: Circuit layout of the NGD network

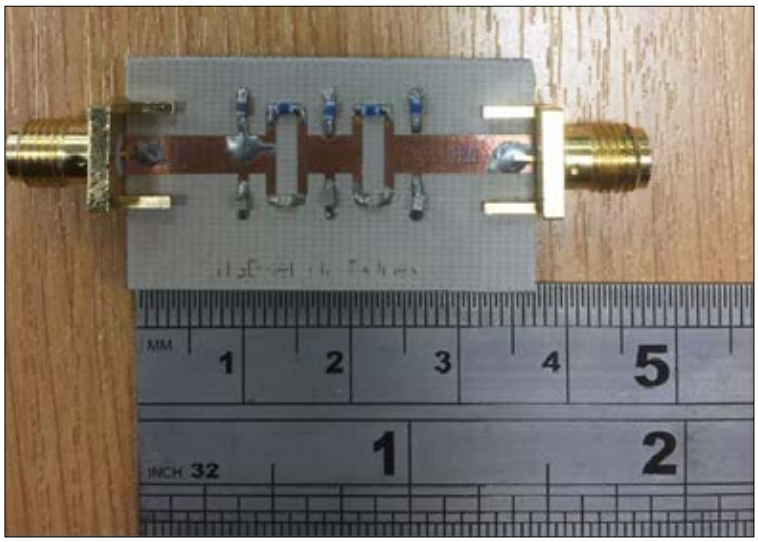


Figure 4. 16: Image of the NGD network prototype

The reflection coefficient (S_{11}) phase and magnitude from measurement and simulation are compared with an ideal non-Foster network in Figure 4.17. It should be noted that the measurement results of the NGD prototype are presented using the extracted S-parameters from the vector network analyser VNA. To distinguish between the demonstrated results, the simulation results are represented in a continuous trace and the experimental results are represented by a dashed trace. In the frequency range from 1.2 GHz- 1.37 GHz both measured and simulated results closely follow that of the ideal non-Foster network with an increasing reflection phase by 27.3 degrees as depicted in Figure 4.17, which indicates NGD behaviour in that bandwidth. However, there are about 10 dB losses associated with the NGD networks which need be compensated. A novel technique involving a reflection amplifier and a Lange coupler will be used for this purpose in the next chapter. Moreover, the locus of the synthesised negative slope of the NGD network is plotted on the Smith chart in Figure 4.18. It shows that the reactance is decreasing with increasing frequency from 1.2 GHz to 1.37 GHz and also rotates counter clockwise. Furthermore, the obtained group delays (GD) from both results are plotted in Figure 4.19. The measured prototype exhibits a negative group delay of -1.62 ns over the NGD bandwidth of 0.3 GHz. Moreover, the simulated model generates an NGD of -0.93 ns over the bandwidth of 0.14 GHz. It should be clarified that the proposed NGD network here is simulated and measured with extra lengths of microstrip transmission lines to be connected with the SMA connectors and they will be de-embedded on the final synthesised non-Foster reactive NGD element, which will be introduced in Chapter 5.

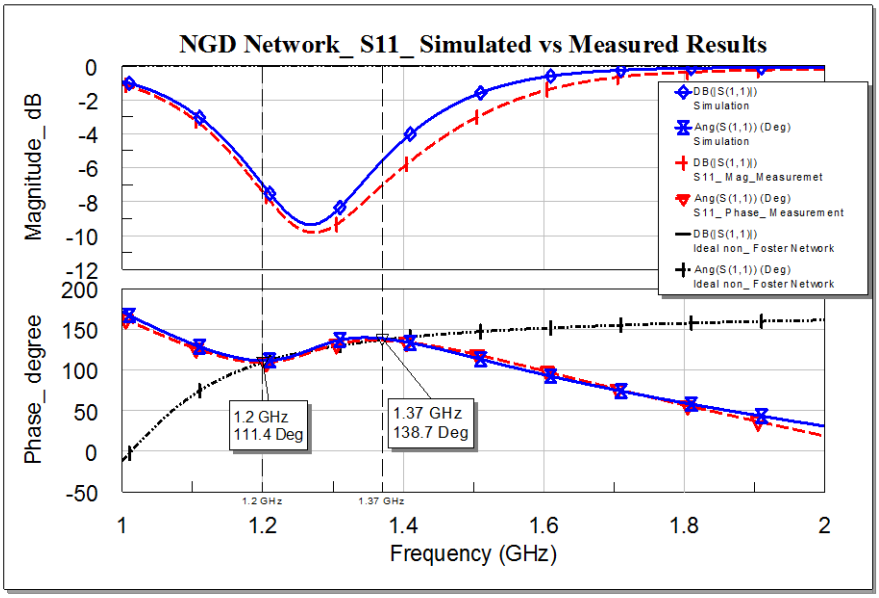


Figure 4. 17: The S_{11} magnitude and phase plots of the NGD network from simulation and experiment

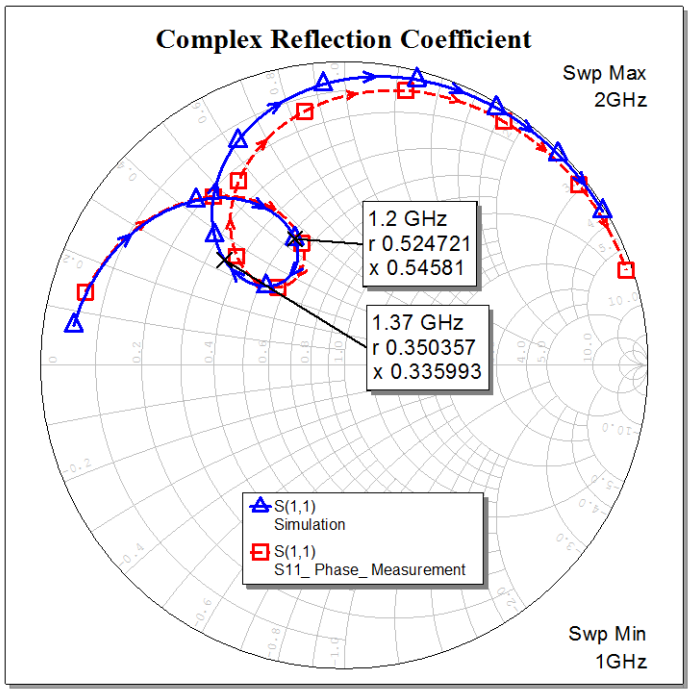


Figure 4. 18: Simulation and measurement results of the complex reflection coefficient plotted on the Smith chart

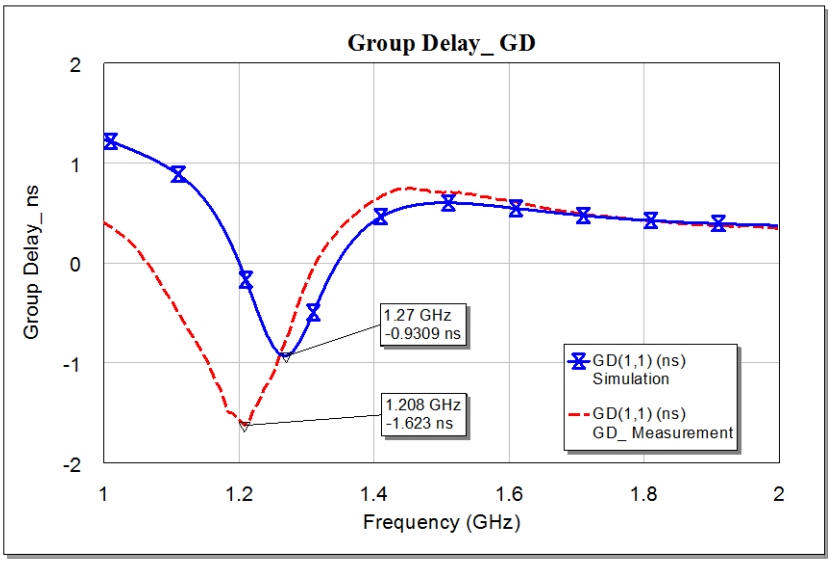


Figure 4. 19: Simulated and measured group delay (GD) responses obtained from the realistic reflection-type NGD network

Table 4.3 summarises the performance of the realised reflection type NGD-network using LC resonators in term of the realisable bandwidth, losses, reflection coefficient phase and group delay.

Table 4. 3: Summary of the performance of the realised reflection-mode NGD network using LC resonators

Prototype	Realisable NGD Bandwidth	Losses dB	S_{11} Phase increased by	Group delay
NGD-based non-Foster circuit using LC resonators	170 MHz between 1.2- 1.37 GHz	10 dB	27.3 degrees	-1.62 ns

4.4 Reflection–Type NGD Network Design Using Open and Short Shunt Stubs

NGD behaviour can be synthesised, using circuits with distributed elements as an alternative way to overcome the lumped elements' limitations such as poor quality at high frequencies and the mechanical implementations difficulties when soldering these elements. Herein, a systematic approach based on the implementation of the shunt LC resonators as open and short transmission line stubs is introduced. To design open and short stubs which act as capacitors and inductors, the electrical length (θ_s) of the stubs must be determined from known capacitors and inductors values. The design methodology in its entirety is presented based on analytical equations and an example is presented to demonstrate how the electrical lengths of the open and shorted circuited stubs are calculated.

Firstly, determining the electrical length of an open stub to act as a capacitor as follows:

The reactance (X_c) of a given capacitor for example with a value of (C= 12 pF) at an operating frequency of 1.3 GHz is calculated as follows:

$$X_c = \frac{-1}{2\pi f C}$$

$$X_c = \frac{-1}{2\pi x 1.3 x 10^9 x 12 x 10^{-12}} = -10.2\ \Omega$$

Now the reactance of the capacitor (X_c) is equilised with the reactance of an open stub (X_{stub}) as follows:

$$X_c = X_{stub}$$

Where,

$$X_{stub} = \frac{-Z_s}{tan\theta_s}$$

Where, Z_s is the characteristic impedance of the stub and is assumed to be 50 Ω.

Therefore,

$$-10.2 = \frac{-50}{tan\theta_s}$$

Therefore, the electrical length of the stub is ($\theta_s = 78.5\ degrees$)

Secondly, finding the electrical length of a short circuit stub to act as an inductor as follows:

The reactance (X_l) of a given inductor for example with a value of (L= 3.6nH) at an operating frequency of 1.3 GHz is calculated as follows:

$$X_l = 2\pi fL$$

$$X_l = 2\pi \; x \; 1.3 \; x \; 10^9 x \; 3.6 \; x \; 10^{-9} = 29.4 \; \Omega$$

$$X_l = X_{stub}$$

$$X_l = Z_s tan\theta_s$$

$$29.4 = 50 \; tan\theta_s$$

$$tan\theta_s = 0.588$$

Therefore, the electrical length of the stub $\theta_s = 30.5 \; degrees$.

This design procedure was carried out to the shunt LC resonators of the NGD network of Fig 4.20. Consequently, fine tuning for the values of the electrical length of the stubs was carried out for optimising the NGD structure with the aid of Microwave Office. A circuit schematic of the proposed NGD circuit using ideal components is depicted in Figure 4.16. Moreover, a realistic NGD network has been designed using Microwave Office, fabricated and tested. The implementation uses a Taconic RF_35_0600 substrate with relative permittivity Ɛr = 3.5 and dielectric

thickness H = 1.52 mm. To obtain more accurate results, realistic Modelithics models of ATC 600S capacitors and Coilcraft CLC 0603CS inductors are employed in the simulation amongst distributed microstrip transmission line sections. The circuit schematic, structure layout and the image of the prototype are depicted in Figures 4.21, 4.22 and 4.23, respectively.

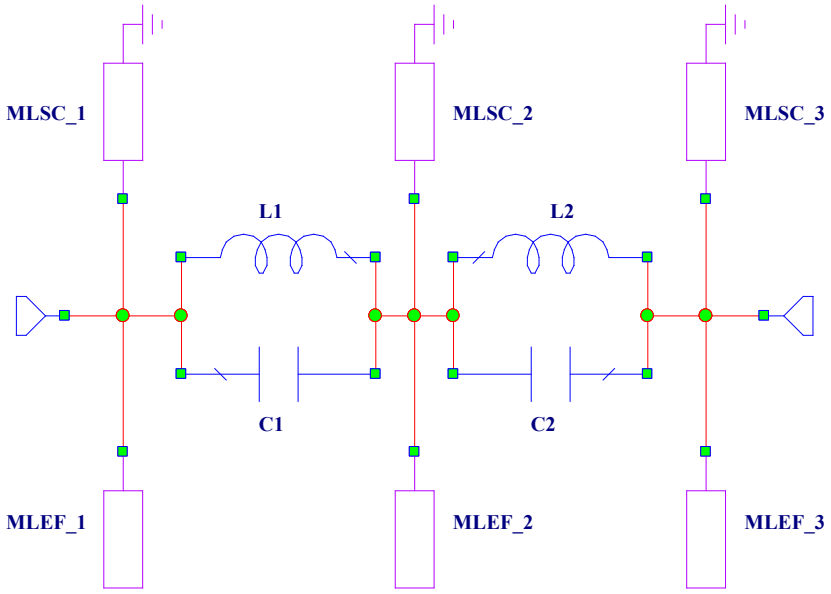


Figure 4. 20: Circuit schematic of the NGD network realised using ideal components, where, MLSC denotes to a short microstrip line stub and MLEF denotes to an open microstrip line stub.

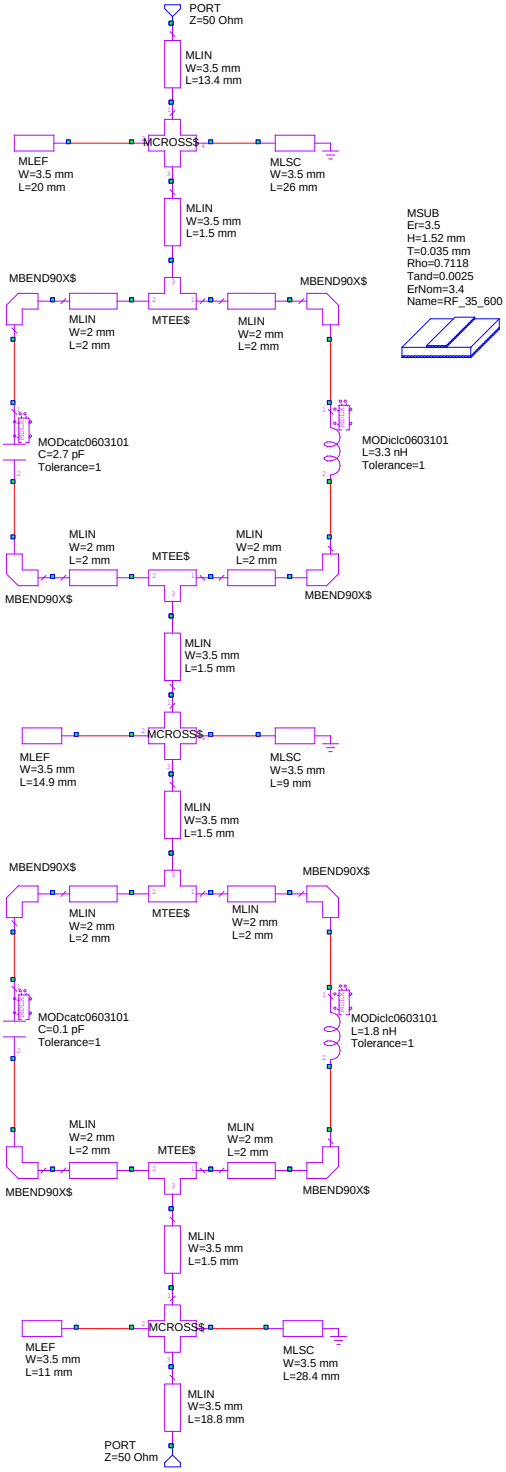


Figure 4. 21: Circuit schematic of the NGD network realised using open-short stubs

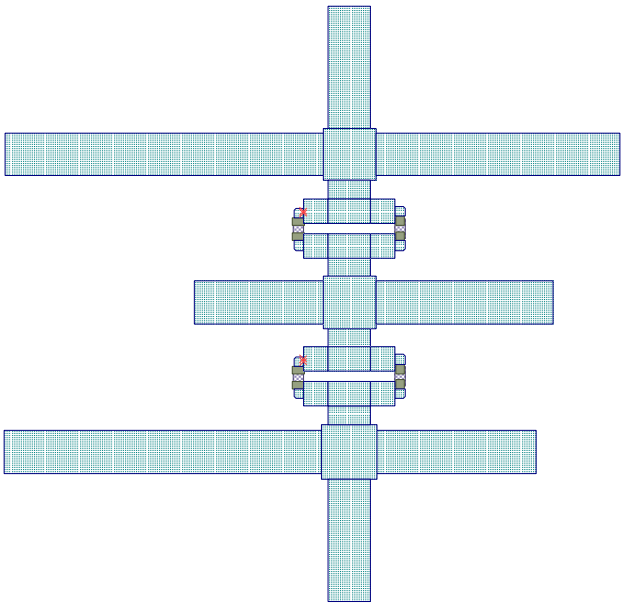


Figure 4. 22: NGD network circuit layout

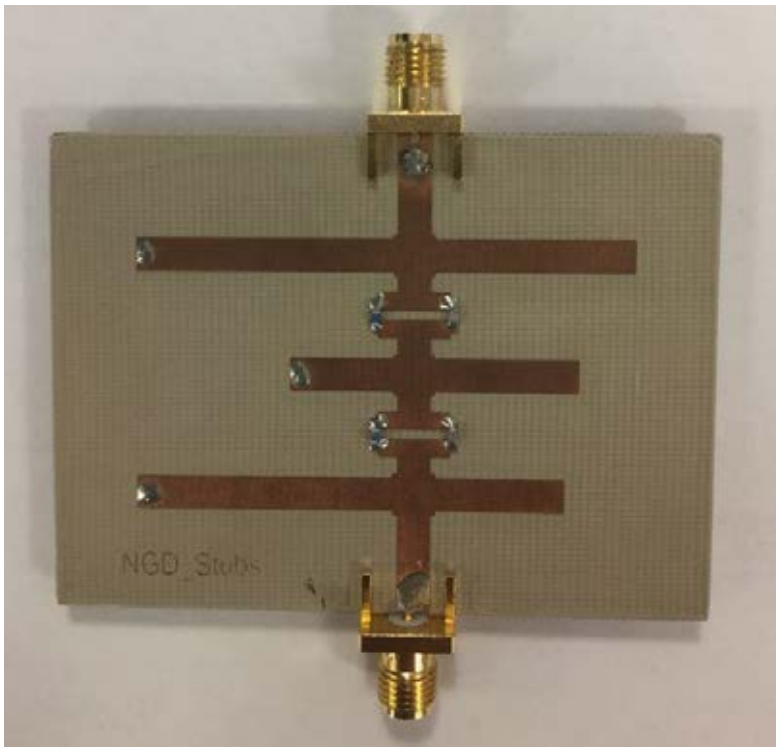


Figure 4. 23: Image of the NGD network prototype

The responses of the phase in degrees and magnitude in dBs of the S_{11} obtained from simulation and experiment are compared with each other and plotted in Figure 4.24. The measurement results of the NGD prototype are presented using the extracted S-parameters from the vector network analyser VNA. Both results are in good agreement and showing NGD behaviour with an NGD bandwidth of 116 MHz and a positive reflection phase gradient with frequency from 1.32 – 1.47 GHz by 25.6 degrees. However, this NGD network is a "lossy" structure and has about 8 dB, an inherent loss which needs to be compensated. Both results of the associated reflection coefficient are plotted on the Smith chart in Figure 4.25. From the graph, we can see the rotations of the reactances are rotating anti-clockwise and decreasing with increasing frequency.

The obtained group delay (GD) results from simulation and measurement are compared in Figure 4.26. Both measured and simulated results generate NGD level of about -0.65 ns at a bandwidth of 0.15 GHz and -0.86 at a bandwidth of 0.15 GHz respectively. Table 4.3 gives a comparison between the proposed NGD networks in term of the realisable bandwidth, losses, reflection coefficient's phase and group delay.

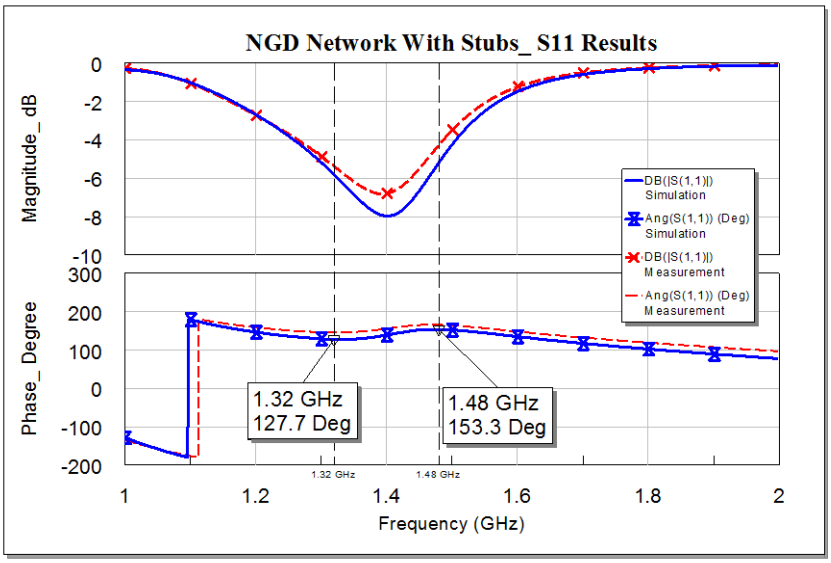


Figure 4. 24: Simulated and measured results of S_{11} magnitude and phase of the reflection-type NGD network realised using stubs

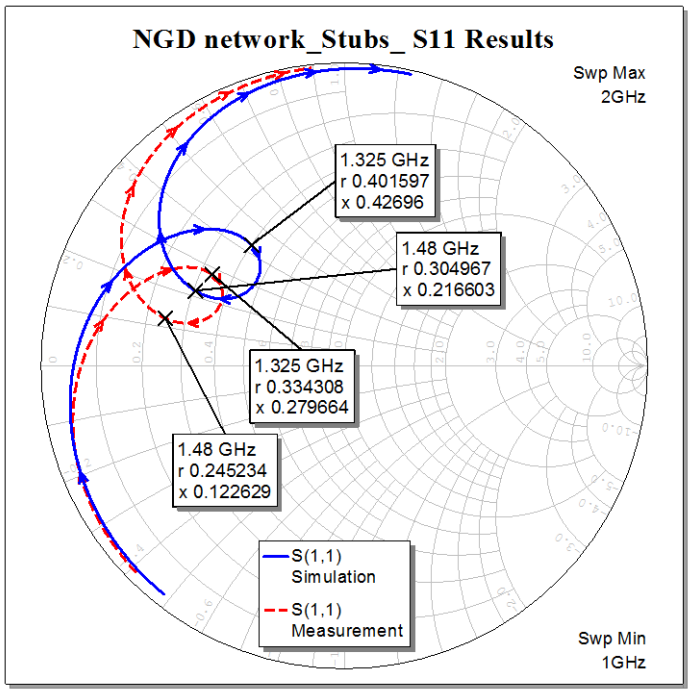


Figure 4. 25: Simulation and measurement results of the complex reflection coefficient (S_{11}) plotted on the Smith chart

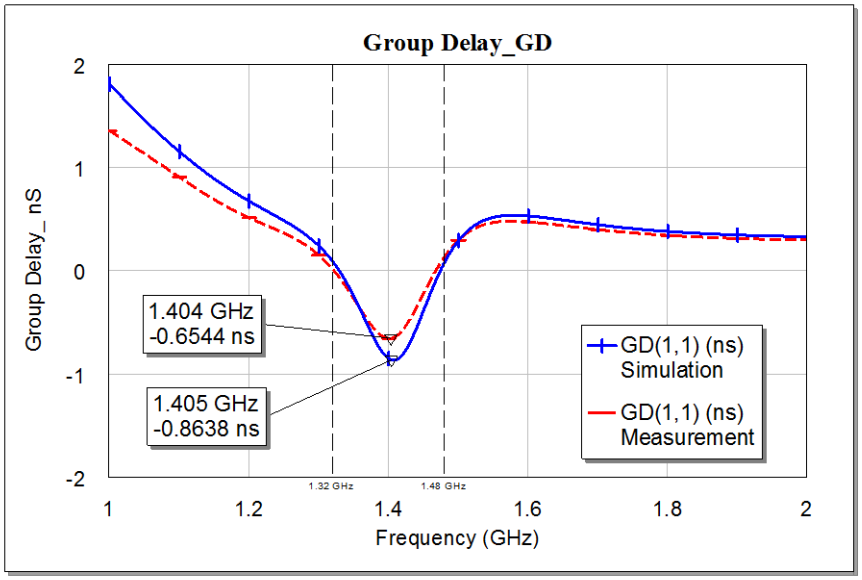


Figure 4. 26: Simulated and measured group delay (GD) responses obtained from realistic reflection-type NGD network using stubs

Table 4. 4: Summary of the performance of the realised reflection-mode NGD networks

Prototype	Realisable NGD Bandwidth	Losses dB	S_{11} Phase increased by	Group delay
Reflection-type NGD network using LC resonators	170 MHz between 1.2- 1.37 GHz	10 dB	27.3 degrees	-1.62 ns
Reflection-type NGD network using stubs	116 MHz between 1.48- 1.32 GHz	8 dB	27.3 degrees	-0.65 ns

4.5 Summary

This chapter has presented a new method for the design of reactive networks with non-Foster behaviour. The concept of the proposed NGD network was augmented with a design methodology based on analytical equations to quantify its operation.

The realised NGD network using the initial calculated LC values gave a good starting point in term of increasing S_{11} phase at the desired frequency range. Consequently, an optimised NGD structure using realistic LC components was designed. Both ideal circuits generated NGD behaviour at the frequency range of interest.

Finally, a realistic reflection-mode NGD network was designed by implementing LC resonators in five sections along with transmission lines forming a "lossy" network with counter-clockwise phase response. In addition, another NGD network model was designed using open and short stubs. As a proof of concept, both prototypes were experimentally validated.

Results from simulation and experiment were in good agreement. Studying the S-parameters of both reflection-type NGD circuits reveals that the phase of S_{11} is an increasing function of frequency, which implies non-Foster behaviour at that bandwidth. Both reflection-types NGD networks using LC resonators and stubs exhibit NGD behaviour of -1.62 ns over a bandwidth of 0.3 GHz and -0.65 ns over a bandwidth of 0.15 GHz respectively.

It was also observed that by cascading more lumped elements sections in the design of the NGD networks, the phase response increases due to the associated losses. Therefore, five LC sections were considered as a working practical compromise. A new perspective in the realisation of NGD networks, with zero loss in a certain bandwidth, which involves a reflection amplifier and a Lange coupler for compensating the NGD networks losses, is presented in Chapter 5.

References

[1] S. Yichuang and J. K. Fidler, "Design of /spl Pi/ impedance matching networks," in Proceedings of IEEE International Symposium on Circuits and Systems - ISCAS '94, 1994, pp. 5-8 vol.5.

[2] M. Şengül and G. Yeşilyurt, "Real frequency design of Pi and T matching networks with complex terminations," in 2017 10th International Conference on Electrical and Electronics Engineering (ELECO), 2017, pp. 1328-1331

CHAPTER 5

SYNTHESISED NON-FOSTER REACTIVE ELEMENTS USING LOSS-COMPENSATED REFLECTION-MODE NGD NETWORKS

This chapter introduces a novel technique to compensate the inherent losses of the NGD networks in the reflection mode. Key steps in the methodology including the design of a negative resistance reflection amplifier and a Lange coupler are investigated and experimentally validated. The advantage of this novel design is that the overall NGD response is provided by passive circuits which should make it easier to achieve stable behaviour. The reflection amplifier is connected the isolated port of the coupler to provide the required gain that compensates the losses. The proposed technique can be very attractive in antenna matching applications where both transmit and receive capabilities are required.

5.1 A Novel Loss Compensation Technique for Reflection-mode NGD Networks

This section introduces a new methodology for compensating the losses of the NGD networks. It is realised by combining two "lossy" reflection-type NGD networks and a negative resistance reflection amplifier with a 3 dB quadrature hybrid coupler in a

balanced structure. The operating principle of the adopted technique presented in Figure 5.1 is augmented with design equations quantifying their operation and presenting the design methodology in its entirety.

The effective input reflection coefficient at the input port (Γ_{in}) of the coupler is:

$$\Gamma_{in} = \frac{b_1}{a_1} \tag{5.1}$$

The wave emerging out of the input port is b_1 can be written as :

$$b_1 = S_{11}a_1 + S_{12}a_2 + S_{13}a_3 + S_{14}a_4 \tag{5.2}$$

To determine b_1, it is necessary to find out the incident waves (a_2, a_3 and a_4) which go into the individual ports 2, 3 and 4 of the coupler first , meaning that find out a_2, a_3 and a_4 in terms of a_1.

$$a_2 = \Gamma_{NGD}b_2 \tag{5.3}$$

Where, Γ_{NGD} is the reflection coefficient of the NGD network at port 2.

$$a_3 = \Gamma_{RA} b_3 \tag{5.4}$$

Where, Γ_{RA} is the reflection coefficient of the reflection amplifier at port 3.

$$a_4 = \Gamma_{NGD} b_4 \tag{5.5}$$

Where, Γ_{NGD} is the reflection coefficient of the NGD network at port 4. Assuming that the coupler is an ideal 3dB reciprocal coupler, thus,

$$S_{11} = S_{22} = 0$$

$$S_{12} = S_{21} = -0.707$$

$$S_{13} = S_{31} = 0$$

$$S_{14} = S_{41} = -j0.707$$

$$S_{23} = S_{32} = -j0.707$$

$$S_{24} = S_{42} = 0$$

$$S_{34} = S_{43} = -0.707$$

By substituting S_{11}, S_{12}, S_{13} and S_{14} into euqation 2, b_1 becomes:

$$b_1 = S_{12}a_2 + S_{14}a_4$$

$$b_1 = -0.707a_2 - j\,0.707a_4$$

$$\mathbf{b_1 = -0.707(a_2 + ja_4)} \qquad (5.6)$$

To find out a_2, and a_4, b_2 and b_4 must be determined first

$$b_2 = S_{21}a_1 + S_{22}a_2 + S_{23}a_3 + S_{24}a_4$$

As, $S_{21} = -0.707$, $S_{22} = 0$, $S_{23} = -j0.707$ and $S_{24} = 0$, Thus, b_2 becomes:

$$b_2 = S_{21}a_1 + S_{23}a_3$$

$$b_2 = -0.707a_1 - j\,0.707a_3$$

$$\mathbf{b_2 = -0.707(a_1 + ja_3)}$$

By substituting $b_2$into equation 3, a_2 becomes:

$$\mathbf{a_2 = -0.707\,\Gamma_{NGD}(a_1 + ja_3)}$$

To find out b_4

$$b_4 = S_{41}a_1 + S_{42}a_2 + S_{43}a_3 + S_{44}a_4$$

As, $S_{41} = -j0.707$, $S_{42} = 0$, $S_{22} = 0$, $S_{43} = -0.707$ and $S_{44} = 0$,Thus, b_4 becomes:

$$b_4 = S_{41}a_1 + S_{43}a_3$$

$$b_4 = -j0.707a_1 - 0.707a_3$$

$$\mathbf{b_4 = -0.707(\,ja_1 + a_3)}$$

By substituting $b_4$into equation 4, a_4 becomes:

$$\mathbf{a_4 = -0.707\,\Gamma_{NGD}(ja_1 + a_3)}$$

By substituting a_2 and a_4 into equation 6, b_1 becomes:

$$\mathbf{b_1 = -0.707(a_2 + ja_4)}$$

$$b_1 = -0.707[-0.707\,\Gamma_{NGD}(a_1 + ja_3) - 0.707\,\Gamma_{NGD}(ja_1 + a_3)]$$

$$b_1 = 0.707x0.707\,\Gamma_{NGD}[\,(a_1 + ja_3) + j(ja_1 + a_3)]$$

$$b_1 = 0.707x0.707\,\Gamma_{NGD}[a_1 + ja_3 - a_1 + ja_3]$$

$$\mathbf{b_1 = ja_3\Gamma_{NGD}} \qquad (5.7)$$

To find out a_3, b_3 must be determined first

$$b_3 = S_{31}a_1 + S_{32}a_2 + S_{33}a_3 + S_{34}a_4$$

As, $S_{31} = 0$, $S_{32} = -j0.707$, $S_{33} = 0$ and $S_{34} = -0.707$, Thus, b_3 becomes:

$$b_3 = S_{32}a_2 + S_{34}a_4$$

$$\mathbf{b_3 = -j0.707a_2 - 0.707a_4}$$

$$b_3 = -j0.707[-0.707\Gamma_{NGD}(a_1 + ja_3)]$$
$$- 0.707[-0.707\,\Gamma_{NGD}(ja_1 + a_3)]$$

$$b_3 = j0.707x0.707\,\Gamma_{NGD}a_1 - 0.707x0.707\Gamma_{NGD}a_3$$
$$+ j0.707x0.707\,\Gamma_{NGD}a_1 + 0.707x0.707\Gamma_{NGD}a_3$$

$$\mathbf{b_3 = j\,\Gamma_{NGD}a_1}$$

By substituting b_3 into equation 4, a_3 becomes:

$$a_3 = \Gamma_{RA} b_3$$

$$\mathbf{a_3 = j\Gamma_{RA}\,\Gamma_{NGD} a_1}$$

By substituting a_3 into equation 7, b_1 becomes:

$$\mathbf{b_1 = j a_3 \Gamma_{NGD}}$$

$$b_1 = -\Gamma_{RA}\Gamma_{NGD}\Gamma_{NGD} a_1$$

By substituting b_1 into equation 1, Γ_{in} can be found

$$\Gamma_{in} = \frac{b_1}{a_1}$$

$$\mathbf{\Gamma_{in} = -\Gamma_{RA}\Gamma_{NGD}^2} \qquad (5.8)$$

Therefore, equation (5.8), mathematically presented the concept of the proposed loss compensation technique demonstrated in Figure 5.1. The reflection coefficient of the received signal at the input port is a result of the reflection coefficients of the reflection amplifier in addition to the two NGD networks. Moreover, the effect of the NGD behaviour of the realised NGD-based non-Foster circuit is the double effect of the NGD devices as a result of sending the signal through them twice in a balanced structure. The direct and coupled ports of the coupler are both connected to reflection-type NGD networks. The reflected signals passing back into the coupler recombine at the isolation port and are amplified by the FET reflection amplifier. The amplified signals pass back into the coupler, reflecting again from the NGD devices, finally recombining at the coupler input port.

In order to make the combining effect work, as the coupling ratio is low and the structure is reciprocal, then the vast majority of the reflected signal from the output ports goes to the isolated port (port 3) because there is no cancellation of the direct reflection and the magnitude S_{41} is much smaller than the S_{21} magnitude. If the hybrid coupler can achieve a coupling factor of 3 dB then the two reflected signals from the NGDs would be 180 degrees out of phase and will cancel each other. If the coupling ratio is not 3 dB then the reflected signal from ports 2 and 4 are not equal. Therefore, they won't perfectly cancel out. In this work, a 3 dB hybrid coupler is employed in the design of the NGD-based reactive non-Foster element.

The new loss compensation method involves three separate components, named above, in the design to form the final synthesised non-Foster NGD circuit. Although the final loss compensated NGD-based non-Foster network is working fine using simulation, because of the involvement of different components and the employment of an active circuit in the design, it is difficult to identify the problem if all the components together are fabricated on the same board the first time. Therefore, each circuit has been modelled, built, tested and evaluated separately to verify that it is working as expected and the modelling approach is correct.

Moreover, having a systematic design methodology by characterising the parasitic positive group delay (PGD) in the reflection amplifier and the coupler will result in known how much negative group delay needed when the NGD network is designed to over compensate for the PGD. This can be potentially done as a further study. Simulation and experimental results for the individual components are presented and evaluated. Subsequently, all the aforementioned components are integrated together in a balanced structure to construct the final synthesised one-port non-Foster element.

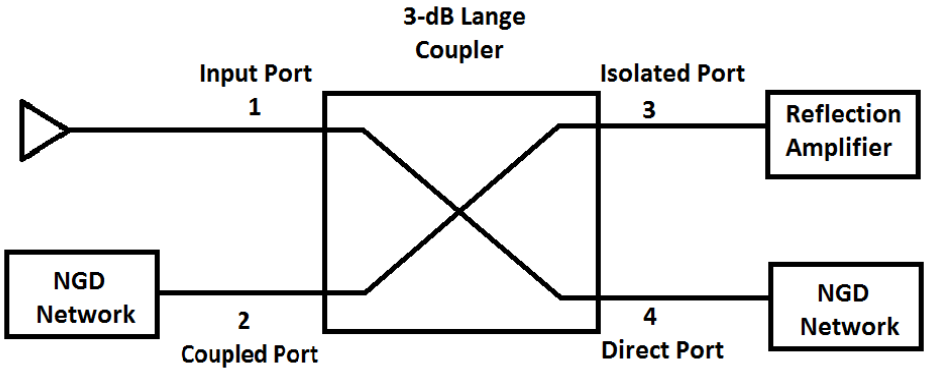


Figure 5.1: Loss-compensated NGD network using reflection amplifier procedure

5.2 Negative Resistance Reflection Amplifier Design and Experiment

The first key step in the implementation of the compensation technique for the realisation of the final synthesised non-Foster reactive element is the design of the negative resistance reflection amplifier. In references [1] and [2], the employment of microwave transistors in negative resistance reflection mode was presented. This approach has advantages over the conventional transmission mode amplifiers in achieving arbitrarily high gain with a limited bandwidth, whilst maintaining low-noise performance for such devices [1]. Three configurations for negative resistance FET-based elements to form active networks in the design of an optimum noise measure reflection amplifier were presented in [1], and a schematic of the configuration chosen to be used in the loss compensation technique is depicted in Figure 5.2.

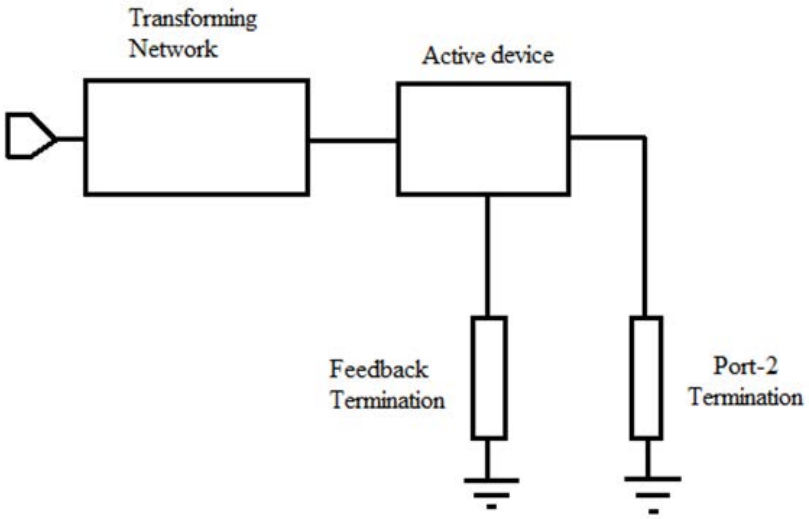


Figure 5.2: Schematic layout of an active two-port device configured as a negative resistance amplifier [1, 2]

In this work, a negative resistance FET-based reflection amplifier is designed and its performance is presented by simulation. A (ATF33143) transistor is used as an active device in the design and its datasheet is depicted in Appendix A. Furthermore, a capacitor is employed as a series reactive feedback at the source termination. In addition, an inductor is utilised as a reactive load termination at the drain.

In this design, the source capacitor and the drain inductor are used to generate the appropriate negative resistance. Moreover, instead of using a transforming network in the design, a capacitor is added in series to the transistor's input gate to tune out the reactive part and negate the negative imaginary part of the input impedance of the device. The proposed negative resistance amplifier structure is shown in Figure 5.3.

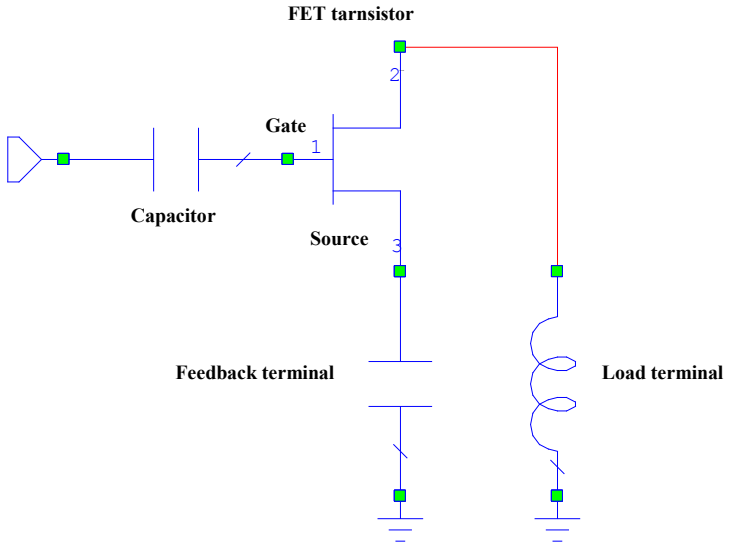


Figure 5.3: AWR circuit schematic of the ideal negative resistance amplifier

5.2.1 Design and Fabrication Procedure

The task of designing a negative resistance amplifier using field effect transistor technology is divided into two parts; firstly, creating a one-port negative resistance device by choosing and determining the load port and the feedback terminating impedances. The second stage in the design process is to derive the input impedance transformer, also called the transforming network, to generate the required gain response as well as to maintain stability [1].

In this work, the purpose of designing a negative resistance FET-based reflection amplifier is to generate the required reflection gain and optimise it to achieve broader bandwidth, aiming to compensate the losses of the NGD networks. Analytical approach to present the design methodology in its entirety is demonstrated.

Mathematical equations to obtain the reactive terminated reactances of an ideal reflection amplifier are presented. The frequency of design is chosen to be in the middle of the synthesised NGD behaviour of the NGD network, therefore, the frequency (f =1.29 GHz). The load port and the feedback terminating reactances are calculated as follows:

For example, if the chosen feedback terminal capacitor is C= 2 pF, then it's reactance can be calculated as the following:

$$X_f = \frac{1}{2\pi fC} \tag{5.9}$$

$$X_f = \frac{1}{2\pi x 1.29 x 10^9 x 2 x 10^{-12}}$$

Therefore, $X_f = 1.6\ \Omega$

In addition, if the chosen load terminal inductor is L= 10 nH, then it's reactance can be computed as follows:

$$X_{load} = 2\pi fL \tag{5.10}$$

$$X_{load} = 2\pi x 1.29 x 10^{9} x 10 x 10^{-9}$$

Therefore, $X_{load} = 81.7\Omega$

Using the AWR Microwave Office for designing the topology, the imaginary and real parts of the input impedance of the reflection amplifier can be obtained and plotted on a rectangular graph as depicted in Figure 5.4. From the complex input impedance values can be determined at the desired frequency (here, for example, is 1.29 GHz).

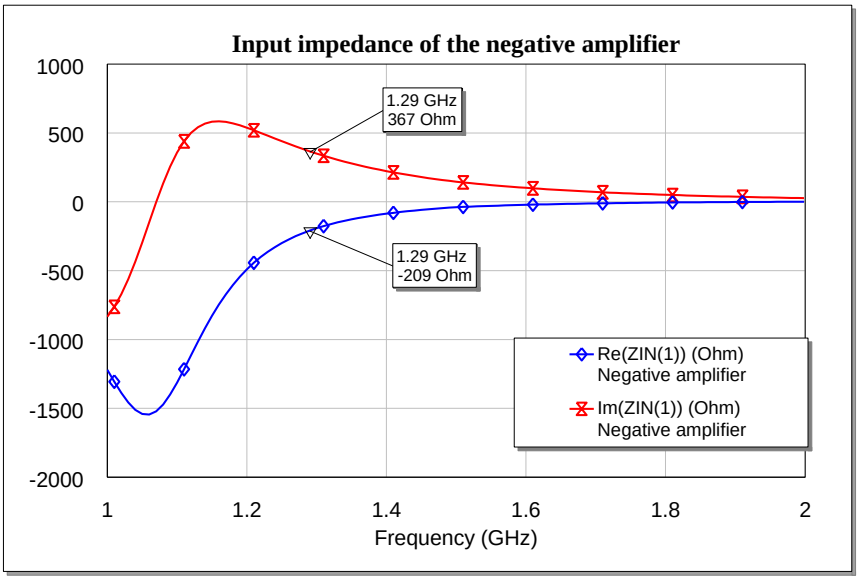


Figure 5.4: The simulated input impedance of the ideal reflection amplifier

The complex input impedance (Z_{in}) at 1.29 GHz is ($Z_{in} = -209 + j367$) .

To compensate the reactive part (imaginary part) of the input impedance of the amplifier, a capacitor is added in series to the transistor's gate as depicted in Fig 5.3.

$$X_c = \frac{1}{2\pi f C}$$

Where $X_c = 367\Omega$

Therefore, $C = \frac{1}{2\pi f X_c}$

$$C = \frac{1}{2\pi x 1.29 x 10^9 x 367} = 0.4\ pF$$

In order to design a practical negative resistance reflection amplifier, there is a need to include transmission line sections and the required DC bias network to establish the correct operating point. Therefore, the (ATF33143) transistor is biased by introducing a DC bias decoupling network, to establish the correct operating point. The design was simulated using the Microwave Office for fast optimisation. The realistic schematic and its associated layout including the biasing circuitry are shown in Figures 5.5 and 5.6 respectively. Moreover, Figure 5.7 shows the front and back views of the fabricated circuit board of the realistic reflection amplifier.

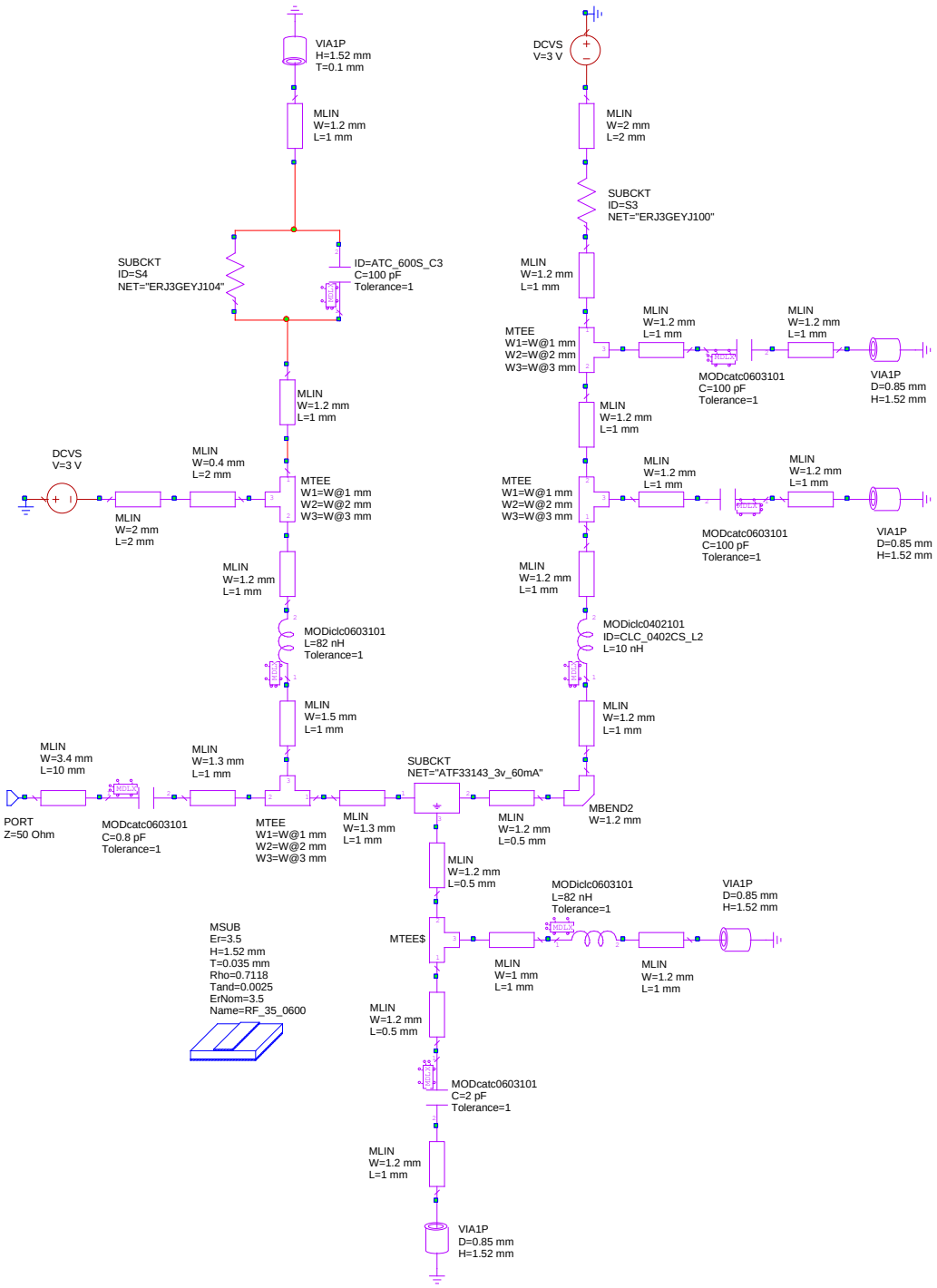


Figure 5.5: AWR circuit schematic of the realistic reflection amplifier with biasing networks at the gate and the drain terminals

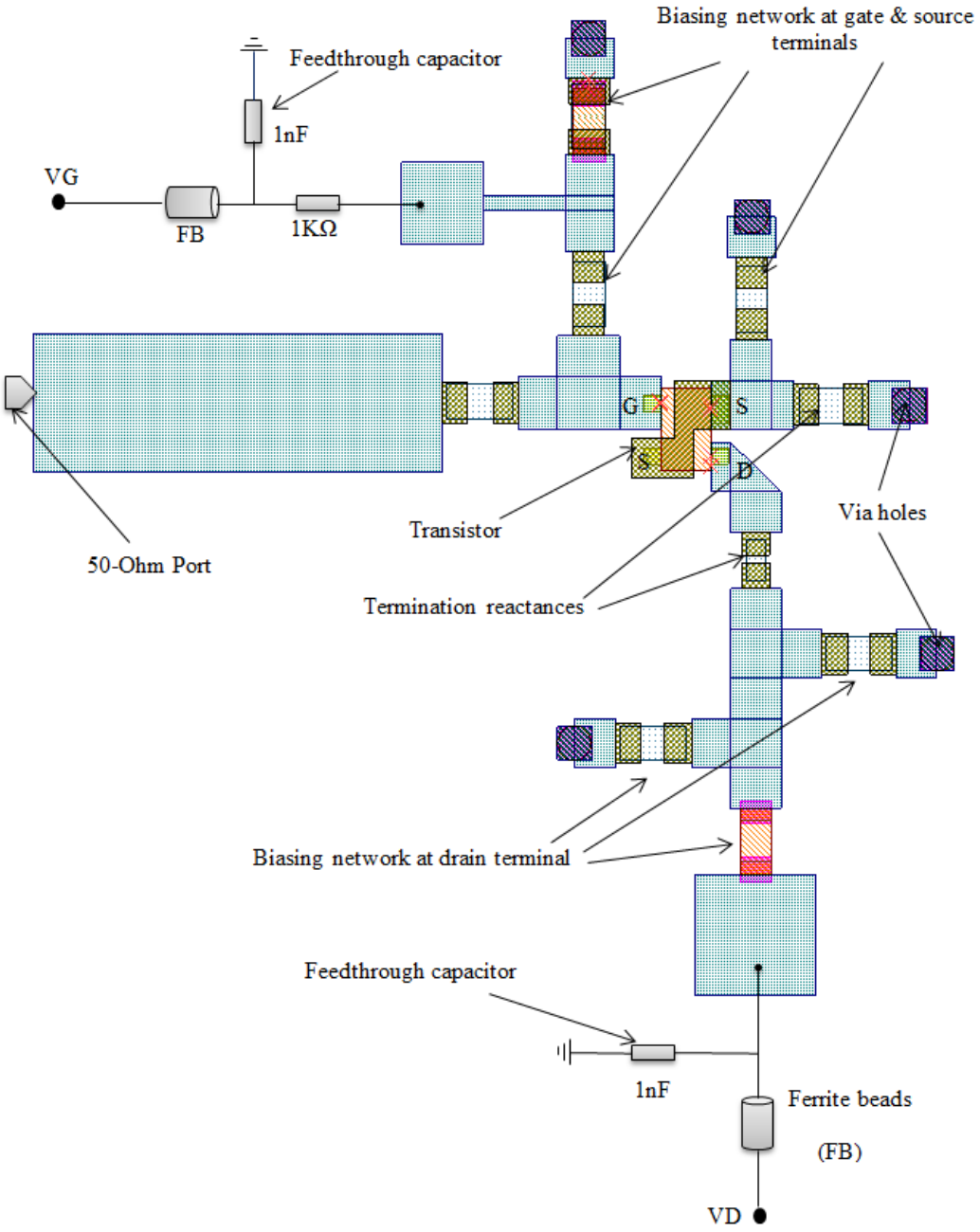
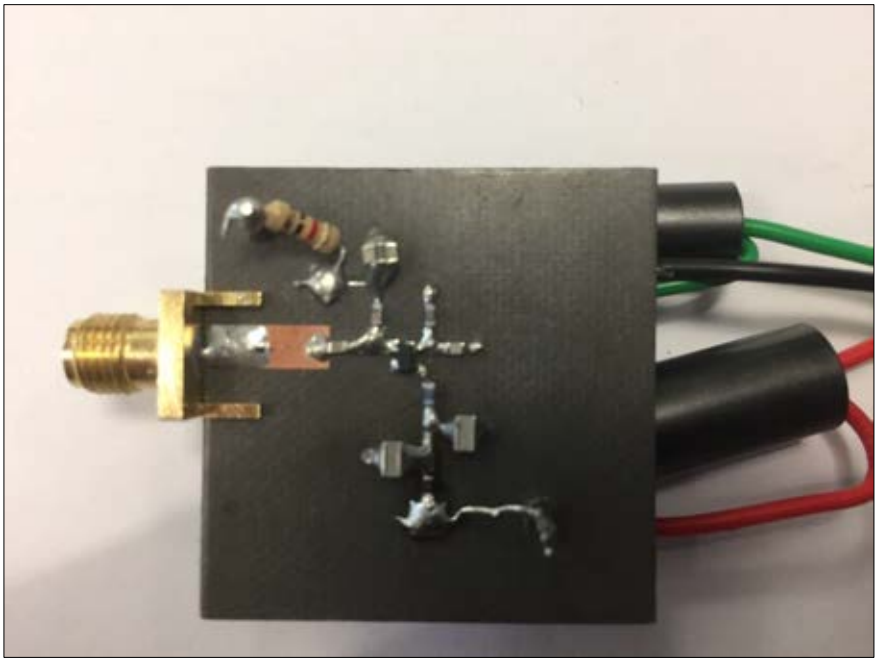
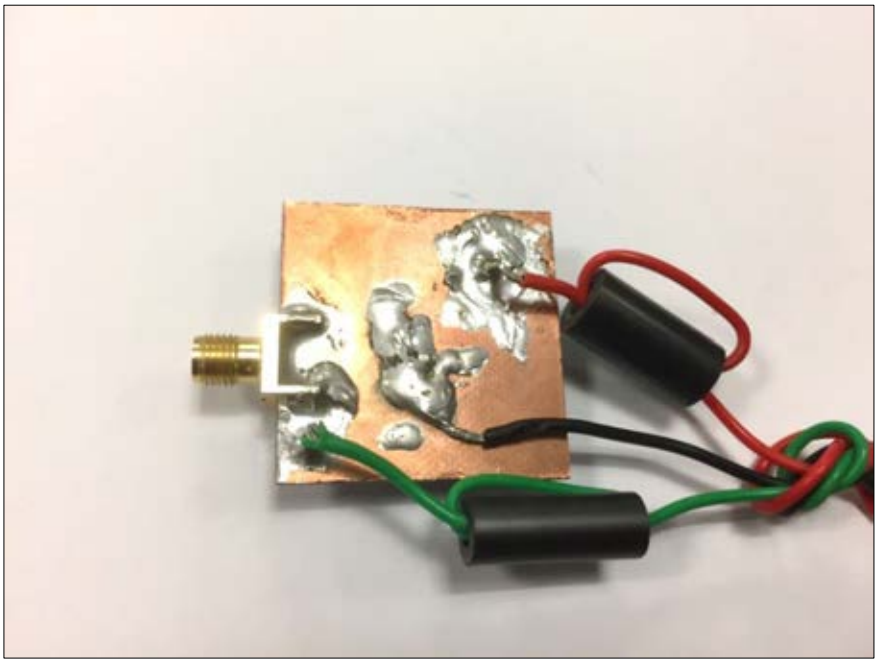


Figure 5.6: The reflection amplifier layout with the biasing circuitry



(a)



(b)

Figure 5.7: Images of the fabricated reflection amplifier and the biasing circuitry: (a) front view; (b) back view

5.2.2 Stability Analysis Methods

The stability factors K and B1 can't be used to check the stability of the proposed FET-based reflection amplifier because it is a one-port active device. Microwave Office offers alternative approaches to internal stability analysis to reduce the likelihood of an unstable design.

5.2.2.1 Nyquist Stability Measured with Modified Gamma Probe STABN_GP2

One rigorous approach to finding the stability characteristics of the FET-based reflection amplifier is by applying Nyquist criteria to the open loop frequency domain response. The Nyquist stability criteria state that if the open loop function G, when plotted on the complex plane, encircles the -1 point in the clockwise direction, then the closed-loop system will be unstable.

In this work, the Nyquist stability measured with modified gamma-probe (STABN_GP2) measurement in Microwave Office is used for inspection of the stability of the amplifier. STABN_GP2 is used for plotting the open-loop gain function in conjunction with the gamma-probe (GPROBE2) element for inspection of the stability. When plotting STABN_GP2, the frequency should be swept over the entire range where instability could occur. The GPROBE2 element is connected in series with the input gate of the transistor to measure the internal reflection

coefficients required for internal stability measurements at the reference plane where it is inserted as shown in Figure 5.8.

Figure 5.9 illustrates the simulated open loop function G of the (STABN_GP2) measurement plotted on a polar graph from 100 MHz to 10 GHz. As it can be seen, G does not encircle the -1 point in a clockwise sense. Therefore, the proposed FET-based reflection amplifier is considered stable.

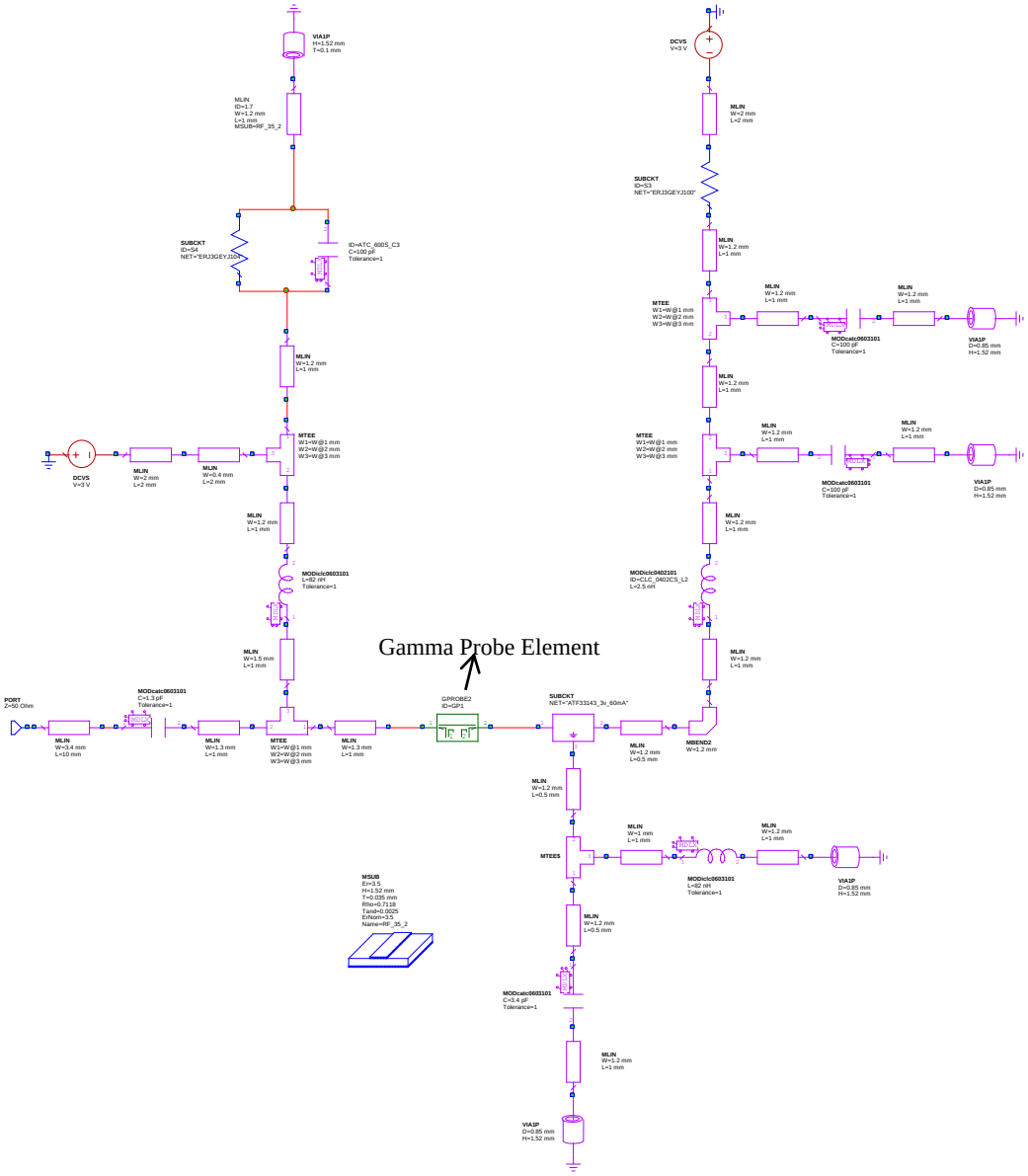


Figure 5.8: Nyquist Stability Measured with Modified Gamma-Probe applied to the FET-based reflection amplifier

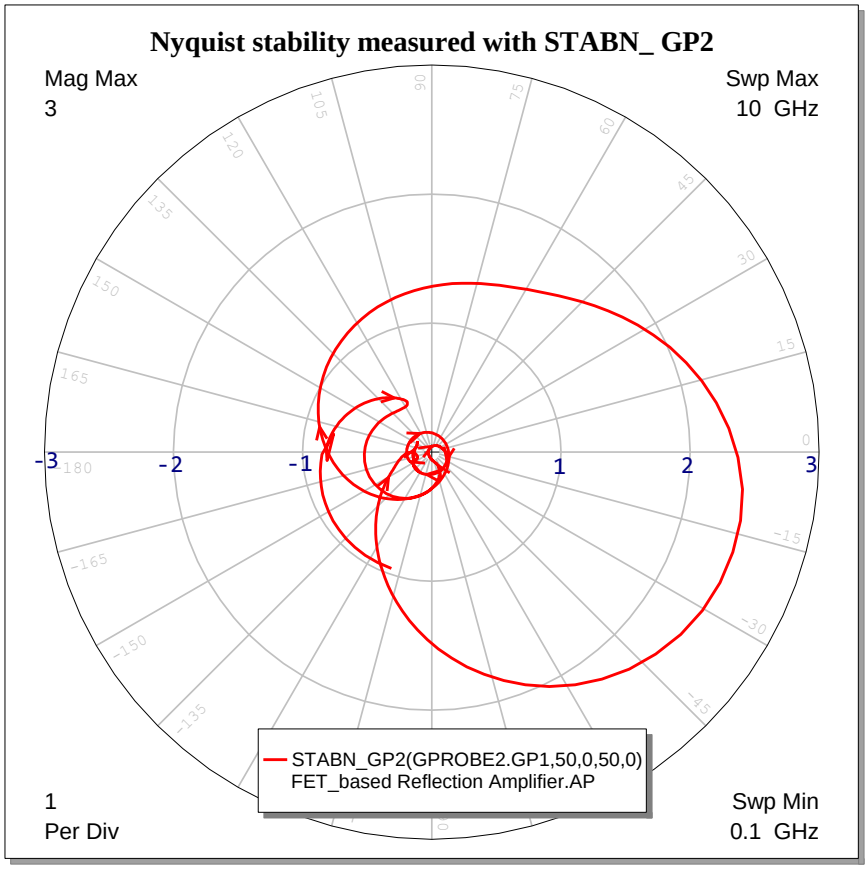


Figure 5.9: Stability analysis through the Nyquist diagram to detect the instability of the FET-based reflection amplifier. The open loop function G, does not encircle the -1 point in the clockwise direction, meaning that the amplifier considered stable

5.2.3 Stability Checks for the Prototype in the Laboratory

In the beginning, when the amplifier was tested, it was proven to fulfil the definition of an oscillator, an amplifier with "a positive feedback". As a first attempt to solve the design stability issues, 1 $k\Omega$ and 10 Ω resistors were added in series with the FET gate and drain terminals respectively, and ferrite beads (FB) were employed on each of the supply rails (Vg & Vd). Then, the RF stability was checked using the spectrum

analyser, but there was no significant effect and as a result, we found that the oscillations were at about 30 MHz spacing from 500 MHz to 3 GHz, but were tuneable over a narrow range by varying the gate bias as depicted in Figure 5.10(a). The amplifier often started to oscillate with switching (VDS) on, the power out being about +12–14 dBm. The FET was changed and it worked for a short time then oscillated again. After setting the DC conditions, it was running at 3V VDS but drew 300 mA when it burst into oscillation.

As a second attempt, the decoupling biasing network was redesigned to include low-pass filters in the drain and source supplies to compensate for the RF signals associated with the power supply wires. 1nF solder mount feed-through capacitors (datasheet is in Appendix A) were added to the gate and drain supplies; carbon film low-value resistors were used to connect them to the surface mounted device parts (bias point etc.); the resistors are "lossy" coils by their internal construction. The results were promising; the 30 MHz comb to over 3 GHz disappeared with the exception of a single spurious output of +3.2 dBm at 1.26 GHz as seen in Figure 5.10(b). The ferrite beads on the supply cable have a negligible effect before adding the feedthrough capacitors and a minimal effect afterwards, so the feedthrough capacitors are the main aid to stability. Subsequently, the biasing conditions were adjusted by reducing the current at the drain supply. A negative voltage was observed at the gate generated from the positive supply, due to the internal construction of the FET. The possible explanation is that the DC power bias circuit has high impedance at the gate. In addition, there is an interaction between the power supply and the FET

gate, which is acting like a diode and rectifying the RF signal to generate a negative voltage on the gate. The gate bias was changed to a shunt source, using a low-value resistor (1kΩ nominal) and supplying the bias voltage to it so that the rectified RF supplied bias had a minimal effect on the operating point. Then the DC power supply keeps the bias point steady by adding current through this resistor. Finally, the amplifier worked with no sign of oscillation detected by the spectrum analyser, as shown in Figure 5.10(c). Consequently, the amplifier was tested and its performance was measured using the vector network analyser (VNA) as depicted in Figure 5.11.

The measured FET-based reflection amplifier was generating about 15 dB gain, however, it was suffering from stability problems. Thus, it was decided to present the performance of the reflection amplifier with its simulated results in the context of the loss compensated, reflection-mode NGD antenna matching network as shown in the next section, in order to allow the principle of NGD operation with reflection amplifiers to be demonstrated despite this practical difficulty.

Other technologies using for example Tunnel and Gunn diodes might be used as an alternative approach for synthesising negative resistance devices. In reference [3], a low power reflection amplifier using a Ga-As AI301A tunnel diode was proposed. By extracting the S-parameter of the tunnel diode, a reflection amplifier was designed to have a reflection gain at 890 MHz for RFID systems in UHF band. The fabricated circuit generated 17 dB reflection gain at 890 MHz. Moreover, the Tunnel diode-based reflection amplifier was designed to be free from oscillations to remove

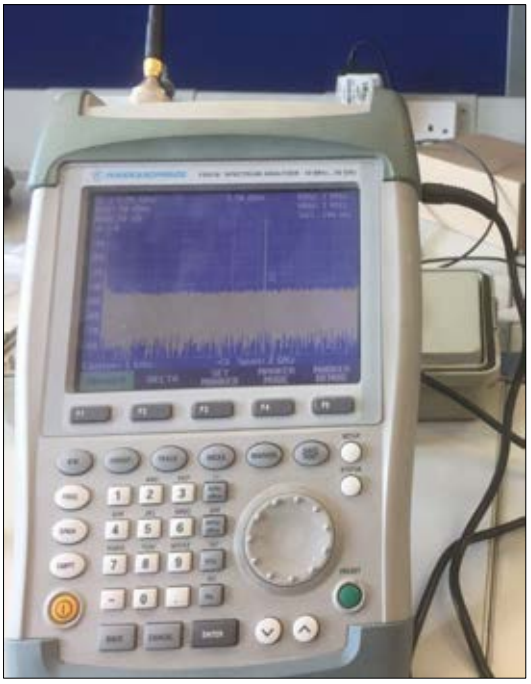
undesired harmonics from the reflected signal and to avoid signal to noise ratio degradation. This behaviour was verified by measurements of the output frequency spectrum of the fabricated device [3].

Consequently, two of these tunnel diode-based reflection amplifiers with similar performance integrated with a microstrip BLC to realise a bidirectional amplifier have been presented in [4]. As a result, a low-power, full-duplex bidirectional amplifier operating in the 915 MHz was achieved. The fabricated bidirectional amplifier produced 9 dB transmission gain between and 22 dB return loss at the input-output ports.

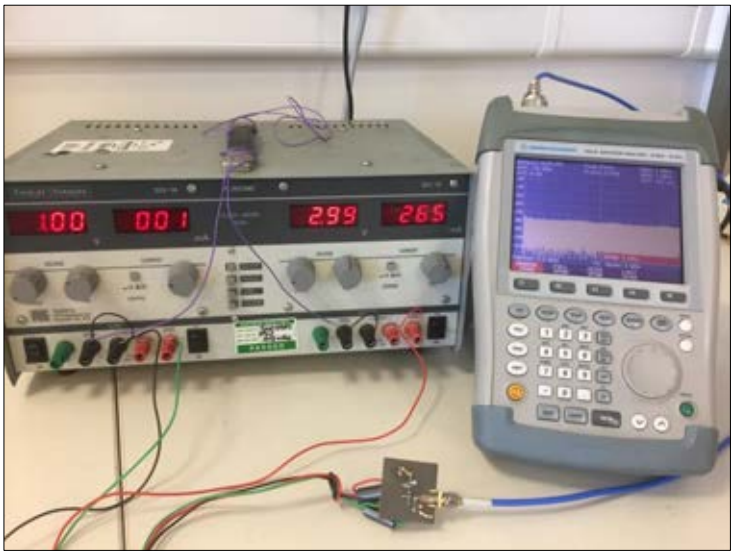
However, neither specific stability analysis to check the stability characteristic of the tunnel-based reflection amplifiers and bidirectional amplifiers, nor group delay measurement to know how much positive group delay produced by the devices were presented in the papers [3, 4].



(a)



(b)



(c)

Figure 5.10: Testing the reflection amplifier stability using a spectrum analyser (a) The amplifier was oscillating about 30 MHz spacing from 500 MHz to 3 GHz; (b) the amplifier was oscillating only at 1.26 GHz; (c) the amplifier worked with no sign of oscillation

Table 5. 1: Biasing stable conditions

Transistor terminals	Voltage (V)	Current (mA)
Drain	5.31	222
Gate	0.22	0

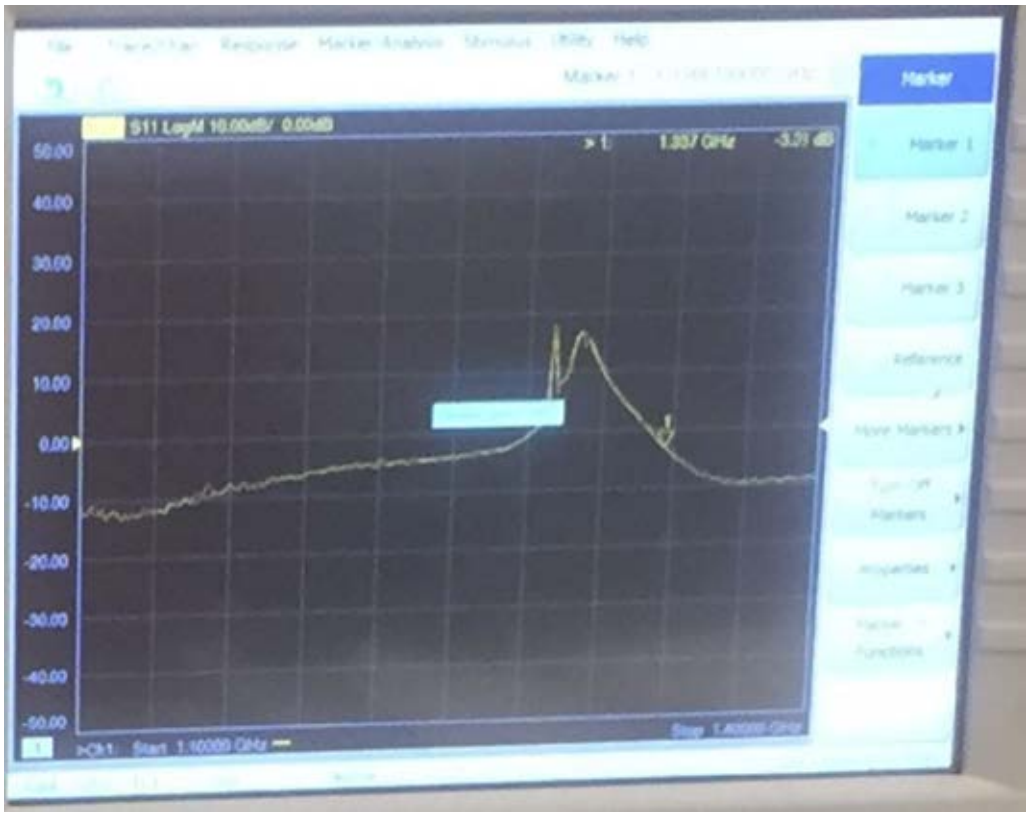


Figure 5.11: Photograph of the measured S_{11} magnitude of the reflection amplifier at the biasing stable conditions in the lab

5.2.4 Simulation Results

As discussed in section 5.2.2, because of the practical problems in maintaining stable operation, the performance of the reflection amplifier is presented using simulation results. Figure 5.12 shows the reflection coefficient obtained from the simulated model of the negative resistance reflection amplifier of Fig 5.5. At the frequency range from 0.5 GHz to 1.9 GHz, the amplifier was generating a reflection gain with a maximum amplitude of 25.84 dB at 1.29 GHz. The amplifier generates the required gain needed to compensate the losses of the NGD networks in the implementation of the overall circuit. However, as a drawback, the narrow bandwidth of the reflection amplifier limits its utilisation in wideband applications.

Figure 5.13 shows the plot of negative resistance simulation results. The results show what the amplifier exhibits a negative resistance from 0.5 GHz to 2 GHz. It should be noted that from 1.2 GHz to 2 GHz, the reactive imaginary part of the input impedance is very close to zero and tuneable; this is because a capacitor is added in series to the gate of the transistor.

Another important parameter in the performance of the design, which is the group delay (GD) produced by the amplifier. Figure 5.14 shows the amount of the positive group delay contributed by the amplifier. From 1.23 GHz- 1.34 GHz, the amplifier exhibits a positive group delay with a maximum amplitude of 12.69 ns at 1.29 GHz. It has a proportional relation with the reflection coefficient S_{11} magnitude. It should

be noted that the positive group delay of such active circuits is inversely proportional to the amplifier's bandwidth. In this case, as the reflection amplifier is a narrow-band, thus, it produces an inevitably large amount of positive group delay. This undesired positive group delay will be over compensated using the NGD networks in the overall design. Table 5.2 gives a comparison between the proposed FET-based reflection amplifier and another reflection amplifier using a tunnel diode presented in [3], in term of the realisable bandwidth, group delay, reflection amplifier and stability.

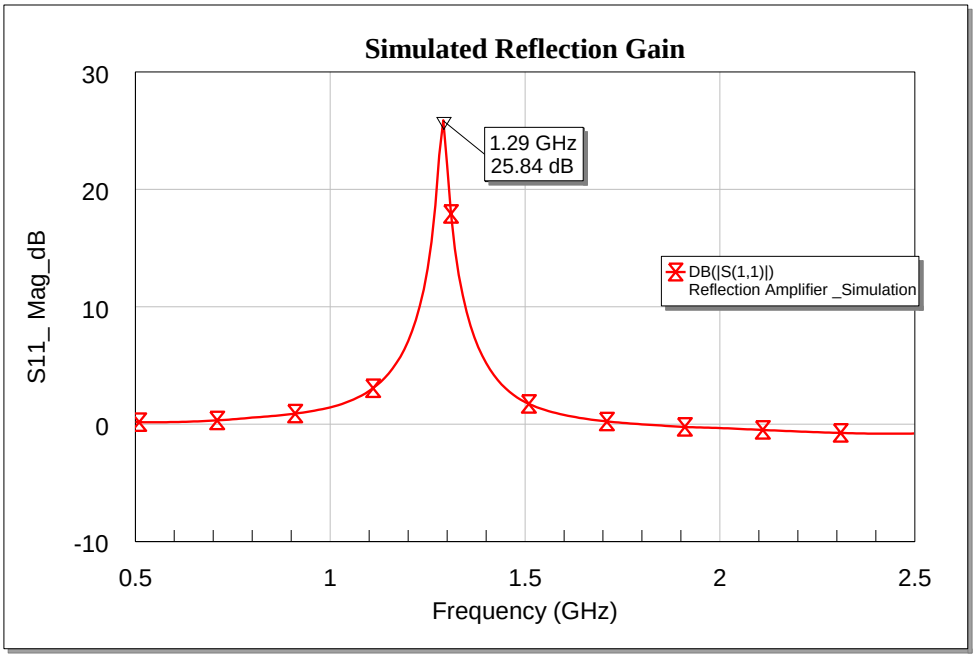


Figure 5.12: Reflection gain obtained from negative resistance amplifier

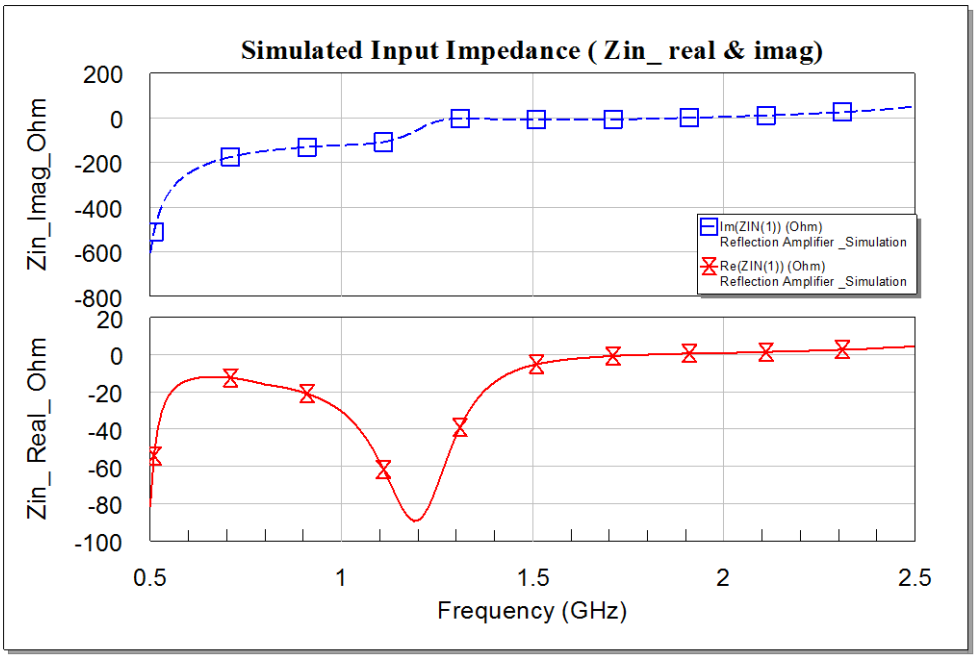


Figure 5.13: Negative resistance plot of the reflection amplifier

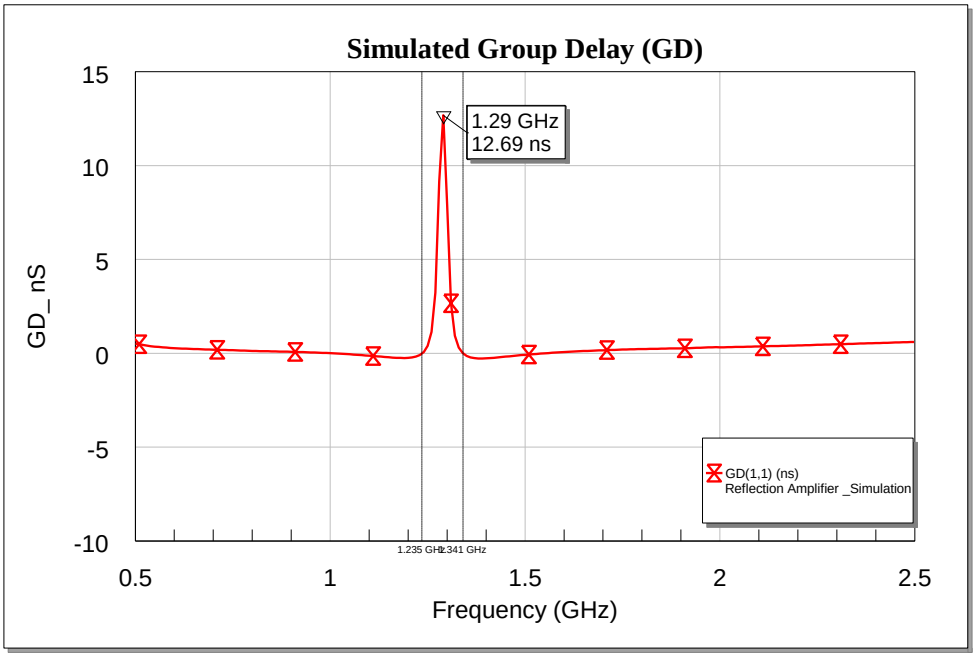


Figure 5.14: Group delay obtained from negative resistance amplifier

Table 5. 2: comparison between the proposed FET-based reflection amplifier and another tunnel diode-based reflection amplifier

Active circuit type	Technique used	Bandwidth	Reflection gain	Group delay	Stability analysis
FET-based Reflection amplifier	(ATF33143) FET transistor	1.23- 1.34 GHz	25.4 dB at 1.29 GHz	12.6 ns at 1.29 GHz	Nyquist criteria
Tunnel diode-based reflection amplifier	Ga-As AI301A tunnel diode	8.7 - 9.1 GHz	17 dB at 890 MHz	Not given	Not given

5.3 Lange Coupler Design and Experiment

The second key step in the design of the final synthesised non-Foster reactive element using loss-compensated NGD networks is the design of a quadrature hybrid coupler. In this work, a Lange coupler is used to demonstrate the principle. It is used to double the effect of the NGDs' response as a result of sending the RF signal through them twice in a balanced structure. Other forms of quadrature hybrid couplers could be used, such as multilayer couplers or branchline couplers, as appropriate in the chosen circuit medium. The Lange coupler is a four-port interdigitated structure which constitutes a quadrature hybrid with a 3 dB coupling

ratio and 90-degrees phase shift difference between the output ports. A circuit schematic of an ideal Lange coupler is shown in Figure 5.15.

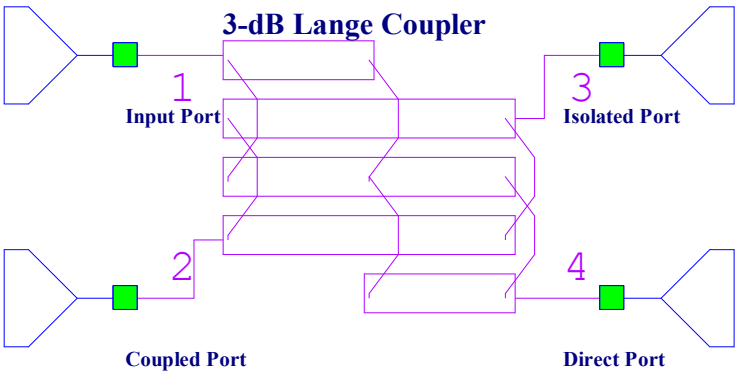


Figure 5.15: Ideal Lange coupler schematic layout

5.3.1 The Design Procedure

The symmetry of the proposed Lange coupler's structure is beneficial, as any port could be used as an input port, and the isolated port is on the same side as the input port. In addition, the output ports are on the other side of the junction from the input port. An even-odd mode characteristic impedance technique is used to design and analyse the operation of the proposed Lange coupler. For more details, and examples of this scheme, readers are referred to [5]. For such a microstrip coupled line, a design graph shown in Figure 5.16 is used to determine the width of the strips and the gap spacing between them: for a given dielectric constant and characteristic impedances, there is a set of even-mode (Z_{0e}) and odd-mode (Z_{0o}) impedances [5].

The implementation described here uses Taconic substrate type RF_35_0600_C1/C1. To design a 3-dB hybrid Lange coupler with a centre frequency of 3 GHz, we need to calculate the even-mode and odd-mode line impedances. To do that, firstly we determine the coupling (C) using the following equation [5].

$$C = 10^{\frac{coupling\ cofficient}{20}} \tag{5.11}$$

$$C = 10^{\frac{-3dB}{20}} = 0.707$$

Thus, even mode characteristic impedance (Z_{0e}) can be determined using this equation [5]:

$$Z_{0e} = \frac{4C - 3 + \sqrt{9 - 8C^2}}{2C\sqrt{(1-C)/(1+C)}} Z_0 \tag{5.12}$$

$$Z_{0e} = \left[\frac{(4x0.707) - 3 + \sqrt{9 - (8x0.707^2)}}{2x0.707x\sqrt{(1-0.707)/(1+0.707)}}\right] x50$$

$$Z_{0e} = \frac{2.828 - 3 + 2.236}{2x0.707x0.414} = 176\,\Omega$$

To find the odd-mode characteristic impedance (Z_{0o}), the following equation is used [5]:

$$Z_{0o} = \frac{4C + 3 - \sqrt{9 - 8C^2}}{2C\sqrt{(1 + C)/(1 - C)}} Z_0 \tag{5.13}$$

$$Z_{0o} = \left[\frac{(4x0.707) + 3 - \sqrt{9 - (8x0.707^2)}}{2x0.707x\sqrt{(1 + 0.707)/(1 - 0.707)}}\right] x50$$

$$Z_{0o} = \frac{2.828 + 3 - 2.236}{2x0.707x2.414} = 52.6\ \Omega$$

Plotting (Z_{0e}) and (Z_{0o}) on the even-odd mode characteristic impedance design data coupled microstrip lines graph as depicted in Figure 5.16, the values of the width (W) of the tracks and the gap (S) between them can be approximately read.

$$\frac{S}{d} \cong 0.075$$

Where d is the height of the substrate which is 1.52 mm.

Therefore, $\frac{S}{1.52} \cong 0.075$, thus $S = 0.114\ mm$

Also, $\frac{W}{d} \cong 0.8$

and d is the height of the substrate which is 1.52 mm.

Therefore, $\frac{W}{1.52} \cong 0.8$, thus, $W = 1.216\ mm$

Now, the quarter wavelength of the Lange coupler's fingers is determined by using the following equations [5]:

$$V = \frac{c}{\sqrt{\varepsilon_r}} \tag{5.14}$$

Where c is the speed of light in vacuum, then

$$V = \frac{c}{\sqrt{3.5}} = 0.54c$$

$$\lambda = \frac{V}{f} \tag{5.15}$$

Where $V$is the speed of light and $f$is the frequency of the design which is 3 GHz.

$$\lambda = \frac{0.54x3x10^{38}}{3x10^{9}}$$

$$\lambda = 54\ mm$$

The quarter wavelength of the fingers l is determined as follows:

$$l = \frac{\lambda}{4} = \frac{54}{4} = \ 13.5\ mm$$

Therefore, l =13.5 mm

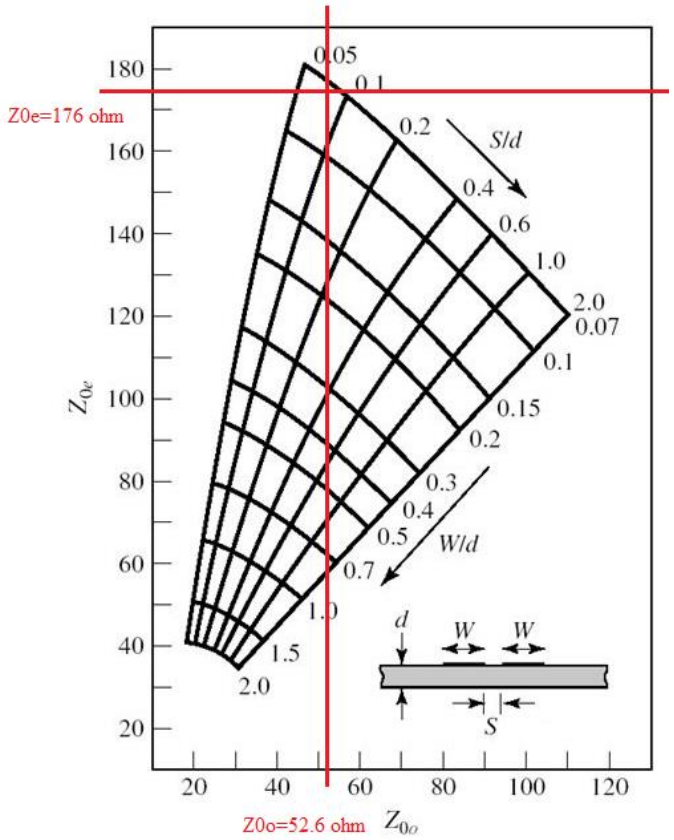


Figure 5.16: Even- and odd-mode characteristic impedance design data for coupled microstrip lines [5]. This implementation uses a substrate with a dielectric constant of 3.5.

5.3.2 Coupler Assessment

To choose the most suitable hybrid coupler to comply with the final non-Foster circuit requirement, an assessment was made between the proposed realistic Lange coupler, an ideal Lange coupler, commercial surface mount couplers, and a branch line coupler. It should be noted that the commercial couplers were assessed using their S-parameters which were downloaded from the corresponding companies' websites. The datasheets for the commercial couplers are in Appendix A. All the

couplers were used as four-port sub-circuits, where three ports were short circuits and one port as a 50 Ω. Figure 5.17 shows the simulated group delay and reflection coefficient magnitude obtained from the used couplers. In the frequency range of interest, the proposed Lange coupler was the most suitable for use because it generated less positive group delay and had lower loss. Consequently, this proposed structure was fabricated and experimentally validated.

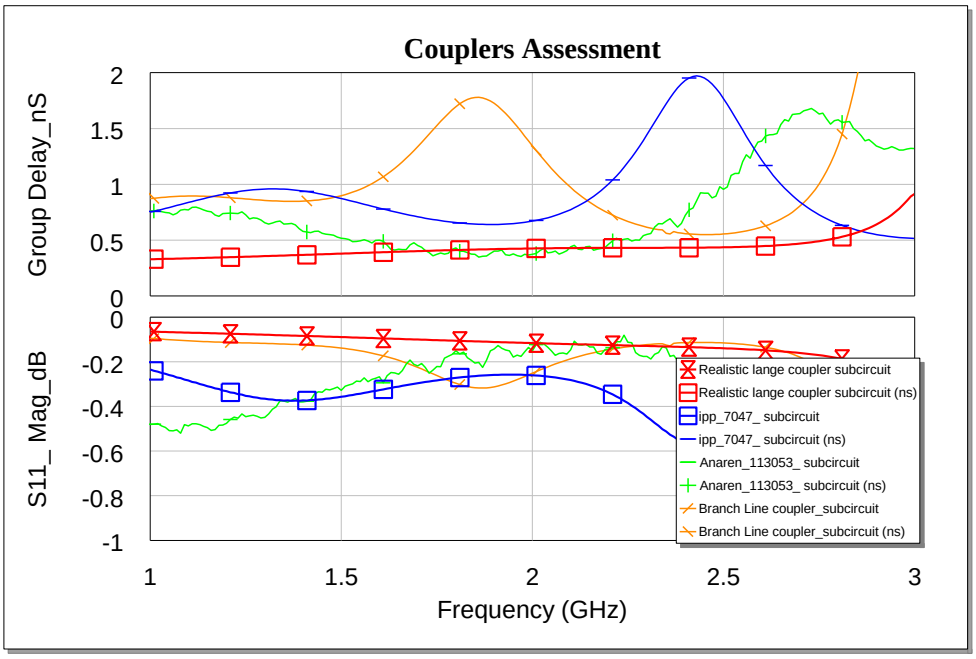


Figure 5.17: Group delay and S_{11} magnitude obtained from the assessed couplers

In this work, a realistic Lange coupler is designed using NI AWR Microwave Office and then tested. Due to the compact size of the design, the four ports of the coupler were folded in a way that can be manufactured. The circuit schematic and its associated layout of the proposed design are shown in Figures 5.18 and 5.19 respectively. It should be noted that extra 10 mm transmission lines are added to connect the four ports of the coupler with the measurement ports of the network analyser, in order to measure its S-parameters. They will be de-embedded later when the coupler is used in the implementation of the final design of the reactive non-Foster element.

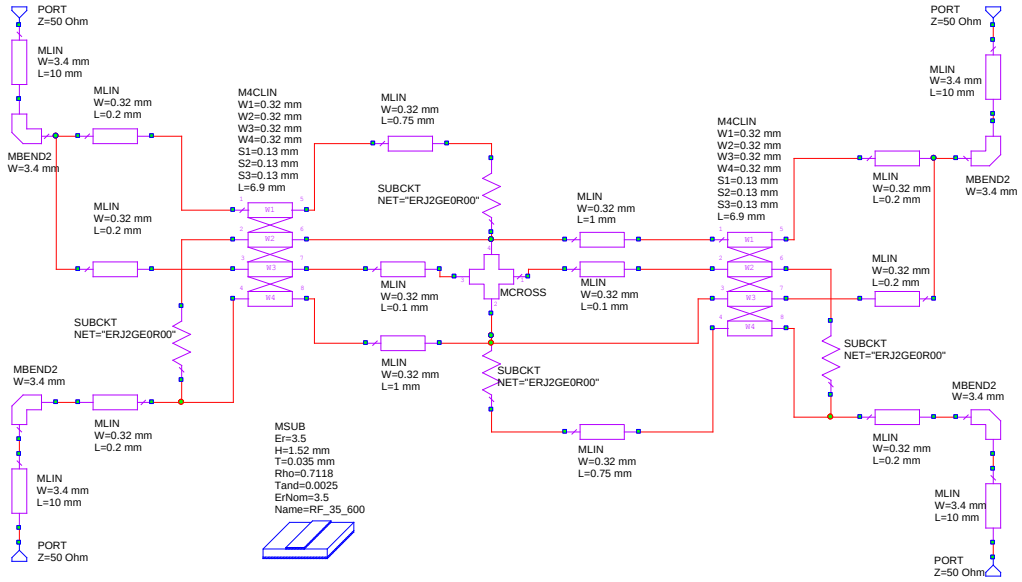


Figure 5.18: Realistic Lange coupler schematic layout

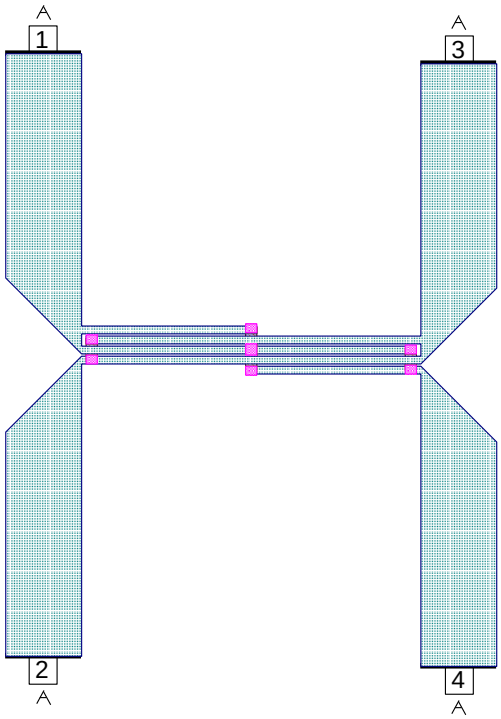


Figure 5.19: Structure layout of the realistic Lange coupler

5.3.3 The Fabrication Procedure

The circuit has been fabricated and manufactured on a double-sided printed circuit board (PCB) where the rear side was a full copper ground plane. The test board was printed on Taconic substrate type RF_35_0600_C1/C1. The challenging feature for manufacturing the prototype on a PCB board in the laboratory was the (0.13 mm) gap between the tracks of the coupler and assembling (0603) surface mount resistors, amongst the other parts on it. Fortunately, it was possible to wire bond the tracks of the coupler. Some bond wires were needed to form air-bridges and connect the strips of the prototype. The wire bonding was achieved using an ultrasonic ball bonder. An

electrostatic spark melted the tip of some gold wire forming a small ball, hanging from the wire. A ceramic bonding tool then pushed the ball down onto the bonding site and vibrated at ultrasonic frequencies to form the bond. The attached wire was then pulled over to the second bonding site where the wire was wedge bonded by smearing the wire across the copper, detaching the wire from the bonding machine and completing the bridged connection. Due to the wire's small diameter, this forms a robust link between the two tracks.

An image of the fabricated circuit is depicted in Figure 5.20. Four SMA connectors were carefully soldered to test the circuit. It is to be noted that all ports are 50 Ω. A photograph of the prototype when it was connected with a two-port vector network analyser in the lab to measure its S-parameters is depicted in Figure 5.21.

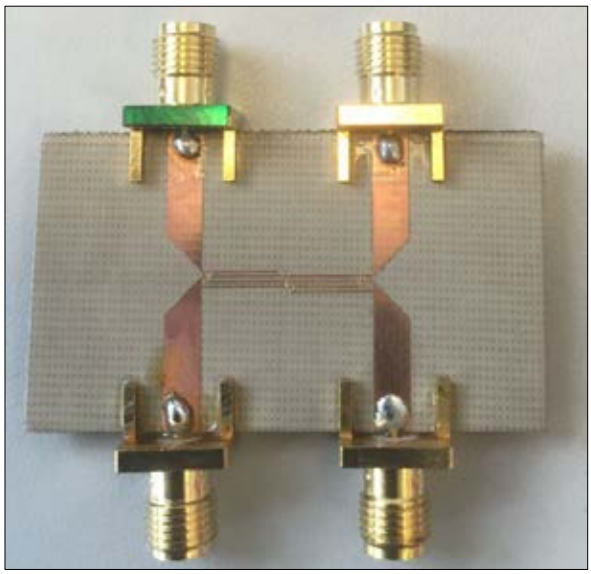


Figure 5.20: Image of the fabricated circuit board

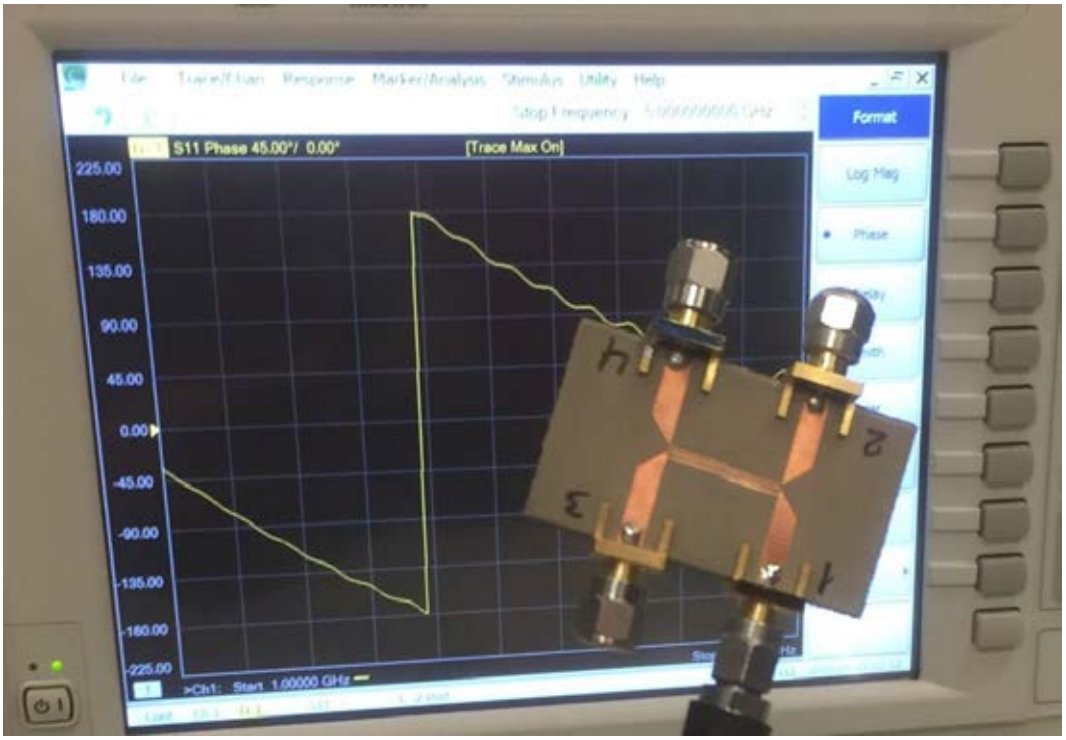


Figure 5.21: Photograph of the measured S_{11} phase response of the fabricated circuit board in the test station

5.3.4 Lange Coupler Simulated and Measured Performance

Fine tuning and optimisation were carried out to refine the design which can be integrated with the other components, forming the final synthesised non-Foster reactive element. The coupling between outputs 2 and 4 obtained from simulated and experimental results after measurements from the experimental setup using vector network analyser shown in Fig 5.21 is depicted as a comparison in Figure 5.22. The design frequency was 3 GHz and the frequency range from 1.0 to 5.0 GHz. At the frequency range from 2.0 to 4.0 GHz, the coupling factors obtained from simulation

and measurement are approximate -3.5 dB and -5.0 dB respectively. It is observed that the simulated S_{21} and S_{41} are approximately 3.5 dB. Furthermore, at the frequency range of interest, the measured S_{41} closely follows that of those simulated at almost -3 dB. However, the measured S_{21} shows an approximate 1.5 dB deviation below the same simulations at the same bandwidth. This implies that the coupled port receives less power than the direct port, possibly due to dimensional inaccuracy in the coupler fabrication.

Furthermore, the output balance plot is depicted in Figure 5.23. This graph shows the characteristics of the output ports. The amplitude balance and the phase balance achieved from the simulation are 1.6 ± 0.3 dB and 1.6 ± 0.3 degrees; whereas, the measured magnitude and phase balances' responses are 3 ± 1 dB and 97.5 ± 4.5 degrees. The difference in phase angle between the two output ports obtained is close to 90 degrees with the respect to the input.

The return loss at port 1 and the isolation at port 3 are depicted in Figures 5.24 and 5.25 respectively. The input and isolated ports obtained from the simulation results receive signals that are down by more than 14 and 17 dB respectively; whereas, the magnitudes of the S_{11} and S_{31} obtained from the measurement are down by more than 10 dB and 11 dB respectively. This implies that the manufactured prototype is not well matched and isolated compared to the simulated model. This can be attributed to the mechanical implementation difficulties of the design. Moreover, changes in any of the design parameters could affect all of the S-parameters.

An important consideration in the choice and design of the hybrid coupler is the amount of the positive group delay that it contributes. Simulated and measured group delays that are contributed by the proposed Lange coupler are plotted in Figure 5.26. As seen from the graph, the proposed coupler generates an approximately 0.2 ns positive group delay in the frequency range from 2- 4 GHz. It should be clarified that as a drawback, this undesirable amount of positive group delay reduces the value of the NGD; thus, it has an impact on the performance of the final reactive non-Foster element. Thus, it has to be overcompensated by the NGD networks. Table 5.3 shows the electrical specifications of the simulated and measured Lange coupler.

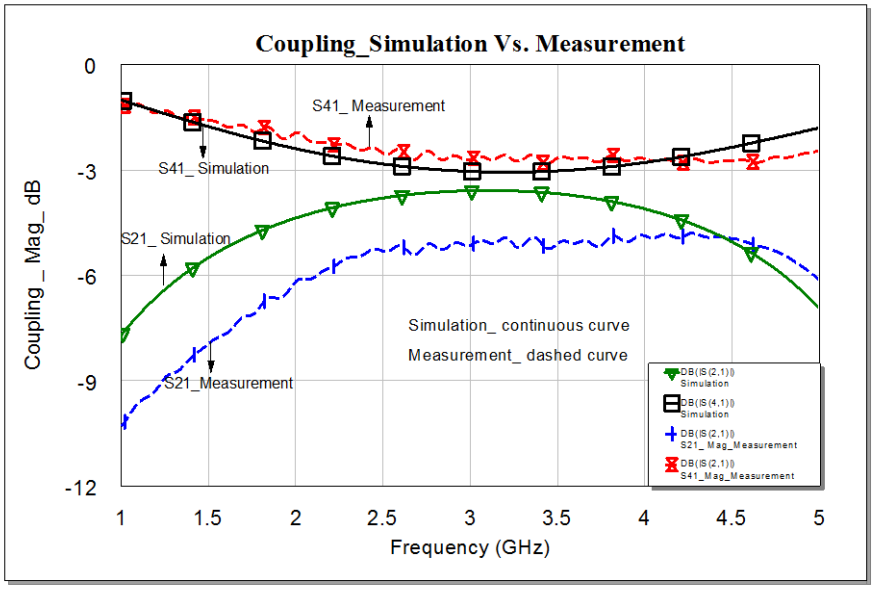


Figure 5.22: Coupling simulation and measurement results obtained from the Lange coupler

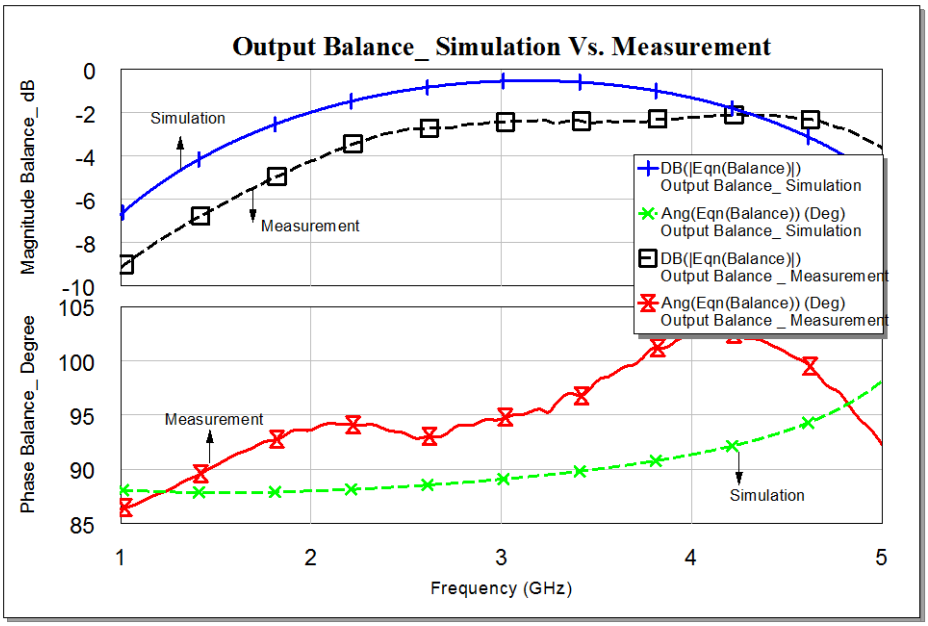


Figure 5.23: Output balance at ports 2 and 4 obtained from simulation and measurement

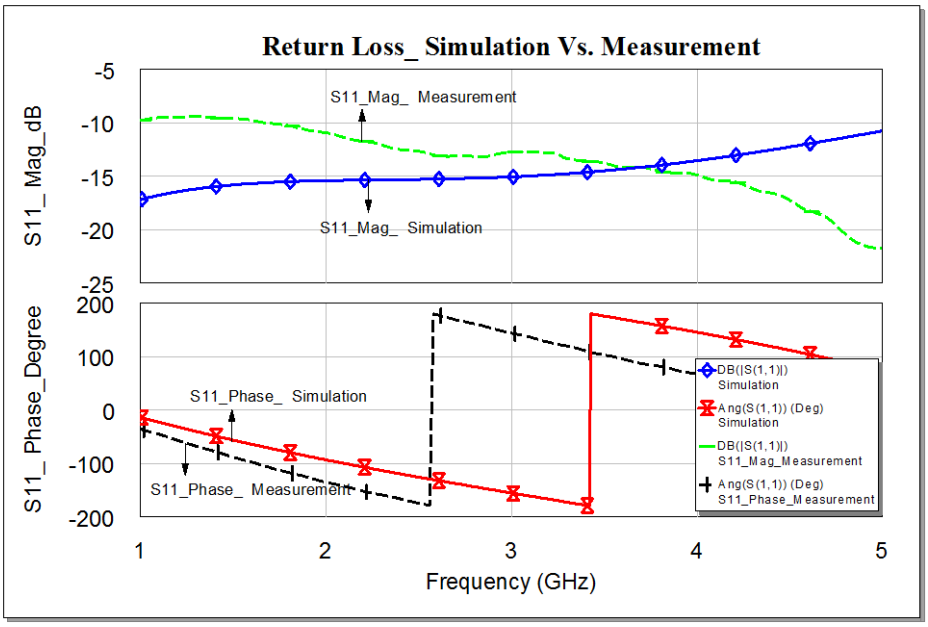


Figure 5.24: Return loss simulation and measurement results obtained from the Lange coupler

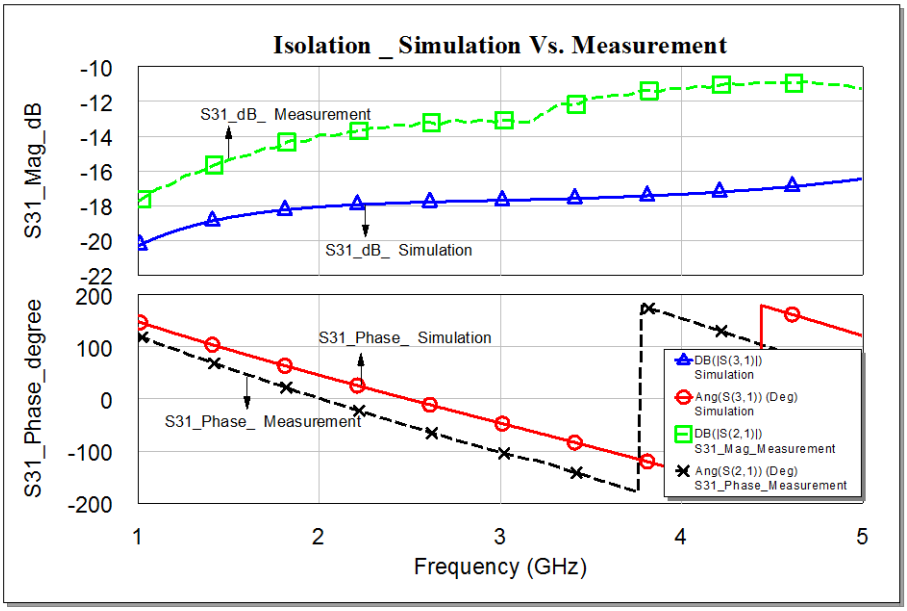


Figure 5.25: Isolation simulation and measurement results obtained from the Lange coupler

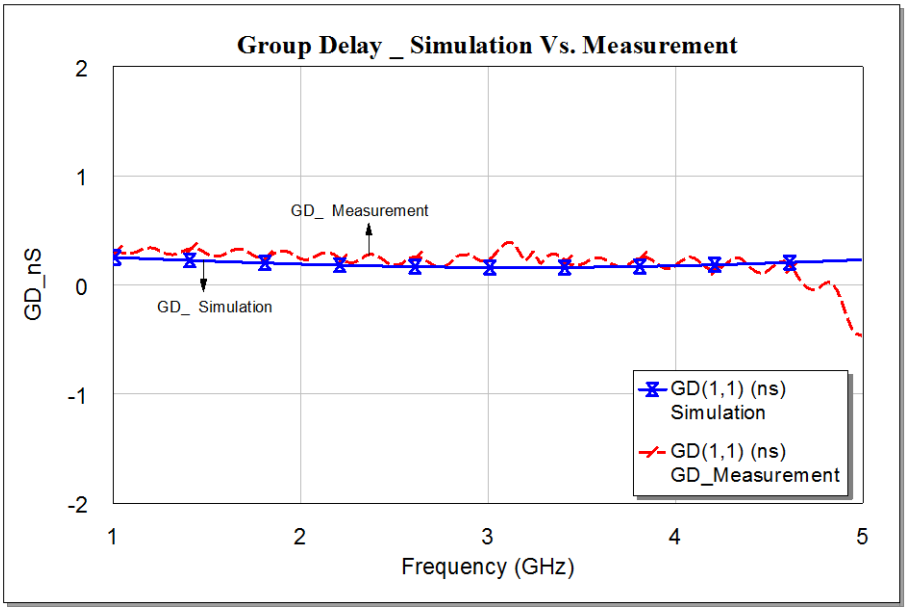


Figure 5.26: Group delay simulation and measurement results obtained from the Lange coupler

Table 5. 3: Electrical specifications of the designed Lange coupler based on measurement and simulation results

Parameter	Frequency Range (GHz)	Simulation	Measurement
Coupling	2.0 to 4.0	-3.5 dB	-5 dB
Isolation		< -17 dB	< -11 dB
Return loss		< -14 dB	< -10 dB
Phase balance		90 ± 2 degrees	97.5 ± 4.5 degrees
Amplitude balance		1.6 ± 0.3 dB	3 ± 1 dB
Group delay		< 0.2 nS	< 0.2 nS

5.4 The Implementation of the Lange Coupler with the NGD Networks

This section presents the design and experimental characterisation of the combination of the Lange coupler with the NGD networks without the FET reflection amplifier. The design consists of two reflection-type NGD networks which are connected to the direct and coupled ports of the Lange coupler. The isolated port of the Lange coupler is connected once to a 50 Ω measurement port and secondly to a short circuit. The short circuit is there to provide a 0 dB reflection coefficient. Then, the gain required from the amplifier can be determined by the reflection coefficient of the complete simulation. The model was designed, simulated and optimised within Microwave Office. Its electrical circuit schematic is presented in Figure 5.27 and the practical circuit layout is depicted in Figure 5.28.

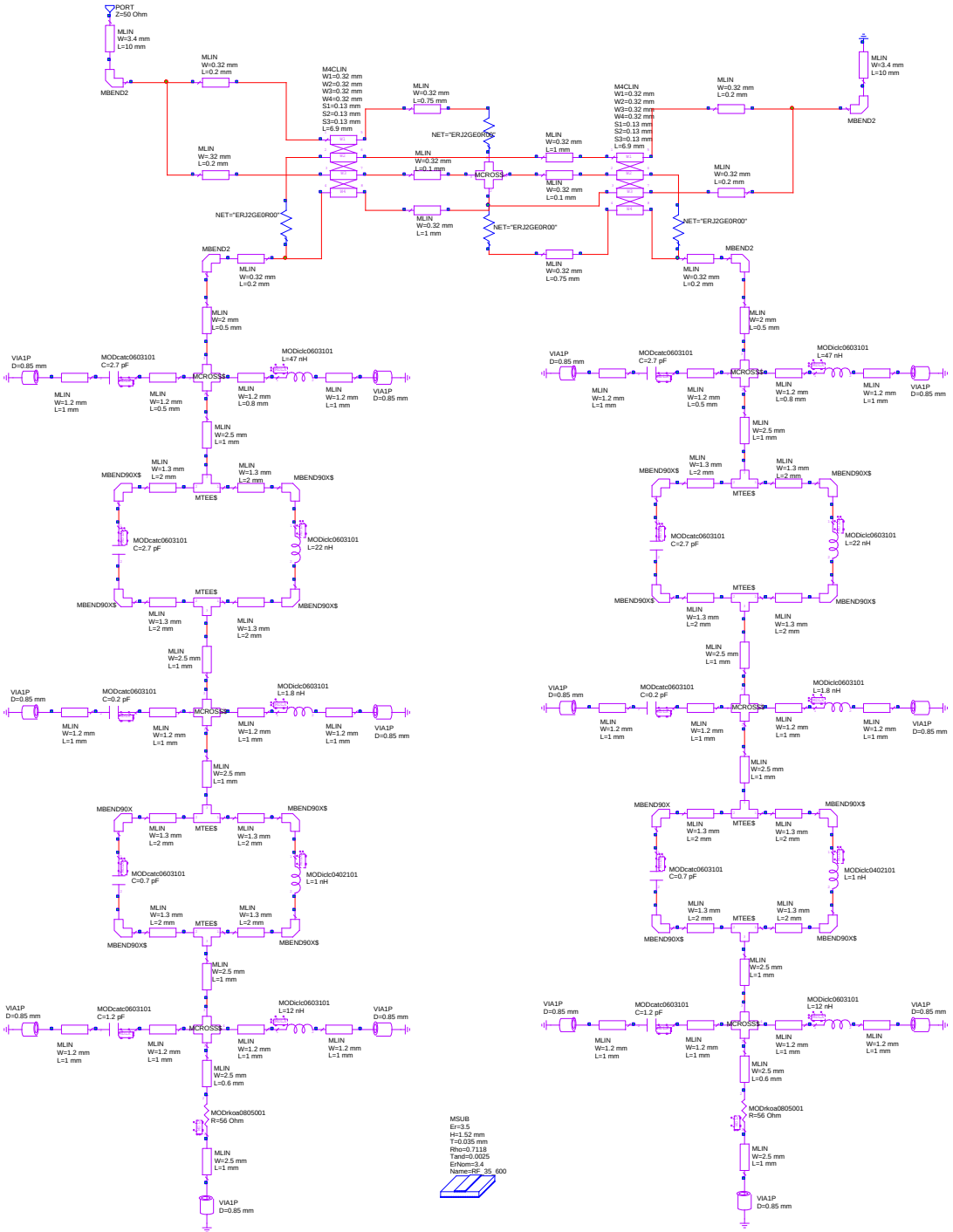


Figure 5.27: Electrical circuit schematic based on the combination of a Lange coupler with NGD networks

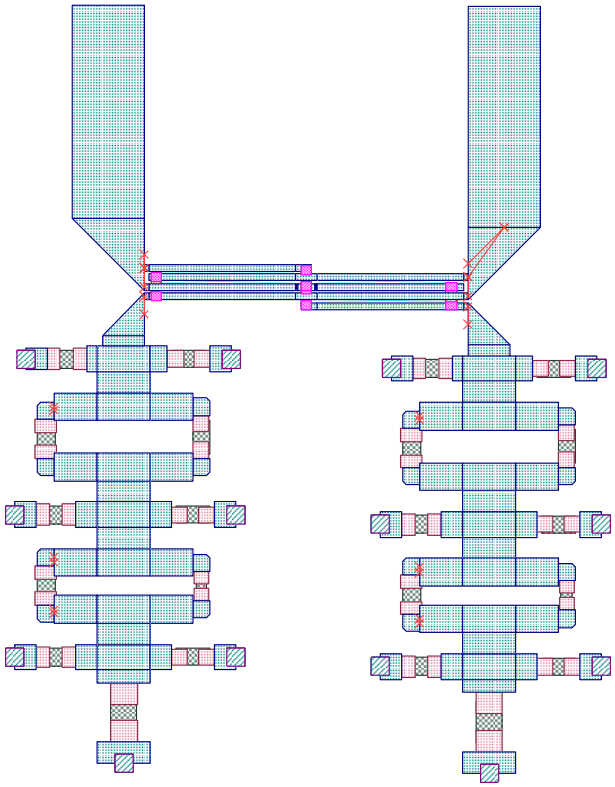


Figure 5. 28: Layout structure of the combination of a Lange coupler with NGD networks

5.4.1 Simulation and Measurement Results

Two measurements were carried out using the VNA in the lab to measure the performance of the prototype. The first measurement was performed when the isolation port of the Lange coupler was connected to a 50 Ω port. The circuit schematic for this implementation is presented as sub-circuits in Figure 5.29. Figure 5.30 shows an image of the prototype when it was tested in the lab using the network analyser.

Figure 5.31 presents the reflection coefficient (S_{11}) phase and magnitude responses from simulation and measurement for the design. Both measured and simulated results are in good agreement with each other, and show NGD behaviour between 1.25 GHz to 1.4 GHz with an increasing phase by 23 degrees. This gives a good indication that the approach we are using is working as expected. The measured prototype suffers from 7.7 dB losses and the simulated model produces -5.8 dB losses. This is attributed to some additional losses that appear due to soldering of components. Moreover, from the graph, we notice that the design model suffers from losses; as the required reflection gain to compensate the losses of the circuit is obtained from the reflection amplifier and we have not applied it yet to the overall structure. Thus, the overall circuit is "lossy". Figure 5.32, presents the measured and simulated results of the group delay of the overall structure. The fabricated structure generates a negative group delay of -0.72 ns over a bandwidth of 0.15 GHz, whereas;

the simulated circuit generates a negative group delay of -1.26 ns over a bandwidth of 0.08 GHz.

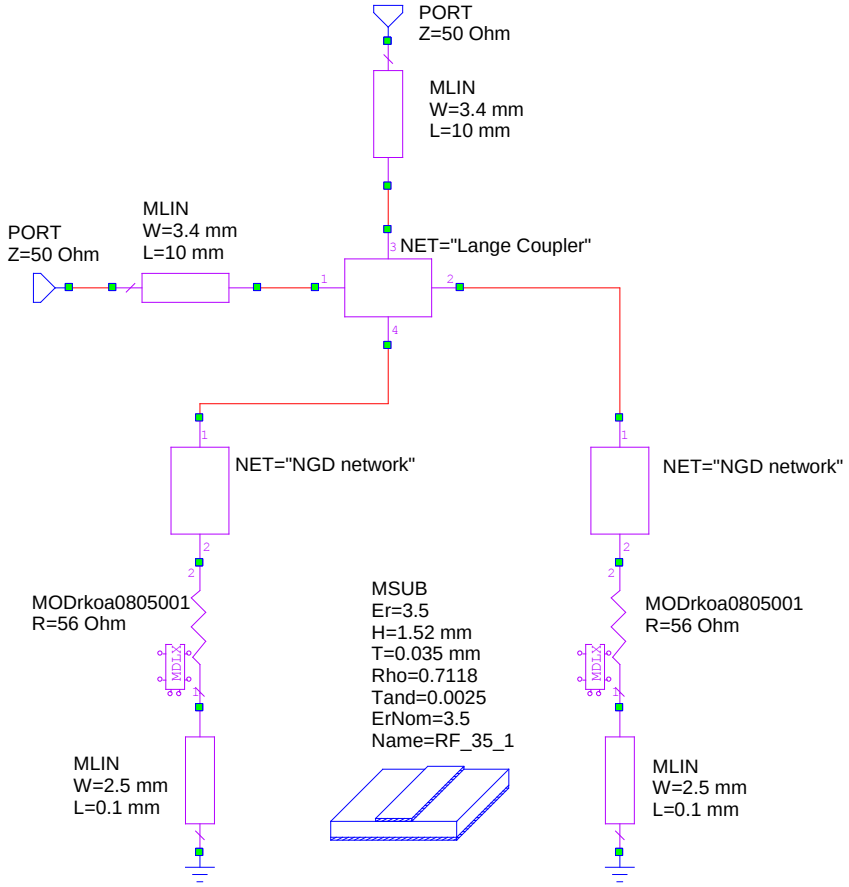


Figure 5.29: Schematic of the combination of a Lange coupler with NGD networks, where the Lange coupler isolated port is connected to 50 Ω port. The “NGD network” sub-circuit is from Fig. 4.8. The “Lange coupler” sub-circuit is from Fig. 5.18.

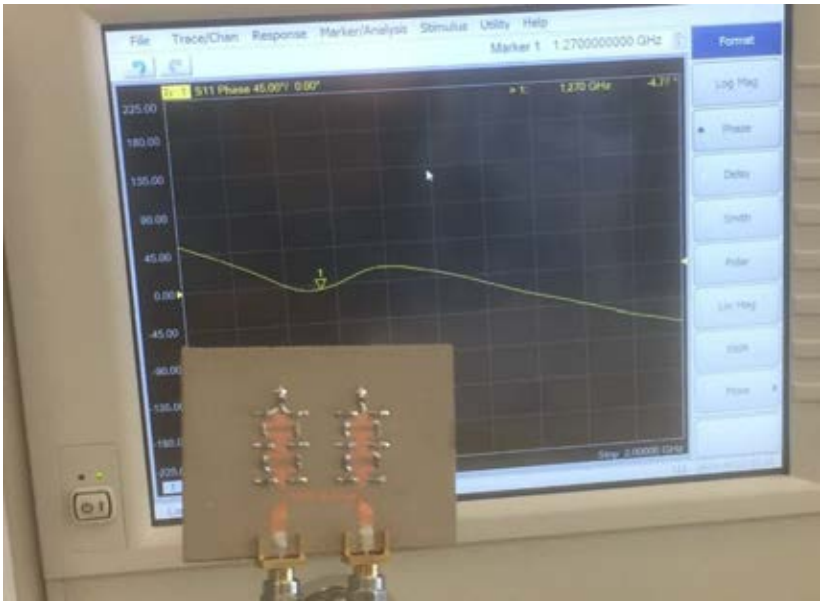


Figure 5.30: Photograph of the S_{11} magnitude of the prototype. The prototype consists of a Lange coupler connected at its outputs to two NGD networks; whereas its input and isolated ports are connected to the VNA through 50 Ω measurement ports.

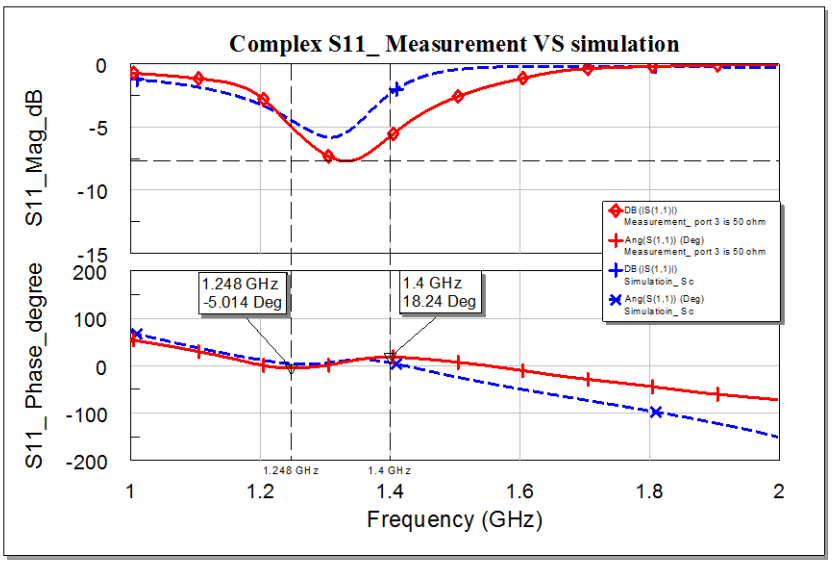


Figure 5.31: Reflection coefficient response plots obtained from measurement and simulation for the combination of the Lange coupler and NGD networks of Fig. 5.29

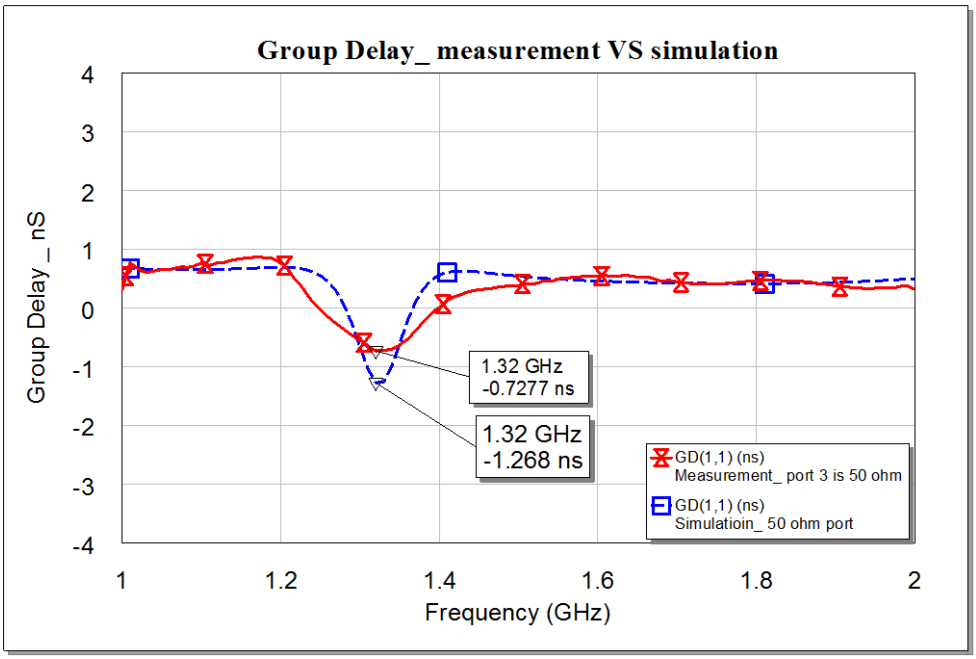


Figure 5.32: Simulated and measured group delay (GD) responses obtained from overall structure displayed in Fig. 5.29

The second measurement was carried out for the prototype when the isolated port of the Lange coupler was connected to a short circuit. Figure 5.33 shows the circuit schematic of this implementation of Lange coupler and NGD networks as sub-circuits. Furthermore, a photograph of the model when it was tested is shown in Figure 5.34. Measurement and simulation of the reflection coefficient phase and magnitude are compared in Figure 5.35. Both results are in good agreement and exhibit non-Foster behaviour from 1.3 GHz to 1.41 GHz. The measured prototype generates 4.7 dB losses and the simulated circuit suffers from 5.8 dB losses. It should be noted the measured phase response of the design is almost flat. This can be

attributed to fact that the positive group delay of the Lange coupler reduces the value of the NGD. Moreover, the structure suffers from inherent losses because of the implementation of the NGD networks which need to be compensated by amplification. This can be accomplished by employing the reflection amplifier in the overall structure as shown in the next section. Moreover, measured and simulated group delay results obtained by the overall circuit are depicted in Figure 5.36. Measured results reveal that the fabricated circuit generates group delay of -0.15 ns over a bandwidth of 0.11 GHz; whereas simulation result shows that the circuit produces a group delay of -0.5 ns over a bandwidth of 0.08 GHz. Table 5.4 summarises the performance of both prototypes when in term of the realisable bandwidth, losses, and reflection coefficient phase and group delay

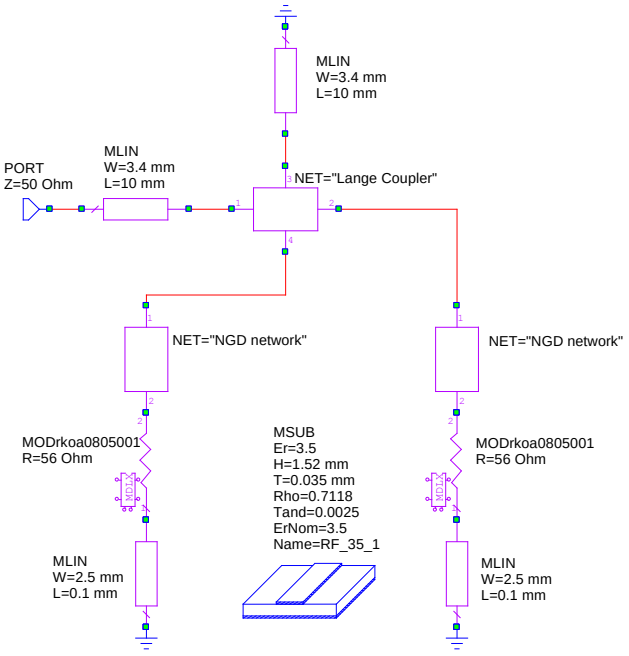


Figure 5.33: Schematic of the combination between a Lange coupler with NGD networks. The “NGD network” sub-circuit is from Fig. 4.14. The “Lange coupler” sub-circuit is from Fig. 5.18.

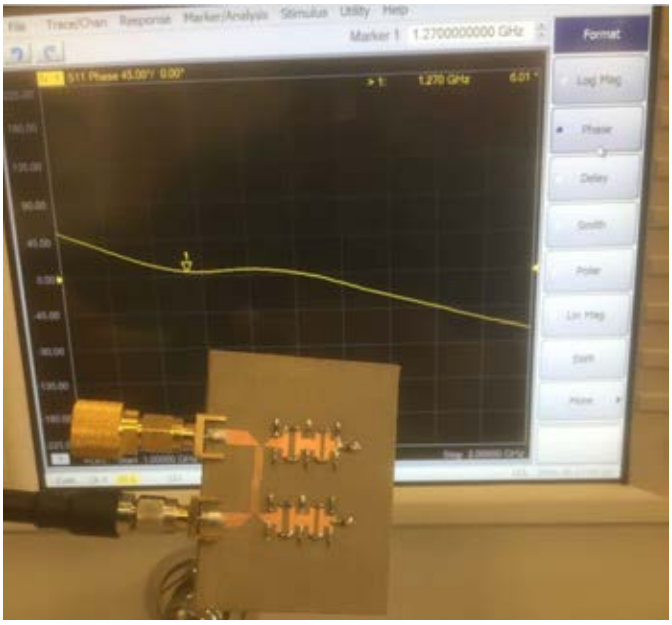


Figure 5.34: Photograph of the S_{11} magnitude of the combined NGD networks with a Lange coupler. Two NGD networks are connected to the outputs of the coupler, the coupler's input port is connected to the VNA through 50 Ω measurement port and the isolation port is connected to a short circuit.

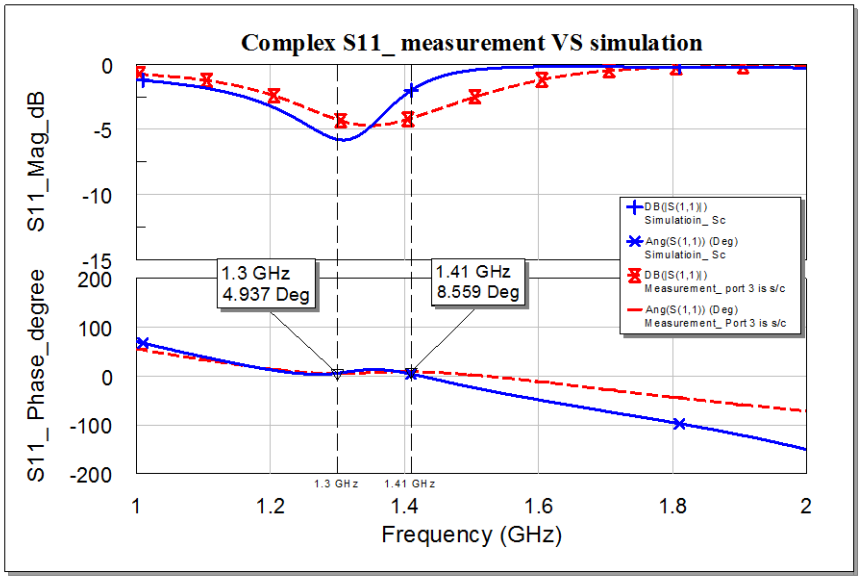


Figure 5.35: Reflection coefficient response plots obtained from measurement and simulation for the combination of the Lange coupler and NGD networks of Fig. 5.33

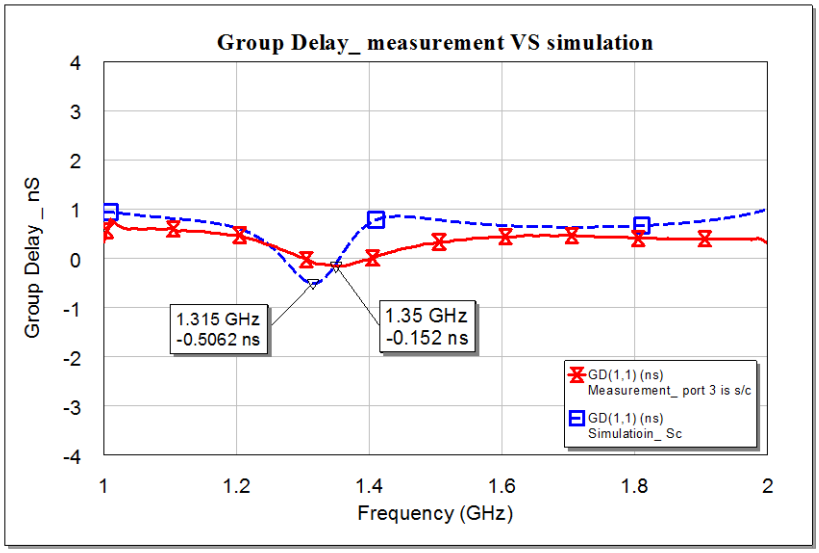


Figure 5.36: Measured and simulated group delay response obtained from overall structure displayed in Fig. 5.33

Table 5. 4: Summary of the performance of both Lange couplers NGD network prototypes

Prototype	Realisable NGD Bandwidth	Losses dB	S_{11} Phase increased by	Group delay
The combination of a Lange coupler with NGD networks, where the Lange coupler isolated port is connected to 50 Ωport	150MHz between 1.25 - 1.4 GHz	7.7 dB	23 degrees	-0.72 ns
The combination of a Lange coupler with NGD networks, where the Lange coupler isolated port is connected to a short circuit	110MHz between 1.3 - 1.41 GHz	4.7 dB	3.6 degrees	-0.15 ns

5.5 Final Synthesised Non-Foster Reactive Element Using Loss-Compensated NGD Networks

As mentioned at the beginning of the chapter, the new loss compensation scheme involves three separate components in the realisation of the final NGD-based non-Foster network. It is realised by combining the NGD networks and a negative resistance reflection amplifier in a balanced structure with a Lange coupler. All the individual circuits have been modelled and experimentally validated. In this section, all the aforementioned components are combined together to construct a new structure which behaves as a reactive non-Foster element (particularly a negative capacitor) in a limited bandwidth in the microwave frequency region.

The overall NGD-based non-Foster structure is designed, simulated and optimised using the AWR Microwave Office. The schematic of the NGD-based non-Foster network is presented as sub-circuits in Figure 5.37. Moreover, the AWR circuit schematic of the realistic structure with the distributed elements and the biasing network is depicted in Figure 5.38. It should be noted that all the extra transmission lines which were added to the individual components to connect them with the measurement ports are de-embedded in the overall design. Figure 5.39 shows the associated circuit layout of the overall NGD-based non-Foster structure.

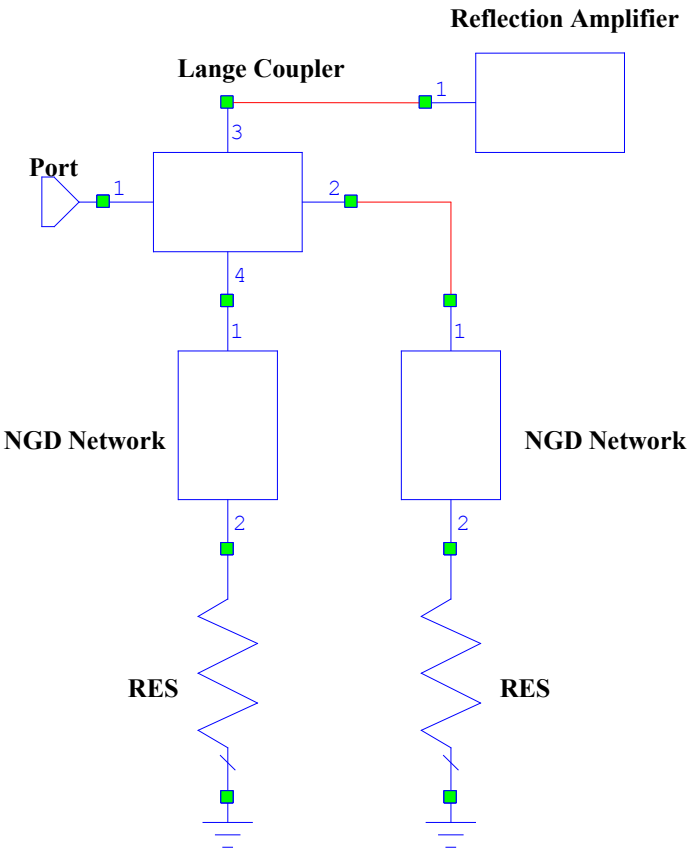


Figure 5. 37: Schematic presents the overall NGD-based non-Foster reactive element using loss compensation NGD networks technique. The “NGD Network” sub-circuit is from Fig. 4.14. The “Reflection Amplifier” sub-circuit is from Fig. 5.5. The “Lange Coupler” sub-circuit is from Fig. 5.18.

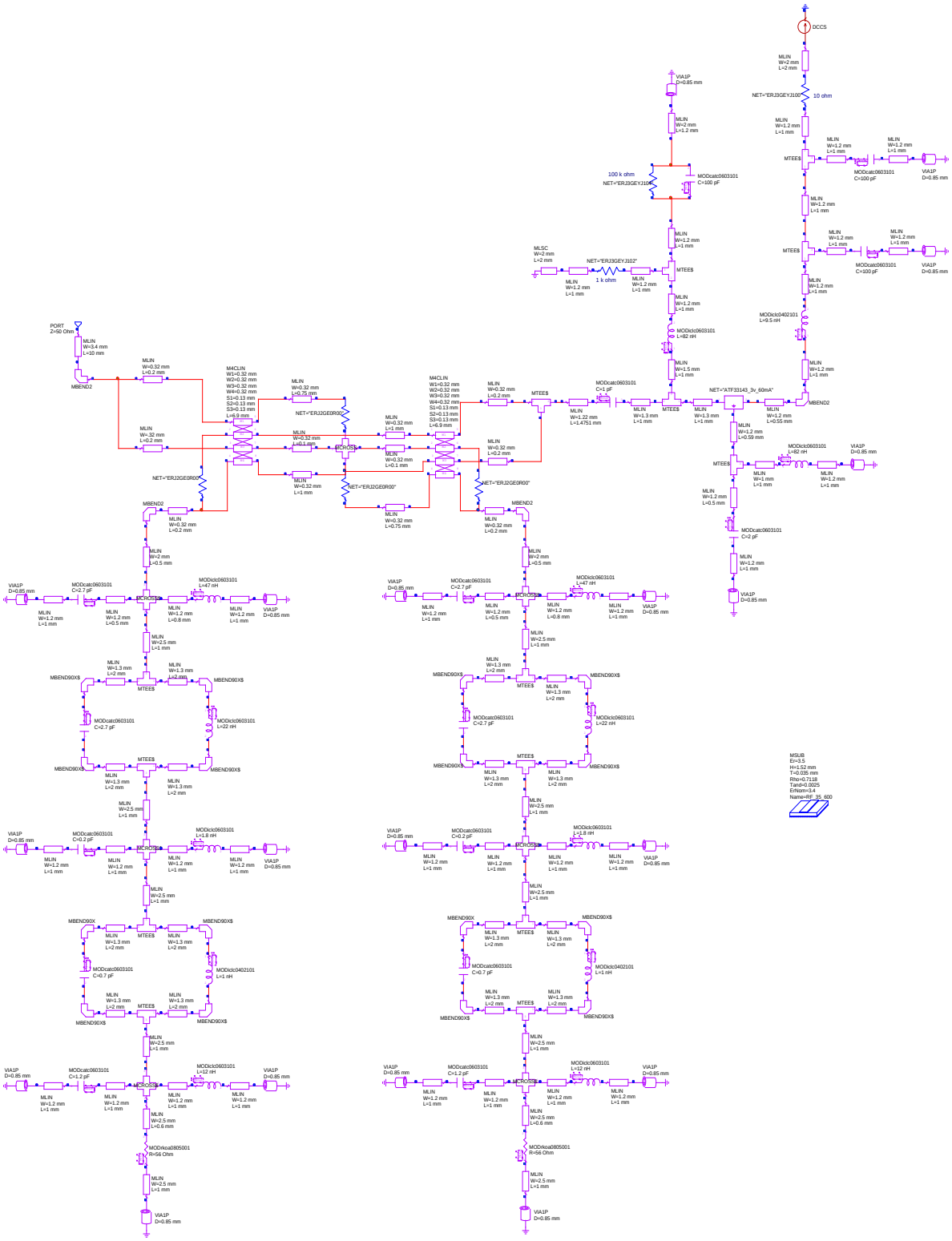


Figure 5. 38: Schematic of the final NGD-based non-Foster network

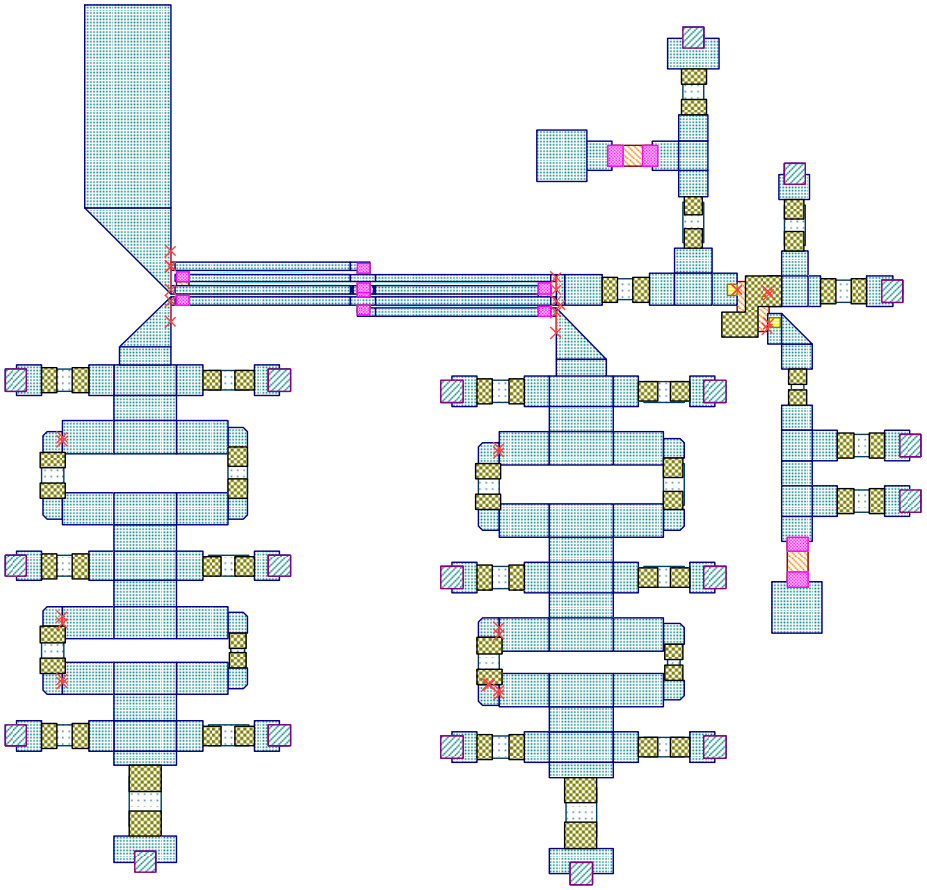


Figure 5.39: AWR circuit layout for the NGD-based non-Foster network

5.5.1 Simulation Results

The reflection coefficient magnitude and phase obtained from the overall NGD-based non-Foster network is depicted in Figure 5.40. The overall structure exhibits NGD behaviour from 1.21 GHz to 1.43 GHz. Studying its S-parameters shows that there is an increasing positive reflection phase in that bandwidth with a very close to 0-dB reflection coefficient and negligible total loss. This indicates that the overall NGD-based non-Foster network in that frequency region is acting as a negative

capacitor. Figure 5.41 shows the locus of the synthesised negative reactance slope of the loss-compensated NGD network was rotating counterclockwise with increasing frequency on the Smith chart. Furthermore, as it can be observed from Figure 5.41, there is no sign of oscillation in our frequency region as the trajectory of the reflection coefficient is not outside the Smith chart perimeter. Therefore, the overall NGD-based non-Foster structure is expected to be stable. Moreover, the group delay introduced by the overall circuit is illustrated in Figure 5.42. The overall circuit generates about (-2 ns) negative group delay over a bandwidth of 0.22 GHz from 1.21 – 1.43 GHz. The overall loss-compensated NGD networks exhibit a non-Foster behaviour over that bandwidth.

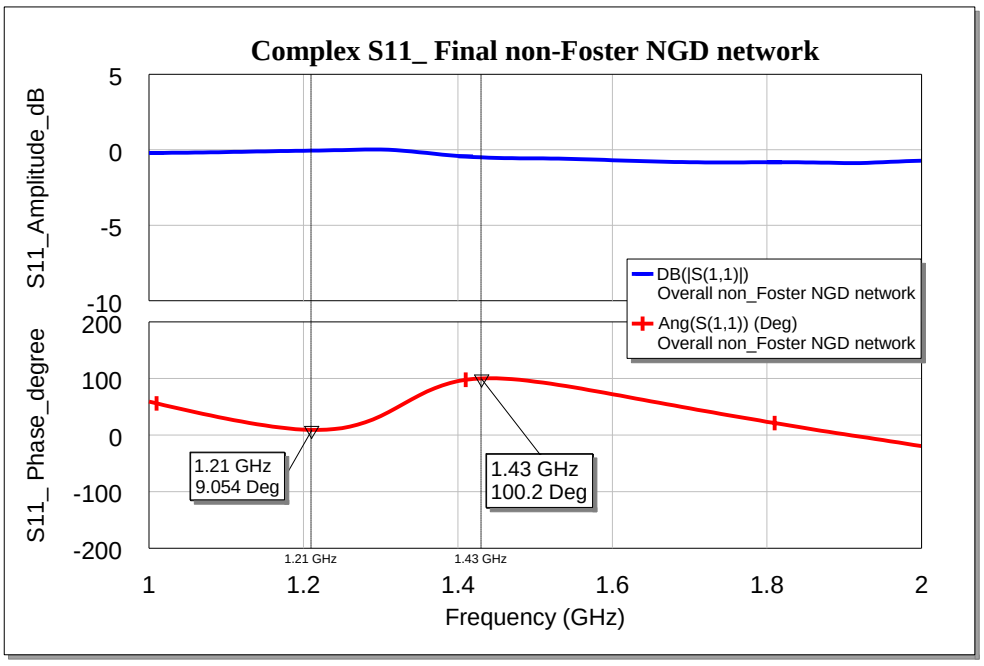


Figure 5.40: Reflection coefficient response plots for the overall NGD-based non-Foster network shown in Fig. 5.38

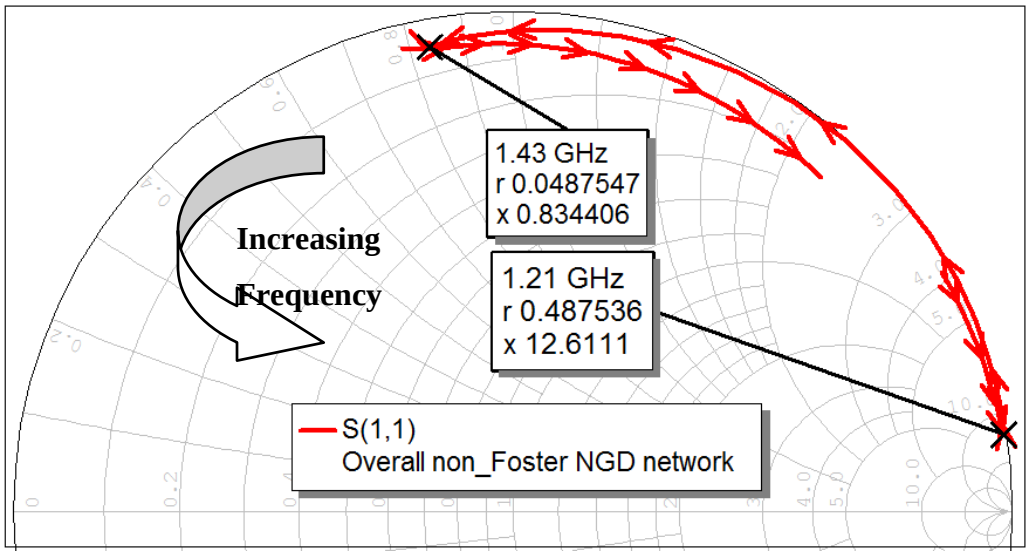


Figure 5.41: Rotation of the reflection coefficient of the NGD-based non-Foster network of Fig. 5.38

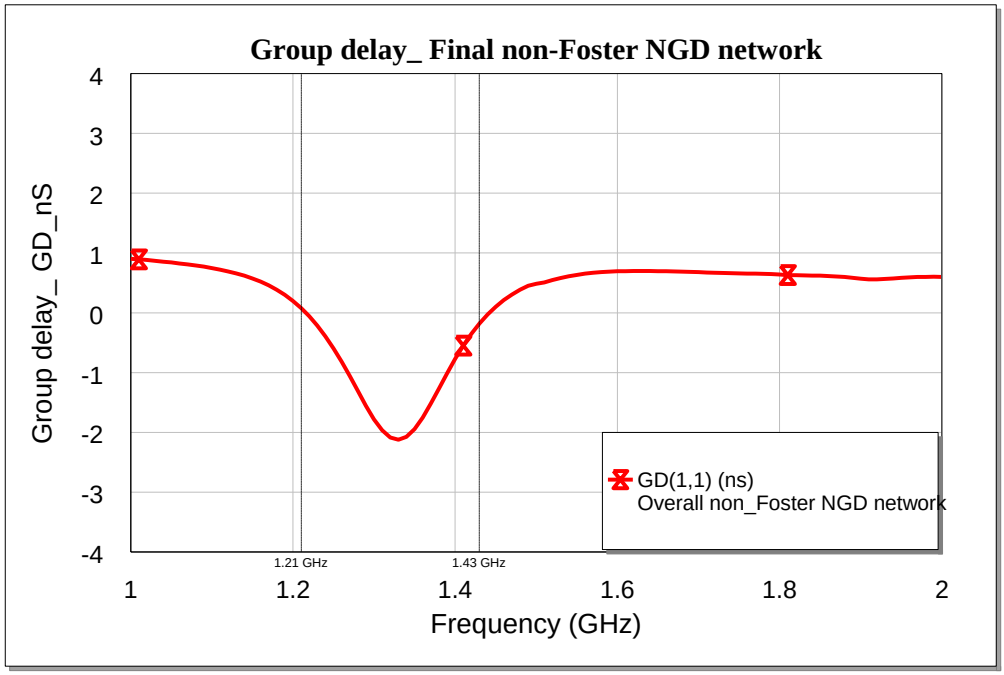


Figure 5.42: Group delay response for the final NGD-based non-Foster network Fig. 5.38

5.5.2 Stability Analysis of the NGD-Based Non-Foster Circuit

The stability of the proposed NGD-based non-Foster circuit is checked using the Nyquist stability measured with modified gamma-probe (STABN_GP2) measurement available in Microwave Office. The GPROBE2 element is connected in series with the input gate of the transistor to measure the internal reflection coefficients required for internal stability measurements at the reference plane where it is inserted. The simulated open loop function G of the (STABN_GP2) measurement plotted on a polar graph from 0.1 GHz to 10 GHz is depicted in Figure 5.43. The open loop function G does not encircle the -1 point in a clockwise sense, thus, the overall NGD-based non-Foster reactive circuit is considered to be stable. Moreover, Table 5.5 presents a comparison between the performance of our proposed loss-compensated reflection–mode NGD-based non-Foster circuit and a loss-compensated transmission–mode NGD-based non-Foster circuit presented in [6], in term of the realisable bandwidth, losses, and reflection and transmission coefficients, group delay and stability analysis.

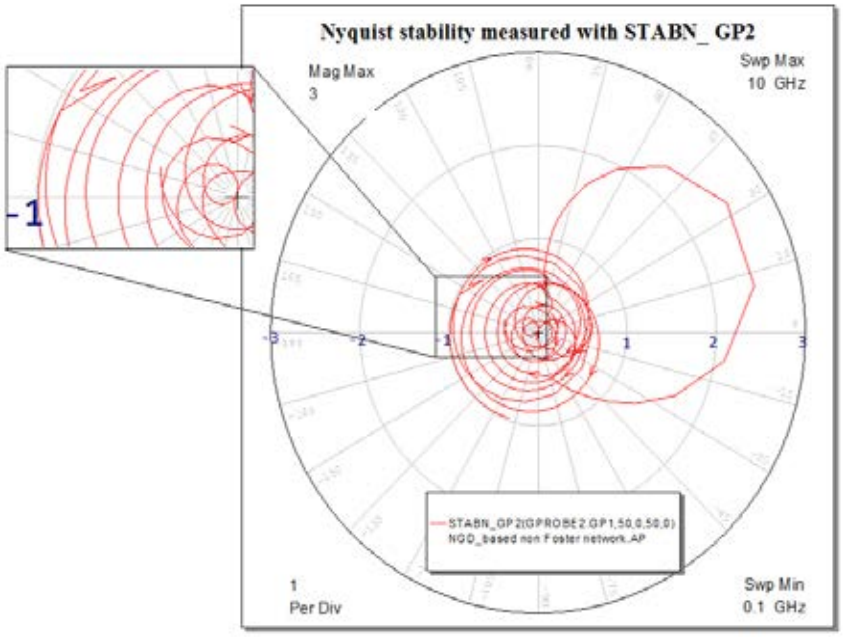


Figure 5.43: Stability analysis through the Nyquist diagram to detect the instability of the FET-based reflection amplifier. The open loop function G, does not encircle the -1 point in the clockwise direction, thus, the NGD-based non-Foster circuit is considered stable

Table 5. 5: Comparison between the proposed NGD-based non-Foster circuit and an NGD-based non-Foster circuit presented in [6]

Non-Foster circuit	Type of NGD network	Active circuit utilised	Realisable NGD Bandwidth	Losses	S_{11} Phase increased by	Group delay	Stability Analysis
Proposed NGD-based non-Foster circuit	Reflection mode using LC resonators	FET-based reflection amplifier	220 MHz between 1.21 and 1.43 GHz	≈ 0 dB	91.15 degrees	-2 ns	Nyquist criteria
NGD-based non-Foster circuit in [6]	Transmission mode using RLC resonators	Regular transmission amplifier	700MHZ between 1.3 and 2 GHz	≈ 0 dB	20 degrees	Not given	Not given

Finally, in order to illustrate the concept of the loss-compensation technique in this implementation, the S_{11} magnitude and phase of the overall structure are compared to a stand-alone NGD network in Figure 5.44. Studying their S-parameters shows that there is an increasing phase response of the reflection coefficient in both structures with a zero loss obtained from the overall structure in the bandwidth of interest as expected. This can be attributed to the losses associated with the NGD networks being compensated by amplification obtained from the negative resistance reflection amplifier when the circuits were combined to realise the final synthesised non-Foster NGD network.

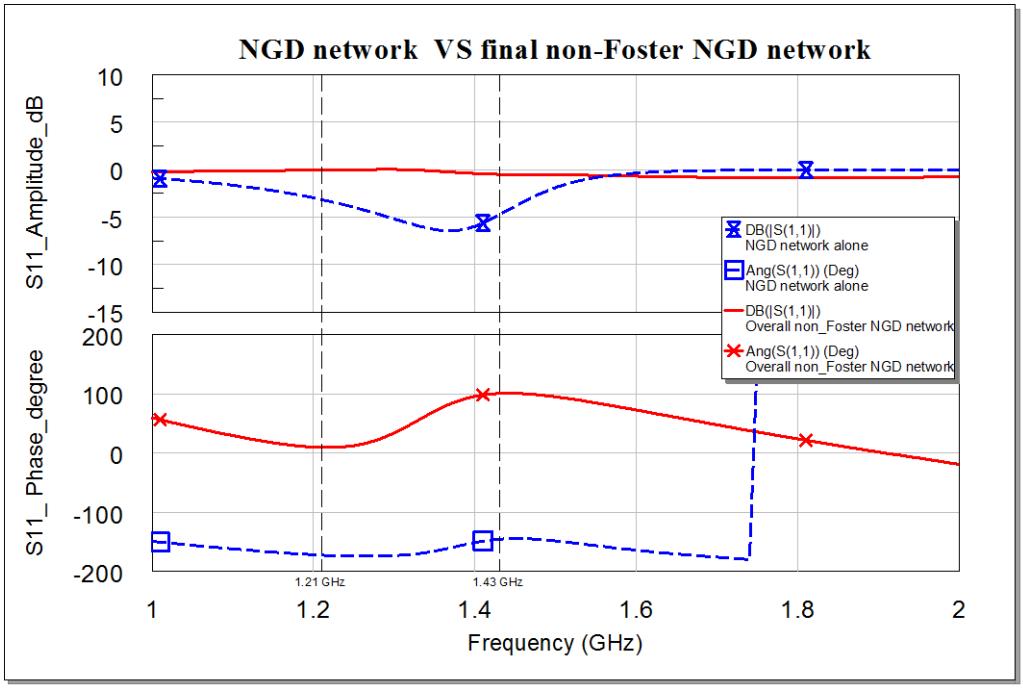


Figure 5.44: S_{11} phase and magnitude plots obtained from the stand-alone NGD network of Fig. 4.14 and the loss-compensated NGD network of Fig. 5.38

5.6 Summary

In this chapter, a novel technique to compensate the inherent losses of the NGD networks in the reflection mode and realising a new class of reactive non-Foster elements has been developed. It provides a new route of synthesising networks with the non-Foster property at a certain bandwidth. It involves a negative resistance amplifier and a Lange coupler to compensate the inherent losses of the NGD networks. Each component has been individually designed and experimentally tested. Measured and simulated results seemed to agree with each other, proving their theoretical concepts. Stability analysis using the Nyquist criteria to detect the instability of the reflection amplifier was performed using Microwave Office, showing that the active circuit is working stable.

A systematic design methodology which starts by characterising the parasitic elements like the Lange coupler and the reflection amplifier is possible. Knowing how much positive group delay these components produce is necessary at the beginning. This helps for designing the NGD network using the method developed in Chapter 4, with a sufficient amount of negative group delay to overcompensate for the unwanted positive group delay produced by the parasitic elements. This systematic approach will provide a new route for synthesising networks with non-Foster behaviour over a limited frequency range. This systematic synthesis procedure can be suggested as a further work for other researchers.

Consequently, an implementation of two reflection-type NGD networks with a Lange coupler has been experimentally validated. Finally, all the circuits were integrated together in a balanced structure forming the final synthesised non-Foster reactive element. Moreover, simulation results from the final circuit were compared to a stand-alone “lossy” NGD network. They showed how this novel technique was able to compensate the losses of the NGD network in a specific frequency range by amplification obtained from the reflection amplifier. The stability of the NGD-based non-Foster network was assessed by Nyquist techniques and simulation results showed that the proposed circuit is working stable. Although the reflection amplifier brings its own stability issues, this separation of functions into separate elements makes it easier to establish stability than in the case of a conventional NIC approach; which typically uses two transistors and creates the problem of establishing the desired reactance trajectory in a single complex element design. The new class of the reactive non-Foster element is applicable to antenna matching, where both transmit and receive functions are required. The potential use of this overall circuit through simulation in antenna matching applications is presented in Chapter 6.

References

[1] P. Gardner and D. K. Paul, "Optimum noise measure configurations for transistor negative resistance amplifiers," Microwave Theory and Techniques, IEEE Transactions on, vol. 45, pp. 580-586, 1997.

[2] P. Gardner and D. K. Paul, "Aspects of the design of low noise, negative resistance, reflection mode transistor amplifiers," IEEE Transactions on Microwave Theory and Techniques, vol. 39, pp. 1869-1875, 1991.

[3] F. Farzami, S. Khaledian, B. Smida, and D. Erricolo, "Ultra-low power reflection amplifier using tunnel diode for RFID applications," in 2017 IEEE International Symposium on Antennas and Propagation & USNC/URSI National Radio Science Meeting, 2017, pp. 2511-2512.

[4] S. Khaledian, F. Farzami, D. Erricolo, and B. Smida, "A Full-Duplex Bidirectional Amplifier With Low DC Power Consumption Using Tunnel Diodes," IEEE Microwave and Wireless Components Letters, vol. 27, pp. 1125-1127, 2017.

[5] D. M. Pozar, Microwave Engineering, 3rd ed. New York, NY, USA: Wiley, 2005.

[6] H. Mirzaei and G. V. Eleftheriades, "Realizing Non-Foster Reactive Elements Using Negative-Group-Delay Networks," Microwave Theory and Techniques, IEEE Transactions on, vol. 61, pp. 4322-4332, 2013.

CHAPTER 6

ANTENNA MATCHING NETWORK USING NEW CLASS OF NON-FOSTER REACTIVE ELEMENTS

This chapter presents the potential use of the synthesised reactive non-Foster element using reflection-type NGD networks in antenna matching applications as it enables both transmit and receive operations without having to switch the configuration. It explores a new analysis of the equivalent circuit of the non-Foster element based on its reflection coefficient variation with frequency. In order to demonstrate one plausible application of the final non-Foster NGD device, a suitable electrically small patch antenna and its equivalent circuit are designed; and through simulation, the application to antenna matching is demonstrated. To prove that the equivalent RLC network can represent an electrically small antenna in practice, a planar monopole patch antenna is designed and with an external matching circuit, made a broader band by the addition of the final non-Foster NGD network.

6.1 Realisation of an Equivalent Circuit Model for the Final Synthesised Non-Foster Element

In this section, a systematic approach is introduced to show how the reflection coefficient (S_{11}) variation with frequency of the final NGD-based non-Foster network of Fig 5.38 in the bandwidth of interest, can be represented by an equivalent LC circuit model. The extra length of the transmission line that connects the overall structure with the measurement port is de-embedded here. However, the impedance trajectory cannot be represented by a single negative capacitor or a single negative inductor because the impedance trajectory of a single negative element doesn't agree well with the impedance response of the proposed non-Foster NGD network. A better fit is achieved in the frequency range from 1.21 GHz to 1.43 GHz, when the impedance is modelled by an equivalent circuit of a shunt negative capacitor and a shunt negative inductor, connected in a parallel branch as depicted in Figure 6.1.

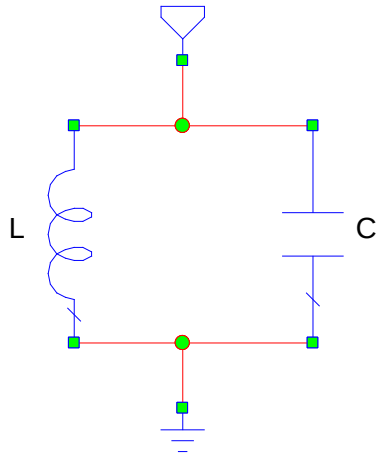


Figure 6.1: Schematic of the LC equivalent circuit model for the NGD-based non-Foster network in the bandwidth of interest, where ($L < 0, C < 0$)

To design the shunt equivalent circuit model, the initial values of the negative capacitor and the negative inductor can be determined from the following derivations:

The susceptance (b) is

$$b = \omega c - \frac{1}{\omega L} \tag{6.1}$$

The values of C and L can be found for the best fit. From Figure 6.1, the denormalized b = -0.0712 @ 1.43 GHz and the denormalized b = -0.0082 @ 1.21 GHz. Applying both susceptance values into equation (6.1), we get:

$$\omega c - \frac{1}{\omega L} = -0.0712 \qquad @1.43\ \text{GHz} \tag{6.2}$$

$$\omega c - \frac{1}{\omega L} = -0.0082 \qquad @1.21\ \text{GHz} \tag{6.3}$$

$$\frac{\omega^2 LC - 1}{\omega L} = -0.0712 \qquad @1.43\ \text{GHz} \tag{6.4}$$

$$\frac{\omega^2 LC - 1}{\omega L} = -0.0082 \qquad @1.21\ \text{GHz} \tag{6.5}$$

$$\omega_1^2 \mathrm{LC} - 1 = -0.0712\ \omega_1\ \mathrm{L} \quad @1.43\ \mathrm{GHz} \tag{6.6}$$

$$\omega_2^2 \mathrm{LC} - 1 = -0.0082\ \omega_2 \mathrm{L} \quad @1.21\ \mathrm{GHz} \tag{6.7}$$

Divide equation (6.6) by ω_1^2 to find LC

$$\mathrm{LC} = \frac{-0.0712\mathrm{L}}{\omega_1} + \frac{1}{\omega_1^2} \tag{6.8}$$

Divide equation (6.7) by ω_2^2 to find LC

$$\mathrm{LC} = \frac{-0.0082}{\omega_2} + \frac{1}{\omega_2^2} \tag{6.9}$$

By equalising equations (6.8) and (6.9) the values of L can be determined as follows:

$$\frac{-0.0712\mathrm{L}}{\omega_1} + \frac{1}{\omega_1^2} = \frac{-0.0082\mathrm{L}}{\omega_2} + \frac{1}{\omega_2^2} \tag{6.10}$$

$$\frac{-0.0712\mathrm{L}}{\omega_1} + \frac{0.0082\mathrm{L}}{\omega_2} = \frac{1}{\omega_2^2} - \frac{1}{\omega_1^2} \tag{6.11}$$

$$\left(\frac{-0.0712}{\omega_1}+\frac{0.0082}{\omega_2}\right)\mathrm{L}=\frac{1}{\omega_2^2}-\frac{1}{\omega_1^2} \tag{6.12}$$

Finding ω_1 and ω_2

$$\omega_1 = 2\pi f_1 = 2\pi x1.43 = 8.98\ \mathrm{GHz} \tag{6.13}$$

$$\omega_2 = 2\pi f_2 = 2\pi x1.21 = 7.61\ \mathrm{GHz} \tag{6.14}$$

By substituting ω_1 and ω_2 into equation (6.12), the value of L can be calculated as follows:

$$\left(\frac{-0.0712}{8.98}+\frac{0.0082}{7.61}\right)\mathrm{L}=\frac{1}{(7.61)^2}-\frac{1}{(8.98)^2} \tag{6.15}$$

Therefore,

$$\mathrm{L} = -0.7\ \mathrm{nH}$$

By substituting L value into equation (6.6),the value of C can be calculated as follows:

$$(8.98)^2 x(-0.7)x\,C - 1 = -0.0712 \text{ x } 8.98 \text{ x } (-0.7) \qquad (6.16)$$

Therefore,

$$C = -25.6 \text{ pF}$$

The calculated negative LC values give a good starting point, for fitting the susceptance trajectory as shown in Figure 6.2. However, there is a deviation in the middle. Therefore, a better fit is obtained by further optimisation of negative L and C values using AWR design environment. The final obtained values of the negative capacitor and the negative inductor are $(C = -27\text{pF})$ and $(L = -0.62\text{nH})$ respectively. As a result, the associated reflection coefficient phase variation response of the equivalent LC circuit closely follows that of the final synthesised non-Foster NGD circuit in the frequency range between 1.285 GHz–1.4565 GHz as depicted in Figure 6.3. Figure 6.4 shows the imaginary part of the input admittance response (Y_{in}) of the synthesised negative LC equivalent circuit which follows that of the final non-Foster circuit from 1.258 GHz to 1.46 GHz.

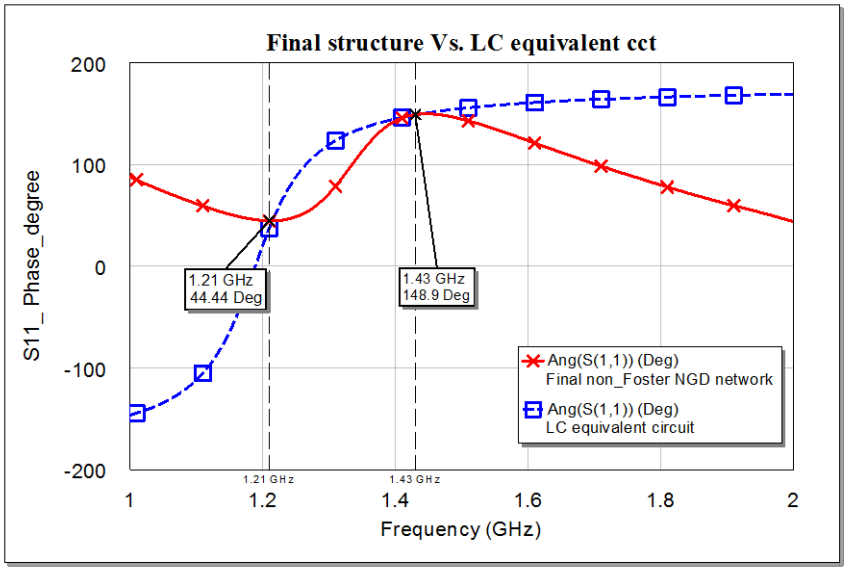


Figure 6.2: S_{11} phase response of the final synthesised non-Foster element of Fig 5.38 versus the phase response obtained from an ideal non-Foster network modelled using an equivalent circuit of Fig 6.1 with values of (C = -25.6 pF) and (L = -0.7 nH)

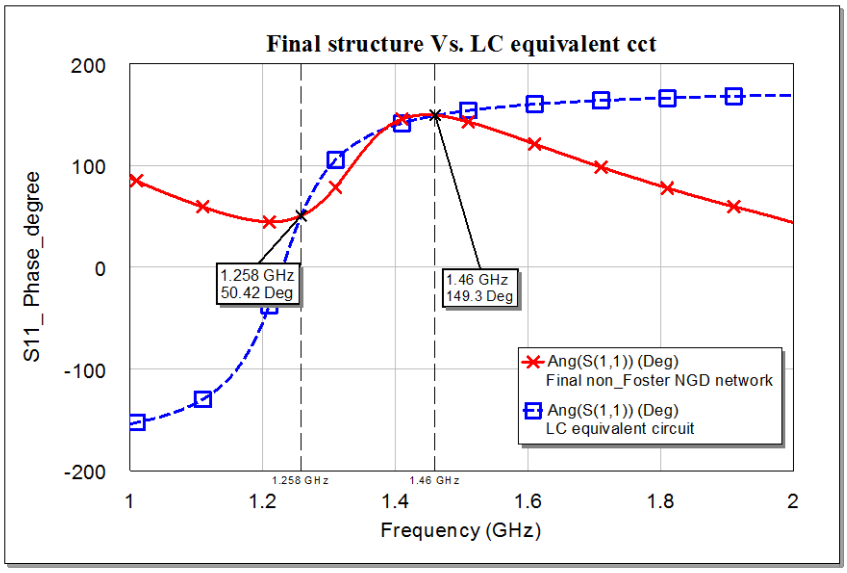


Figure 6.3: S_{11} phase response of the final synthesised non-Foster element of Fig 5.38 versus the phase response obtained from an ideal non-Foster network modelled using an equivalent circuit of Fig 6.1 with values of (C = -27 pF) and (L = -0.62 nH)

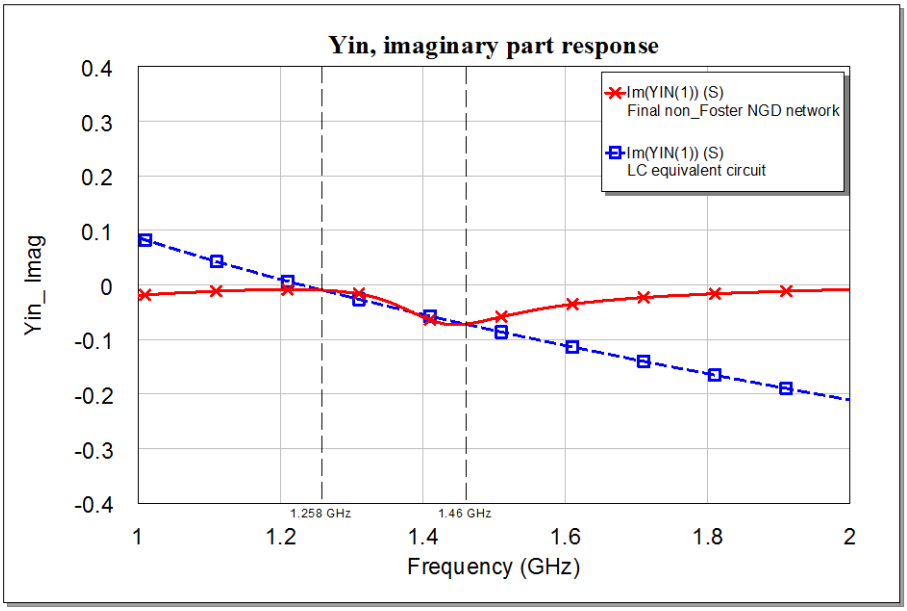


Figure 6.4: The input admittance imaginary parts response of the final non-Foster NGD network and the synthesised LC equivalent circuit of Fig 6.1 with values of (C = -27 pF) and (L = -0.62 nH)

6.2 Realisation of Pure Negative Capacitance from the LC Equivalent Circuit

The effect of the negative inductor can be compensated by employing a positive inductor in shunt with the synthesised non-Foster network, using the LC equivalent circuit model, giving a total inductance of Lp:

$$L_p = \frac{(L_1 \, x \, L_2)}{(L_1 + L_2)} \tag{6.20}$$

Where, L_1 and L_2 are the negative inductor and the positive inductor elements respectively. Then, $(L_1 + L_2 = 0)$. Therefore, $L_p = \infty$. As a result, a pure effective negative capacitance with a value of C = -27 pF can be obtained in the frequency range of interest, as depicted in Figure 6.5; it is in the right range of magnitude for matching electrically small antennas and tuning their frequencies of resonance.

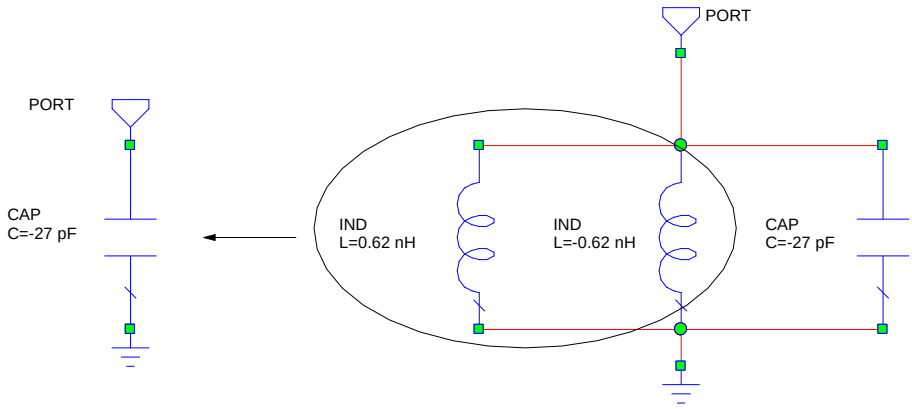


Figure 6.5: AWR circuit schematic shows how a purely negative capacitor is realized from the equivalent circuit model presented in Fig 6.1

6.3 Design of an Electrically Small Antenna

To appreciate the potential benefit of using the NGD-based non-Foster element in antenna matching applications, an electrically small patch antenna (ESPA) is designed to be resonating at a higher frequency than the frequency range where the overall synthesised non-Foster network is working as a negative capacitance. One way to do that is essentially by treating the ESPA as a stub, because an ESPA when

it is not radiating, looks like an open circuit stub. The desired ESPA should be less than a quarter-wavelength long, for example, $\lambda/6$ long transmission line, and looks like a positive capacitance at the design frequency in the middle of the negative capacitance range of the synthesised non-Foster property.

In this work, the chosen frequency of design is in the middle of the negative capacitance range, which is 1.36 GHz. If, as a starting point, the designed ESPA is a $\lambda/6$-long microstrip transmission line, its associated reactance is:

$$Z = -jZ_c \cot \beta l \tag{6.21}$$

Where Z_c is the characteristic impedance of the ESPA as a transmission line and $\beta l = 60^o$. The corresponding capacitance would be ($\omega c = 2\pi f$).

$$\omega c = \frac{1}{Z_c} \tan 60^o \tag{6.22}$$

$$Zc = \frac{\tan 60^o}{\omega c} \tag{6.23}$$

The C value is the opposite of the negative capacitance value of Figure 6.5, which is $C = 27$ pF. Therefore, the characteristic impedance (Zc) of the ESPA is:

$$Z_c = \frac{1.73}{2\pi x 1.36x10^{9}x27x10^{-12}}$$

$$Z_c = 7.5\ \Omega$$

Using the calculator TX LINE of the AWR software and a Taconic RF_35_0600 substrate with relative permittivity $\varepsilon_r = 3.5$ and a dielectric thickness $H = 1.52$ mm, the width (W) and the length (L) of the ESPA are calculated as $W = 37$ mm and $L = 20$ mm. Furthermore, the dimensions of the 50 Ω feeding line for the ESPA are obtained as $W = 3.4$ mm and the length should be short so it doesn't affect the impedance, ideally $L = 2$ mm. Finally, the electrically small microstrip patch antenna is designed and modelled using the electromagnetic AWR Axiem simulator.

The obtained susceptance from the simulation is not at the right range of magnitude for matching the ESPA by the synthesised non-Foster network at the frequency range of interest. It is not at the right value because the calculated length of the patch antenna was long and has got a fringing capacitance on the end of it. In order to compensate for the fringing capacitance effect, the physical length must be reduced and as a result, the susceptance can be reduced to the right value of magnitude for matching the ESPA with different matching networks. An optimisation to the antenna's structure was carried out and as a result an ESPA with dimensions of ($L = 14.1$ mm) and ($W = 23$ mm) was designed, as shown in Figure 6.6. The simulated

ESPA exhibits a -5.493 dB return loss at a resonant frequency of 5.39 GHz and a bandwidth of 11.8% at -3 dB return loss between 5.072 GHz and 5.709 GHz as depicted in Figure 6.7.

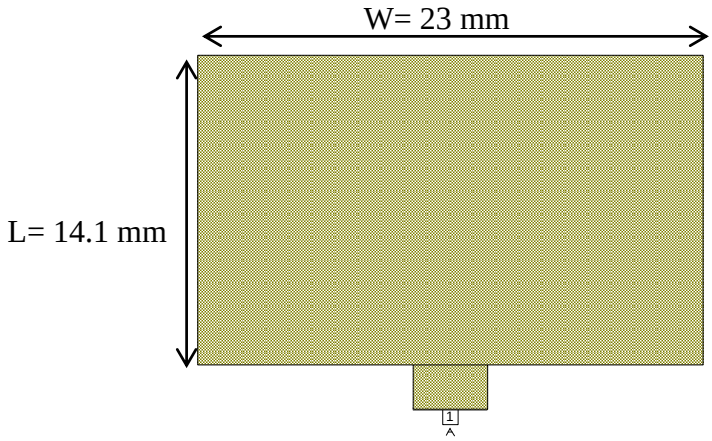


Figure 6.6: AWR circuit schematic of the ESPA with dimensions of (W = 23 mm) and (L = 14.1 mm), designed on a Taconic RF_35 substrate

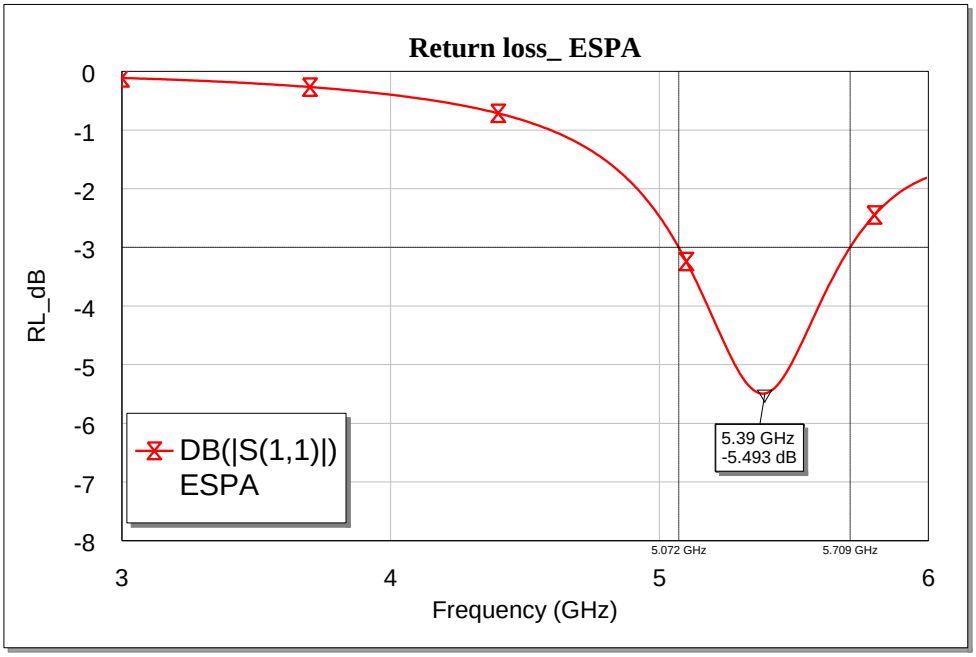


Figure 6.7: The simulated return loss of the ESPA

The modelled antenna produces a susceptance value of ($15.55\Omega^{-1}$) at 1.36 GHz as shown in Figure 6.8 and it is at the right value of magnitude to match the antenna with different matching techniques and tune its frequency of resonance. The real and imaginary parts of the input impedance of the ESPA are presented in Figure 6.9. The ESPA acts as a positive capacitor from 1 GHz to 1.53 GHz and beyond that, it behaves as a positive inductor. To match the antenna and tune its resonance frequency to the desired frequency of operation which is 1.36 GHz, the proposed NGD-based non-Foster network and its equivalent LC circuit are employed as non-Foster matching networks, as demonstrated in the next section.

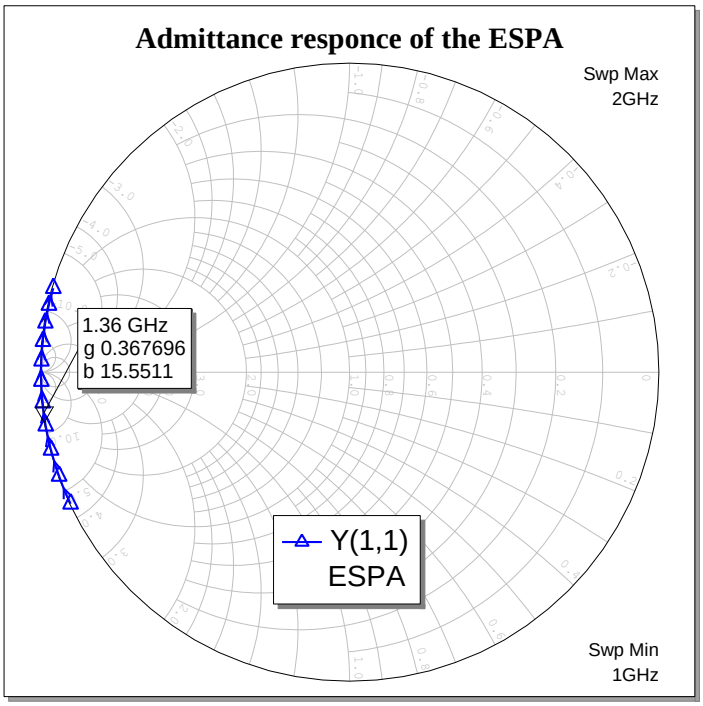


Figure 6.8: The obtained susceptance and conductance values of the ESPA of Fig 6.7

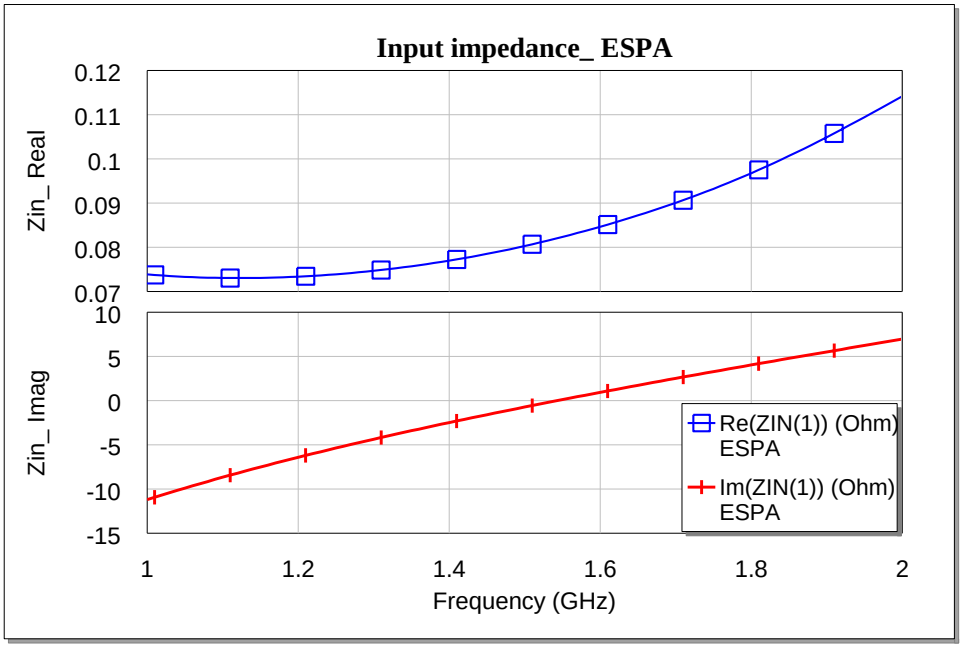


Figure 6.9: The complex input impedance of the ESPA

6.4 Antenna Matching Network Application

In this section, the proposed NGD-based non-Foster network is implemented as a non-Foster matching network with the ESPA as depicted in Figure 6.10. Also, the ESPA is matched with the ideal non-Foster network of Fig 6.5 and with an ideal negative capacitor of a value of (C = -27 pF). Moreover, the ESPA is matched with a Foster matching network which consists of a positive inductor of a value (L = 0.62 nH). All the impedance matching networks were connected in shunt with the proposed ESPA and simulated using an AWR design environment.

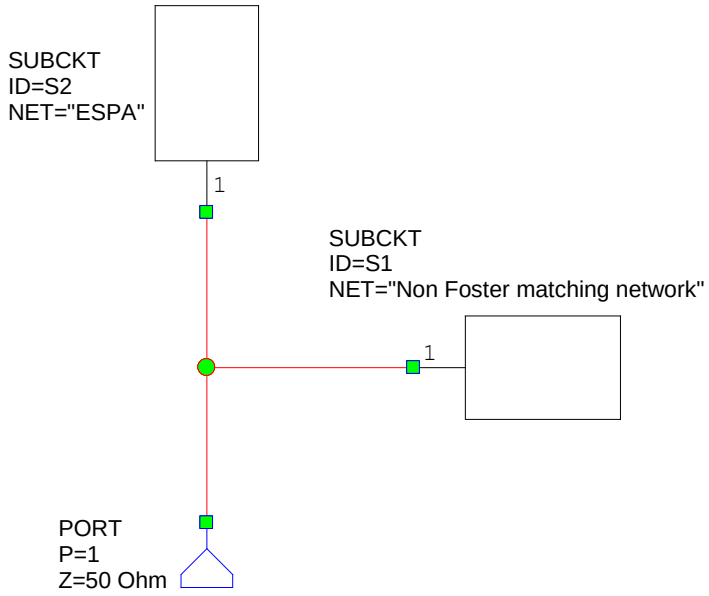


Figure 6.10: AWR schematic of the ESPA matched with non-Foster matching technique

Figure 6.11 demonstrates the simulated return loss (RL) of the ESPA matched with different matching techniques. It was possible to tune down the resonance frequency of the antenna to the frequency range of interest. This demonstration proves that the realised ideal non-Foster network from the NGD-based non-Foster network is working as good as an effective negative capacitor of a value of (-27 pF) in the frequency range of interest, as it produced -5.9 dB return loss at 1.36 GHz and within a bandwidth of 1.4% at -3 dB return loss. The antenna matched with a Foster positive inductor has a return loss of -3.97 dB at 1.34 GHz and a bandwidth of 1.35% at -3 dB return loss; whereas, the antenna matched with our NGD-based non-Foster circuit obtains a return loss of -4.17 dB at 1.36 GHz and a bandwidth of 1.63% at -3 dB return loss. The non-Foster matching network gives a slightly deeper resonance compared to the Foster matching network.

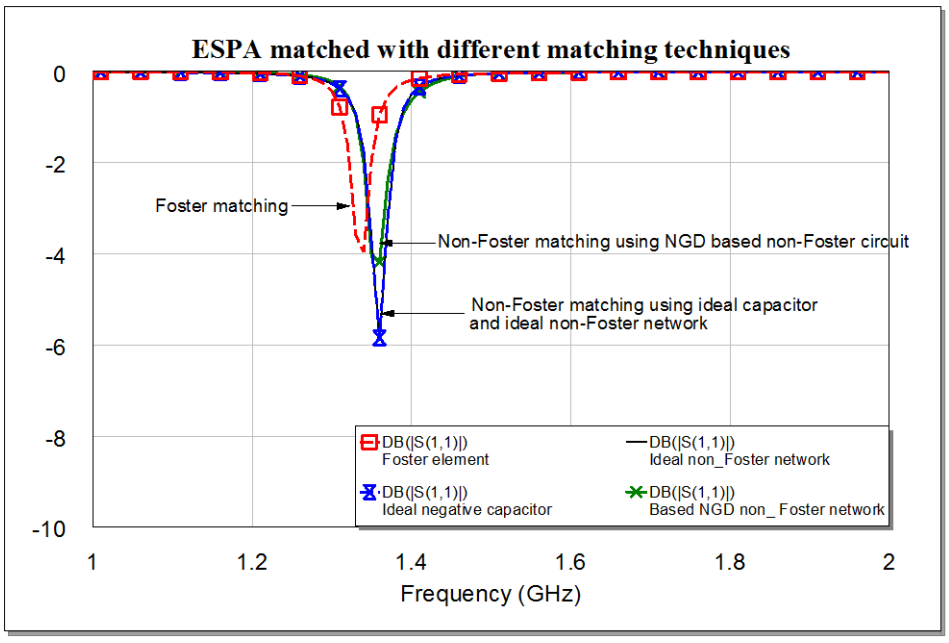


Figure 6.11: Simulated RL for the ESPA matched with different matching networks

The factor preventing broadband and perfect matching using the non-Foster technique with this specific antenna is that the ESPA suffers from small radiation resistance values at the bandwidth of interest. Moreover, the normalised conductance value of the antenna, which is (g = 0.368) shown in Fig 6.8, is not at the right value of magnitude and ideally should be close to one.

One way to change the conductance of the antenna to the right value, which is approximately one, is to vary the length and the width of the antenna while keeping its susceptance value approximately constant. This leads to a change in the radiation resistance of the ESPA and to get a good depth of resonance and probably a wider performance. Many attempts have been carried out through a systematic approach to get the conductance value of the antenna close to one and to keep the susceptance value constant; however, none were successful.

An alternative way is introduced in the following section where the overall non-Foster NGD network is represented as a negative inductor instead of a negative capacitor in the bandwidth of interest. Furthermore, the ESPA is represented by an equivalent circuit model. As a result, it is possible to match the antenna at the desired frequency and to have a broader bandwidth.

6.5 Circuit Model of Microstrip Patch Antenna

Due to the difficulty of designing an ESPA with the correct admittance values to be matched with the synthesised negative capacitor and to find out the potential of the synthesised negative inductor in antenna matching networks, the antenna is represented in the form of a resonant RLC network. The chosen shunt RLC resonant circuit is depicted in Figure 6.12. To take the feeding line into consideration, it is represented by an inductive reactance [1- 2]. The RLC values of the modelled circuit and the inductive reactance of the feeding line are optimised and obtained using an AWR circuit schematic simulator. The objective is to design an ESPA which resonates at a higher frequency than our frequency band of interest.

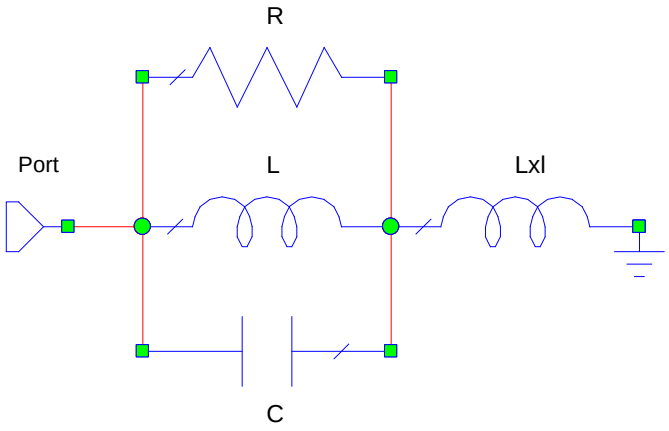


Figure 6.12: RLC equivalent circuit of ESPA. The optimised RLC values are (R = 7 Ω), (L = 0.13 nH), (C = 49 pF) and (L_{XL} = 0.39 nH)

The simulated antenna equivalent RLC network has a return loss of -2.424 dB at 2 GHz and a bandwidth of 10.6% at -2 dB return loss as shown in Figure 6.13. The antenna is not at resonance and is also not well matched. Figure 6.14 and Figure 6.15 illustrate the input impedance and the input admittance of the ESPA's equivalent circuit respectively. In the frequency range from 1 GHz to 2 GHz the antenna equivalent circuit behaves as a positive inductance. Therefore, to match it with a non-Foster matching network, a negative inductor must be employed to cancel out the inductive reactance and obtain a broadband performance.

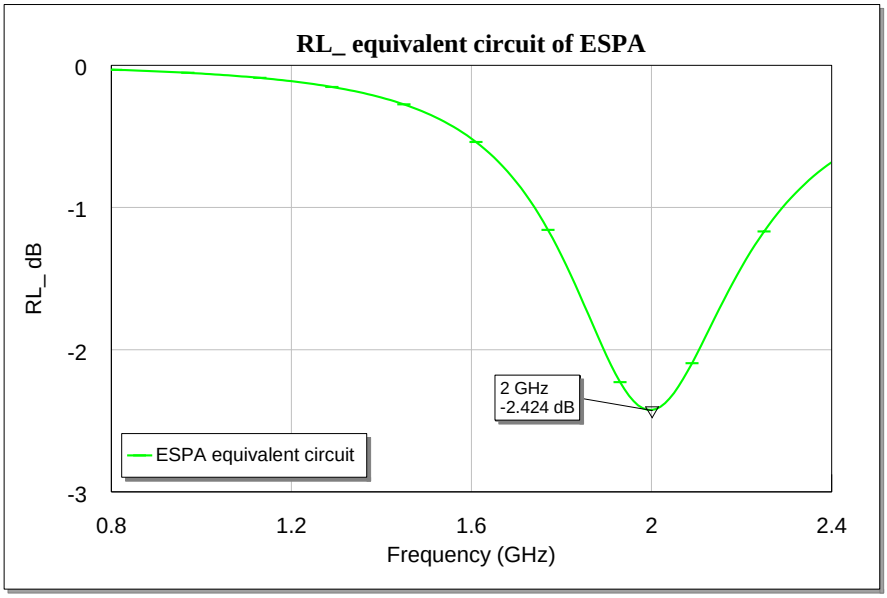


Figure 6.13: Simulated return loss (RL) of the ESPA circuit model shown in Fig 6.12

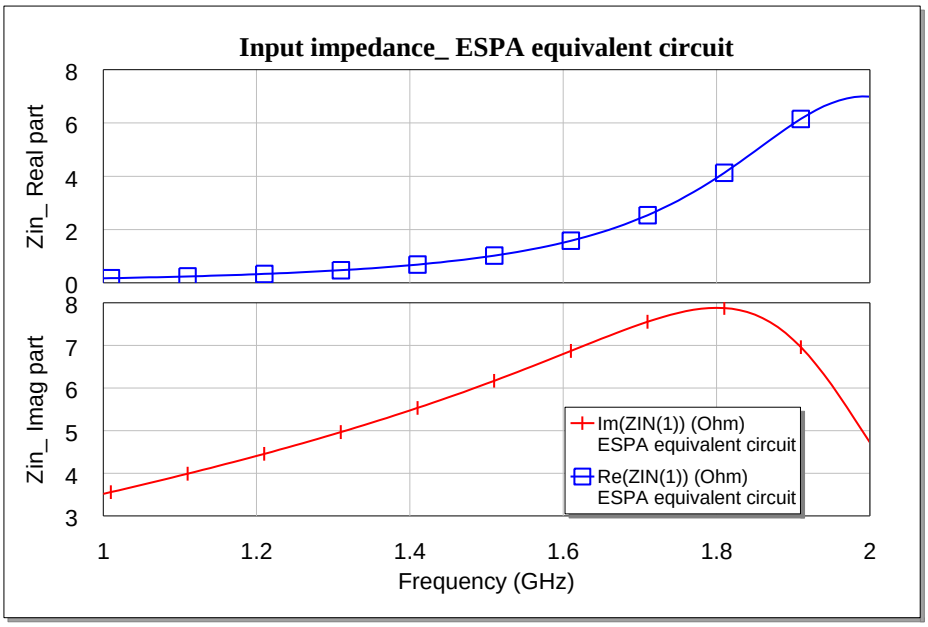


Figure 6.14: The complex input impedance of the ESPA's equivalent circuit

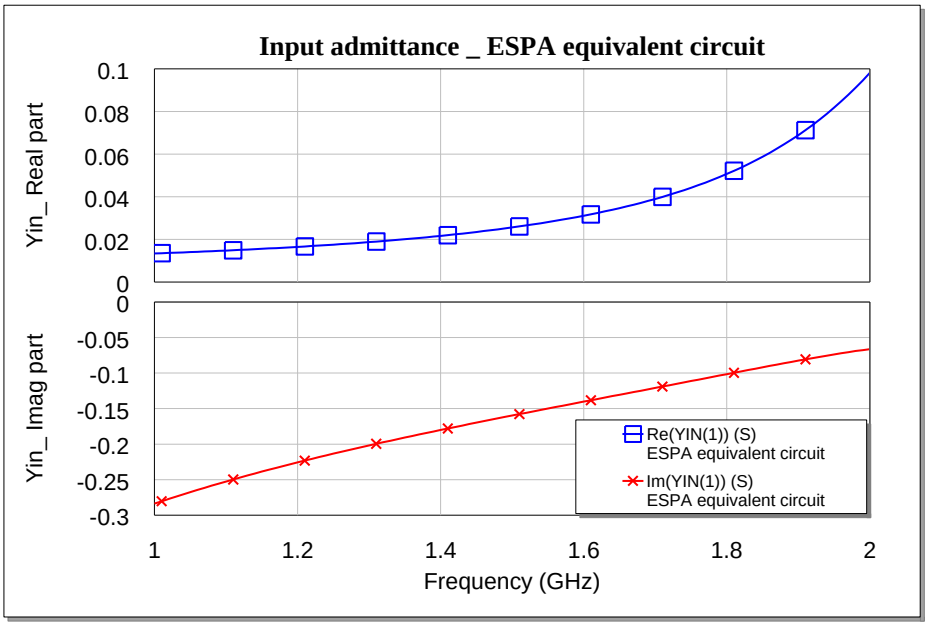


Figure 6.15: The complex input admittance of the ESPA's equivalent circuit

6.6 Realisation of a Pure Negative Inductance from the LC Equivalent Circuit of the Final Synthesised Non-Foster Element

Herein, the effect of the negative capacitor can be compensated by employing a positive capacitor in shunt with the synthesised LC equivalent circuit model of the final NGD-based reactive non-Foster network, giving a total capacitance of Cp:

$$C_p = C_1 + C_2 \tag{6.24}$$

Where, C_1 and C_2 are the negative capacitor and the positive capacitor elements respectively. Then, $(C_1 + C_2 = 0)$. Therefore, $C_p = 0$. As a result, a pure negative inductance with a value of L = -0.62 nH can be obtained in the frequency range of interest, as shown in Figure 6.16; and it is in the correct range of magnitude for matching electrically small antennas, to broaden their bandwidth and tune their frequencies of resonance [1].

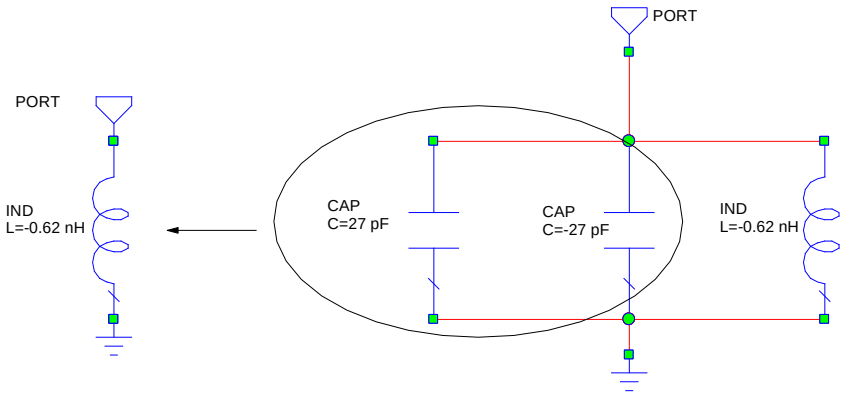


Figure 6.16: AWR circuit schematic shows how a purely negative inductor is realized from the equivalent circuit model presented in Fig 6.1

The imaginary part responses of the input impedance and the input admittance of the synthesised negative inductor from the non-Foster NGD network's equivalent circuit of Fig 6.1 are shown in Figure 6.17. In the frequency range from 1 GHz to 2 GHz, the synthesised ideal non-Foster inductor has input impedance with negative imaginary part values and input admittance with positive imaginary part values.

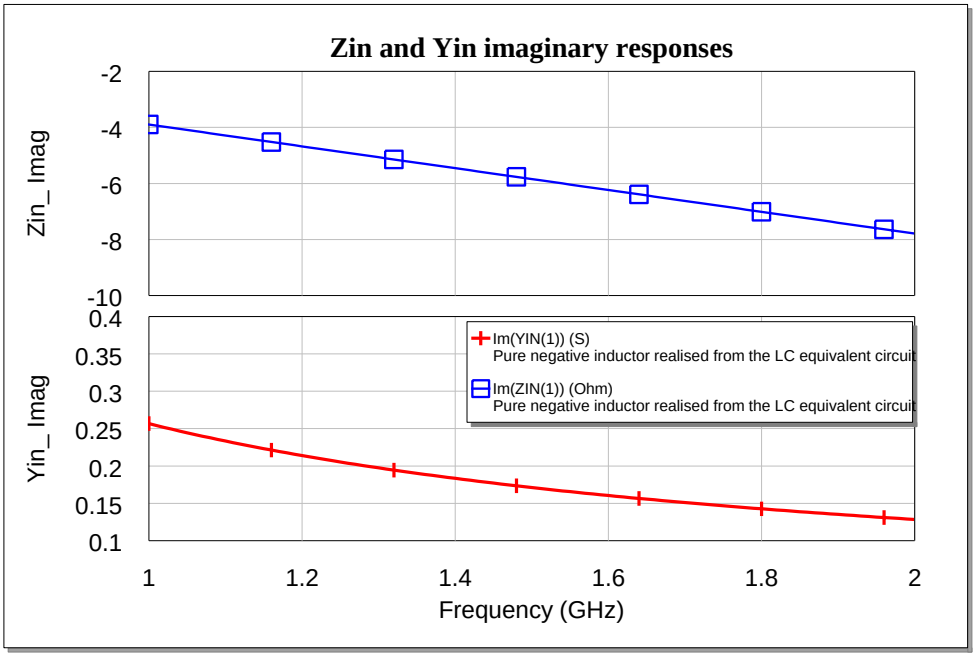


Figure 6.17: The input impedance and the input admittance of the realised negative inductor from the non-Foster NGD network's equivalent circuit model

Figure 6.18 reveals that this synthesised negative inductor can be used as a shunt non-Foster matching network, to match the ESPA's equivalent circuit of Fig 6.12 in the frequency range of interest; as it has the opposite susceptance response. When they are matched in shunt, the inductive admittance of each other will be cancelled

out and as a result, a pure admittance of approximately zero is obtained for a large frequency range; therefore, a broadband matching antenna can be achieved.

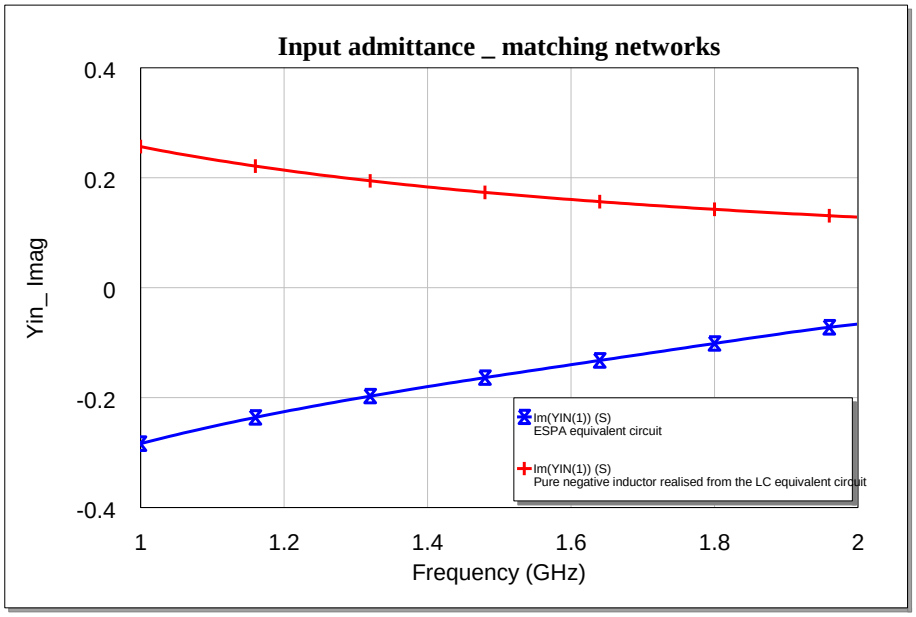


Figure 6.18: Comparison between the input impedance imaginary part response of the ESPA equivalent circuit and the realised pure negative inductor

6.7 Matching Network with the ESPA Circuit Model

To demonstrate the advantages of using non-Foster elements to achieve a wideband antenna matching, an ideal non-Foster network of the RLC equivalent model of the ESPA is impedance matched with Foster matching network and non-Foster matching networks. Consequently, it is also matched with an ideal negative inductor with a value of $(\mathrm{L} = -0.62\ \mathrm{nH})$. The Foster matching network consists of a positive

capacitor with a value of (C = 27 pF). The simulated reflection coefficient (S_{11}) of the antenna with different matching techniques is depicted in Figure 6.19. As it can be seen, it was possible to match the antenna and tune down its resonance frequency to the desired frequency range of interest using different matching techniques. The antenna matched with the Foster matching network obtains a return loss better than -10 dB between 1.224 GHz and 1.285 GHz within the bandwidth of 4.86% at 1.25 GHz (61 MHz of useful bandwidth). Whereas, the antenna matched with the ideal non-Foster network has a return loss better than -10 dB between 1.203 GHz–1.528 GHz within the bandwidth of 23.97% at 1.36 GHz (325 MHz of useful bandwidth). Furthermore, the antenna matched with the overall synthesised non-Foster reactive NGD network has a return loss better than -10 dB between 1.242 GHz and 1.462 GHz within the bandwidth of 16.33% at 1.28 GHz and 1.39 GHz (220 MHz of useful bandwidth). The antenna matched with non-Foster matching networks reveals a significant improvement by achieving a broader bandwidth performance than that obtained when the same antenna was passively matched.

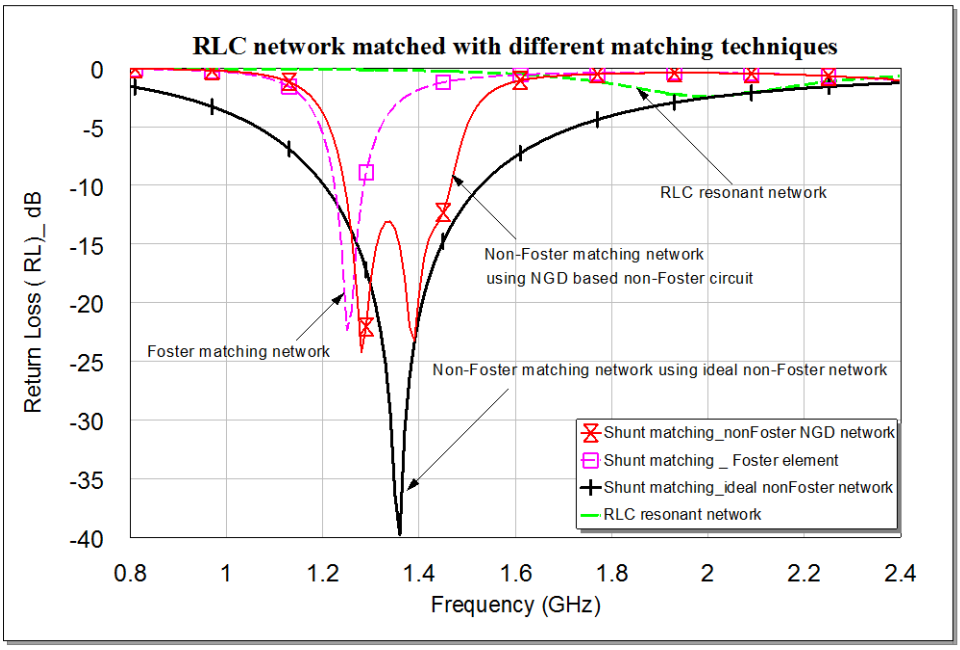


Figure 6.19: Simulated return loss (RL) for the RLC resonant network matched with different matching networks

6.8 Design of a Planar Monopole Patch Antenna (PMPA)

To demonstrate that the RLC equivalent circuit model of Fig 6.12 represents an electrically small antenna in practice, a planar monopole patch antenna is designed using an AWR EMSight simulator to achieve approximately the same characteristic performance of the antenna RLC equivalent circuit and to be resonating at higher frequency than the negative capacitance range of the synthesised non-Foster property, as shown in Figure 6.20. The simulated antenna has a return loss of (-14.49 dB) and is resonating at 1.78 GHz, as depicted in Figure 6.21.

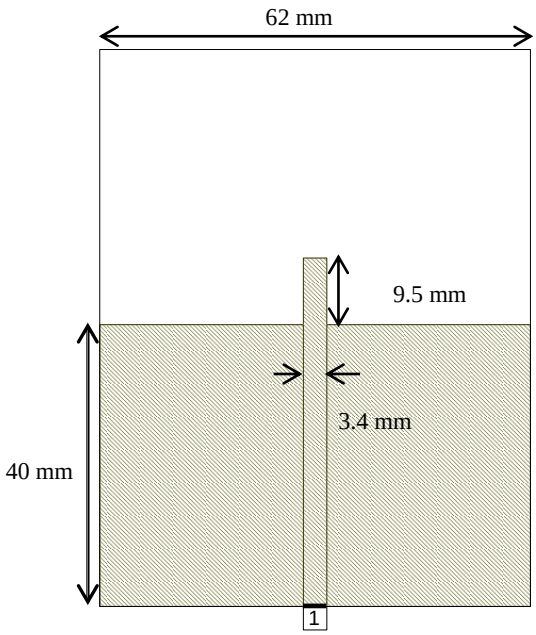


Figure 6.20: Geometry of the planar monopole patch antenna

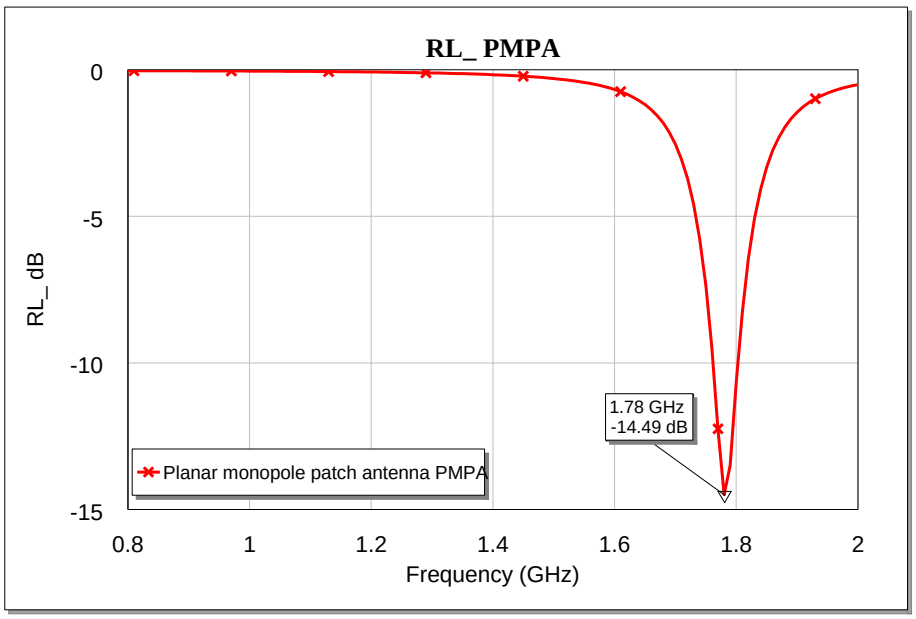


Figure 6.21: Return loss response of the proposed simulated PMPA

Figure 6.22 shows the real and the imaginary parts of the input impedance of the proposed PMPA. As the antenna is electrically small, it suffers from a very small radiation resistance. It has a positive reactance below its resonance.

Figure 6.23 presents input admittance conductance and susceptance of the proposed PMPA. In the frequency range from 1 GHz to 1.63 GHz the PMPA has a fairly constant negative inductive susceptance response.

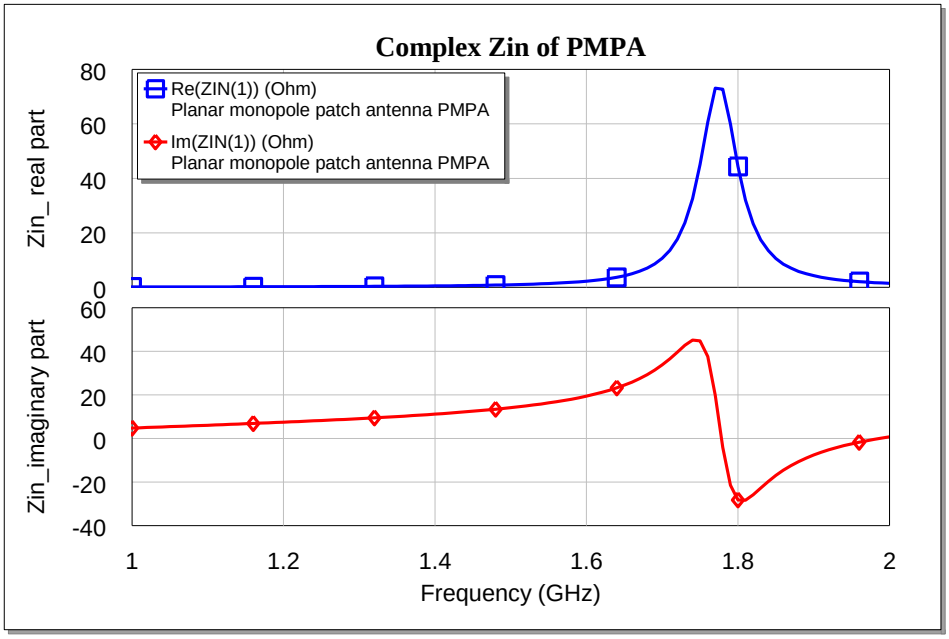


Figure 6.22: Input impedance response of the PMPA

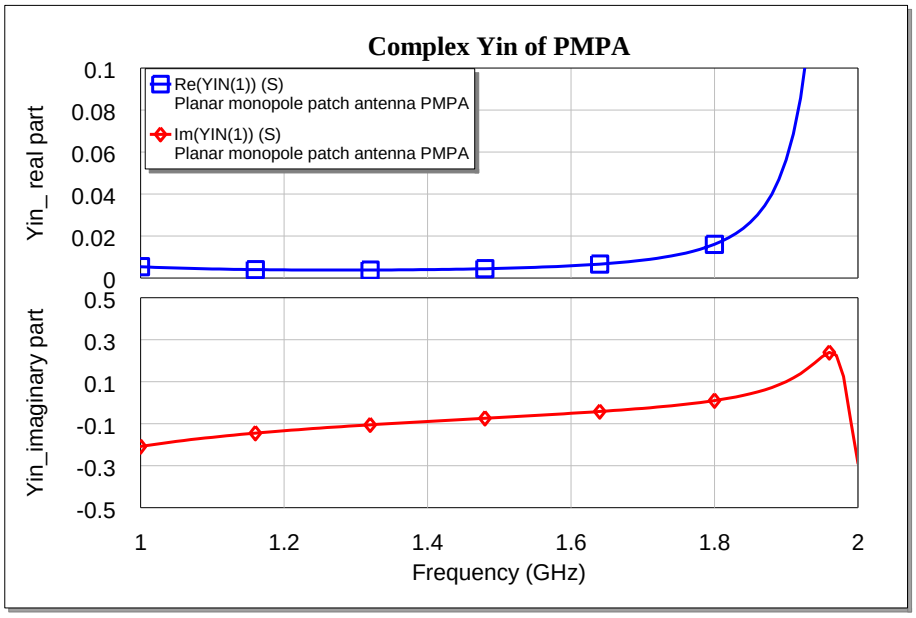


Figure 6.23: Input admittance response the PMPA

6.9 Impedance Transformer Network

In this section, an external matching network is developed to transform the impedance of the planar monopole patch antenna to 50 Ω to shift down its frequency of operation and obtain a perfect match at the desired frequency range of interest. The transformation network consists of a parallel capacitor and a series inductor as shown in Figure 6.24. The shunt capacitor is employed to add enough positive susceptance to move the PMPA impedance onto the 50 Ω circle on the Smith chart. The inductor is connected in series to add enough inductive reactance to transfer the PMPA's impedance to 50 Ω on the Smith chart, as depicted in Figure 6.25.

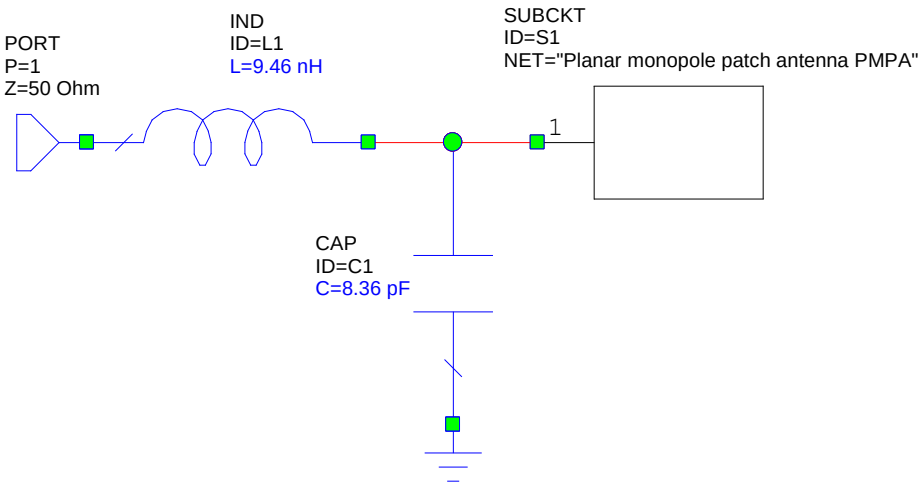


Figure 6.24: Schematic of the planar monopole antenna with the impedance transformer network, where (C = 8.36 pF) and (L = 9.46 nH)

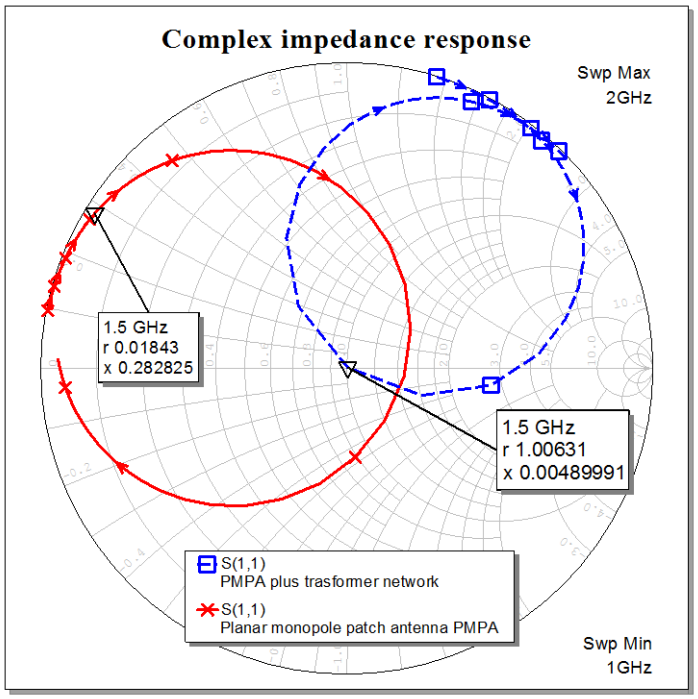


Figure 6.25: Impedance response of the PMPA alone and when it is connected to the admittance transformer network on the Smith chart

Figure 6.26 shows the simulated return loss response of the proposed PMPA alone and when it is connected to the external transformation network. By employing the impedance transformer network to the terminal of the PMPA, it was possible to tune down the resonance frequency of the antenna to the desired frequency of operation and also achieve a better, deeper matching. Moreover, the antenna with the external matching circuit exhibits a return loss better than -10 dB between 1.487 GHz-1.515 GHz within the bandwidth of 1.9% (14 MHz of useful bandwidth) and resonating at 1.5 GHz.

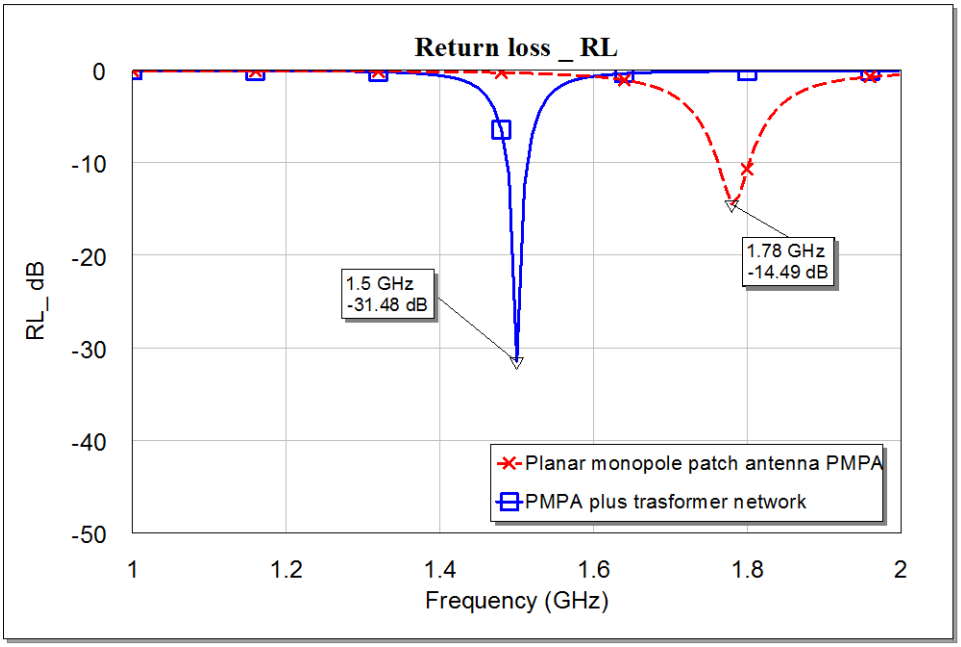


Figure 6.26: Simulated return loss of the PMPA alone and when it is connected to the impedance transformer network

6.10 Antenna Matching Network

In this section, our NGD-based non-Foster network is employed as a non-Foster matching network at the terminal of the proposed planar monopole patch antenna with the impedance transformer network. Its performance is compared with the performance of the same antenna when it is matched with a Foster positive capacitor matching network. The schematic of the matched antenna with the final synthesised non-Foster element using reflection-mode NGD networks is demonstrated as sub-circuits in Figure 6.27.

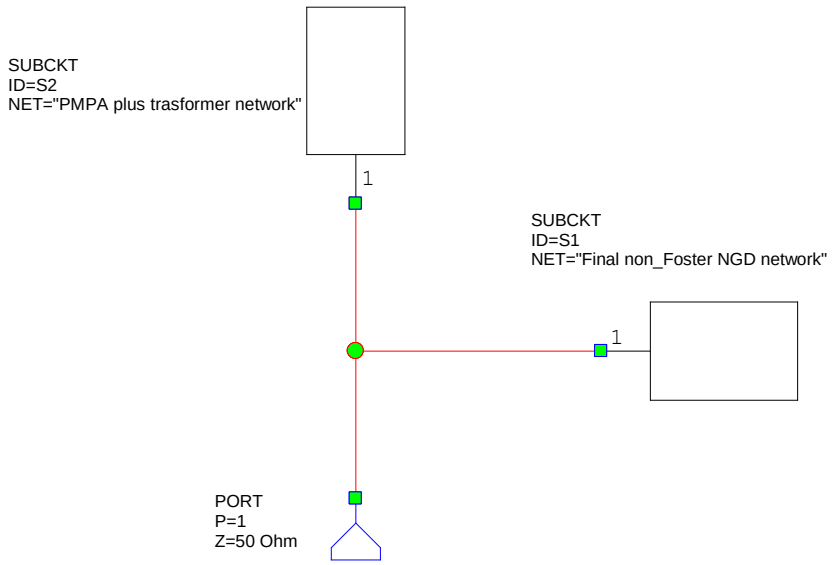


Figure 6.27: Schematic of the PMPA matched with non-Foster matching technique

The simulated reflection coefficient (S_{11}) of the antenna matched with different matching techniques is depicted in Figure 6.28. The results of the antenna matched with the Foster matching network reveals -3.54 dB return loss at 1.49 GHz and a

bandwidth of 31.6% at -3 dB return loss. The antenna matched with the non-Foster NGD network exhibits a return loss better than -10 dB between 1.46 –1.54 GHz within the bandwidth of 5.8% (43.5 MHz of useful bandwidth). It was possible to match the planar monopole antenna with the transformer network below its resonance and broaden the performance, using our proposed non-Foster reactive element. Furthermore, simulation results of the antenna matched with non-Foster matching networks reveal a significant improvement in terms of the bandwidth compared to the antenna itself and compared to that which is obtained when the same antenna was passively matched.

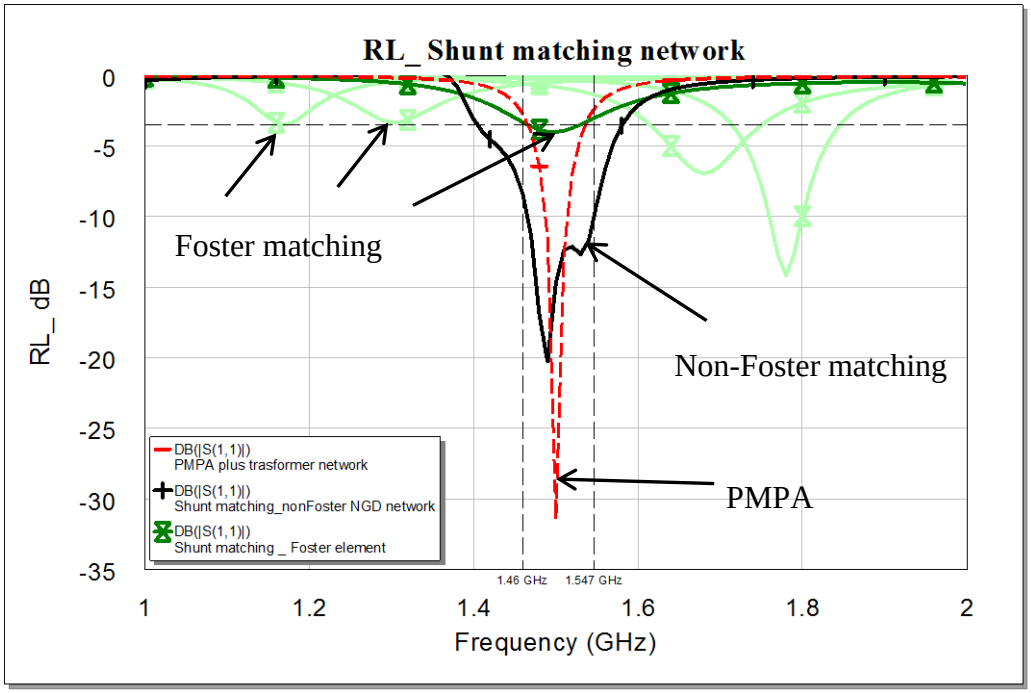


Figure 6.28: Simulated return loss (RL) for the PMPA matched with different matching networks

6.11 Stability Analysis

The stability analysis of the proposed NGD-based non-Foster circuit connected to the planar monopole patch antenna is performed using the Nyquist stability measured with modified gamma-probe (STABN_GP2) measurement offered by Microwave Office. The GPROBE2 element is connected in series with the input gate of the transistor to measure the internal reflection coefficients required for internal stability measurements at the reference plane where it is inserted. The simulated open loop function G of the (STABN_GP2) measurement plotted on a polar graph from 0.5 GHz to 3 GHz is depicted in Figure 6.29. As it can be seen from the graph, the open loop function does not encircle the -1 point in a clockwise sense, thus, the overall NGD-based non-Foster circuit with the monopole antenna can be considered to be having a stable operation.

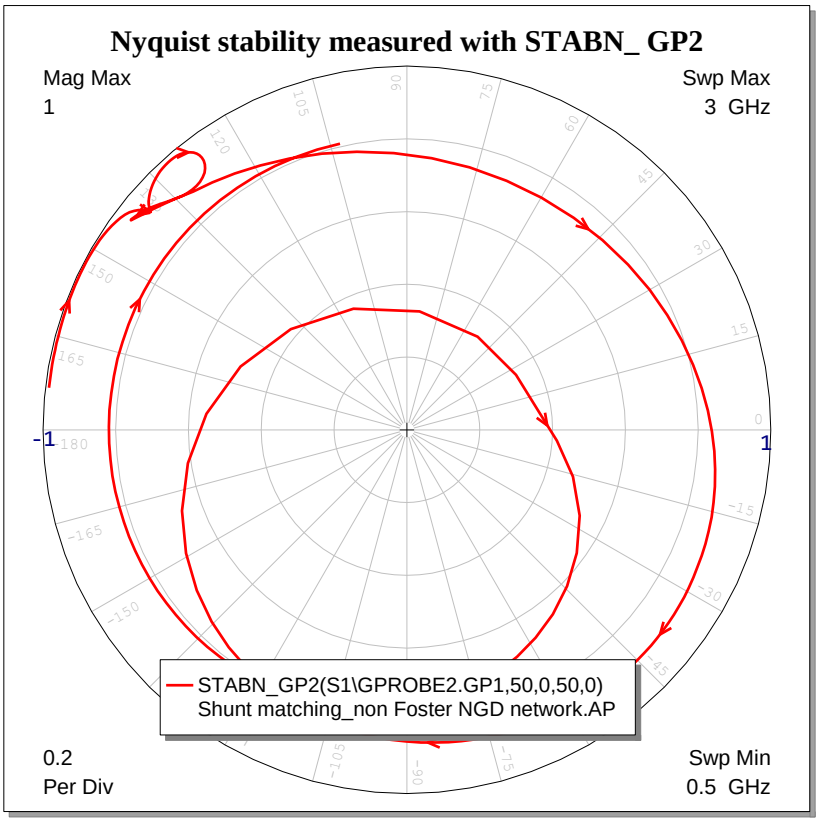


Figure 6.29: Stability analysis through the Nyquist diagram to detect the instability of the NGD-based non-Foster circuit connected with a planar monopole patch antenna (PMPA). The open loop function G, does not encircle the -1 point in the clockwise direction, thus, the overall combination is considered to be having a stable operation.

The performance of the different electrically small antennas and their equivalent circuits are summarised in Table 6.1, and their implementations with different matching techniques are presented in Table 6.2.

Table 6. 1: Summary of the performance of the employed antennas

Type of antenna	Rep Model	Resonance Frequency (GHz)	Return loss RL (dB)	BW%
ESPA	Simulation	5.39	-5.493	11.8% at -3 dB RL
RLC resonant network	Simulation	2	-2.424	10.6% at -2dB RL
PMPA	Simulation	1.78	-14.49	2.3% at -10 dB RL
PMPA plus transformer network	Simulation	1.5	-31.48	1.9% at -10 dB RL

Table 6. 2: Summary of the performance of the electrically small antennas matched with different matching networks

Type of antenna	Unmatched antennas		Foster matching		NGD-based non-Foster matching	
	Resonance Frequency (GHz)	BW%	Resonance Frequency (GHz)	BW%	Resonance Frequency (GHz)	BW%
ESPA	5.39	11.8% at -3 dB RL	1.34	1.4% at -3 dB RL	1.36	1.63% at -3 dB RL
RLC resonant network	2	10.6% at -2 dB RL	1.25	23.97% at -10 dB RL	1.28 & 1.39	16.33% at -10 dB RL
PMPA plus transformer network	1.5	1.9% at -10 dB	1.49	Not performed	1.46	5.8% at -10 dB RL

6.12 Linearity and Noise Considerations

The use of an amplifier within the NGD-based antenna matching circuit discussed in Chapter 5 implies that there will be some operational limitations arising from non-linearity and noise. Full assessment of these effects would need to be done on a case by case basis when considering detailed transceiver designs. However, order of magnitude estimates of the problems can be made using the following simple analysis.

6.12.1 Non-Linearity

In FET based negative resistance low noise amplifiers operating in X-band, practical measurements of 1 dB gain compression point gave results of around -8 dBm, considerably lower than for transmission mode amplifiers using the same device [3]. This was rationalised on the basis that in a reflection mode amplifier, the gate terminal sees the voltage amplitude associated with the amplifier output. Thus to a first approximation, the output 1 dB gain compression point of a negative resistance amplifier can be expected to be of the same order of magnitude as the 1 dB compression point of a transmission mode amplifier referred to the input port.

For the device used in this thesis, the data sheet in Appendix (A) shows a typical output 1 dB compression point of 21 dBm, and gain of 13.5 dB, giving an estimate of the 1 dB compression at the input port of 7.5 dBm. This limitation needs to be

taken into consideration to assess possible non-linear signal distortion of the transmitted signal. A more accurate and detailed estimate of non-linear effects would require detailed non-linear modelling of the transistor.

6.12.2 Noise Performance

It has been shown in [4] that the noise performance of transistors in reflection mode can be made comparable to those in transmission mode, with the appropriate choice of reactive terminations. Figure 6.30 shows a circuit configuration which consists of a circulator connected to the reflection amplifier circuit of Fig 5.5 to find the noise temperature. The simulation result shown in Figure 6.31 shows that, even without optimising for noise, the reflection mode amplifier has a low noise temperature of about 70 K. Moreover, another circuit configuration of a circulator connected with the NGD developed in the thesis, in reflection mode first presented in Fig 5.38 is shown in Figure 6.32. Figure 6.33 shows that there is a considerably higher noise temperature result (800 K) than what was obtained from the case of the reflection amplifier itself. This is because of the lossy NGD networks integrated with the design from which the signal reflects, before reaching the reflection amplifier.

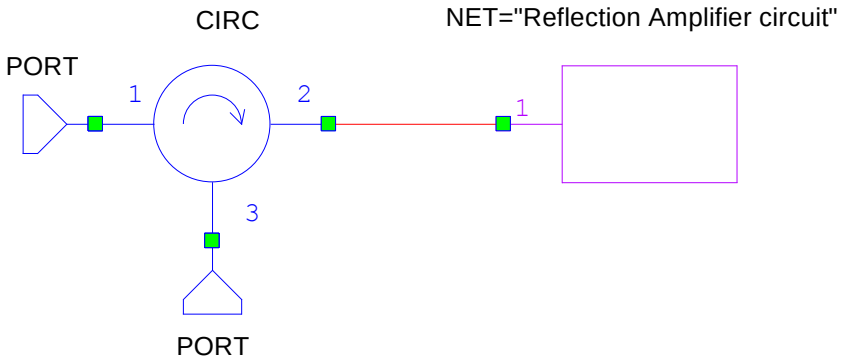


Figure 6.30: Circuit configuration of a circulator connected with the reflection amplifier presented in Fig 5.5 for noise simulation

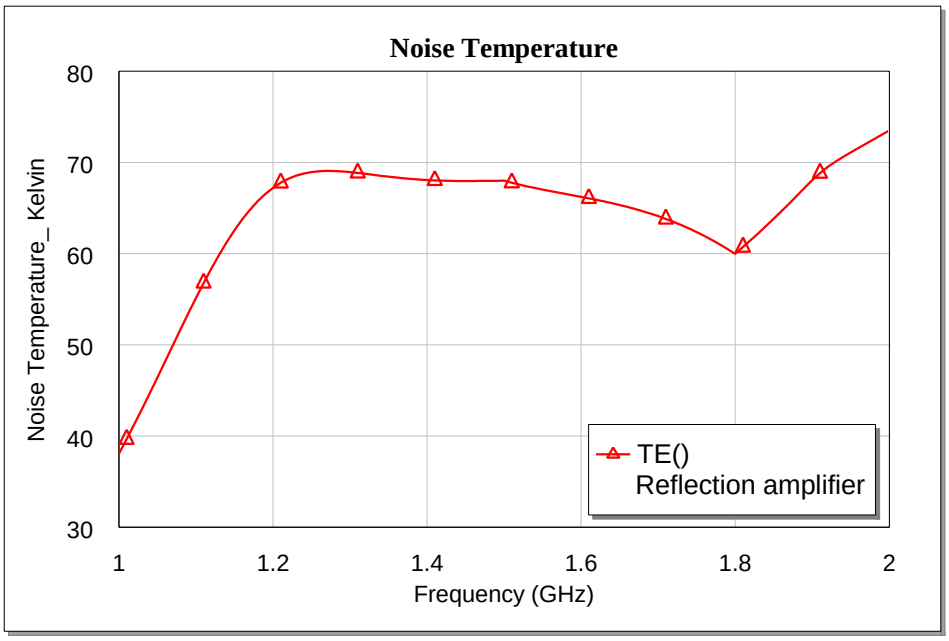


Figure 6.31: Noise temperature simulation results

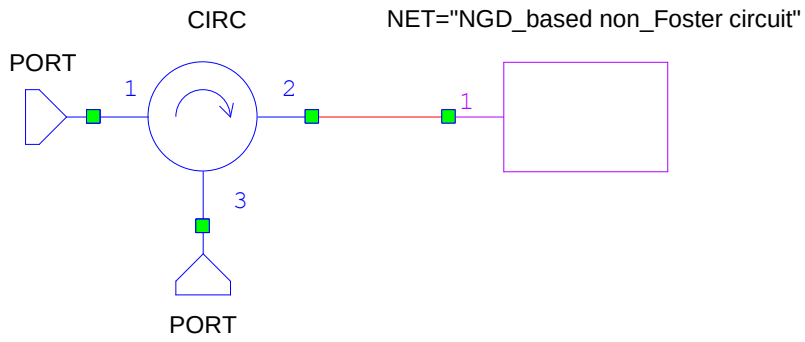


Figure 6.32: Circuit schematic comprises of a circulator connected with the NGD-based non-Foster network presented in Fig 5.38 for noise simulation

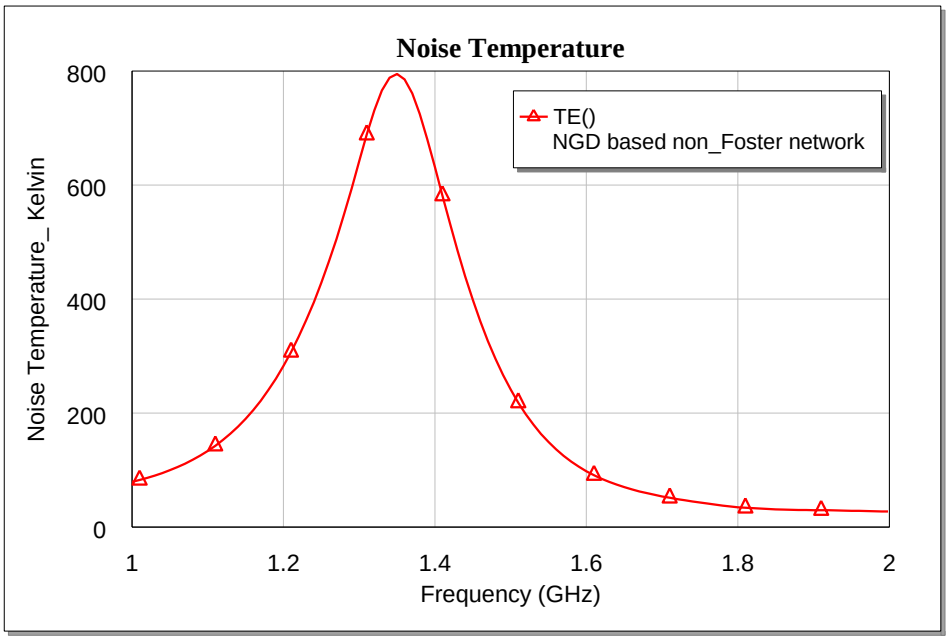


Figure 6.33: Noise temperature simulation results

As it can observed from Figure 6.33, the noise temperature peaks in the middle of the frequency range where NGD behaviour occurs. This additional noise, uncorrelated with the antenna noise, would need to be accounted for in the receiver

sensitivity calculation. This could limit the applicability of this antenna matching method in some noise limited application areas.

6.13 Summary

This chapter has investigated the capability of the synthesised non-Foster reactive element using reflection-mode NGD networks in providing a wideband matching network with electrically small antennas in the microwave frequency region. A new analysis of the equivalent circuit model for the non-Foster NGD network, based on the impedance trajectory of the network in the frequency range of interest has been developed. Then, an ESPA was designed using the electromagnetic AWR Axiem simulator. The proposed antenna had the correct susceptance value to be matched with different matching techniques. However, its radiation resistance values were too small to perform a perfect wideband antenna matching network.

An alternative technique was developed based on the representation of the ESPA with an RLC equivalent network and by representing the final synthesised non-Foster NGD network as a pure negative inductor. By matching the antenna circuit model with different matching networks, it was possible to tune its resonance frequency to the desired frequency range of interest and to achieve a broader bandwidth.

A planar monopole patch antenna (PMPA) was designed using an AWR EMSight simulator to obtain approximately the same characteristic performance of the RLC equivalent circuit of Fig 6.11. The new antenna was connected to an impedance transformer network to tune its resonance frequency to the desired frequency of operation. Finally, PMPA was matched using our NGD-based non-Foster network and with a Foster matching network. Broadband antenna matching was obtained using our proposed non-Foster NGD reactive network. It is a significant achievement, compared with the performance of the antenna alone and when it was matched with a traditionally passive Foster matching technique.

Stability analysis using the Nyquist criteria to detect the instability of the NGD-based non-Foster circuit connected with a planar monopole patch antenna (PMPA) was performed. The open loop function G of the Nyquist plot does not encircle the -1 point in the clockwise direction, thus, the overall combination is considered to be stable.

Approximate calculations of the non-linear and noise performance have been introduced, showing that there could be some degradation at each end of the dynamic range when using this method in an integrated transceiver, and these would need to be taken into account on a case by case basis in future transceiver design.

References

[1] F. Abboud, J. P. Damiano, and A. Papiernik, "Simple model for the input impedance of coax-fed rectangular microstrip patch antenna for CAD," IEE Proceedings H - Microwaves, Antennas and Propagation, vol. 135, pp. 323-326, 1988.

[2] J. J. Wang, Y. P. Zhang, C. Kai Meng, and A. C. W. Lu, "Circuit model of microstrip patch antenna on ceramic land grid array package for antenna-chip codesign of highly integrated RF transceivers," IEEE Transactions on Antennas and Propagation, vol. 53, pp. 3877-3883, 2005.

[3] P. Gardner, "Novel Techniques in Low Noise Microwave Transistor Amplification," Ph.D. Thesis, The University of Manchester Institute of Science and Technology, 1992.

[4] P. Gardner and D. K. Paul, "Aspects of the design of low noise, negative resistance, reflection mode transistor amplifiers," Microwave Theory and Techniques, IEEE Transactions on, vol. 39, pp. 1869-1875, 1991.

CHAPTER 7

CONCLUSIONS AND FUTURE WORK

7.1 Summary

This thesis explores novel microwave engineering techniques for the realisation and implementation of passive and active electronic circuits; in particular, realising reactive non-Foster elements based on loss-compensated reflection-type NGD networks at the microwave frequencies. The conclusions, constituting a summary of the main contributions of the thesis, are presented in the following:

- Based on the relation between NGD networks and reactive non-Foster elements, which was explored in Chapter 3, it is shown that a class of a non-Foster element can function as an NGD network and vice versa. The NGD response can be synthesised using non-Foster elements in different configurations. Loss-compensated NGD networks have been proposed as an alternative approach for designing non-Foster reactive elements.

- A novel technique for designing reflection-type NGD networks starting from design equations to quantify their operation has been introduced in Chapter 4. Finally, a reflection-mode NGD network was designed and experimentally

validated. Experiment and simulation results were in good agreement and showed that the proposed network exhibits NGD of 1.62 ns over a bandwidth of 0.3 GHz from 1.2 to 1.37 GHz. However, the NGD network has about 10 dB loss which must be compensated.

- A novel technique to compensate the inherent loss of the NGD network in the reflection mode and realising a new class of reactive non-Foster elements has been investigated and explored in Chapter 5. It provides a new route for synthesising networks with non-Foster behaviour over a limited frequency range. It employed a negative resistance amplifier and a Lange coupler for the compensation of the losses of the NGD networks.

  Each component has been individually designed and experimentally validated. Although, the designed negative resistance reflection amplifier was shown by simulation using Nyquist technique is working stable. The fabricated structure was suffering from stability issues. Therefore, it was decided to present its performance with its simulated results in the context of the loss compensated, reflection-mode NGD antenna matching network, in order to allow the principle of NGD operation with reflection amplifiers to be demonstrated.

  Consequently, an implementation of two reflection-type NGD networks with a Lange coupler has been experimentally validated. Finally, all the circuits were combined together in a balanced structure forming the overall NGD-based non-

Foster reactive element. The stability of the NGD-based non-Foster network was assessed by Nyquist techniques and simulation results showed that the proposed circuit is working stable. Despite the stability concerns associated with the practical implementations reflection amplifier, this separation of functions into separate elements makes it easier to establish a stable behaviour compared to the conventional NIC approach; which typically uses two transistors and creates the problem of establishing the desired reactance trajectory in a single complex element design. The advantage of the new proposed NGD-based non-Foster structure is that the main NGD property is obtained by passive elements, which have no stability concerns and are well behaved.

- Chapter 6 has demonstrated the potential use of the synthesised non-Foster reactive element using reflection-mode NGD networks to improve the matching bandwidth with an electrically small antenna at its terminals. New analysis to explore an equivalent circuit model for the non-Foster NGD network based on the impedance trajectory of the network in the frequency range of interest has been investigated. The NGD-based non-Foster network was connected with a planar monopole patch antenna (PMPA) and by the addition of an external impedance transformer to the antenna's terminal; the bandwidth of the antenna has been increased over a wider frequency range. It was a significant achievement compared with the performance of the antenna alone and when it is matched with a passive matching network.

Stability analysis using the Nyquist criteria to detect the instability of the NGD-based non-Foster circuit connected with PMPA was performed and simulation results showed that the overall circuit is stable. Finally, the performance of NGD-based non-Foster network in terms of the non-linearity and noise were characterised. The approximate calculations of these operational limitations revealed that there could be some degradation at each end of the dynamic range when using this technique in an integrated transceiver, and these would need to be taken into account on a case by case basis when designing a transceiver in future.

7.2 Conclusions

- NGD networks in reflection-mode using cascaded LC resonators terminated in resistive load can be incorporated into non-Foster networks using a novel configuration based on a Lange coupler and a reflection amplifier.

- A simple equivalent circuit model (-L, -C) of the proposed NGD-based non-Foster network can be used to deploy the non-Foster network in an antenna matching network.

- The operational limitations of this approach arise from the stability, noise and non-linearity, all stemming from the reflection amplifier.

- Theoretical analysis based on Nyquist approach shows that stability can be achieved but practical implementation issues can cause stability problems.

- The noise arising in the non-Foster element is relatively high because of the lossy NGD networks from which the signal reflects, before reaching the reflection amplifier. In receive applications this limitation should be taken into account.

- The non-linearity will occur because of the non-linearity of the active negative resistance device. This issue has to be taken into account in transmit mode applications.

7.3 Future Work

The work presented in the thesis was devoted to the realisation of a new class of non-Foster reactive elements in the microwave frequency band. The concepts developed in the research can be further improved and applied to new electromagnetic and microwave applications. Below are some recommendations that can be carried out:

- Produce a systematic synthesis procedure which starts from a required group delay slop to a network design. To do that, the parasitic elements such as the Lange coupler and the reflection amplifier have to be characterised first. By knowing how much positive group delay (GD) each element would contribute,

and then an NGD network can be designed to give a specific amount of negative group delay to overcompensate the unwanted positive GD of the parasitic.

- The employed FET reflection amplifier was narrow bandwidth and generated a large positive group delay. Improving the performance of these active devices can provide a better way to compensate the losses of the NGD network and will have a positive impact on designing wideband NGD-based non-Foster networks.

- Employing other techniques such as tunnel and Gunn diodes for realising the reflection amplifier may result in reduced stability concerns. Some existing examples in the literature were introduced in Chapter 5.

- Using bi-directional amplifiers at the terminals of the NGD networks, the losses of these networks can be compensated and as a result, transmission for more details directional amplifiers can be suggested as a means for designing fully established, bi-lateral, non-Foster NGD networks. an example of designing a tunnel diode- based bidirectional amplifier was presented earlier in Chapter 5. Other approaches for realising bidirectional amplifiers exist in the literature, for example, using two transistor-based reflection amplifiers and microstrip BLC, two identical unilateral amplifier plus two RF circulators and a network of amplifiers in MMIC technologies. More details on these techniques can be found [1, 2, 3 and 4].

- The operational limitations associated with the NGD-based antenna matching networks such as non-linearity and noise needs to be fully assessed which can be done on a case by case basis when considering detailed transceiver designs.

- Design more and different types of electrically small antennas, such as dipole antennas that can be matched with the realised non-Foster NGD network over a limited frequency range.

- Design wideband NGD-based non-Foster networks to suit given electrically small antennas for specific applications, building upon the techniques established in this thesis primarily for low frequencies applications.

References

[1] S. Khaledian, F. Farzami, D. Erricolo, and B. Smida, "A Full-Duplex Bidirectional Amplifier With Low DC Power Consumption Using Tunnel Diodes," IEEE Microwave and Wireless Components Letters, vol. 27, pp. 1125-1127, 2017.

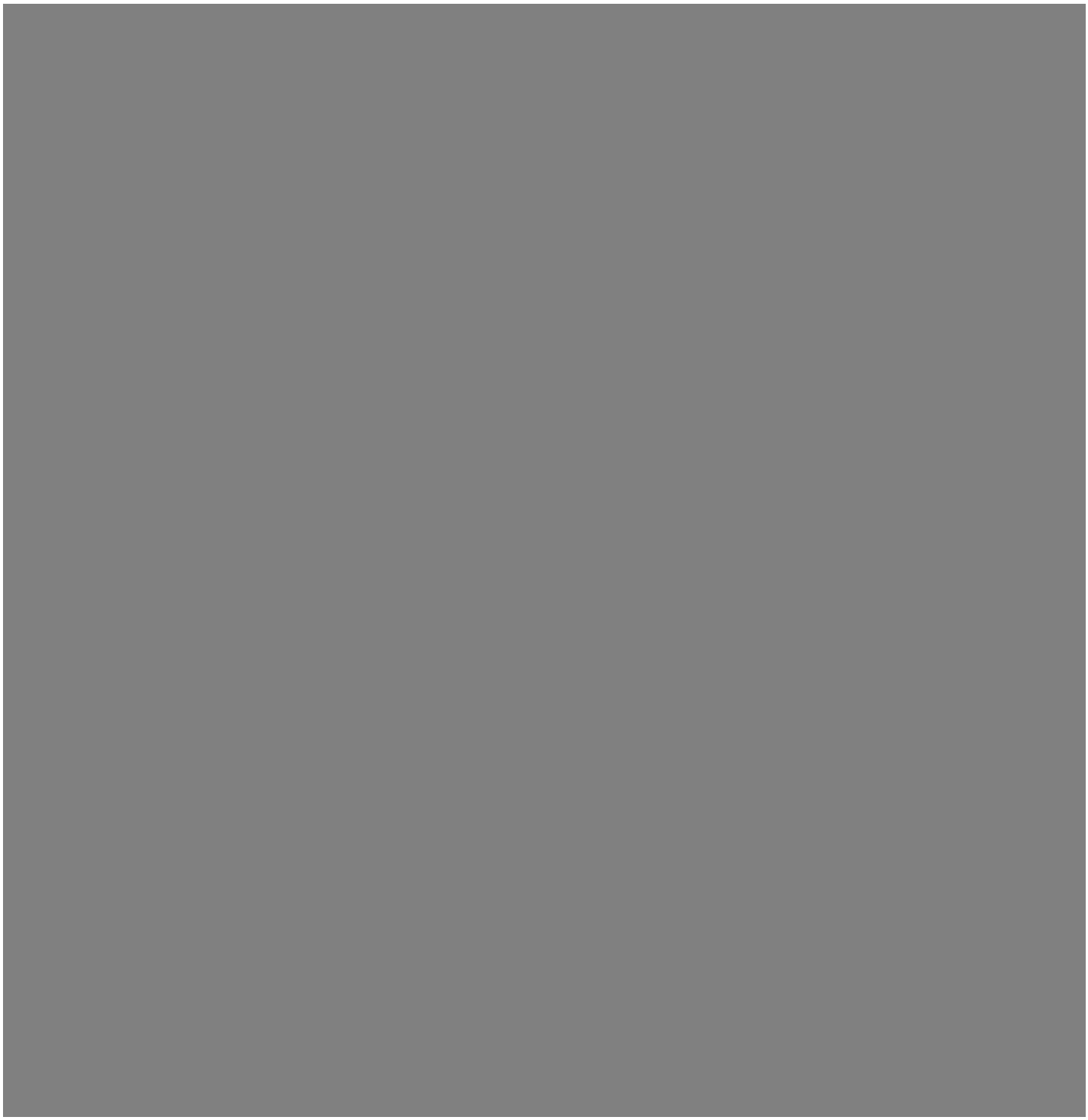
[2] C. Shyh-Jong, C. Shing-Ming, and L. Yang-Chang, "A novel bi-directional amplifier with applications in active Van Atta retrodirective arrays," IEEE Transactions on Microwave Theory and Techniques, vol. 51, pp. 542-547, 2003.

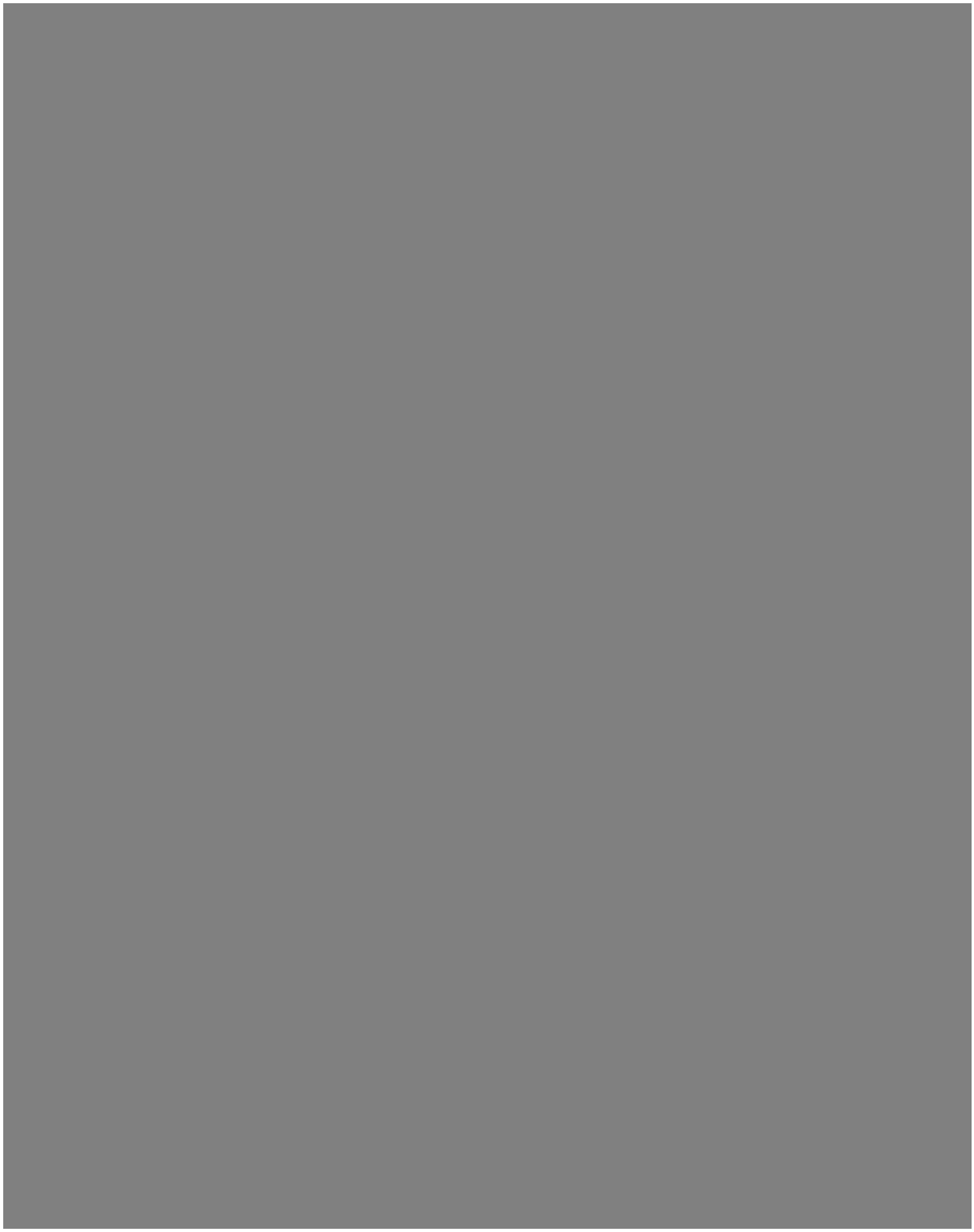
[3] A. S. A. Bechteler and T. F. Bechteler, "Switchless bidirectional amplifier for wireless communication systems," Microwave and Optical Technology Letters, vol. 49, pp. 1888-1890, 2007.

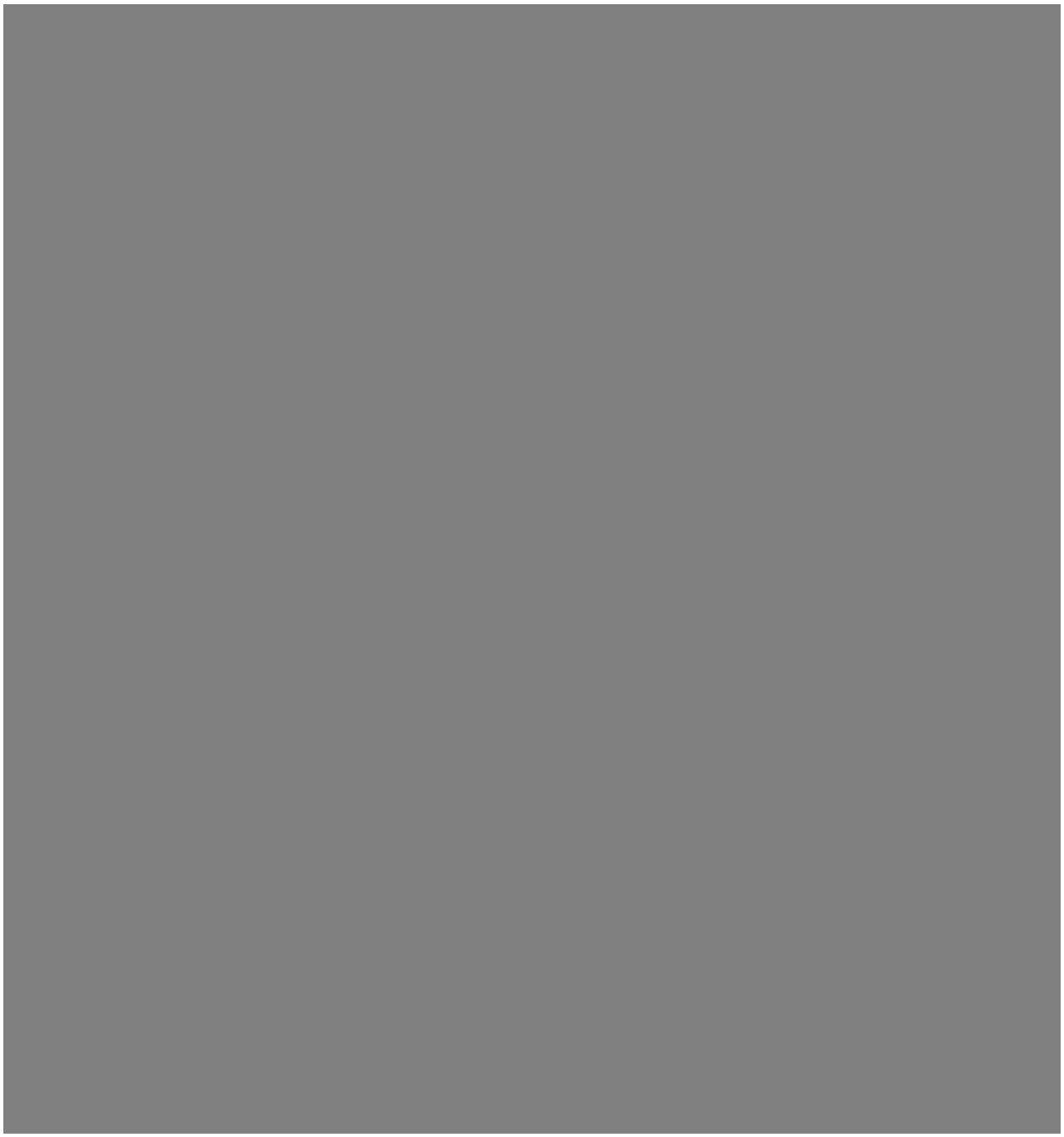
[4] D. Kim, D. H. Lee, S. Sim, L. Jeon, and S. Hong, "An X-Band Switchless Bidirectional GaN MMIC Amplifier for Phased Array Systems," IEEE Microwave and Wireless Components Letters, vol. 24, pp. 878-880, 2014.

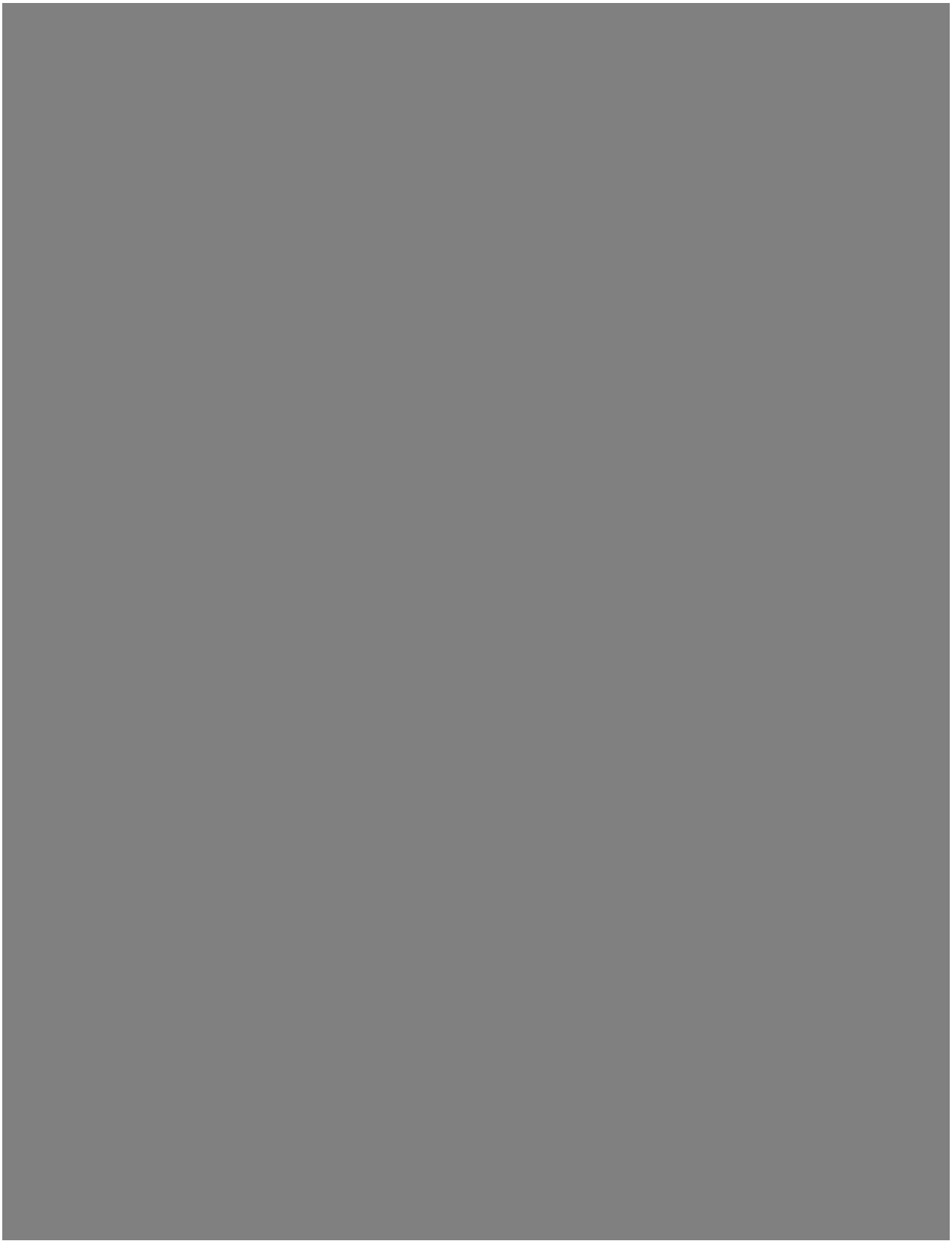
APPENDIX A

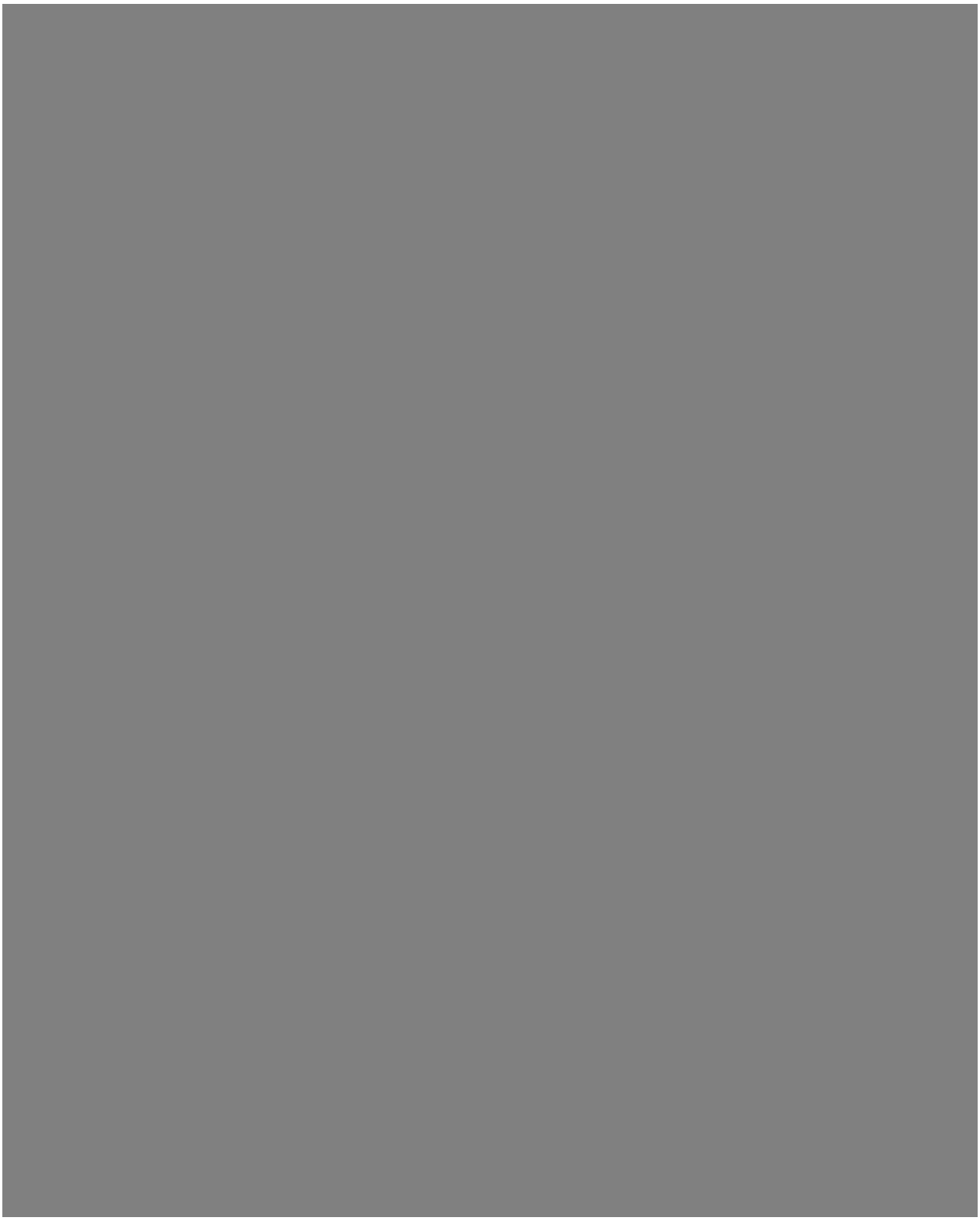
COMPONENTS DATA SHEETS



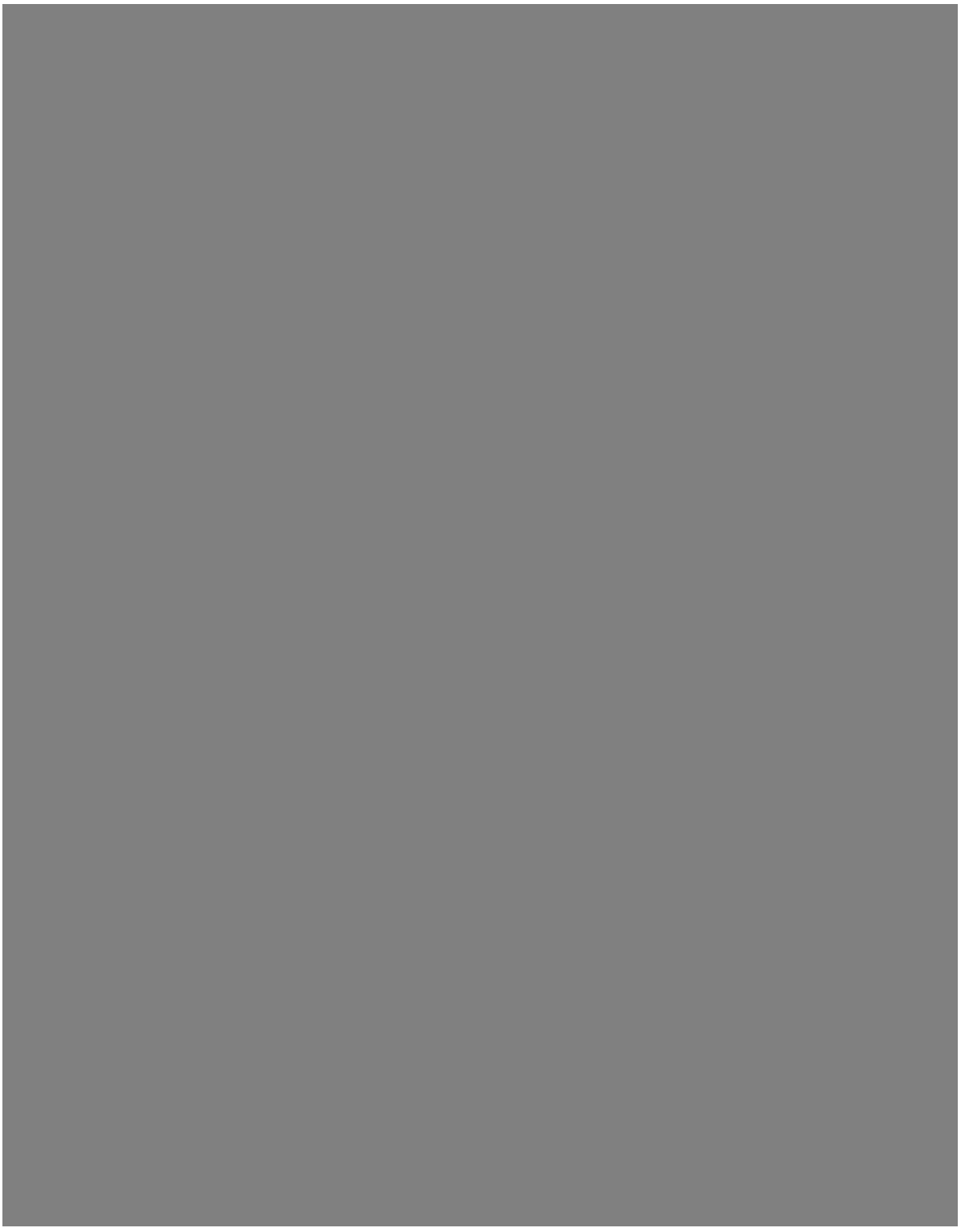


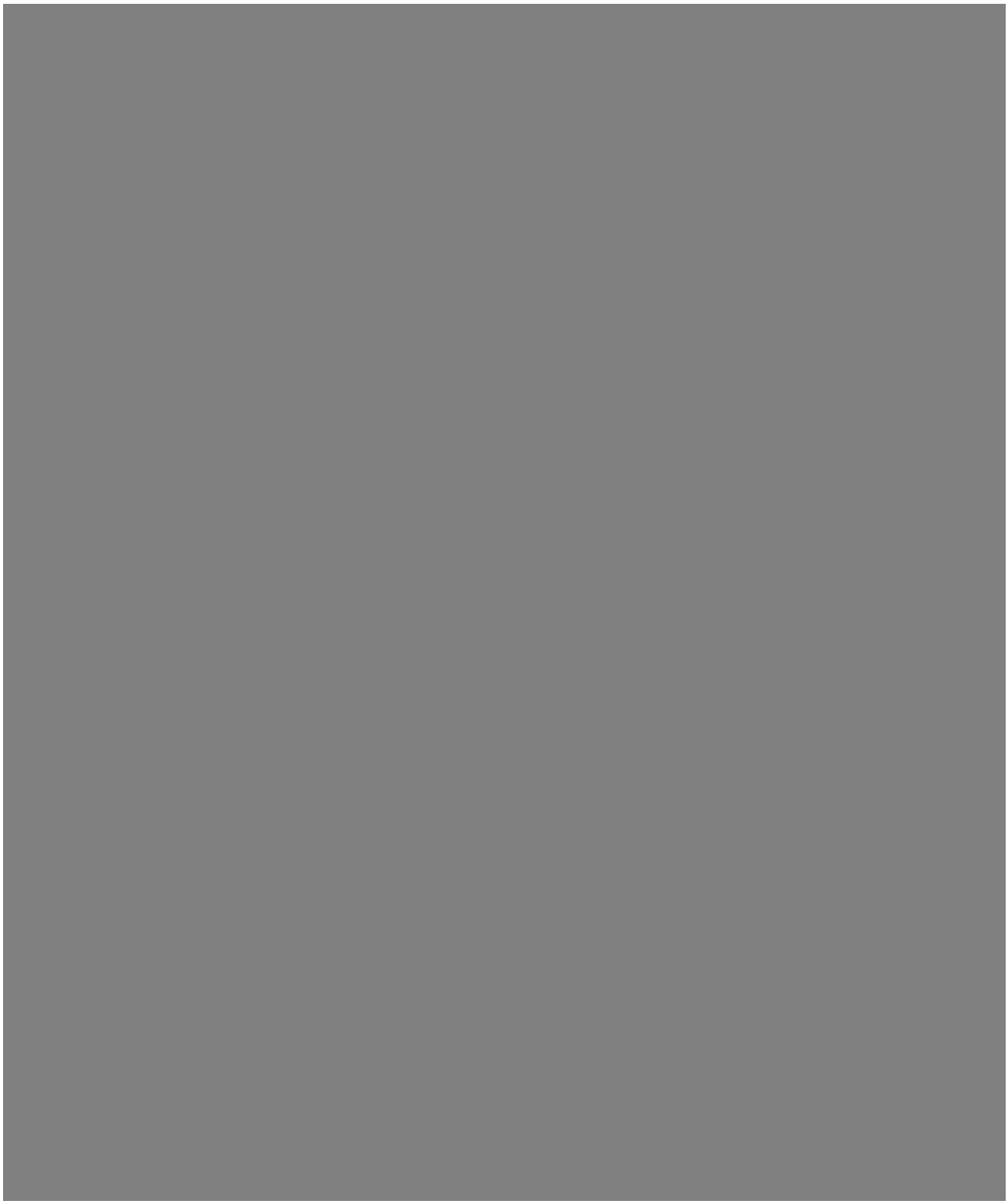


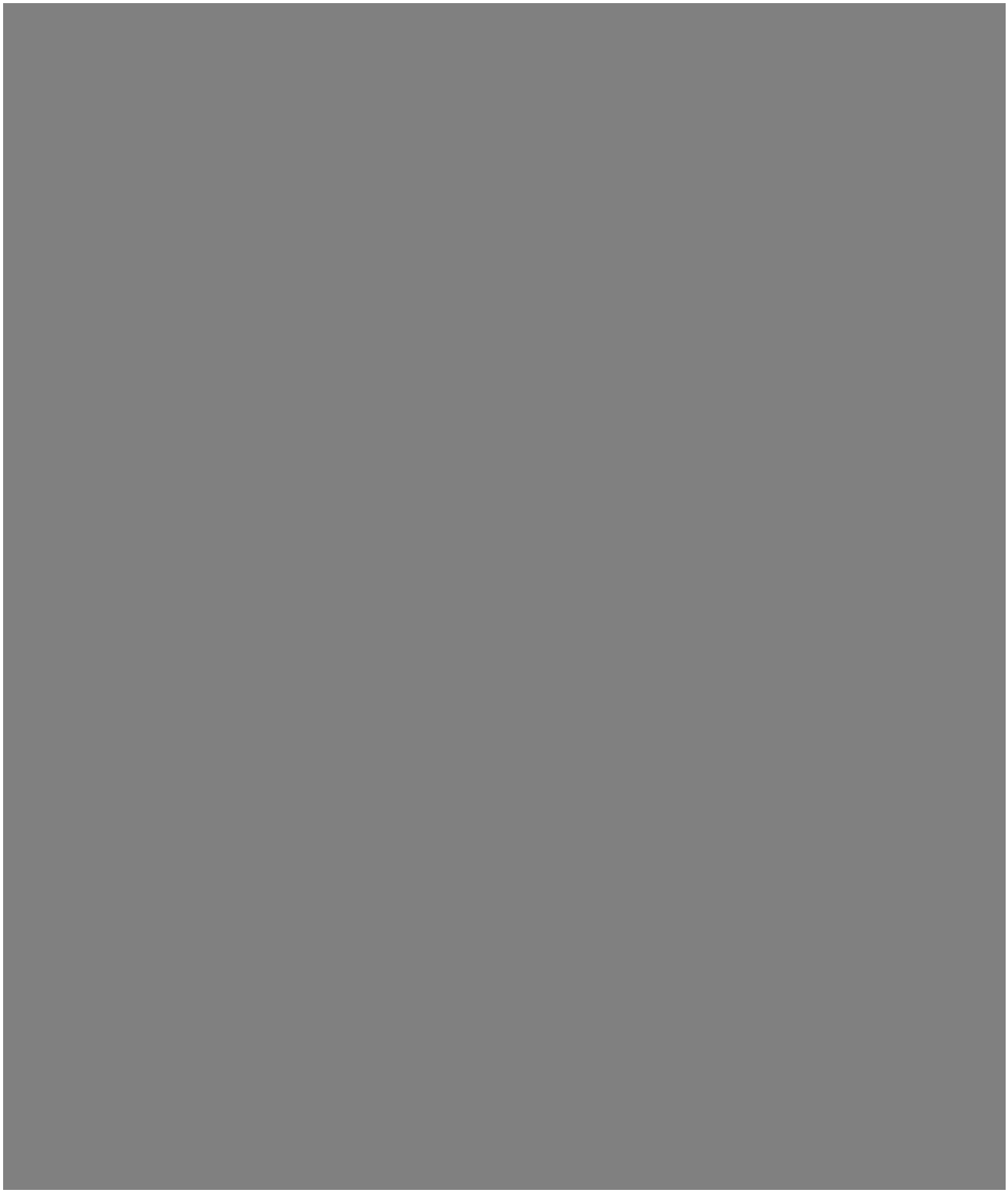


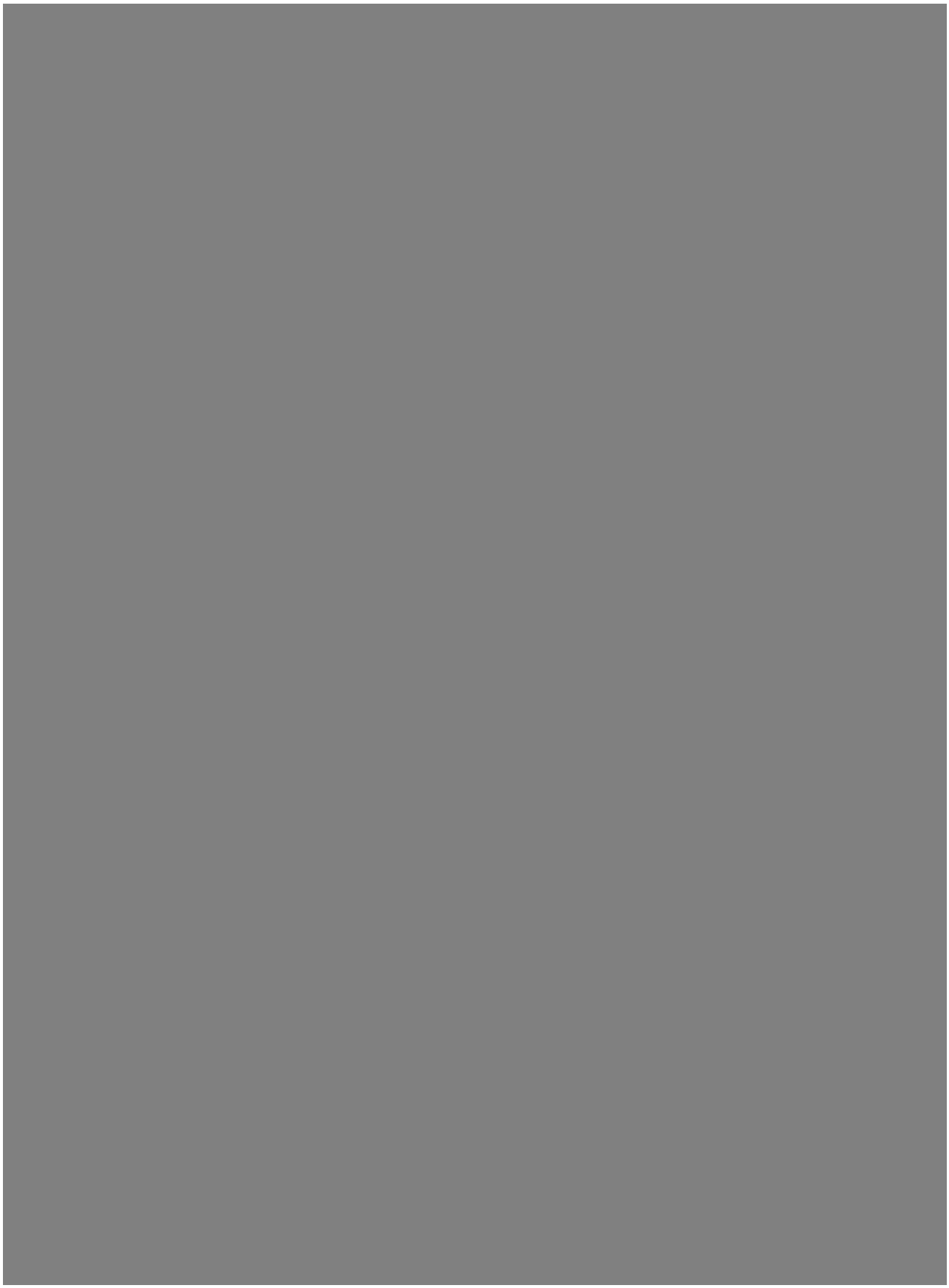


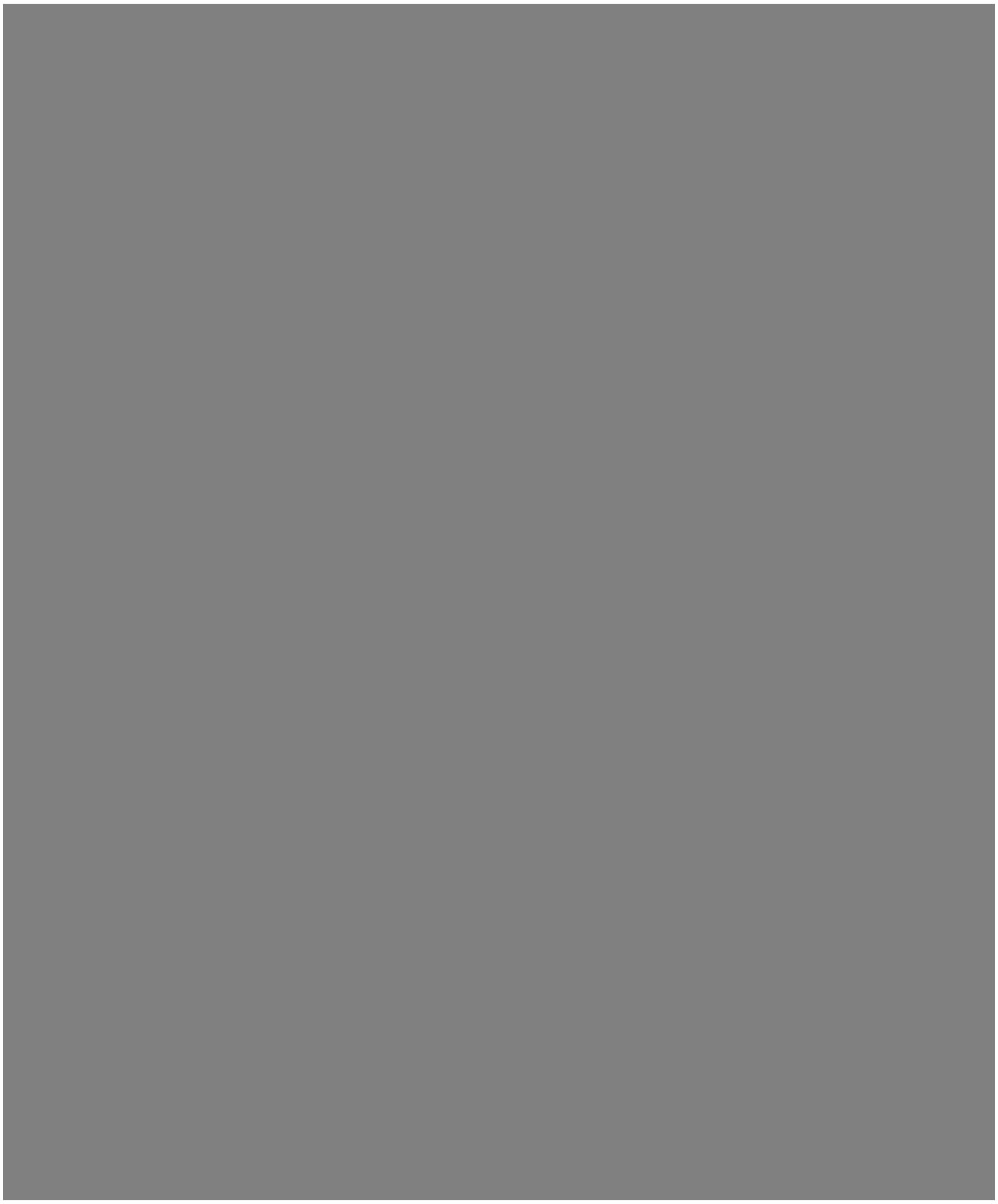


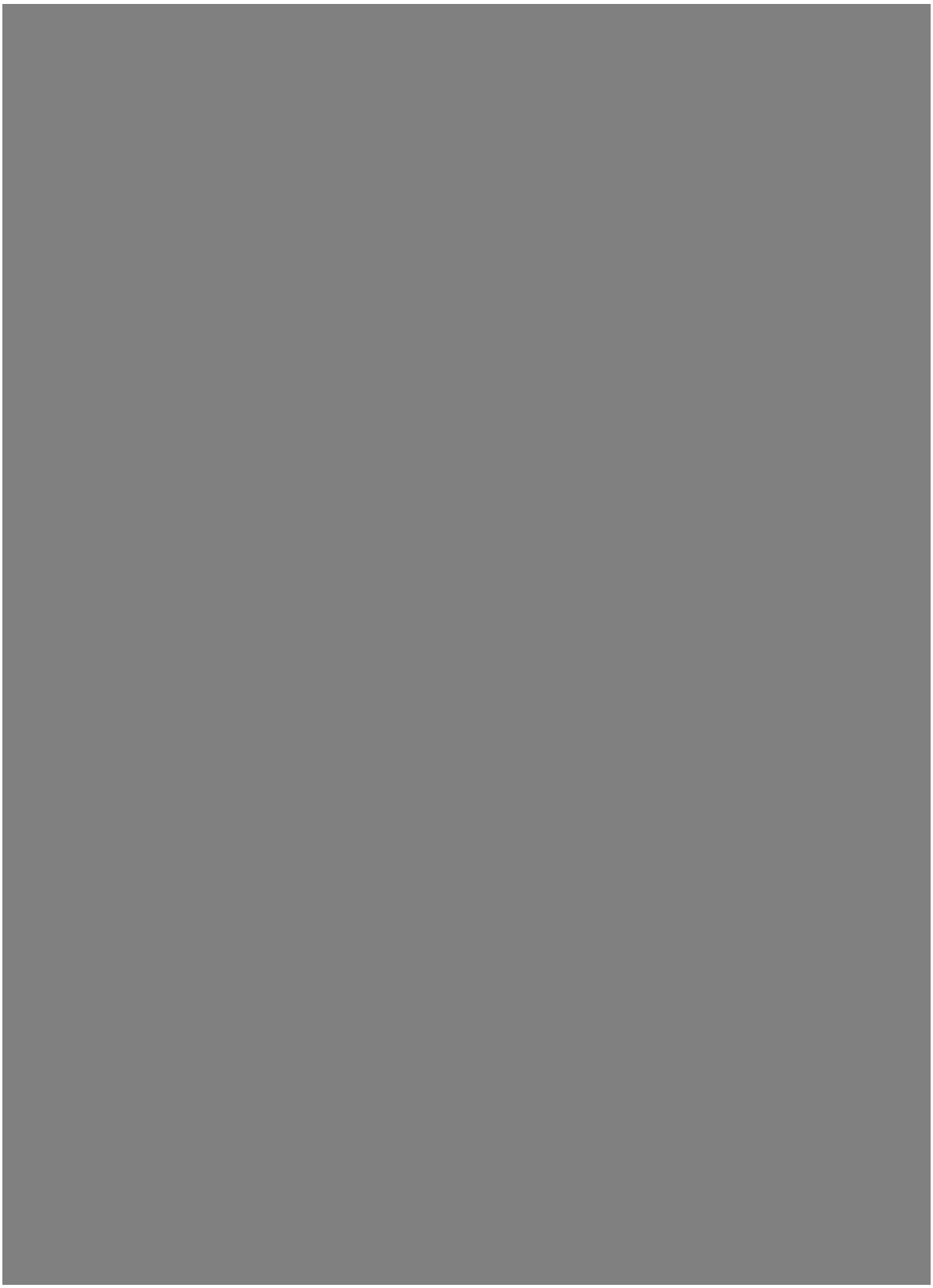


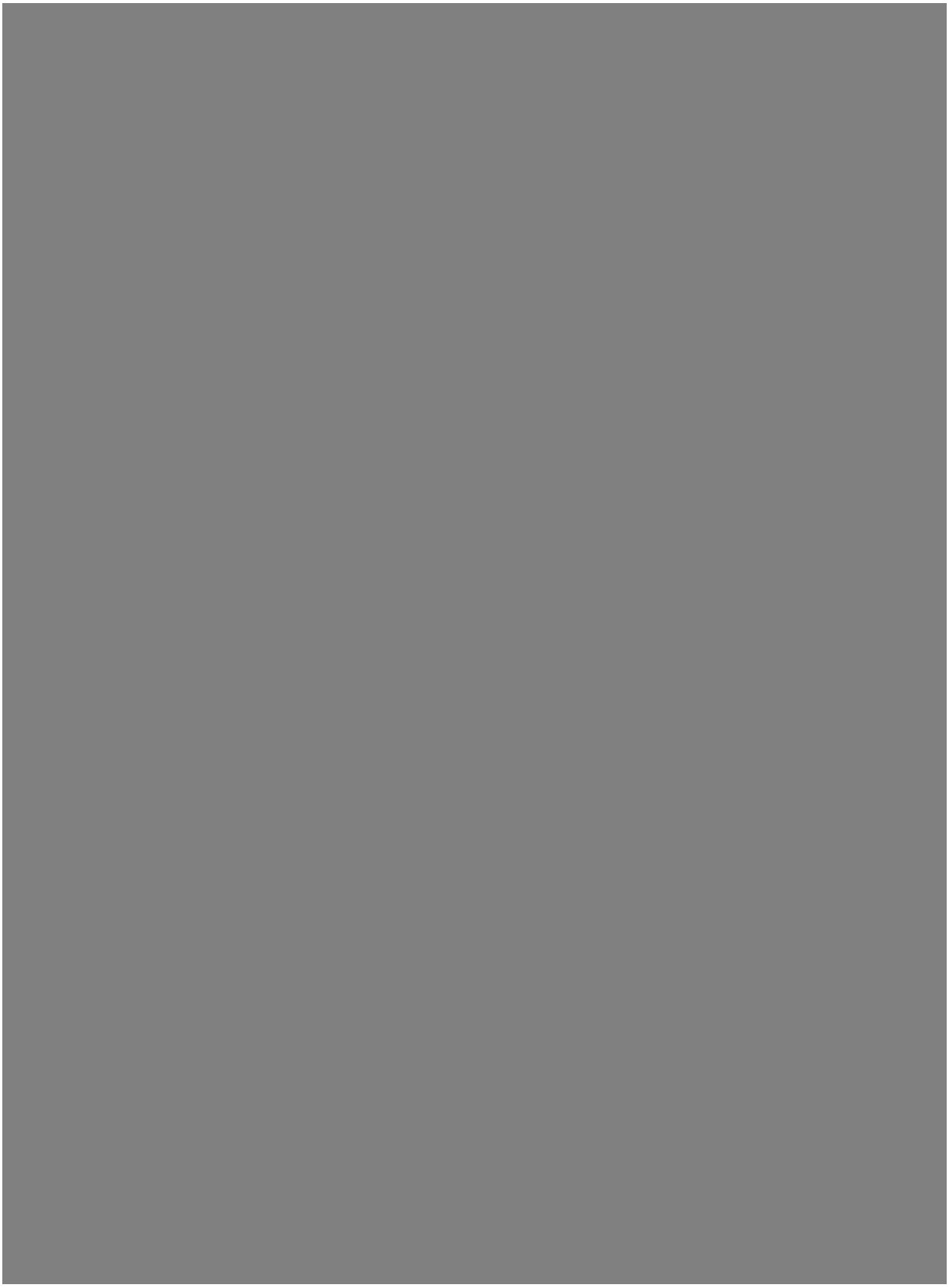


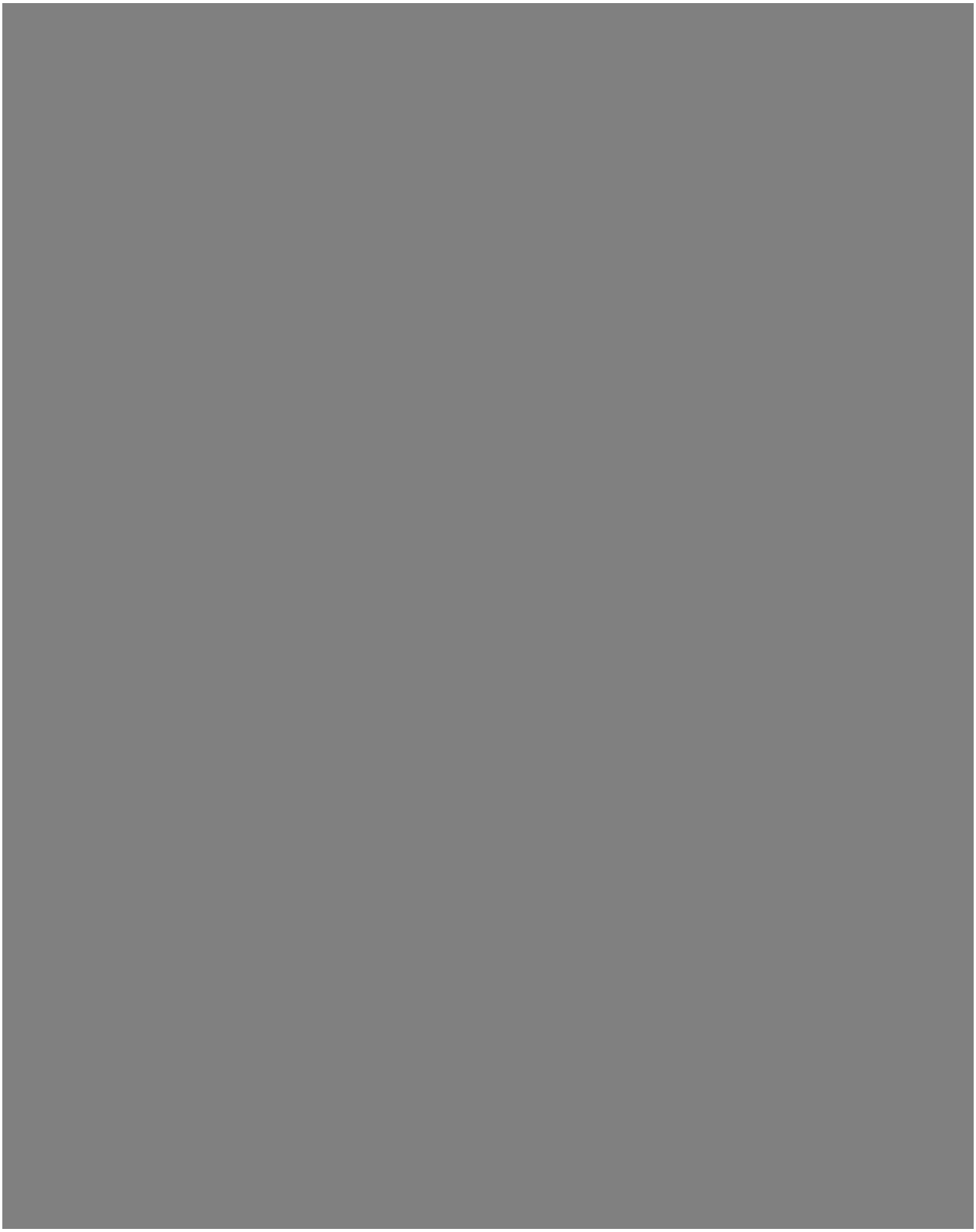


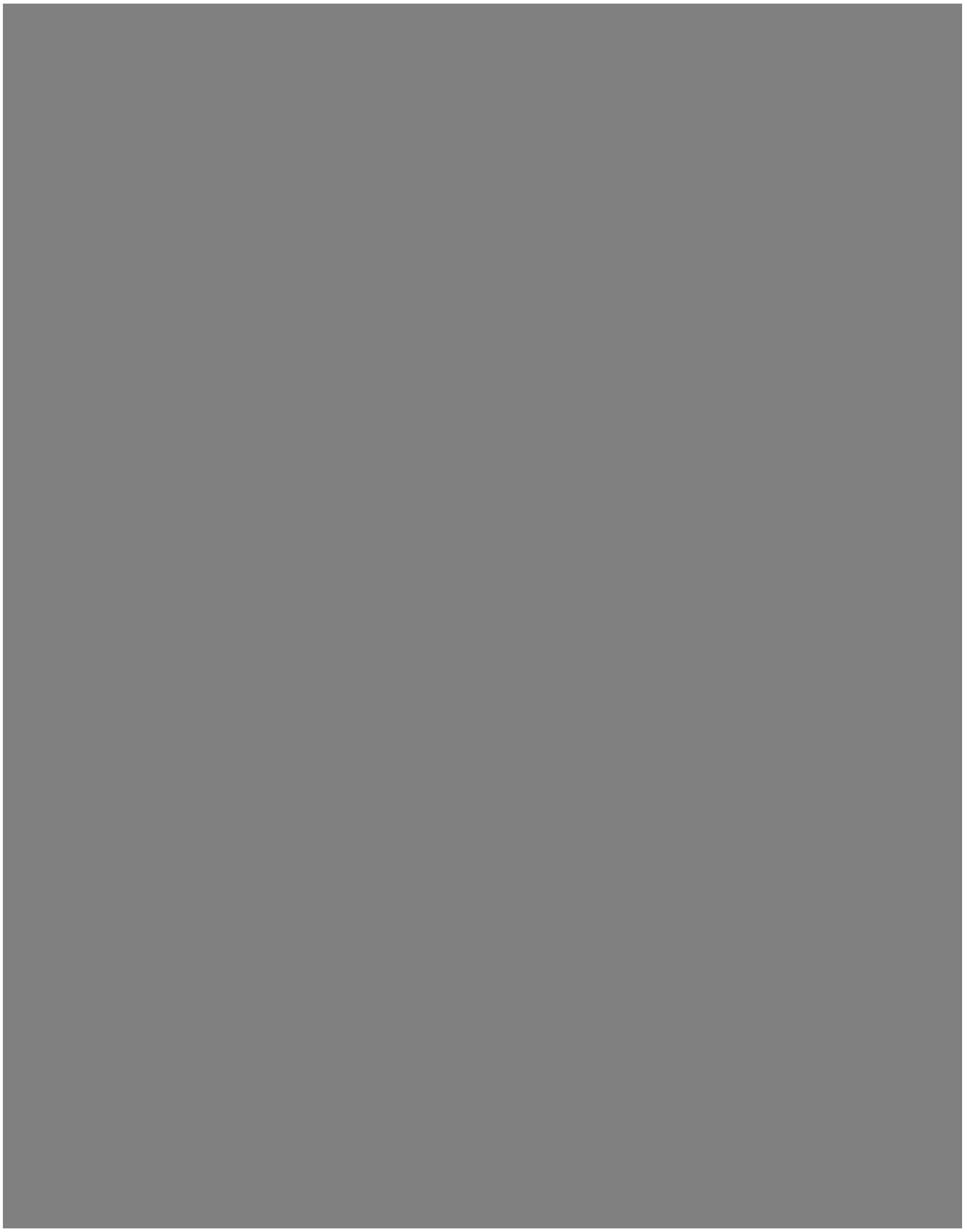


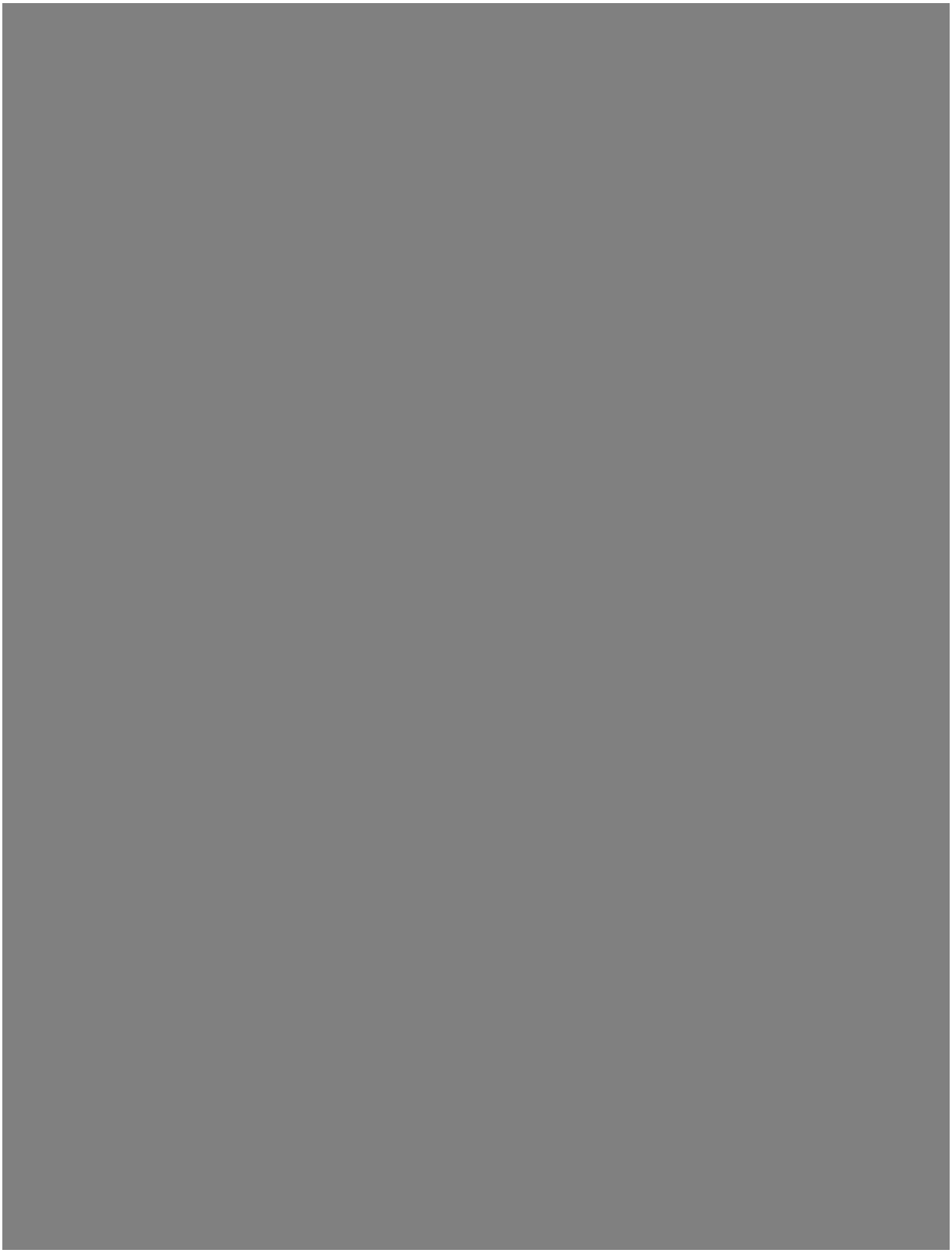


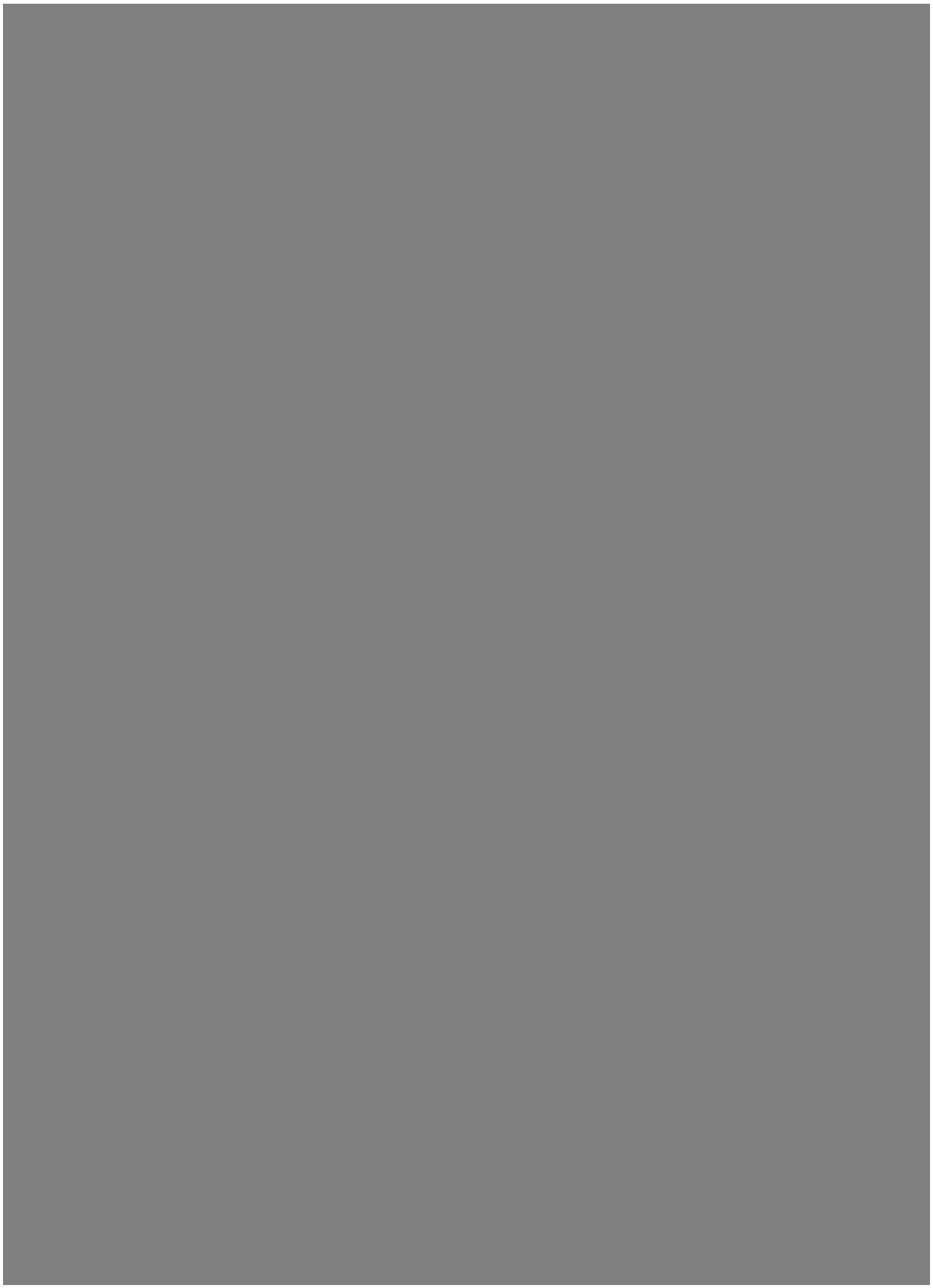


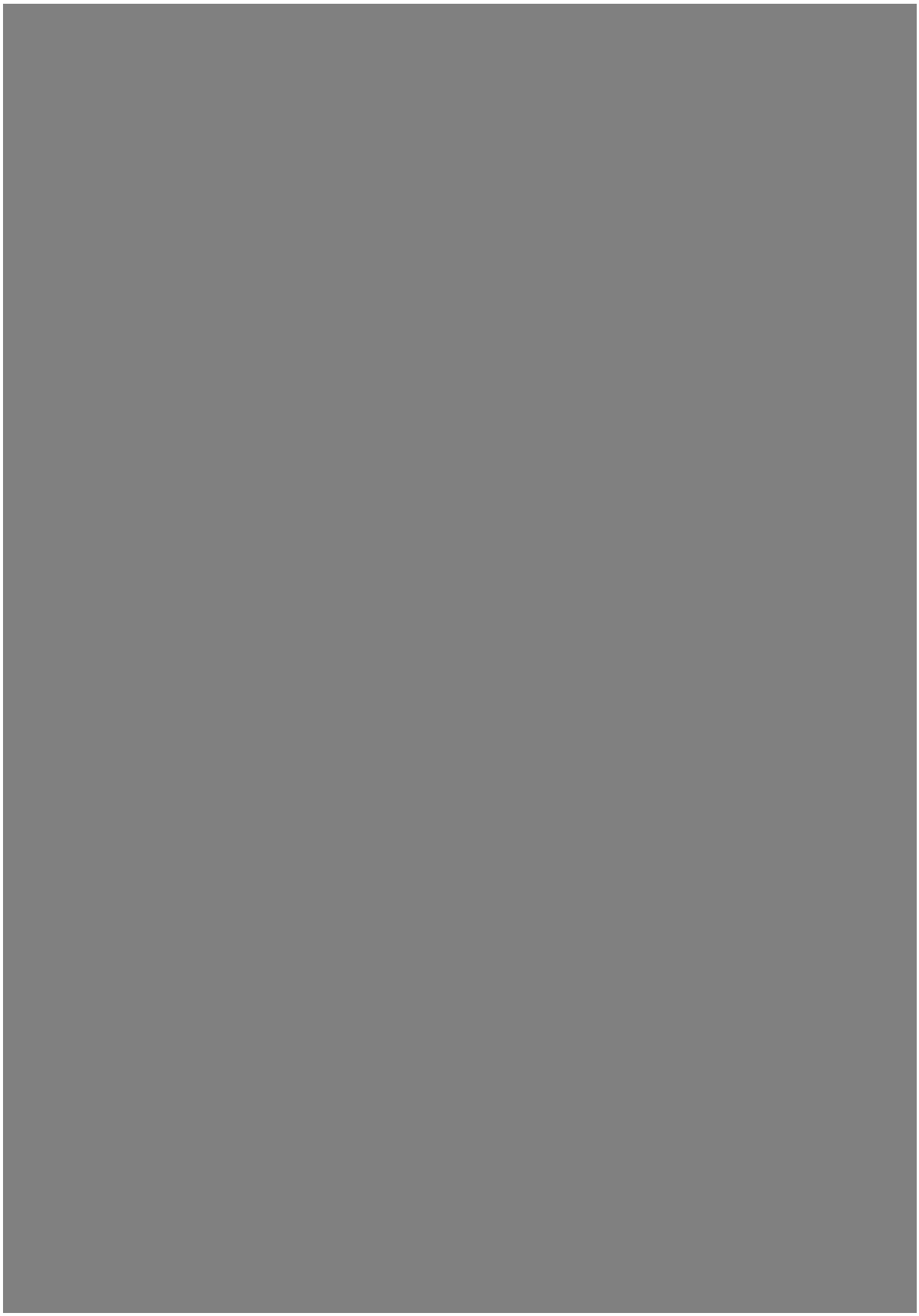




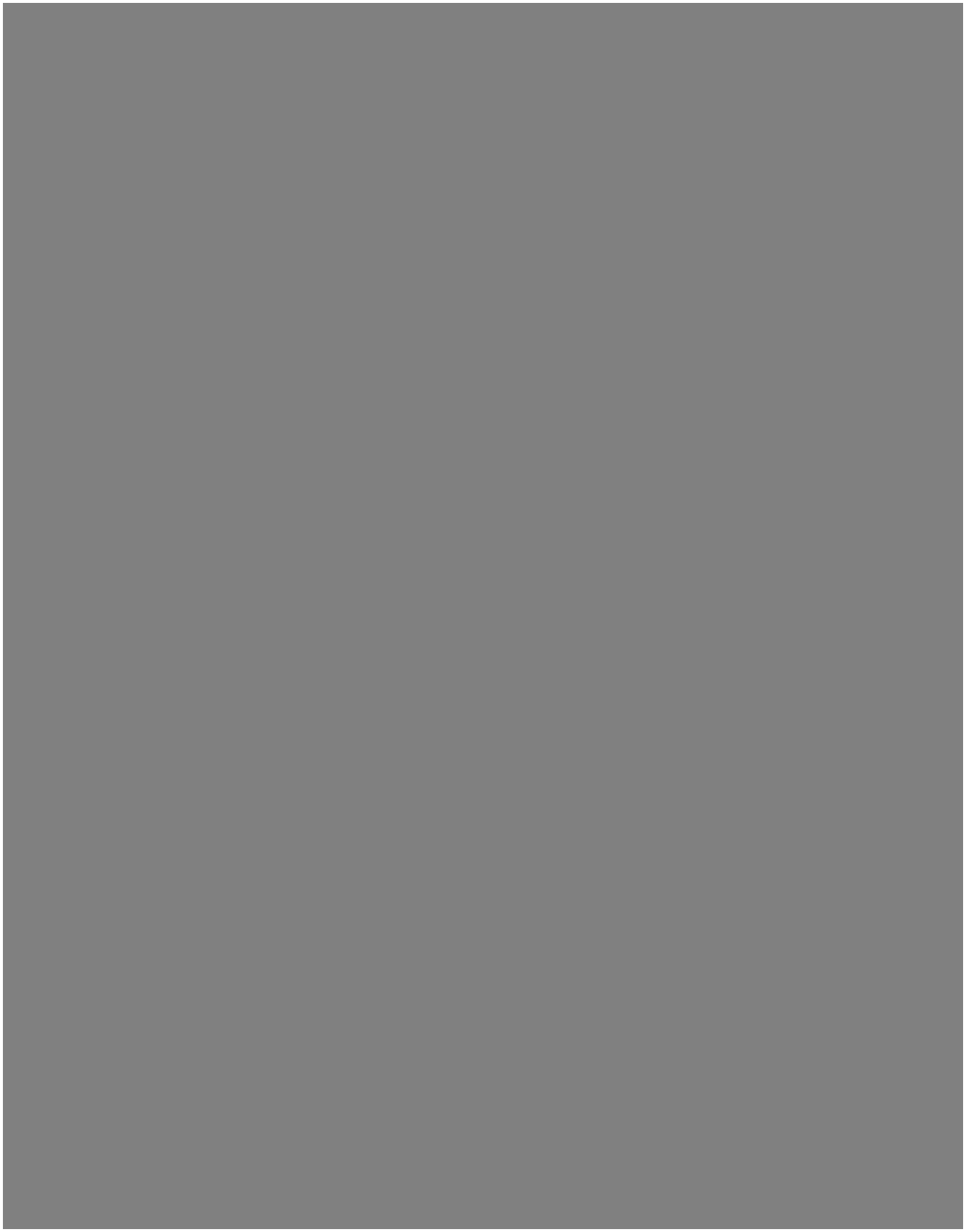


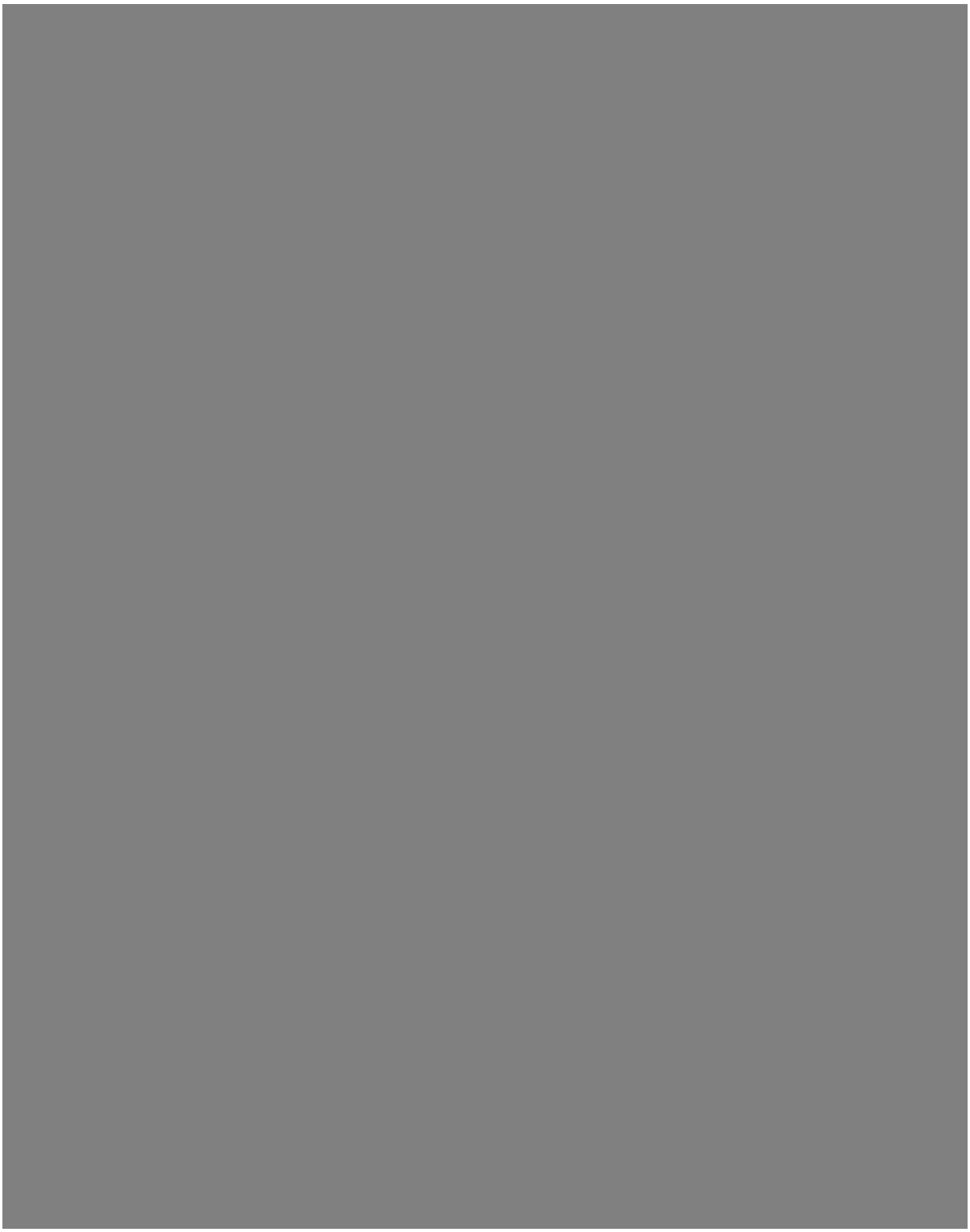


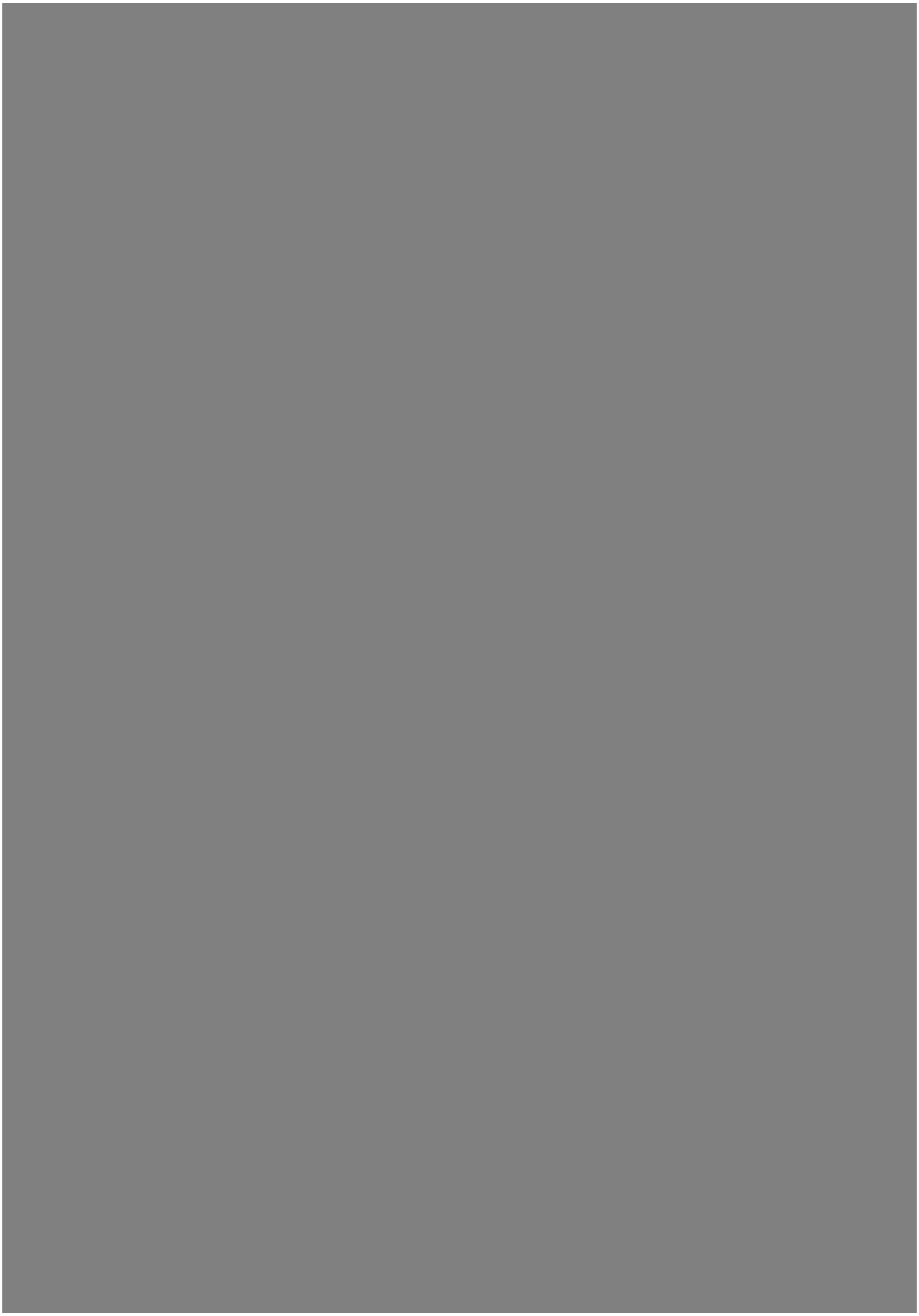


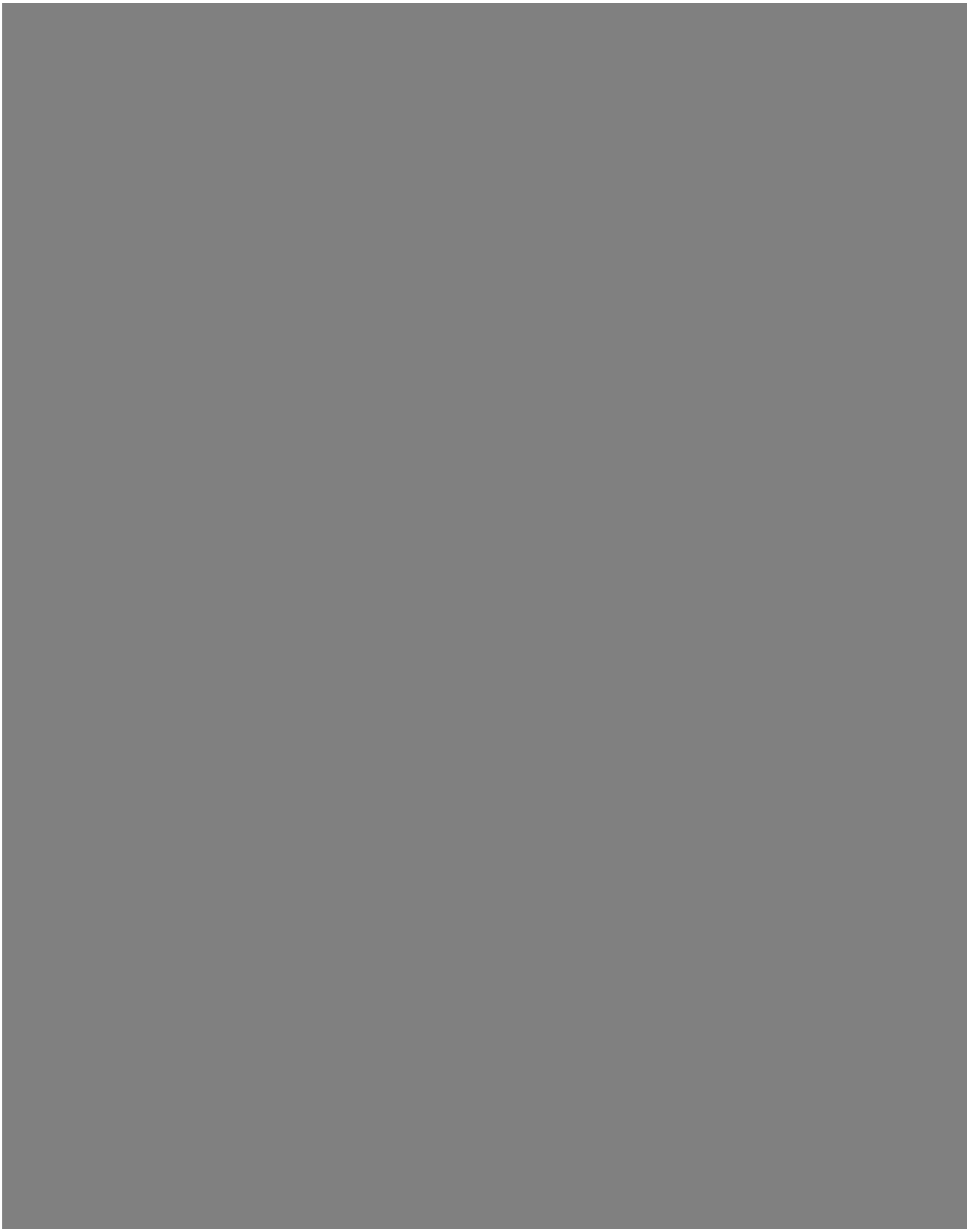


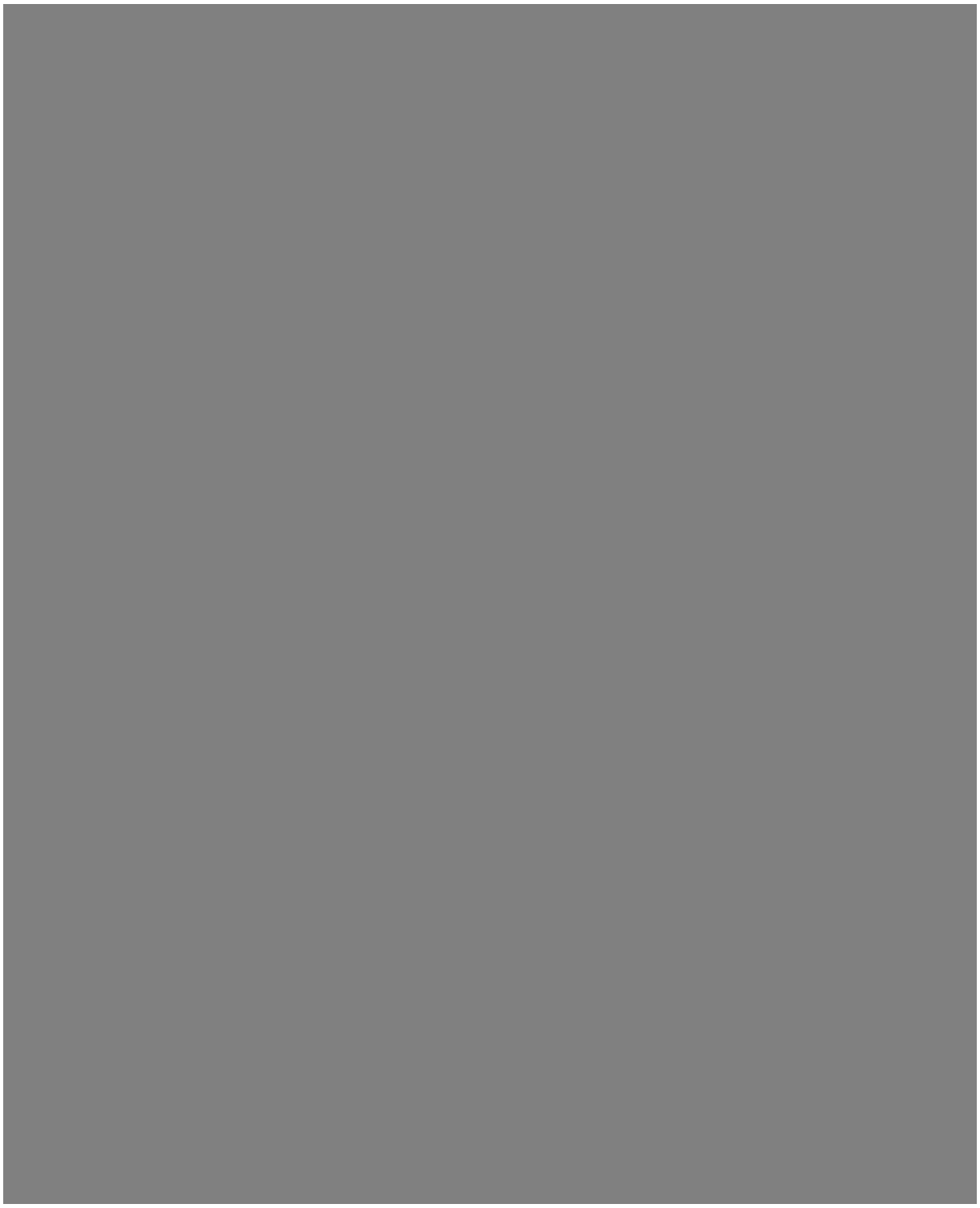


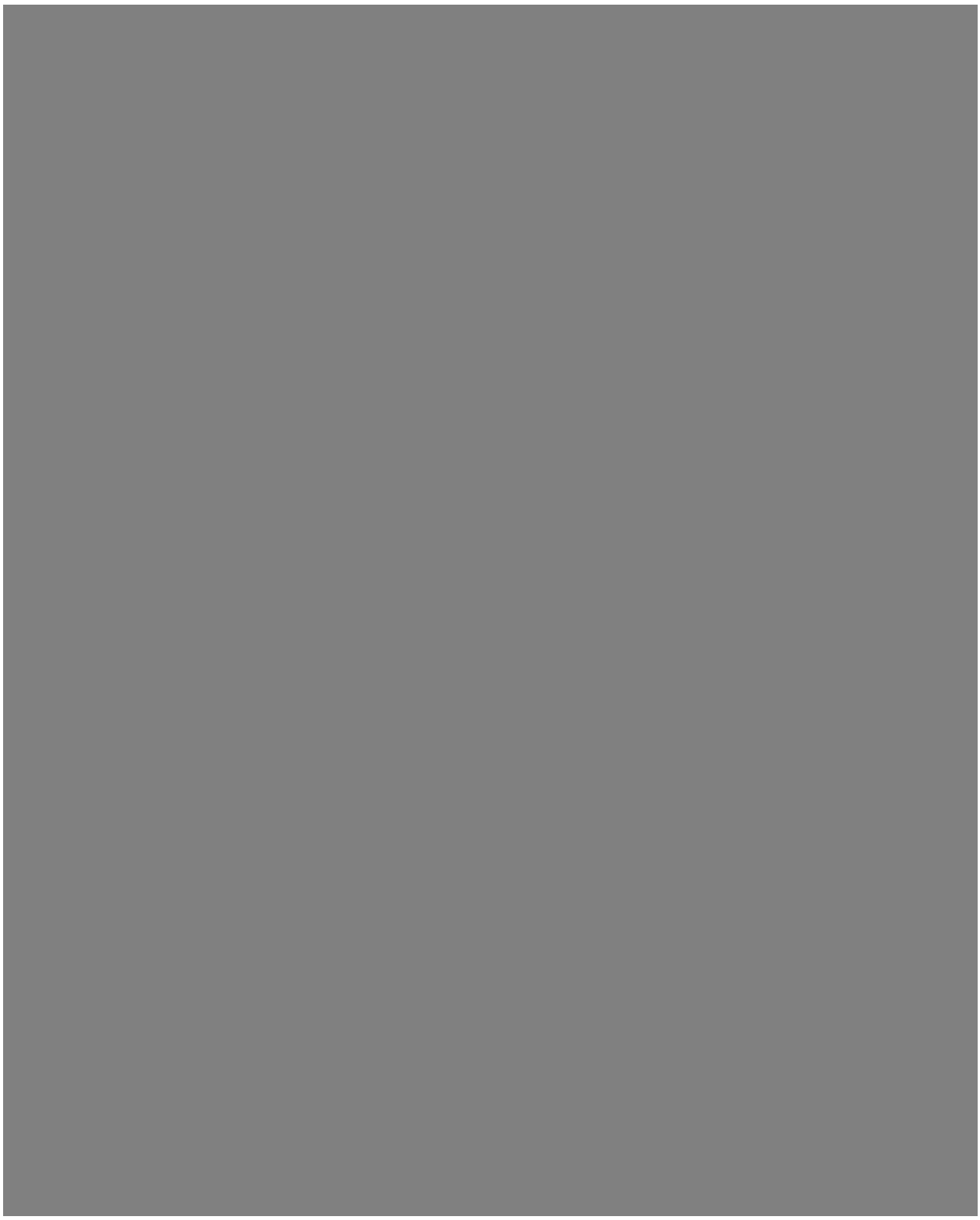






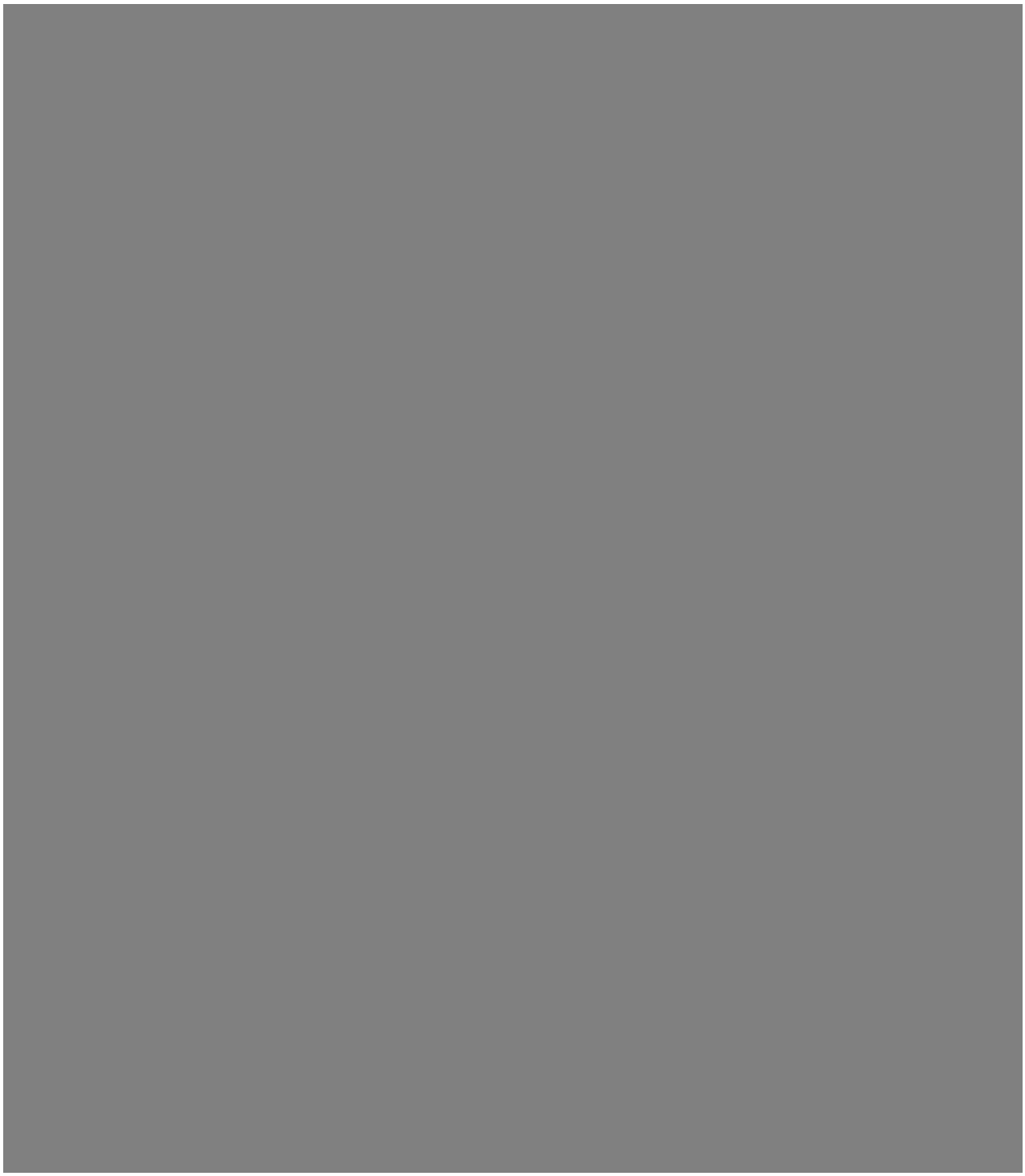


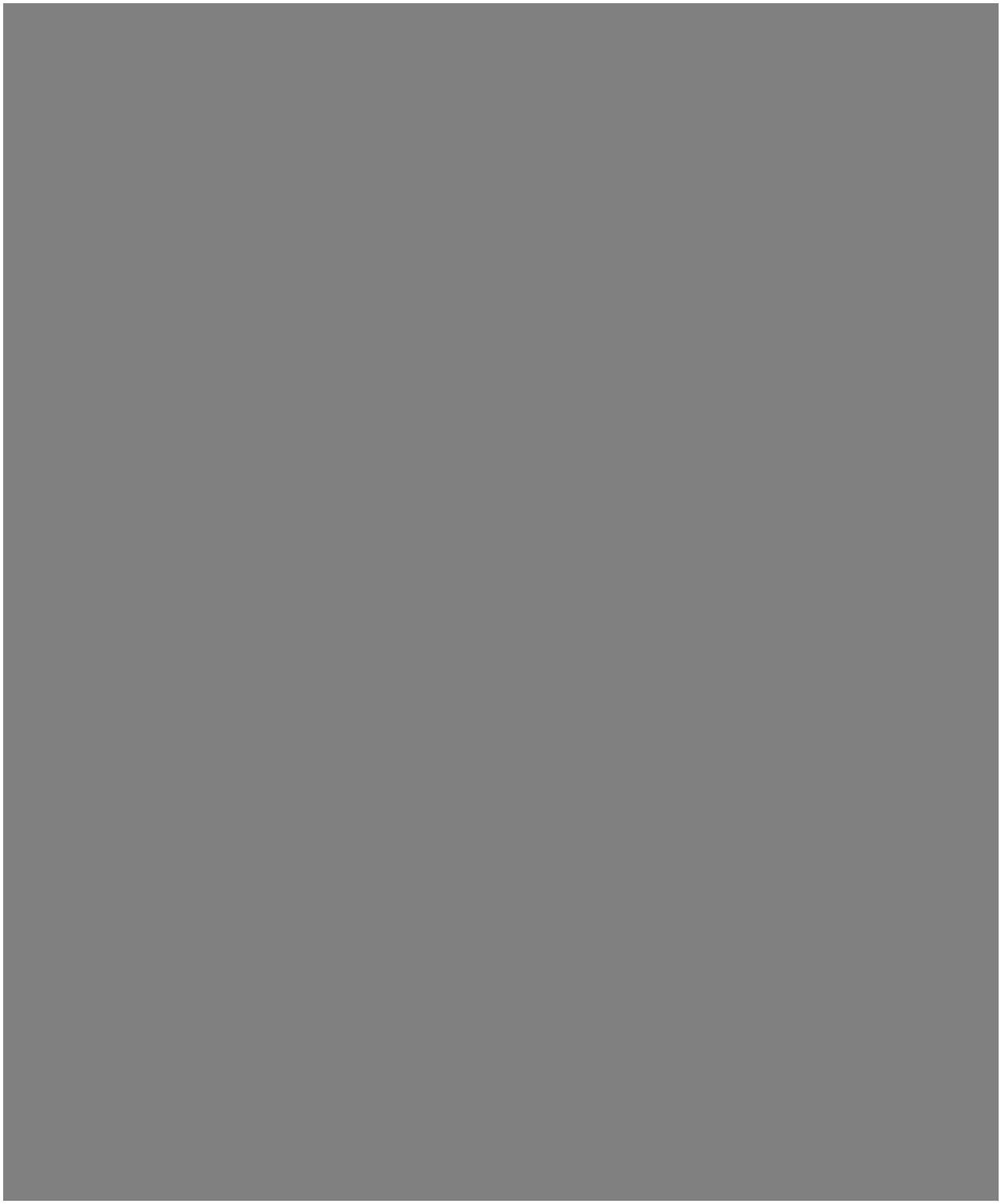


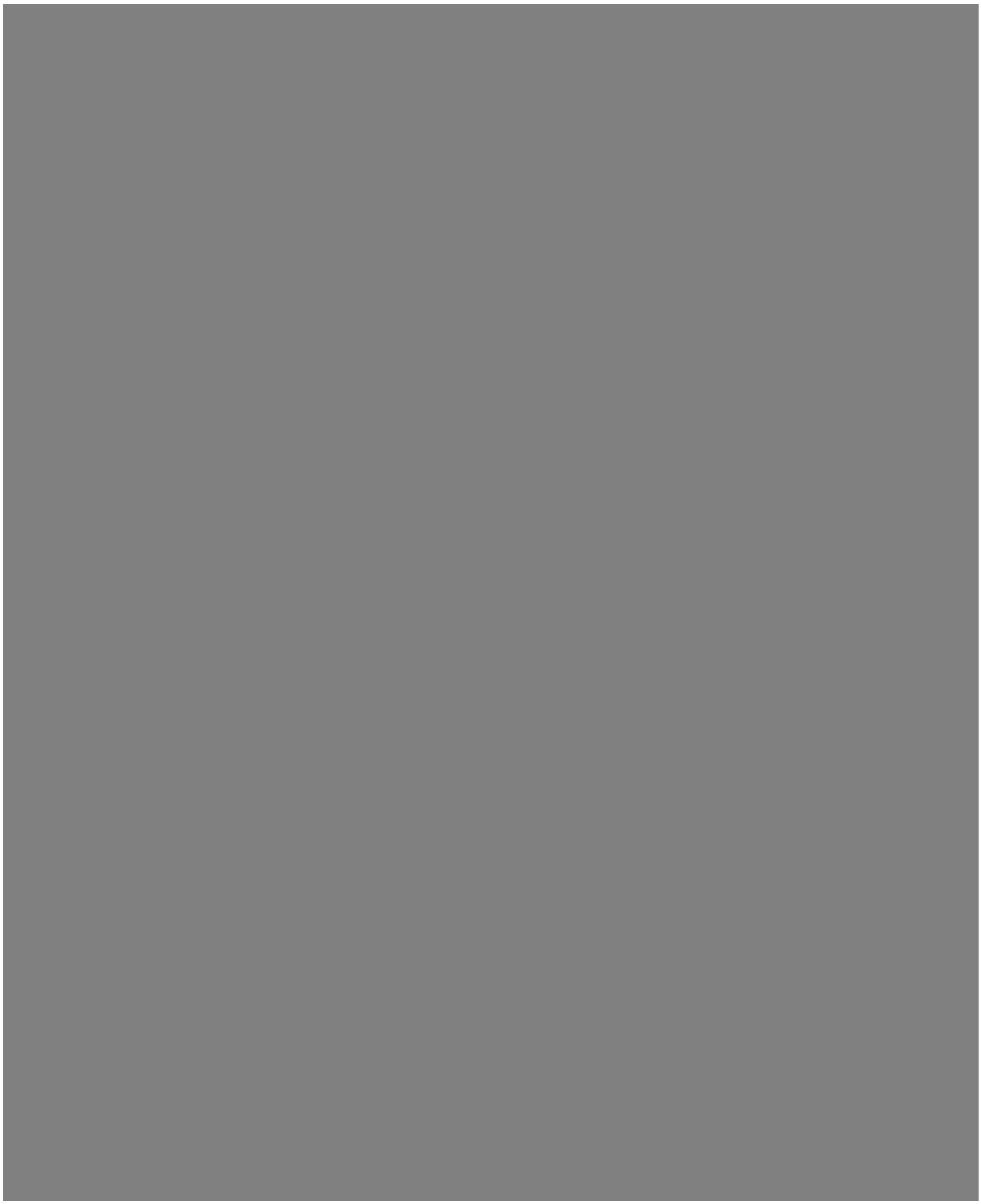


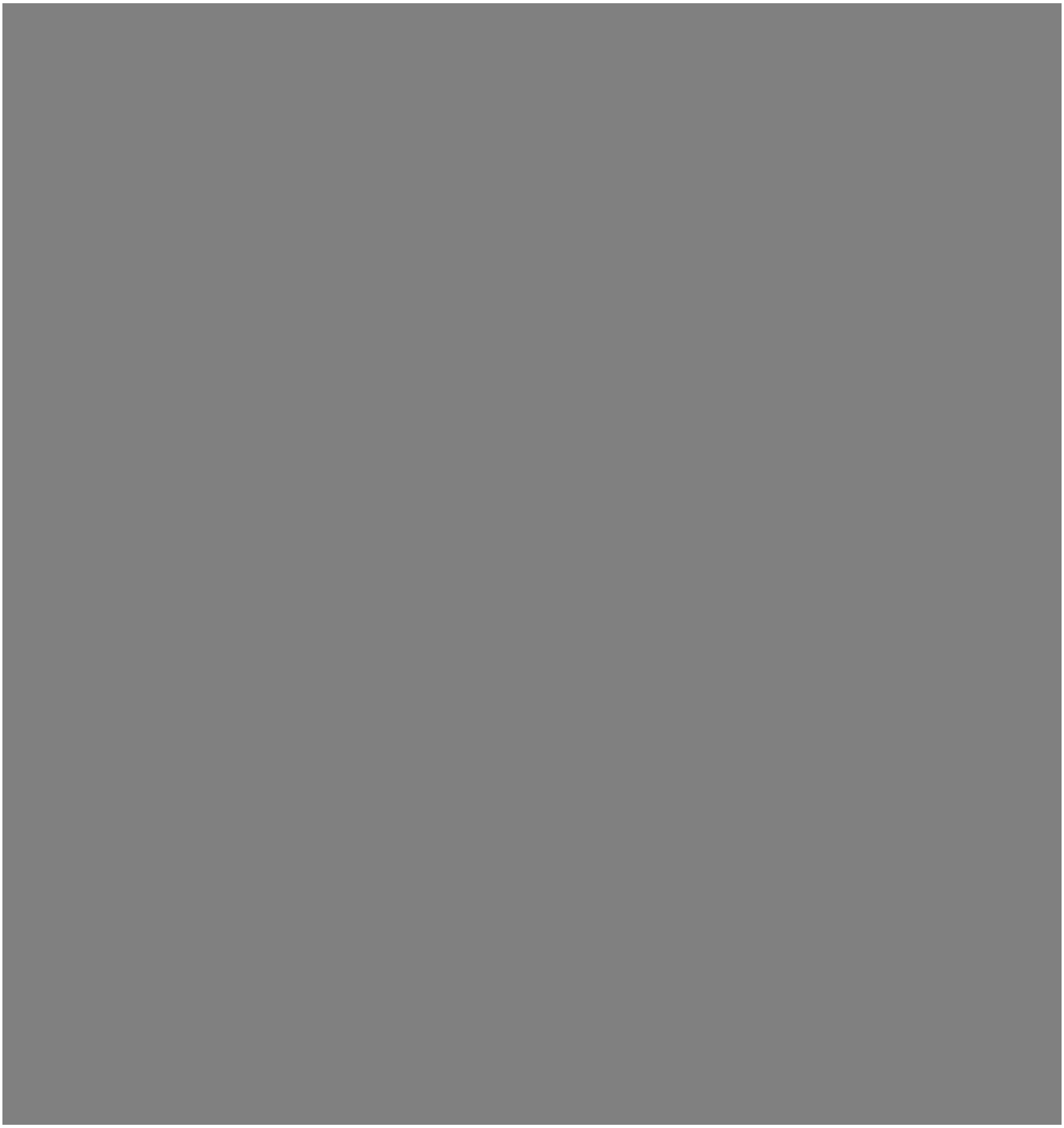
APPENDIX B

NI AWR Design Environnent









B. 2 Starting NI AWR/ MWO

The following main window displays.

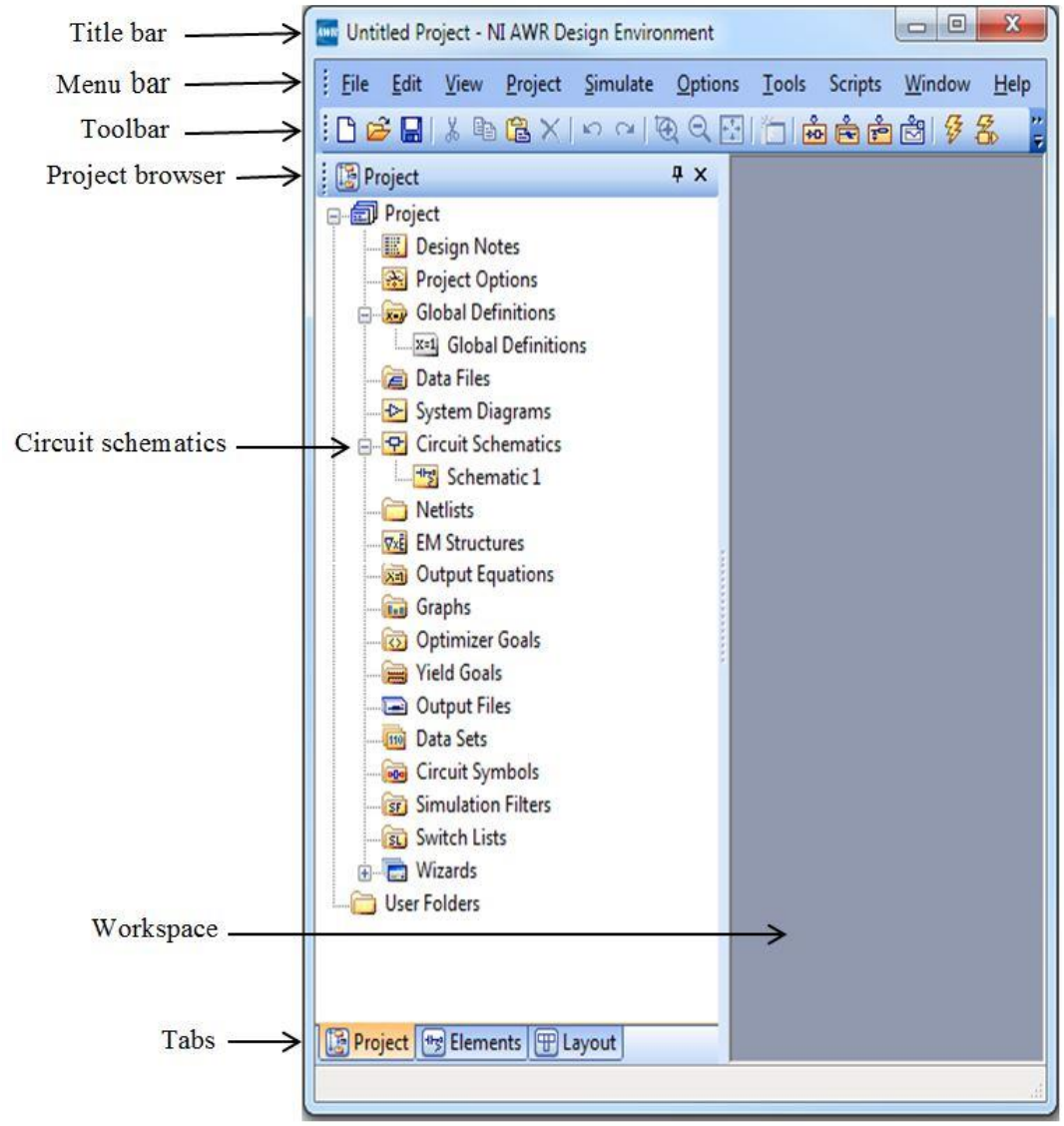


Figure B.1: AWR main window displays

B. 3 Specifying the Simulation Frequency

1. Click on Options > Project Options in the Project Browser.

2. Click the Frequencies tab.

3. Type "1" in Start, "2" in Stop, and "0.01" in Step, and then click Apply.

4. Click OK.

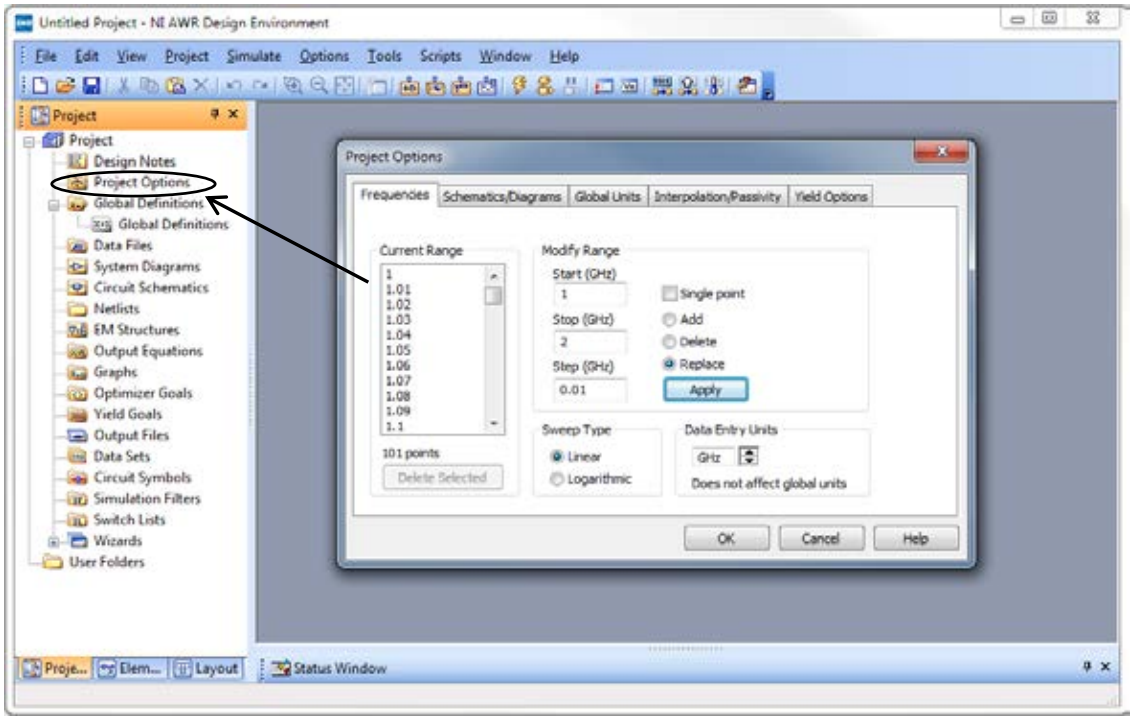


Figure B.2: Specifying the Simulation Frequency

B. 4 Creating a New Circuit Schematic for the Design

1- Right-click on **Circuit Schematics** in the Project Browser, choose **New Schematic**, and then specify

2- After you name the schematic, a window for it opens in the workspace and the Project Browser displays the new item as a sub-node under **Circuit Schematics.**

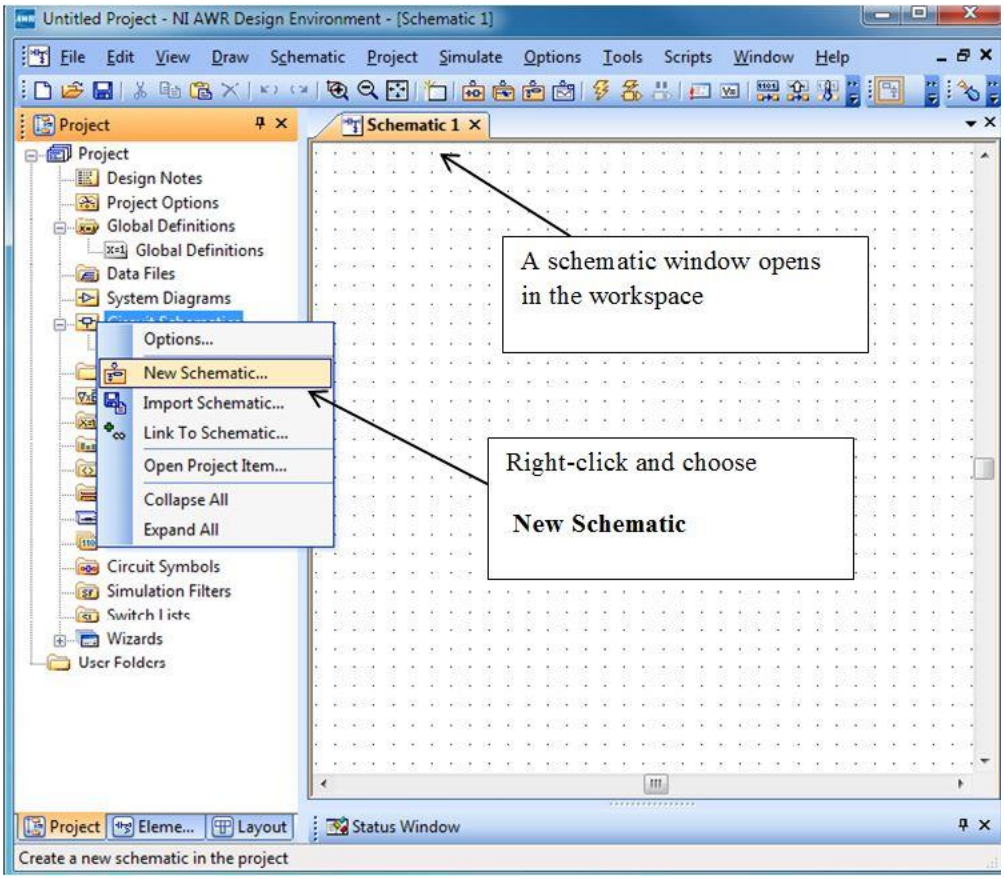


Figure B.3: creating a new circuit schematic

B. 5 Placing Elements in a Schematic

To place elements on a schematic:

1. Click the **Elements** tab to display the Element Browser. The Element Browser replaces the Project Browser window.

2. Under **Circuit Elements**, expand the **Lumped Element** category and select the desired model from the bottom window and drag it to the schematic to design the circuit as depicted in the figure below.

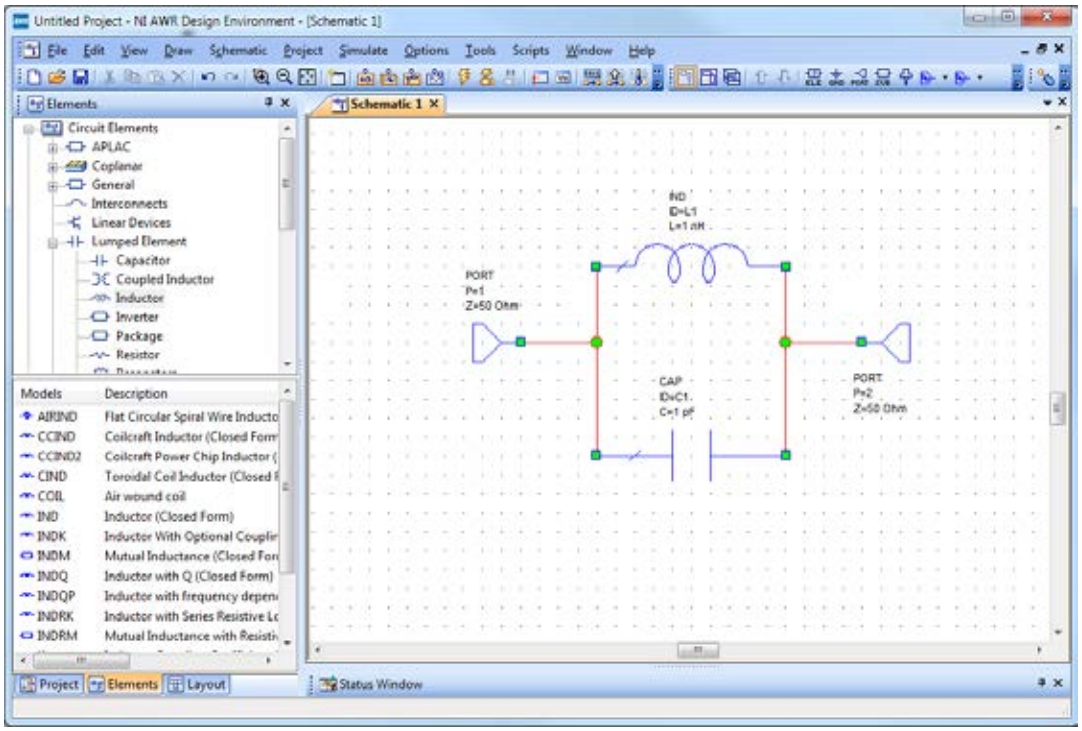


Figure B. 4: placing the desired element to the circuit schematic

B. 6 Creating Output Graphs and Measurements

Right-click on **Graphs** in the Project Browser and choose **New Graph** to display a dialogue box in which to specify a graph name and graph type. An empty graph display in the workspace and the graph name displays under **Graphs** in the Project Browser. The results can be viewed in various graphical forms such as rectangular graph type or Smith chart... etc.

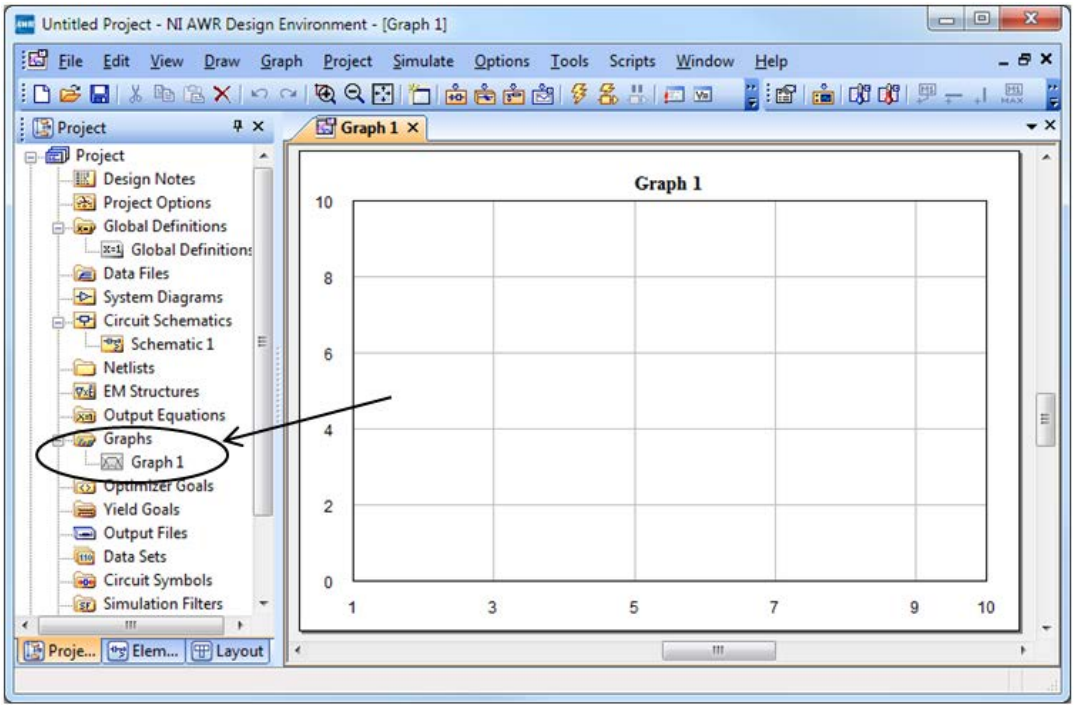


Figure B. 5: Creating graphs to display the results

To specify the data that you want to plot, right-click the new graph name in the Project Browser and choose **Add Measurement**, a dialogue box will display to allow

you to choose from a comprehensive list of measurements. Consequently, the design is ready to be simulated by hitting the simulation button displayed in the toolbar.

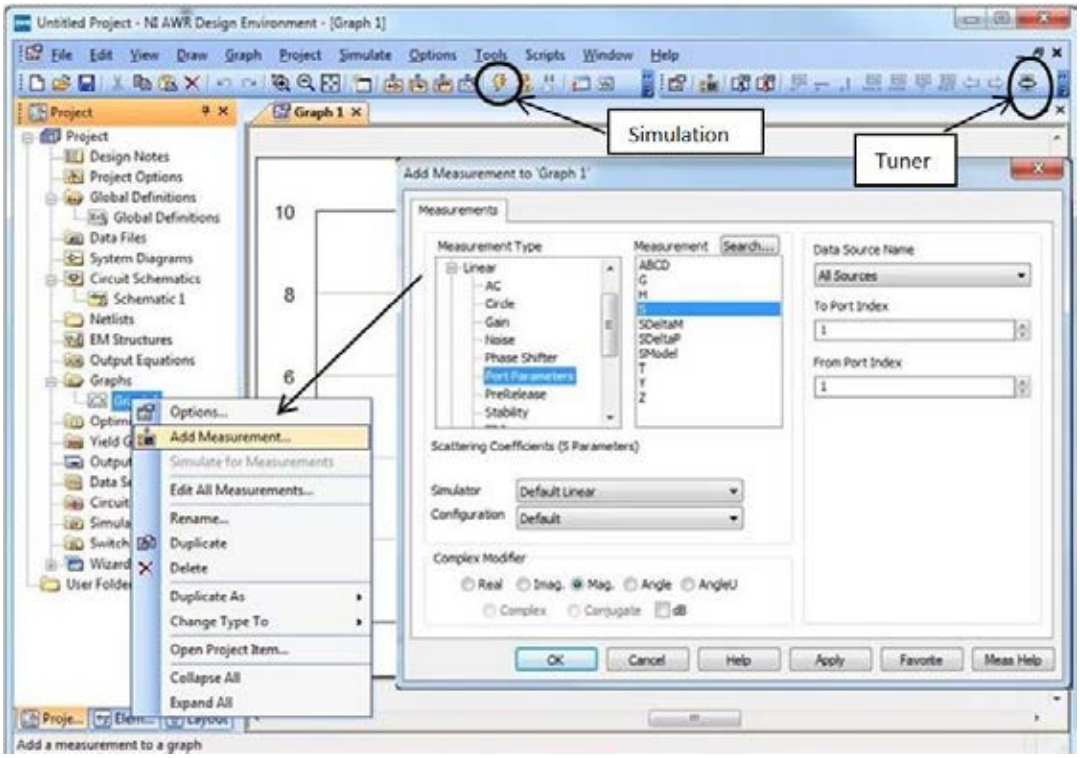


Figure B. 6: Specifying the wanted measurement type to be plotted

There are additional tools and features that can be very useful for optimising the design parameters for specific goals for such as tuner and optimiser which are available in the toolbar and they need set up prior utilising them.